




 Cite this: *RSC Adv.*, 2025, 15, 42771

# Emerging nano sensing technologies for the detection of biological and chemical food toxins

 Mohsin Javed,<sup>a</sup> Afzal Shah,<sup>a</sup>  \*a Sidra Nasir,<sup>b</sup> Sidra Pervaiz<sup>c</sup> and Hazrat Hussain <sup>a</sup>

This document presents advancements in contemporary detection technologies aimed at ensuring food quality and safety. It explores a range of sophisticated sensing platforms designed to identify harmful substances in food products. The integration of nanomaterials and microfluidics has significantly enhanced these detection techniques, resulting in improved sensitivity, specificity and response times. Additionally, the document emphasizes the importance of developing portable and user-friendly sensing devices, which not only facilitate practical applications of these technologies but also address the challenges and potential solutions associated with their implementation. Emerging trends, including smartphone-based detection systems and the incorporation of artificial intelligence for data analysis, are also examined, showcasing their potential to revolutionize food safety protocols. This review emphasizes the critical importance of advanced sensing technologies in mitigating risks associated with foodborne toxins, ensuring the integrity of the global food supply chain, and highlighting the necessity for ongoing research and development to meet the dynamic challenges of food safety. It offers a comprehensive analysis of the sources, toxicity characteristics, and detection challenges linked to various classes of toxins, followed by an overview of innovative sensor-based techniques for detecting food toxins. By consolidating existing knowledge, this comprehensive review establishes a foundation for future improvements in food quality and safety measures.

 Received 14th September 2025  
 Accepted 15th October 2025

DOI: 10.1039/d5ra06960b

[rsc.li/rsc-advances](https://rsc.li/rsc-advances)

## 1. Introduction

Innovative technologies, including electrochemical and optical sensing systems, microfluidic platforms, and nanomaterial-based biosensors, are being developed to enable the rapid, accurate, and on-site detection of biological and chemical contaminants in food. Advancements in sensing technologies play a critical role in achieving Sustainable Development Goal 2 (Zero Hunger) by ensuring that food distributed globally is safe. By reducing exposure to hazardous pathogens, mycotoxins, heavy metals, and pesticide residues, these technologies are crucial for achieving SDG 3 (Good Health and Well-being). With contaminated food affecting millions each year and being a significant contributor to global illness, the integration of advanced sensing technology into regular food monitoring is crucial for preventing outbreaks, reducing healthcare costs, and enhancing consumer confidence. As the global community works towards meeting the SDGs by 2030, investing in next-generation food toxin detection systems is imperative for safeguarding food safety.

Toxins are produced by various organisms, including bacteria, algae, fungi, plants, and animals, for purposes such as competition, defense, or predation. Toxins do not pose a threat to the organisms that produce them; however, they can be detrimental to other creatures. Toxins have the potential to elicit an immune response.<sup>1</sup> A notable example of such toxins is snake venom, which causes critical pathologies when injected through a bite. Aflatoxin is the most commonly found toxin in stored moldy grains, nuts, and fruits. Warm and humid conditions promote the growth of fungi that produce this toxin.<sup>2</sup> Environmental pollution and the application of agricultural chemicals further exacerbate the generation of toxins. While these agents do not naturally occur in food, they can contaminate the food supply through environmental pollution.<sup>3</sup> For instance, crops or animals absorb heavy metal ions from soil or water, and these ions then make their way into the food chain.<sup>4</sup> Exposure to toxins through ingestion, inhalation, or direct contact can lead to a range of adverse health effects, which vary depending on their physical, chemical, or biological characteristics.<sup>5</sup> Several chemical toxins have been reported to cause cellular death by blocking cellular metabolism or impairing nerve impulse transmission.<sup>6</sup>

The availability of toxin-free food is crucial for survival and promoting overall well-being. Technological innovations in food science have enhanced food production and processing systems, facilitating the global distribution of food to support

<sup>a</sup>Department of Chemistry, Quaid-i-Azam University Islamabad, 45320, Pakistan.  
 E-mail: afzals\_qau@yahoo.com

<sup>b</sup>Department of Applied Chemistry, Government College University Faisalabad, 38040, Pakistan

<sup>c</sup>Department of Chemistry, Government College University Faisalabad, 38040, Pakistan



population growth.<sup>7</sup> Precision agriculture and genetically modified organisms have contributed to increased food production and improved quality in agricultural systems. The unintentional entry of trace amounts of chemical substances into food can pose significant health risks to humans, underscoring the urgent need for rigorous food safety measures.<sup>8</sup> As the food industry evolves, it faces critical food safety challenges that represent a substantial global concern for both public health and economic stability. Food security and safety have become universal priorities due to international food adulteration scandals. Adequate food safety protection relies on stringent regulatory frameworks and comprehensive monitoring systems to safeguard public health and uphold consumer trust in national food supplies.<sup>9</sup>

The concept of food extends beyond nutritional and cultural aspects to encompass the essential protection of human well-being. Food safety control must focus on monitoring food quality and detecting potential contaminants. The processes of physical, biological, and chemical contamination are primarily associated with the methods used for transporting and storing food products.<sup>10</sup> Pathogenic microorganisms and microbial toxins are the most significant factors in compromising food safety among all the factors that lead to food contamination.<sup>11</sup> In 2010, the WHO reported that foodborne pathogens caused approximately 600 million illnesses and resulted in around 420 000 fatalities. In recent years, there has been a significant rise in foodborne illnesses, impacting all developed countries. Annually, 9.4 million cases of foodborne diseases are linked to recognized pathogenic agents and their toxins, which include 24 confirmed agents.<sup>12</sup> In contrast, around 38.6 million cases arise from unidentified agents and unpredictable distribution systems. The economic impact of these foodborne illnesses is substantial, totaling \$78 billion annually, encompassing costs related to healthcare, unemployment, product recalls, bankruptcies, and legal issues.<sup>13</sup> A significant number of foodborne illnesses are caused by microbial toxins, including botulinum toxin, staphylococcal enterotoxin, and various enterotoxins, as well as mycotoxins produced by fungi and toxins found in seafood. Even minimal exposure to these toxic substances can lead to severe health complications for consumers.<sup>14,15</sup>

Food safety depends on continuous monitoring of biological and chemical toxins. Among these, *Clostridium botulinum* is known for producing botulinum toxin, while certain fungi, such as *Aspergillus* and *Fusarium*, are responsible for producing mycotoxins.<sup>15</sup> The consequences of exposure to foodborne toxins can be severe, leading to a range of illnesses from food poisoning to chronic health issues, and in extreme cases, even death. Food products can become contaminated with chemical toxins, including pesticides, heavy metals, and industrial chemicals, which infiltrate the food supply through environmental pollution, agricultural practices, and food processing methods. Of particular concern are persistent organic pollutants and endocrine-disrupting chemicals, which can accumulate in the human body and disrupt hormonal functions, leading to significant health risks, including the development of cancers and reproductive issues.<sup>16</sup>

Monitoring the presence of toxins is crucial for safeguarding human health. Various testing methods and stringent quality control measures facilitate the identification of potential contamination risks. Regulatory bodies such as the WHO and the Food and Agriculture Organization (FAO) have established maximum permissible levels of toxins in food production. Advances in detection technologies, such as mass spectrometry and chromatography, have significantly enhanced the capability to identify and quantify these toxins, thereby improving safety standards and regulatory compliance. Maintaining rigorous monitoring and strict food regulations is vital to prevent unknown toxins from jeopardizing the food supply. Identifying pathogenic agents and their toxins is essential for addressing food safety challenges.<sup>17</sup> The protection of public health and the preservation of consumer trust in the food supply rely heavily on robust food safety regulations and comprehensive monitoring systems, which should encompass all facets of nutritional heritage and health protection.<sup>18</sup>

Research on biological toxins primarily focuses on low-molecular-weight compounds, such as mycotoxins, which are often produced by fungi under suitable environmental conditions. These biotoxins can be found in various sources and have the potential to contaminate food, animal feed, and seafood during harvesting, processing, storage, and transportation.<sup>19</sup> The presence of biological toxins at harmful levels can lead to food poisoning, particularly when used as agents in biological warfare. Notably, aflatoxin B1 (AFB1), a type of mycotoxin, is linked to liver cancer, affecting approximately 28.2% of diagnosed patients.<sup>19</sup> Additionally, biotoxins are categorized based on their sources, with marine toxins including shellfish toxins, ciguatoxins, and tetrodotoxins, which pose significant health risks. Marine pollutants can enter the food chain, resulting in severe consequences, such as shellfish poisoning, which claims between 750 and 7500 lives globally each year. Bacterial toxins also contribute to foodborne illnesses by inhibiting protein synthesis and causing neurotoxicity. Notably, *Clostridium botulinum* produces the highly lethal botulinum toxin, which can cause death at doses as low as 100 ng.<sup>20,21</sup> When these toxins cannot be effectively reduced or eliminated, it becomes essential to restrict their consumption.<sup>22</sup>

Recent advancements in the detection of biological and chemical toxins in food have been significant, driven by technological innovations and a heightened emphasis on public health safety. This review explores the latest detection methods, utilizing data from 2020 onward, and highlights advanced sensing protocols that improve sensitivity, specificity, and detection speed through developments in nanomaterials and microfluidics. It also addresses the role of electrode modifiers in facilitating electron transport between transducers and food toxins. Furthermore, the emergence of portable and user-friendly sensing devices is emphasized, enabling on-site testing and real-time monitoring, which ultimately bolsters food safety standards and encourages proactive strategies against foodborne illnesses. As the domain of food toxin detection evolves, this review serves as an essential reference for researchers, industry stakeholders, and regulatory bodies committed to protecting public health. It identifies prevalent



detection challenges and offers adaptable solutions, concluding with a focused gap analysis and a roadmap for research priorities aimed at expediting industry and regulatory integration. The review explicitly connects theoretical sensing principles to practical applications by examining how factors such as matrix effects, sample preparation, analytical specificity, and validation processes influence the relevance of ultra-low limits of detection reported under controlled conditions for real-world food testing.

## 2. Sensors and their types

Sensors have become indispensable in modern operations, providing critical data that enhances security protocols and improves efficiency across various industries.<sup>23</sup> Healthcare relies on sensors to track patient vital signs, as this enables the prompt detection of health issues, leading to enhanced patient recovery.<sup>24</sup> Sensors enable precise farming to achieve better water optimization while monitoring the soil ecosystem and advancing agricultural production. Sensors play a crucial role in environmental monitoring systems, assessing air and water quality, and contributing to the resolution of pollution and effective climate change management.<sup>25</sup> Sensors in the food industry monitor contaminants for both safety and quality purposes. The applications demonstrate the necessity of sensors that deliver real-time information to boost automation and upgrade system operational excellence. As advancements in technology continue, the role of sensors will remain critical in advancing safety protocols, streamlining processes, and supporting sustainable growth. In 132 AD, Zhang Heng constructed the seismoscope, which became the initial sensing device for detecting earthquakes.<sup>26,27</sup> Food detection sensors are now essential for monitoring contaminants and evaluating the quality of food products in food safety procedures.<sup>28</sup> The Toronto-based startup TellSpec created the first food-specific detector device, the TellSpec. Raman spectroscopy enables this device to analyze food through scans that reveal allergens, chemicals, nutrients, calories, and ingredients. The device TellSpec was developed following a food allergy incident involving the founder's daughter to provide consumers with precise information about food contents. The SciO helps users select healthier food options, serving as a handheld molecular sensor that utilizes near-infrared light to identify molecular signatures in food.<sup>27</sup> The protection of public health depends on strict food monitoring and thorough regulations, as consumer trust in the food supply requires this level of security. The evolution of sensor technology enhances our ability to detect and neutralize foodborne threats, thereby creating a more secure and diverse food supply chain. A variety of sensors are used to detect biological and chemical toxins present in food, as discussed *vide infra*.

Biosensors serve as analytical devices that combine biological recognition components with transduction systems for detecting specific substances, such as food toxin. Each biosensor contains one or more biological recognition components, including enzymes, antibodies, nucleic acids, or microorganisms, to detect the target substance.<sup>28</sup> The

biological interaction between recognition elements produces a detectable signal, which is then translated by the transducer into electrical, optical, or thermal outputs. A biosensor operates through four distinct operations: starting with the binding of the target analyte to its biological recognition component, followed by signal generation and transduction, and finally signal processing. The sequential operational steps enable biosensors to perform quick and precise detection of analytes.<sup>29,30</sup> Biosensors play a crucial role in ensuring food safety and quality by detecting toxins. Modern biosensors can detect a wide range of toxic compounds, including pathogens, microbial toxins, pesticides, and heavy metals. Biosensors provide immediate monitoring data, enabling the detection of contaminated food products and helping to prevent dangerous consumption and reduce the risk of food-related illnesses.<sup>31,32</sup> The application of nanotechnology and biotechnology has sparked the development of biosensors with greater accuracy and sensitivity, which now serve as fundamental tools in the food industry. Through continuous monitoring, these devices verify that products from production zones meet safety regulations and quality requirements as they are transported to storage and distribution points. Biosensors are essential for fostering consumer confidence in the safety of the food supply.

### 2.1 Electrochemical sensors

Electrochemical sensors utilize electrical signals to transform chemical information, enabling the detection and measurement of food toxins. These devices employ three principal sensing methods: potentiometry, amperometry, and voltammetry.<sup>33</sup> The potentiometric sensor determines electrode potential disparity while sustaining a steady current flow in pH meter applications. Amperometric sensors track the constant voltage-controlled oxidation or reduction current to detect analytes. A changing voltage in voltammetric sensors produces measurable current fluctuations, enabling the detection of complex analyte combinations.<sup>34</sup> When operating electrochemical sensors, the target analyte engages with a chemically sensitive layer attached to the electrode surface. An interaction occurs between the target molecule and the chemically sensitive layer, resulting in modifications to the electrical features that are measured as a distinct signal.<sup>35,36</sup> These sensors obtain enhanced sensitivity and selectivity when their surfaces are modified with specific nanomaterials, enzymes, polymers and specialized recognition elements.<sup>37</sup> Assessing food toxins through electrochemical sensors relies on detecting pesticides, heavy metals, and microbial toxins. Electrochemical sensors offer high precision and fast responsiveness, while providing portability benefits that support real-time testing across the entire food distribution chain, from factory production to end-user consumption.<sup>36</sup> The sensors provide prompt information about toxins to ensure food safety, protect public health, and maintain consumer trust. The advancement of materials science and nanotechnology helps improve electrochemical sensors, thereby extending their usefulness in preserving the food supply.



## 2.2 Fluorescent sensors

Fluorescent sensors serve as analytical devices that detect specific substances using fluorescence-based methods, including the assessment of toxins in food products. Fluorescent sensors utilize specific wavelength-stimulated fluorescent dyes and probes that emit light. The intensity of fluorometric light detection and the variations in wavelength correlate directly with the concentration of the target analyte, enabling quantitative analysis.<sup>38,39</sup> Fluorescent sensing utilizes three fundamental analytical methods: fluorescence resonance energy transfer (FRET), time-resolved fluorescence, and fluorescent quenching. The energy exchange between two fluorophores under FRET detection yields results whose intensity depends on the distance between them, making it suitable for detecting molecular interactions. Time-resolved fluorescence enhances sensitivity by separating background noise and measuring the emission signal over time. The structure of a fluorescent quencher causes a decrease in fluorescence intensity, allowing researchers to detect specific analytes. Flexible fluorescent analytical sensors prove irreplaceable during analyte monitoring because they offer exceptional sensitivity, speed, and high selectivity performance.<sup>40–42</sup> These detectors demonstrate performance in identifying various substances, including infectious agents, toxic chemicals, microbial toxins, heavy metals, and pesticides. Fluorescent probes serve as targeted detectors for DNAs, bacterial toxins, such as botulinum toxin, and aflatoxins produced by molds, facilitating prompt detection and ongoing monitoring of these harmful substances.<sup>43–46</sup> Fluorescent sensors used for food protection prevent contaminated food from being consumed, thereby protecting public health while preserving consumer confidence. Research in nanotechnology and biotechnology has significantly enhanced the capabilities of fluorescent sensors, allowing for the accurate detection of minute quantities of toxins.

## 2.3 Optical sensors

Optical sensors detect variations in light to identify specific substances by measuring their concentrations.<sup>47</sup> The sensor mechanism utilizes a combination of absorption, fluorescence, phosphorescence, and reflectance processes to analyze the characteristics of various analytes. The functioning system of optical sensors creates a photon emission from a light source that interacts with the target analyte.<sup>48</sup> The photodetector detects changes in light properties stemming from the interaction between the light source and its target element. The resulting optical signal provides a precise measurement that correlates directly with the concentration of the substance being analyzed. These sensors are particularly effective in detecting food toxins, thanks to their high sensitivity, remarkable selectivity, and swift response times.<sup>49</sup> They are capable of identifying a wide range of biological and chemical contaminants, including pathogenic agents, toxic microbial substances, insecticides, and heavy metals. Specifically, fluorescence-based optical sensors employ fluorescent dyes in conjunction with quantum dots, which emit light upon binding to their target toxins, facilitating real-time detection and early identification of

these harmful substances. Additionally, surface plasmon resonance (SPR) sensors can detect anionic substances at low concentrations by monitoring changes in the refractive index at the sensor surfaces after the binding of toxin-recognition elements.<sup>50</sup> Optical sensors play a crucial role in food safety by enabling continuous monitoring of food products throughout production, distribution, and consumption. By providing accurate and timely information about the presence of contaminants, these sensors help protect public health and maintain confidence in the food industry.

## 2.4 Spectrometric and chromatographic sensors

Spectrometric and chromatographic sensors serve as fundamental analytical tools that help determine the identification and quantity of food toxins. Mass spectrometry (MS) and infrared spectroscopy (IR) serve as spectrometric sensors due to their ability to detect interactions between electromagnetic radiation and matter.<sup>51</sup> Mass spectrometry determines the presence of chemicals by measuring their mass-to-charge ratio. In contrast, infrared spectroscopy determines chemical composition by analyzing the IR light absorption patterns of molecules.<sup>52</sup> Chromatographic sensors separate mixtures into individual components, such as gas chromatography (GC) and high-performance liquid chromatography (HPLC). Separating volatile compounds occurs through GC methods, whereas HPLC analyzes all nonvolatile substances. The separation process in both methods utilizes fixed environments for each phase to determine how analytes bind with each station, which in turn defines their moving locations. Sample preparation followed by separation, detection, and data analysis comprises the sensor's operational procedure. Mass spectrometry involves applying ions to samples, followed by separation using a mass analyzer, and then detecting their ionization patterns to produce mass spectral output data.<sup>53</sup> When a sample absorbs IR light in infrared spectroscopy, the resulting spectrum provides structural information about the molecules. The basis of chromatographic systems involves placing a sample into a column that uses monitored detectors, including mass spectrometers or UV detectors, to detect separated analytes.

## 2.5 Colorimetric sensors

Colorimetric sensors sense discrete substances through visible color alterations.<sup>54</sup> A color change occurs visibly when these sensors detect target analytes based on chemical processes that produce observable changes in color.<sup>55,56</sup> The degree and tone of the created color directly correspond to the amount of analyte present, which enables quantitative examination. The function of colorimetric sensors depends on a recognition element, such as a chemical reagent or enzyme, that triggers a color reaction when it interacts with the target analyte. A spectrophotometer or direct human observation can effectively monitor color changes, providing both qualitative and quantitative data. The wide application of colorimetric sensors in food safety necessitates their ability to detect various contaminants, including pesticides, heavy metals, and microbial toxins, through the provision of speedy and cost-effective quality monitoring of



## BIOSENSORS

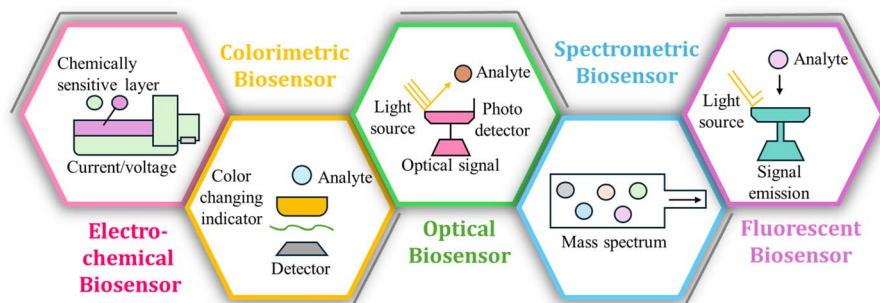


Fig. 1 Biosensor technologies employed in food toxins detection, categorized by their working principles and analytical signals.

food products. Comprehensive overview of biosensor technologies employed in food toxins detection, categorized by their working principles and analytical characteristics is given in Fig. 1 that systematically compares five major biosensor types: (1) electrochemical biosensors, utilizing electrical signals (potentiometry, amperometry, voltammetry) with nanomaterial-enhanced interfaces for real-time, sensitive detection; (2) fluorescent biosensors, leveraging light-emitting probes (FRET, time-resolved fluorescence) for exceptional sensitivity and selectivity; (3) colorimetric biosensors, enabling rapid visual analysis through quantitative/qualitative color changes; (4) spectrometric/chromatographic sensors (MS, IR, HPLC, GC), providing detailed chemical composition and structural data; and (5) optical biosensors (SPR, fluorescence-based), offering real-time, precise monitoring *via* photon-based detection. All platforms share core biosensor attributes, such as bi-recognition, specificity, and response, tailored for diverse food safety applications.

The following sections present biological and chemical toxins along with their respective sensing platforms.

### 3. Biological toxins

Biological toxins pose significant risks to both human and animal health.<sup>57</sup> As discussed *vide supra*, botulinum toxin and aflatoxins are among the most hazardous biological toxins. They are associated with severe health implications, with aflatoxins being linked to serious conditions like liver cancer.<sup>58,59</sup> Tetrodotoxin found in pufferfish cells is highly perilous, as even minuscule amounts can lead to paralysis and death. Biological toxins disrupt biological cell operations by targeting nerve cells, liver function, or renal function, resulting in moderate to severe health consequences.<sup>60</sup> Physical health security is fundamentally linked to the analysis of biological toxins, as their prompt identification enables timely interventions that can prevent outbreaks and ensure public safety. Continued research and development efforts have enabled researchers to devise improved methods for detecting and neutralizing these toxins, thereby ensuring the integrity of food supplies. Fig. 2 presents three primary categories of biological food toxins categorized hierarchically by their origins and representative examples. This

classification highlights the variety of biological toxins present, emphasizing the need for the development of effective sensing platforms to ensure food safety monitoring.

#### 3.1 Mycotoxins

Mycotoxins are harmful substances produced by molds, with “myco” signifying their fungal origin and “toxin” highlighting their toxic characteristics. These are among the most hazardous contaminants in food and animal feed, posing significant health risks to both humans and animals.<sup>55</sup> The contamination of meat with mycotoxins raises critical concerns regarding food safety. It is believed that such contamination leads to considerable economic losses, in addition to public health and food safety issues, although precise calculations of these impacts remain elusive. The term “mycotoxin” was first introduced in 1960 following the death of 100 000 turkeys in the UK due to feed contaminated with secondary metabolites from *Aspergillus flavus*.<sup>61</sup> Mycotoxicosis refers to a health condition resulting from exposure to mycotoxins.<sup>62</sup> These toxins are categorized based on their harmful effects, including nephrotoxins, immunotoxins, hepatotoxins, and neurotoxins. Additionally, they can be classified into four groups based on their cellular injury mechanisms, including allergens, teratogens, carcinogens, and mutagens. Chemically, mycotoxins are derived from amino acids and polypeptide derivatives. Humans can be exposed to these toxins primarily through the consumption of meat from animals that have ingested contaminated feed, as well as through spices that have been infected during the processing of these meats.<sup>63,64</sup> Mycotoxins are implicated in several clinical conditions in humans; for instance, fumonisin B1 has been linked to esophageal cancer in the Balkans, while ochratoxin is associated with endemic nephropathy. Currently, over 400 distinct mycotoxins have been identified.<sup>65,66</sup> A schematic representation illustrating the structures of mycotoxins, their toxic effects on the human body, and their sensor-based detection is provided in Fig. 3.

**3.1.1 Aflatoxins.** Aflatoxins (AFs) are toxic compounds that can trigger allergic reactions. These substances are derived from coumarin and feature a bifuran group linked to the coumarin core, along with either a pentanone or a lactone ring, which



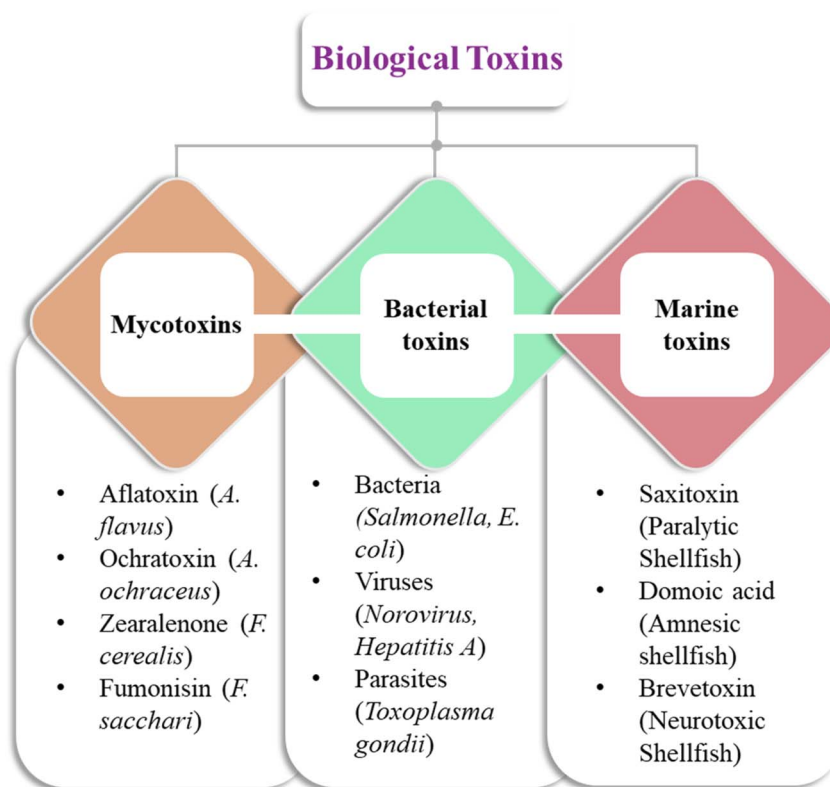


Fig. 2 Classification of major biological toxins demanding the implementation of effective prevention and control measures to safeguard food safety.

distinguishes between the AFB and AFG types.<sup>67</sup> Among the 20 identified aflatoxins, AFB1, AFB2, AFG1, and AFG2 are the most significant. The B-type aflatoxins are produced by *Aspergillus flavus*, while the G-type aflatoxins are generated by *Aspergillus parasiticus*. The biosynthesis of aflatoxins involves at least 25 genes that regulate enzyme production, encompassing 18 enzymatic steps in the process.<sup>68,69</sup> These toxins are commonly found in various food products and animal feeds, with research indicating that at least one aflatoxin was detected in 37.6% of the grain samples analyzed.<sup>70</sup> Research indicates that while rice is generally considered low-risk for AF contamination, some varieties of rice have been found to contain AFB1 and other mycotoxins. The ingestion of contaminated food and animal feed, coupled with the presence of residual aflatoxins, poses serious health risks. AFB1, in particular, is a potent carcinogen in humans and is associated with significant health issues.<sup>71</sup> Acute hepatitis and liver cancer are significantly related, and there are also intermittent acute AF outbreaks that have resulted in fatalities, as highlighted by reports from Kenya concerning lethal aflatoxicosis.<sup>72</sup> While liver cancer is not very common due to the liver's ability to detoxify aflatoxins, the metabolism of AFB1 results in the production of a reactive intermediate known as AFB1-*exo*-8,9-epoxide, facilitated by cytochrome P450 enzymes.<sup>73</sup> The detoxification process is aided by glutathione transferases, suggesting that an unidentified protective mechanism against liver cancer may be associated with the detoxification of AFB1-*exo*-8,9-epoxide. Additionally, AF

eruptions are primarily found in humid and subtropical regions, with a few instances occurring in temperate climates.<sup>73</sup> Climate change has altered the geographical distribution of traditional aflatoxins, making Mediterranean regions increasingly vulnerable to aflatoxin contamination. This vulnerability is driven by rising temperatures, increased CO<sub>2</sub> levels, and changing precipitation patterns, which collectively contribute to a global increase in crop contamination by fungi and aflatoxins.

Before harvest, AFs can significantly impact crops in the field, often in conjunction with drought conditions. The situation becomes even more concerning in storage, where conditions that promote mold growth can exacerbate the problem. Typically, the most critical factors influencing storage quality are the moisture content of the substrate and the relative humidity of the environment. The presence of AFs not only increases mortality rates in agricultural animals but also diminishes the value of grains used as animal feed. Additionally, dairy products can indirectly contain aflatoxins, as cows metabolize AFB1 from contaminated feed into hydroxylated AFM1.<sup>74</sup> Aflatoxins are toxic and carcinogenic to both humans and animals. Chronic exposure can lead to immunosuppression, cancer, and other serious health issues, while acute exposure may result in fatal outcomes.<sup>75</sup> AFB1 is particularly harmful, causing liver damage in affected animals, whose susceptibility varies widely. Research on aflatoxin toxicity has primarily focused on experimental animals or those with



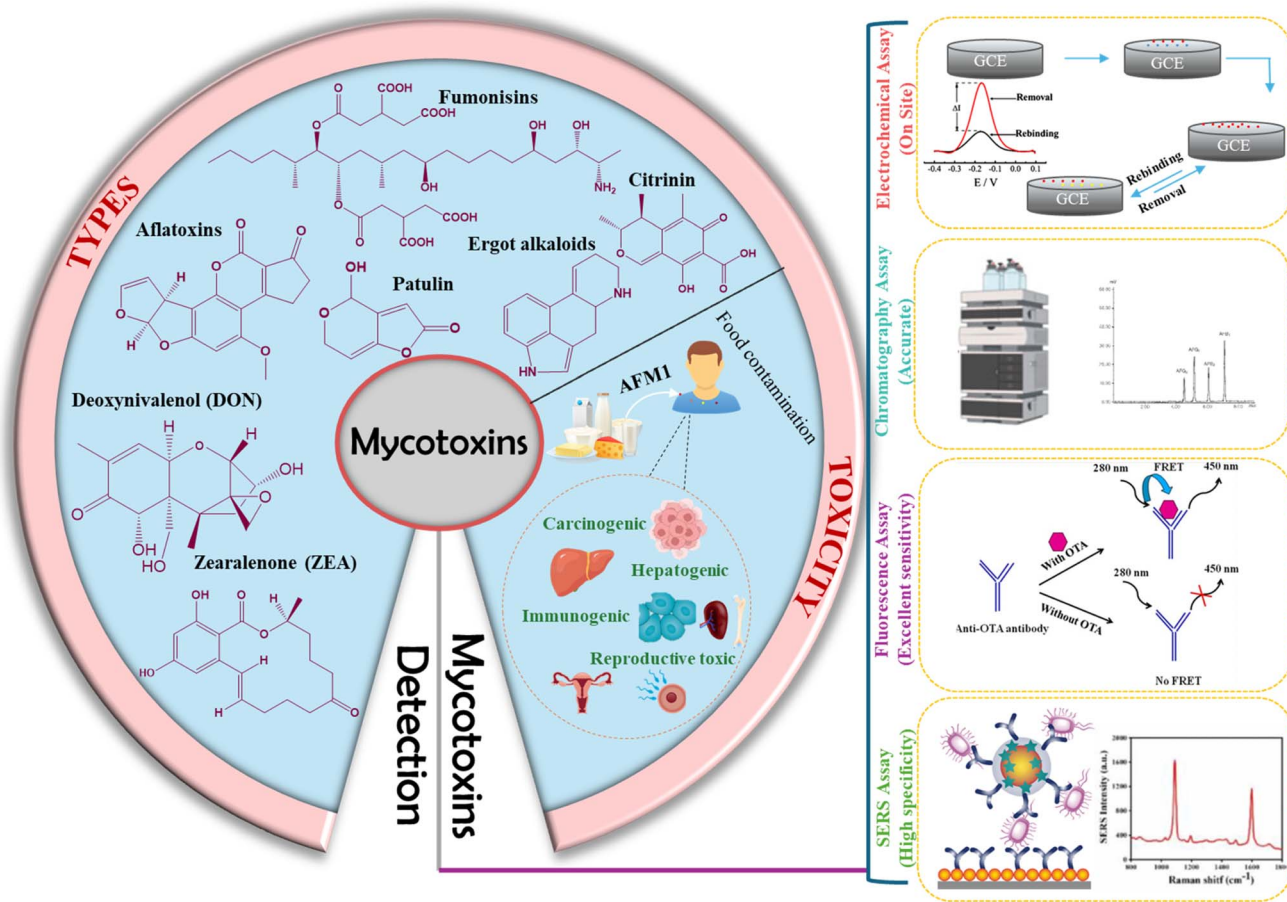


Fig. 3 Schematic representation of the structures of mycotoxins, their toxic effects on the human body, and the methods for their detection using sensor technology.

significant agricultural relevance. The detoxification of aflatoxins occurs in the cytosol and microsomes through a reactive glutathione S-transferase mechanism, which conjugates activated aflatoxins with reduced glutathione.<sup>76</sup> Differences in glutathione transferase and cytochrome P450 systems may influence the susceptibility to aflatoxins across species. Consequently, due to the variability in aflatoxin susceptibility among test species, concluding its effects on humans has proven challenging; however, instances of acute toxicity in humans remain uncommon.<sup>77</sup> Notably, a hepatitis outbreak in India in 1974, linked to aflatoxin-contaminated maize, resulted in the deaths of 100 individuals.<sup>78</sup> Interestingly, a woman who ingested at least 40 mg of pure aflatoxin in a suicide attempt has been reported alive even after more than a decade.<sup>79</sup> Initial fears that aflatoxin was responsible for Reye's syndrome, a neurological disorder affecting children and adolescents, have been disproven, yet aflatoxin remains a recognized toxin. In individuals with hepatitis B, dietary aflatoxin significantly increases the risk of developing primary hepatocellular carcinoma, and epidemiological studies have consistently associated dietary aflatoxin exposure with a heightened risk of liver cancer.<sup>74</sup> Evaluating an individual's lifetime exposure to aflatoxin is complex, and findings from such studies have often been inconsistent.

**3.1.1.1 Detection of AFs.** Aptasensors designed for the electrochemical detection of food toxins facilitate the swift, sensitive, and selective identification of toxins. These sensors utilize aptamers as biorecognition elements, providing high specificity and user-friendliness in complex food matrices. Nodoushan *et al.* developed an electrochemical aptasensor for the detection of AFB<sub>1</sub>, using a nanocomposite of graphene oxide and gold nanowires. The aptasensor detected AFB<sub>1</sub> through specific binding between the toxin and its aptamer, resulting in detachment from the electrode and a measurable decrease in the electrochemical signal *via* DPV. This reflects molecular recognition and disruption of electron transfer.<sup>75</sup> The aptasensor demonstrated a notable change in the peak current of differential pulse voltammetric signals when the aptamer was detached from the electrode surface in the presence of the toxin. It exhibited a linear detection range of 5.0 to 750.0 pM and achieved a limit of detection of 1.4 pM, along with commendable reproducibility. The aptasensor's specificity test showed that it detects AFB<sub>1</sub> over a blank solution and non-specific compounds. Wang *et al.* also designed a simple electrochemical aptasensor that efficiently detected AFB<sub>1</sub>. A gold electrode was modified with an anti-AFB<sub>1</sub> aptamer featuring a methylene blue (MB) redox tag at its 3'-end, in the absence of



AFB<sub>1</sub>, a complementary DNA (cDNA) strand bound to the aptamer, resulting in the MB moving away from the electrode surface and leading to a reduction in current. AFB<sub>1</sub> and cDNA then competed for the MB-tagged aptamer, resulting in the formation of a hairpin structure that drew the MB closer to the electrode, thereby increasing the current. This signal-on electrochemical aptasensor is capable of detecting AFB<sub>1</sub> across a dynamic concentration range from 2 nM to 4 μM. AFB<sub>1</sub> binds specifically to the methylene blue-labeled aptamer, displacing complementary DNA and inducing a hairpin loop that brings the redox tag close to the electrode, thereby enhancing electron transfer and enabling sensitive electrochemical detection.<sup>80</sup> Chen *et al.* introduced a self-calibrating single-probe method for ratiometric electrochemical aptasensors, achieving a detection limit for AFB<sub>1</sub> as low as 0.012 pg mL<sup>-1</sup> by utilizing an internal self-referencing signal. This aptasensor detects AFB<sub>1</sub> based on its selective binding to ferrocene-labeled aptamers, which causes the aptamer to detach from the electrode surface, resulting in a measurable decrease in redox current that enables highly sensitive, ratiometric electrochemical detection under varying pH and temperature conditions.<sup>81</sup>

A recent study introduced a novel electrochemical biosensor that utilizes a multifunctional composite material composed of MOF and MXene. This composite combines a molybdenum-based two-dimensional MOF with Ti<sub>3</sub>C<sub>2</sub> MXene and is applied to a screen-printed electrode (SPE). The article reported the detection of AFB<sub>1</sub> using an electrochemical biosensor, where anti-AFB<sub>1</sub> antibodies are covalently immobilized on an MOF/MXene-modified electrode. Antigen-antibody binding hinders electron transfer, as measured by increased charge transfer resistance in impedance spectroscopy. Remarkably, the sensor demonstrated a low LOD of 8 pg mL<sup>-1</sup>, effectively identifying AFB<sub>1</sub> concentrations between 0.06 and 50 ng mL<sup>-1</sup> using electrochemical impedance spectroscopy (EIS). Additionally, it showed strong performance in key quality metrics, including long-term stability, specificity against interfering substances, and both repeatability and reproducibility.<sup>82</sup> Similarly, Wood *et al.* also detected AFB<sub>1</sub> electrochemically, using a sensor made of molecularly imprinted polymer (MIP) incorporated into a stainless-steel hypodermic needle. The hypodermic needle sensor, constructed from stainless steel, was developed through a meticulous layer-by-layer film coating process that incorporated AFB<sub>1</sub>-imprinted polyaniline (PANI), cellulose nanocrystals (CNC), and MWCNTs biomimetic receptor films. The PANI@MIP/CNC-CNT hypodermic needle sensor demonstrated a remarkable electrochemical capacitance response (approximately 10 minutes) to AFB<sub>1</sub>, exhibiting a linear range of 0–25 nM and LOD of 3 nM. The sensor exhibited commendable reusability, capable of being utilized up to 7 times while maintaining an RSD of 2.8% in its capacitive response. The high current signal in the MIP-enabled stainless-steel hypodermic needle sensor arises from the synergistic effects of conductive MWCNTs, structurally supportive CNC, and redox-active PANI, MIP, which together facilitate rapid electron transfer, enhance electrochemical capacitance, and enable the selective binding of AFB<sub>1</sub>, thereby modulating the charge distribution and amplifying the sensing response.<sup>83</sup> Arzi *et al.* successfully

identified AFB<sub>1</sub> using modified SPCE/MWCNTs/CS.<sup>80</sup> In their electrochemical detection method, the signal was generated by the electrons produced during the reduction of TMB(ox) to TMB(red), facilitated by the HRP enzyme, while maintaining a consistent voltage between +0.2 and +0.3 V. The developed electrochemical immunosensor demonstrated a detection limit of 0.3 pg mL<sup>-1</sup> and a linear working range from 0.0001 to 10 μg L<sup>-1</sup>. The high current signal in this electrochemical immunosensor arises from the synergistic integration of MWCNTs and chitosan on the screen-printed carbon electrode, which enhances conductivity and surface area. At the same time, the enzyme-linked immunoassay mechanism, specifically the HRP-catalyzed redox conversion of TMB, produces a quantifiable electron flow that reflects the competitive binding between AFB<sub>1</sub> and its conjugate, enabling sensitive and specific detection through efficient electron transfer and catalytic amplification. Notably, this immunosensor was effectively utilized on real peanut samples without any pretreatment, and the analysis of spiked samples indicated a recovery rate of 80–127%.

A study focused on the development of a pencil graphite electrode enhanced with reduced graphene oxide (rGO) and gold nanoparticles (AuNPs) for detecting aflatoxin M<sub>1</sub> (AFM<sub>1</sub>) in milk samples. The findings revealed that several factors, including aptamer concentration, incubation time for AFM<sub>1</sub>, and duration of exposure, significantly influenced the sensor's effectiveness. The high current signal in this aptasensor originates from the synergistic enhancement of electron transfer by rGO and AuNPs, which increases conductivity and the electroactive surface area. At the same time, the specific binding of AFM<sub>1</sub> to thiol-modified aptamers immobilized on the electrode surface forms hydrogen bonding and π-π interactions that alter the charge transfer resistance, enabling sensitive and selective detection through EIS. When optimal conditions were met, the EIS technique demonstrated a linear concentration range of 0.5 to 800 ng L<sup>-1</sup>, with a detection limit of 0.3 ng L<sup>-1</sup>.<sup>84</sup> Additionally, a photoelectrochemical aptasensor was created using sensitized PDA@f-MWCNTs/TiO<sub>2</sub> to detect AFB<sub>1</sub> in real samples, including groundnuts and milk. The high current signal in this photoelectrochemical aptasensor arises from the synergistic integration of PDA@f-MWCNTs/TiO<sub>2</sub> nanotube arrays, which enhance visible-light absorption, electron mobility, and charge separation. At the same time, the specific binding of AFB<sub>1</sub> to NH<sub>2</sub>-functionalized aptamers *via* hydrogen bonding and π-π stacking creates a non-conductive complex that modulates electron transfer and photocurrent intensity through steric hindrance and diffusion limitation of the electron donor. This method exhibited a linear range of 0.005–50 ng mL<sup>-1</sup> and an impressive detection limit of 1 pg mL<sup>-1</sup>, showcasing remarkable sensitivity and selectivity for AFB<sub>1</sub> detection.<sup>85</sup> Another method for the rapid assessment of AFM<sub>1</sub> in milk and water has been developed, employing a solvent-free approach for signal evaluation. This technique involves the electrodeposition of two layers of PANI onto a GCE, which serves to encapsulate a DNA aptamer that specifically targets AFM<sub>1</sub>. Through the use of EIS and direct current voltammetry, a notable reduction in the intrinsic activity of PANI was observed upon exposure to the AFM<sub>1</sub> solution. The high current signal in this aptasensor stems from



the redox-active emeraldine form of PANI, which facilitates rapid electron transfer due to its conductive polymer matrix; upon binding of AFB<sub>1</sub> to the NH<sub>2</sub>-functionalized aptamer *via* hydrogen bonding and electrostatic interactions, the analyte induces conformational changes and partial charge shielding, modulating the redox behavior of PANI and enhancing sensitivity through altered electron transfer kinetics. The LOD varied based on the measurement technique, ranging from 1 to 5 ng L<sup>-1</sup> and 3 to 90 ng L<sup>-1</sup>.<sup>86</sup>

An electrochemical immunosensor for AFB<sub>1</sub> has been developed using a composite of graphene quantum dots (GQDs) and AuNPs. The carboxyl groups on the GQDs interact with the amino groups of a crosslinker, resulting in the formation of a GQD-AuNP conjugate. Following the application of this composite onto an indium tin oxide (ITO) electrode, AFB<sub>1</sub> antibodies were introduced. The high current response in this electrochemical immunosensor is attributed to the synergistic enhancement of electron transfer by GQDs and AuNPs, which increase conductivity, surface area, and catalytic activity. At the same time, the specific binding of AFB<sub>1</sub> to immobilized antibodies involves covalent amide bonding and thiol-gold interactions that modulate charge transfer resistance and facilitate sensitive detection through efficient electron tunneling and bio-nano conjugation. The sensor utilized hexacyanoferrate as the electrochemical probe, demonstrating effective performance across a concentration range of 0.1 to 3.0 ng mL<sup>-1</sup> of AFB<sub>1</sub>. This biosensor was subsequently employed to analyze maize samples that had been artificially contaminated. Furthermore, it is conceivable that this approach could be adapted for the

detection of other mycotoxins by utilizing specific antibodies for each toxin.<sup>87</sup> Additionally, Qian *et al.* developed a multi-functional aptasensor capable of dual-channel detection of AFB<sub>1</sub>, which exhibited a linear detection range of 5 to 200 ng mL<sup>-1</sup> and a detection limit of 35 pg mL<sup>-1</sup>. The signal intensification in this aptasensor originates from the catalytic role of AuNPs, which facilitate the deposition of AgNPs and amplify the electrochemical stripping signal through efficient electron transfer at the electrode interface. The sensing mechanism is driven by the specific binding affinity between the thiolated aptamer and AFB<sub>1</sub>, involving non-covalent interactions such as hydrogen bonding and  $\pi$ - $\pi$  stacking, while the Au-S bond between the aptamer and AuNPs ensures stable probe immobilization and effective signal transduction.<sup>88</sup>

A multi-scaled electrochemical biosensor was developed by integrating an aptamer, horseradish peroxidase, and carboxylated polystyrene nanospheres onto a carbon nanofiber/carbon felt platform. The three-dimensional porous structure of the carbon nanofiber and carbon felt, as shown in the FESEM micrographs in Fig. 4, provides an excellent substrate due to its high conductivity and efficient transport of reactants. Horseradish peroxidase and carboxylated polystyrene nanospheres served as signal amplification probes, facilitating the decomposition of H<sub>2</sub>O<sub>2</sub> and improving electrochemical responses. The biosensor employed DPV to detect AFB<sub>1</sub> in soy sauce and wine samples, achieving recovery rates ranging from 87.53% to 106.71%, with a limit of detection of 0.016 pg mL<sup>-1</sup>.<sup>89</sup> Wang *et al.* designed a competitive electrochemical aptamer-based technique to detect AFB<sub>1</sub>. A gold electrode was coated with the

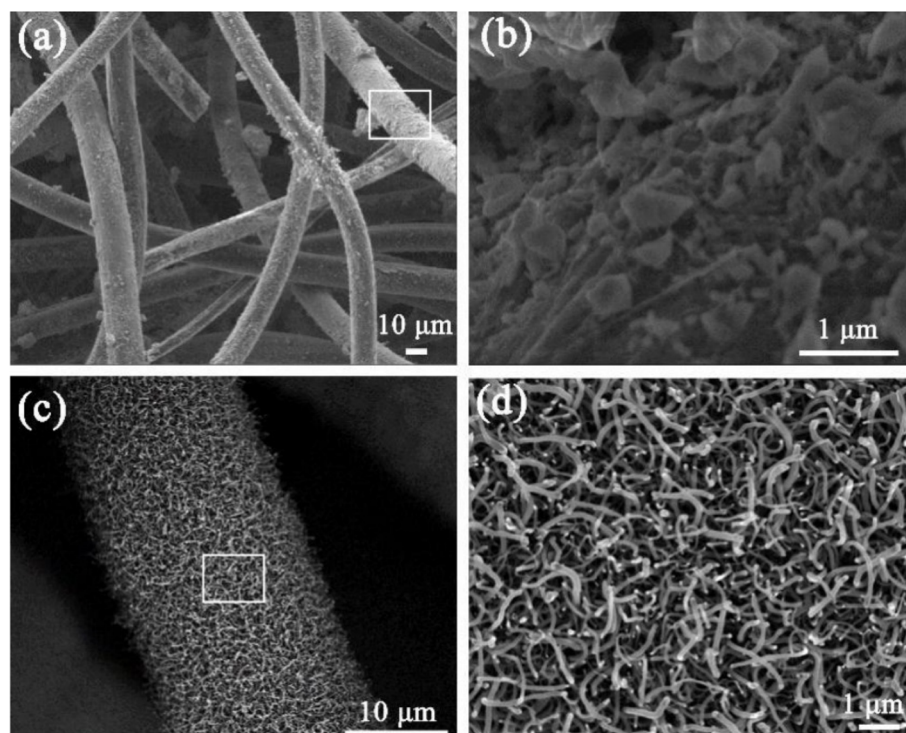


Fig. 4 FESEM micrographs of Ni-Cu oxalate-decorated CF (a and b) and SSE (c and d) at different scales. This figure has been adapted from ref. 89 with permission from MDPI, copyright 2022.



cDNA strand of an anti-AFB<sub>1</sub> aptamer and subjected to a sample solution containing an aptamer labeled with MB. The increase in signal intensity in this competitive electrochemical aptamer-based sensor arises from the proximity of MB to the gold electrode when the MB-labeled aptamer hybridizes with the immobilized cDNA, enabling efficient electron transfer. In the presence of AFB<sub>1</sub>, the aptamer preferentially binds AFB<sub>1</sub> through non-covalent interactions, such as hydrogen bonding and  $\pi$ - $\pi$  stacking, thereby preventing hybridization with cDNA and reducing the proximity of MB, which lowers the current signal and enables selective detection. Under carefully calibrated testing settings, the sensor's dynamic detection range was 2–500 nM, and it identified 2 nM AFB<sub>1</sub>.<sup>90</sup>

The biosensing strategies illustrated in Fig. 5 showcase advanced techniques for detecting aflatoxins in food, emphasizing high sensitivity, selectivity, and multiplexing capabilities. The electrochemical aptasensor (Fig. 5a) utilizes nanomaterials, including rGO, AuNPs, and MOFs, to enhance signal transduction for the detection of AFM<sub>1</sub> in milk. Optical methods, such as colorimetric (Fig. 5b) and fluorometric (Fig. 5c) biosensors, integrate aptamers, MIPs, and quantum dots (CdTe/ZnS) for interference-free and ultrasensitive AFB<sub>1</sub> detection. Further, Fig. 6 also illustrates aflatoxin detection, where Photoelectrochemical (PEC) sensors (Fig. 6a) exploit CuO-g-C<sub>3</sub>N<sub>4</sub> heterojunctions to boost photocurrent responses in molecularly imprinted polymer-based AFB<sub>1</sub> sensing, while ratiometric sensors (Fig. 6b) leverage thionine-graphene nanocomposites to improve accuracy in AFB<sub>1</sub> detection. Additionally, surface-enhanced Raman spectroscopy (SERS) aptasensors (Fig. 6c) enhance sensitivity through the use of UiO-66-NH<sub>2</sub>-modified magnetic beads, enabling the ultra-trace quantification of AFB<sub>1</sub>. Collectively, these approaches highlight the integration of nanomaterials, biorecognition elements, and innovative transduction mechanisms, paving the way for next-generation biosensors in food safety monitoring.

An electrochemical aptasensor was developed to simultaneously detect ochratoxin A (OTA) and AFB<sub>1</sub>. This sensor incorporated haemin and ferrocene within the HKUST-1 MOF, which consists of copper nodes and trimesic acid. The framework was further enhanced by integrating complementary DNA sequences specific to AFB<sub>1</sub> and OTA aptamers, resulting in the formation of Hemin@HKUST-1 and Ferrocene@HKUST-1. The improved current response in this duplexed electrochemical aptasensor arises from the synergistic conductivity of carbon nanodots decorated with AuNPs, which enhances electron transfer between the transducer and redox-labeled aptamer complexes. Upon the specific binding of aflatoxin B1 and ochratoxin A to their respective aptamers, non-covalent interactions, such as hydrogen bonding and  $\pi$ - $\pi$  stacking, displace the ferrocene@HKUST-1 and hemin@HKUST-1 bioconjugates, modulating the redox signal and enabling highly sensitive detection through DPV. DPV was used to measure the current response to the electroactive labels of ferrocene and hemin in the bioconjugates at two potentials simultaneously, in the absence of the two mycotoxins. The detection limits for OTA and AFB<sub>1</sub> mycotoxins were 4.3 and  $5.2 \times 10^{-3}$  ng mL<sup>-1</sup>, respectively, and ranged from  $1.0 \times 10^{-2}$  to 100 ng mL<sup>-1</sup>.<sup>96</sup>

Selvolini *et al.* developed an electrochemical enzyme-linked oligonucleotide array for the rapid detection of AFB<sub>1</sub> by employing a multi-detection assay within a competitive framework. The poly(aniline-anthranilic acid) copolymer (PANI-PAA) was first deposited onto graphite SPC using cyclic voltammetry (CV). AFB<sub>1</sub>-BSA was covalently attached to the PANI-PAA copolymer for immobilization. The resolution was implemented on modified SPCs after the affinity interaction between AFB<sub>1</sub> and apt-BIO. Streptavidin and alkaline phosphatase conjugates were attached to biotinylated complex sensors. The electroactive product derived from 1-naphthyl phosphate, the enzymatic substrate, was identified through DPV. Covalent bonding between the carboxyl groups of the copolymer and the amino groups of the AFB<sub>1</sub>-BSA conjugate ensures stable immobilization, while specific aptamer-AFB<sub>1</sub> interactions, primarily hydrogen bonding and  $\pi$ - $\pi$  stacking, trigger competitive displacement, modulating the enzymatic redox signal for precise detection. Within the range of 0.1 to 10 ng mL<sup>-1</sup>, a dose-response relationship was observed with a detection threshold of 0.086 ng mL<sup>-1</sup>.<sup>97</sup>

Lin *et al.* developed an electrochemical aptasensor for AFB<sub>1</sub> detection by employing layer-by-layer self-assembly. Positively charged poly(diallyl dimethylammonium chloride) nanosheets and negatively charged carboxylated polystyrene nanospheres were arranged in alternating layers on the electrode. Multi-layered sandwich electrodes featured numerous electrochemically active regions and exhibited good conductivity, with amide bonds formed between carboxyl-functionalized polystyrene nanospheres and AFB<sub>1</sub> aptamers. To increase selectivity, ethanolamine and bovine serum albumin were applied to the electrode. Nyquist plots showed that the sample AFB<sub>1</sub> concentration is substantially associated with electrode charge transfer resistance. Among the most successful mycotoxin detection technologies, the improved electrochemical aptasensor has a detection limit of 0.002 ng mL<sup>-1</sup> and stability over 30 days. The electrochemical aptasensor recovered 94.5–103.3% AFB<sub>1</sub> from soy sauce and oil.<sup>98</sup> Using aptamers and AuNPs on a conductive boron-doped diamond electrode, Feng *et al.* constructed an electrochemical aptasensor to detect AFB<sub>1</sub>. The high sensitivity in this boron-doped diamond (BDD)-based electrochemical aptasensor results from the synergistic conductivity of the BDD electrode and AuNPs, which enhance electron transfer and provide abundant active sites for aptamer immobilization *via* strong Au-S covalent bonding; upon specific binding of AFB<sub>1</sub> to the aptamer through hydrogen bonding and  $\pi$ - $\pi$  stacking, the resulting spatial conformation hinders redox probe access, modulating charge transfer resistance and enabling precise, concentration-dependent impedance shifts. With a linear relationship range of  $1.0 \times 10^{-13}$  to  $1.0 \times 10^{-8}$  mol L<sup>-1</sup>, the EIS analysis revealed that the aptasensor had a low detection limit of  $5.5 \times 10^{-14}$  mol L<sup>-1</sup>.<sup>99</sup> Additionally, Meng *et al.* demonstrated the synthesis of a platinum-coordinated titanium-based porphyrin MOF, specifically designed for the development of an aptamer sensor targeting AFB<sub>1</sub>. The high specific surface area of the MOF, coupled with the excellent electrochemical properties of platinum, significantly enhanced the sensor's performance. The modified AFB<sub>1</sub> aptamer sensor exhibited



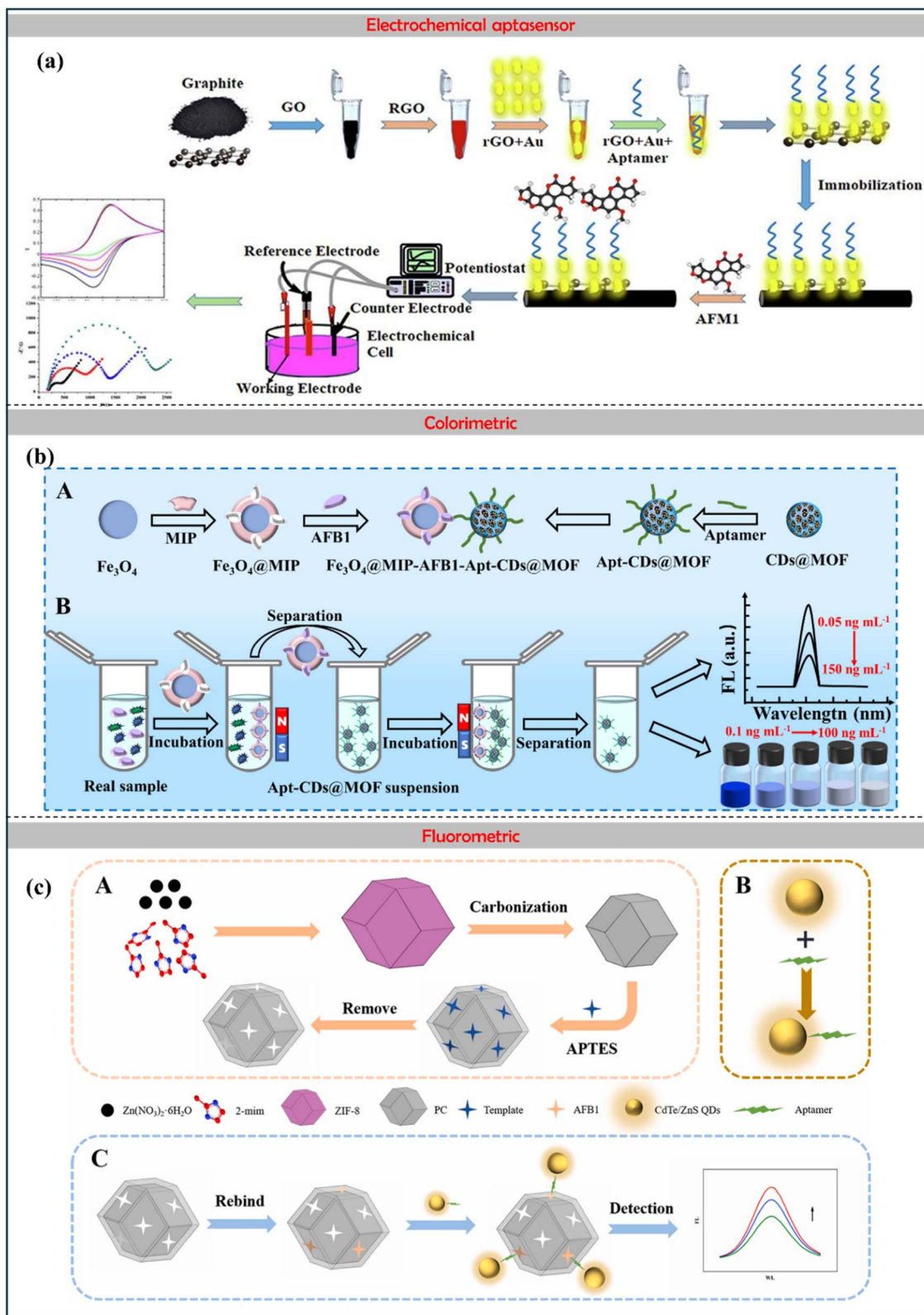


Fig. 5 Electrochemical aptasensor (a) monitoring of Aflatoxin M1 in milk using a novel electrochemical aptasensor based on reduced graphene oxide and gold nanoparticles, reproduced from ref. 84 with permission from Elsevier, copyright 2022. Colorimetric: (b) fluorescence/colorimetric sensor based on aptamers-molecular imprinted polymers synergistic recognition for ultrasensitive and interference-free detection of aflatoxin B<sub>1</sub>, reproduced from ref. 91 with permission from Elsevier, copyright 2025. Fluorometric: (c) schematic illustration of Preparation of the MIP/PC imprint layer (A); preparation of fluorescent CdTe/ZnS-Apt probe (B); and detection of AFB<sub>1</sub> by the sandwich biosensor (C), reproduced from ref. 92 with permission from Elsevier, copyright 2023.



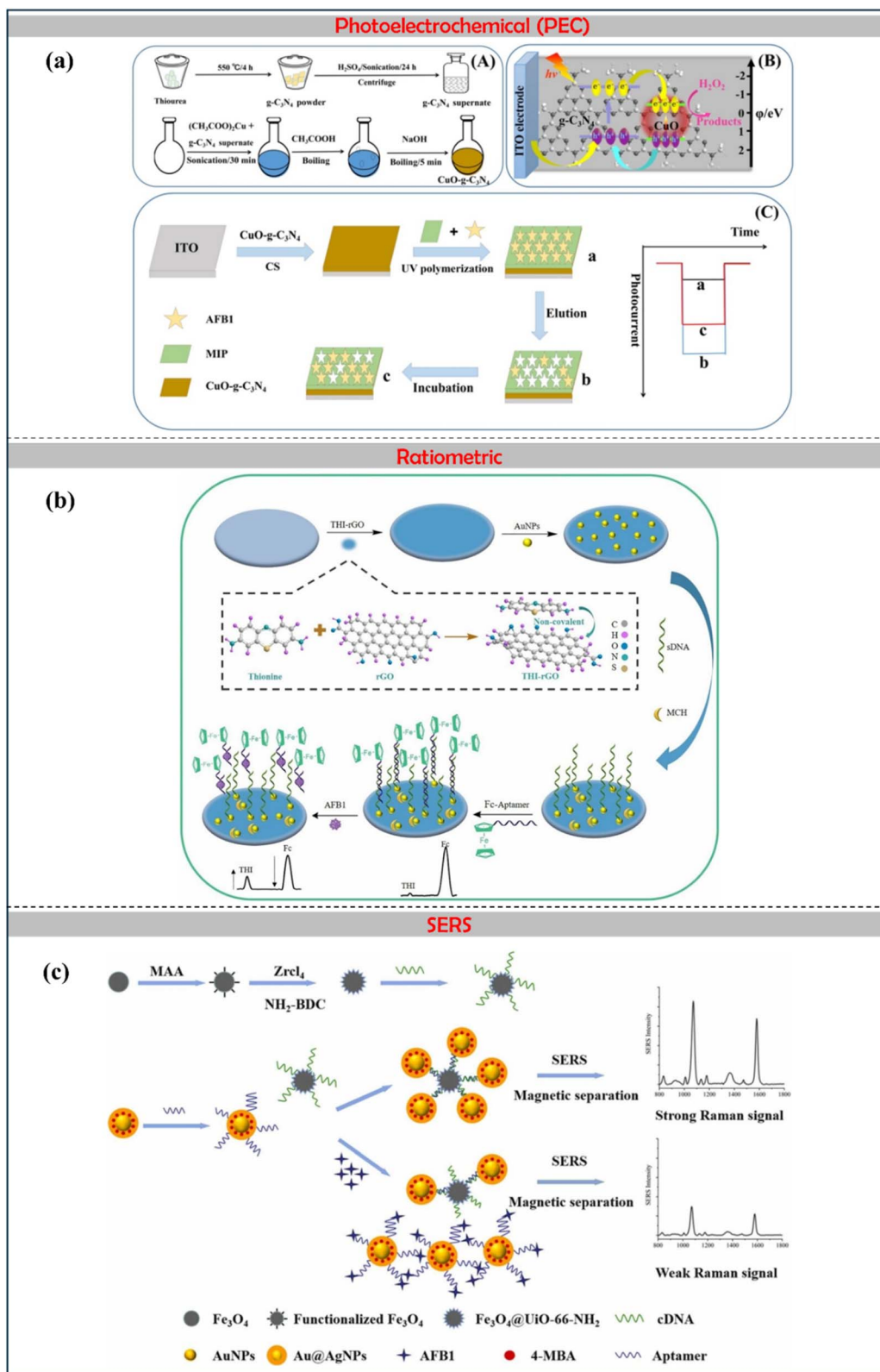


Fig. 6 Photoelectrochemical: (a) construction of CuO-g-C<sub>3</sub>N<sub>4</sub> heterojunction-based MIP-PEC sensors for ultrasensitive detection of aflatoxin B<sub>1</sub>, reproduced from ref. 93 with permission from Elsevier, copyright 2021. Ratiometric: (b) a sensitivity programmable ratiometric electrochemical aptasensor was fabricated based on thionine-graphene nanocomposite for the detection of AFB<sub>1</sub> in peanut, reproduced from ref. 94 with permission from Elsevier, copyright 2020. SERS: (c) development of an ultrasensitive SERS aptasensor for the determination of AFB<sub>1</sub> by modifying magnetic beads with UiO-66-NH<sub>2</sub> for enhanced signal probe capturing, reproduced from ref. 95 with permission from Elsevier, copyright 2023.



a linear detection range of 0.1 to 75  $\mu\text{g L}^{-1}$  and a detection limit of 31  $\text{ng L}^{-1}$ .<sup>100</sup>

Another study introduced a pistachio AF sensor with a confirmatory cross-validation. This sensor utilized a competitive assay integrated with a screen-printed carbon electrode (SPCE) and was assessed through electrochemical methods. The intense signal and improved sensitivity in this electrochemical immunosensor are attributed to the efficient electron transfer facilitated by the SPCE and the catalytic reduction of TMB by HRP-labeled antibodies. In contrast, the specific binding between aflatoxins and monoclonal antibodies, mediated through non-covalent interactions such as hydrogen bonding and hydrophobic forces, modulates the competitive immunoassay response, resulting in a quantifiable current proportional to the analyte concentration. It demonstrated a linear detection range of 0.01 to 2  $\mu\text{g L}^{-1}$  and exhibited excellent repeatability, with RSD of 2%. The detection limits were found to be 0.017  $\mu\text{g L}^{-1}$  in phosphate-buffered saline and 0.066  $\mu\text{g kg}^{-1}$  within the pistachio matrix, both significantly lower than the European regulatory threshold for total aflatoxins in pistachios.<sup>101</sup> Additionally, Gevared and coworkers reported a facile synthesis of AuNP-GQD nanocomposite, which was employed as an electrode modifier for the voltammetric measurement of AFB<sub>1</sub>. The oxidation of AFB<sub>1</sub> using this device resulted in an enhanced electrocatalytic effect, improving the voltammetric response and shifting the peak potential to more positive values. EIS revealed that the modified electrodes exhibited lower charge transfer resistance values. Under optimal conditions, a linear analytical curve was established, yielding detection and quantification limits of 0.47 and 1.5  $\text{nmol L}^{-1}$ , respectively.<sup>102</sup> Table 1 illustrates the various methods used to detect aflatoxins and their corresponding detection limits.

**3.1.2 Ergot alkaloids.** Mycotoxins known as ergot alkaloids (EAs), primarily produced by the *Claviceps* fungus, have been recognized as harmful since the 5th century AD. The term “ergot” is derived from the old French word “argot,” which means “cock’s spur.” Ergotism represents the earliest documented mycotoxicosis, leading to illness in both humans and animals through the ingestion of food or feed contaminated with these alkaloids.<sup>142,143</sup> The earliest recorded epidemic of ergotism, which resulted in the death of more than 10 000 individuals, occurred in France between 944 and 945 AD.<sup>79</sup> Ergotism was widespread in Eastern Russia, Germany, and France between the 9th and 14th centuries.<sup>144,145</sup> Three categories of entheogenic alkaloids—clavines, lysergic acid amides, and ergopeptines—are distinguished by their structural resemblance. Ergotamine and ergosine, the two most well-known ergot alkaloids produced by *Claviceps* species, utilize tetracyclic ergoline rings and are stable alkaloids that are relatively unaffected by heat. Conversely, heating can diminish the levels of ergocornine, ergocristine, ergokryptine, and ergometrine.<sup>146</sup> Alkaloids are categorized into ergopeptines and ergopeptinines, each possessing distinct biological and physicochemical features. The levorotatory isomers of EAs are referred to as ergopeptins, while the dextrorotatory isomers are known as ergopeptinines, with the highest and lowest biological activity found in ergopeptines. The conversion of ergopeptine is

accelerated in aqueous acidic or alkaline solutions. Various species, including *Claviceps purpurea*, *Claviceps fiformis*, *Claviceps africana*, *Epichloë*, and *Neotyphodium*, produce EAs, along with *Aspergillus*, *Penicillium*, and *Blansia*, all of which can significantly affect cereal production.<sup>147,148</sup>

*Sorghum bicolor* agriculture has experienced significant financial setbacks due to the adverse effects of *C. africana*, resulting in declines in seed quality and overall production. Additionally, challenges in harvesting and threshing processes, coupled with restrictions on international seed trade, have further exacerbated these losses.<sup>149</sup> Furthermore, in developing nations, the poisoning of individuals who ingest food infected with sclerotia (the dormant structures of the fungus) indicates that ergotism has not been eradicated and continues to pose a significant threat. In Ethiopia, 47 people died of ergotism in the spring of 1978 after eating barley contaminated with *C. purpurea* sclerotia.<sup>150</sup> Biogenic amine receptors can be bound by endogenous amines, which modify neurotransmission, and their biological effects can be correlated with those of pharmaceuticals due to their structural resemblance to neurotransmitters such as noradrenaline, dopamine, adrenaline, and serotonin.<sup>151</sup> Notwithstanding the laborious extraction of ergot bodies, the grains still contained ergot alkaloids. When grasses or cereals are harvested, *Sclerotia* can contaminate the feed and cereal-based food with EAs. *Sclerotia* are fragmented and blended with flour during cereal milling, rendering them challenging to detect. *C. purpurea* parasitises a minimum of 400 Poaceae species, with the most impacted being cereals such as barley, millet, oats, wheat, rye, and triticale, as well as various weedy grasses.<sup>152</sup>

The primary health concerns associated with EAs in humans and animals are mycotoxins that lead to convulsive and gangrenous ergotism. This condition, one of the earliest recognized diseases linked to mycotoxins, can manifest through symptoms such as hallucinations, convulsions, agalactia, burning sensations, vasoconstriction, and even the loss of limbs due to gangrene following the consumption of contaminated food. Nausea, endocrine dysfunction, vomiting, weakness, numbness, cardiovascular issues, and death are also noted. Ethiopians contracted gangrenous ergotism in 2001 after eating infected barley. Pigs, cattle, sheep, rabbits, and poultry all exhibited symptoms following an EA infection, which was costly for breeders and the meat industry.<sup>153</sup> Animals that consume grains affected with EA may develop a variety of diseases that affect any part of their bodies.<sup>79</sup> Detection of EAs using various methods is discussed in the subsequent section.

**3.1.2.1 Detection of EAs.** Huybrechts *et al.* developed a UHPLC-MS/MS method to comply with the new EU regulation that restricts ergot alkaloids in dry cereal-based infant foods to 20  $\text{ng g}^{-1}$ . This technique enabled the quantification of six specific ergot alkaloids, including ergocornine, ergocristine, ergometrine, ergosine, ergotamine, and  $\alpha$ -ergocryptine, with a detection limit of 0.5  $\text{ng g}^{-1}$ . The method employs enhanced QuEChERS extraction followed by UHPLC-MS/MS analysis, demonstrating high sensitivity, accuracy, and precision. In a study involving 49 samples from Belgium, 26 samples showed no presence of EAs, while 23 contained at least one type of





Table 1 Aflatoxin detection in a variety of food samples using different sensing platforms

S. No.	Method	Analyte	Electrode modifier	Linear range	LOD	Sample	Ref.
1	CV and EIS	AFB <sub>1</sub>	AP/Ti-MOFs-Pt/GCE	0.1–75 $\mu\text{g L}^{-1}$	31 $\text{ng L}^{-1}$	—	100
2	DPV	AFB <sub>1</sub>	—	0.5 nM–4 $\mu\text{M}$	0.07 nM	Cow milk	103
3	DPV	AFB <sub>1</sub>	GCE/RGO/MoS <sub>2</sub> /PANi@AuNPs/Apt/MCH	0.01–1.0 $\text{fg mL}^{-1}$	0.002 $\text{fg mL}^{-1}$	Wine	104
4	DPV	AFB <sub>1</sub>	APT/TDNs/3DOM MoS <sub>2</sub> -AuNPs	0.1 $\text{fg mL}^{-1}$ –0.1 $\mu\text{g mL}^{-1}$	0.01 $\text{fg mL}^{-1}$	Rice, wheat powder	105
5	DPV	AFB <sub>1</sub>	AFB <sub>1</sub> -BSA/PANI-PAA/GSPES	0.1–10 $\text{ng mL}^{-1}$	0.086 $\text{ng mL}^{-1}$	Maize flour	97
6	DPV	AFB <sub>2</sub>	SPCE/PAM/PA/PDA/Apt	0.0001–100 $\text{ng mL}^{-1}$	0.10 $\text{pg mL}^{-1}$	Corn	106
7	DPV	AFM <sub>1</sub>	Apt-modified SPGE	2–600 $\text{ng L}^{-1}$	0.9 $\text{ng L}^{-1}$	Milk and serum	107
8	EIS	AFB <sub>1</sub>	Apt-Fe <sub>3</sub> O <sub>4</sub> @Au/SPCE	0.020–50 $\text{ng mL}^{-1}$	15 $\text{pg mL}^{-1}$	Peanuts	108
9	EIS	AFM <sub>1</sub>	—	5–120 $\text{ng L}^{-1}$	0.5 $\text{ng L}^{-1}$	Milk	109
10	EIS	AFM <sub>1</sub>	Anti-AFM <sub>1</sub> /Fc/SINPs-PpPD/SPCE	10–500 fM	4.53 fM	Milk	110
11	EIS and DPV	AFB <sub>1</sub>	Fe-cDNA/p $\beta$ -CD/AuNPs/GC	0.0001–10 $\text{ng mL}^{-1}$ (EIS) 0.001–10 $\text{ng mL}^{-1}$ (DPV)	0.049 $\text{pg mL}^{-1}$ (EIS) 0.511 $\text{pg mL}^{-1}$ (DPV)	Peanut oil/94.5–106.7%	111
12	SWV	AFB <sub>1</sub>	MBS/CdTe-cDNA1/Apt-SiO <sub>2</sub> @Pbs	0.005–50 $\text{ng mL}^{-1}$	0.511 $\text{pg mL}^{-1}$	Peanuts	112
13	CV	AFB <sub>1</sub>	BSA/anti-AFB <sub>1</sub> /GQD-AuNPs/ITO	0.1–3.0 $\text{ng mL}^{-1}$	4.5 $\text{pg mL}^{-1}$	Maize	87
14	CV	AFB <sub>1</sub>	GO-PB-PTCNH <sub>2</sub> -AuNPs	0.01–100 $\text{ng mL}^{-1}$	0.008 $\text{ng mL}^{-1}$	Wheat	113
15	I-T	AFB <sub>1</sub>	—	1–20 $\text{ng mL}^{-1}$	0.13 $\text{ng mL}^{-1}$	—	114
16	ECL	AFM <sub>1</sub>	Apt-GMNP-GO-L-AgNPs	5–150 $\text{ng mL}^{-1}$	0.01 $\text{ng mL}^{-1}$	Milk	115
17	ECL	AFM <sub>1</sub>	H1/Au NPs/PTCA/GCE	0.0004–400 $\text{ng mL}^{-1}$	0.09 $\text{pg mL}^{-1}$	Milk	116
18	ECL	AFB <sub>1</sub>	Au-PEI@SiO <sub>2</sub> -AFB <sub>1</sub> -BSA	0.01–100 $\text{ng mL}^{-1}$	0.0039 $\text{ng mL}^{-1}$	Milk	117
19	ECL and EC	AFB <sub>1</sub>	—	0.0001–100 $\text{ng mL}^{-1}$ (ECL) 0.0001–100 $\text{ng mL}^{-1}$ (EC)	0.058 $\text{pg mL}^{-1}$ (ECL) 0.018 $\text{pg mL}^{-1}$ (EC)	Peanut	118
20	PEC	AFB <sub>1</sub>	ITO/Zn-SnS <sub>2</sub> /N-GQDs/(EDC/NH <sub>2</sub> )/ aptamer/DA	0.01–20 $\text{ng mL}^{-1}$	3 $\text{ng mL}^{-1}$	Milk	119
21	PEC	AFB <sub>1</sub>	AuNPs-labeled DNA aptamer/Ce- TiO <sub>2</sub> @MoSe <sub>2</sub> /ITO	0.03–200 $\text{ng mL}^{-1}$	10 $\text{pg mL}^{-1}$	Peanut	120
22	PEC	AFB <sub>1</sub>	Au/Ache/TiO <sub>2</sub> NTs	1–6 nM	0.33 nM	—	121
23	PEC	AFB <sub>1</sub>	AFB <sub>1</sub> /Aptamer/erGO/P5Fin/Au/ITO	0.01–100 $\text{ng mL}^{-1}$	2 $\text{pg mL}^{-1}$	Peanuts, wheat	122
24	EIS	AFB <sub>1</sub>	Ab-AFB <sub>1</sub> /BSA/AuNPs-PABA/RGO/GCE	0.01–1 $\text{ng mL}^{-1}$	0.001 $\text{ng mL}^{-1}$	Vegetable oil/unspiked	123
25	EIS	AFB <sub>1</sub>	Ab-AFB <sub>1</sub> /BSA/AuNPs-COOH-GO/GCE	0.05–25 $\text{ng mL}^{-1}$	0.05 $\text{ng mL}^{-1}$	Rice/99–101%	124
26	CV	AFB <sub>1</sub>	SA/Biotin Ab-AFB <sub>1</sub> /SPE	0.00005–5 $\text{ng mL}^{-1}$	50 $\text{fg mL}^{-1}$	Rice milk/unspiked	125
27	DPV	AFB <sub>1</sub>	BSA/Ab-AFB <sub>1</sub> /Mn <sub>2</sub> O <sub>3</sub> /ITO	1 $\text{pg mL}^{-1}$ –10 $\mu\text{g mL}^{-1}$	0.54 $\text{pg mL}^{-1}$	Sweet corn/96–99%	126
28	DPV (indirect HRP)	AFB <sub>1</sub>	Ab-AFB <sub>1</sub> /MWCNTs/Chi/SPCE	0.0001–10 $\text{ng mL}^{-1}$	0.3 $\text{pg mL}^{-1}$	Peanut/unspiked	127
29	CA (direct HRP)	AFM <sub>1</sub>	Ab-AFM <sub>1</sub> /SWCNTs/PET	0.01–1 $\text{ng mL}^{-1}$	0.02 $\text{ng mL}^{-1}$	Milk/unspiked	128
30	PEC	AFB <sub>1</sub>	CsPbBr <sub>3</sub> /TiO <sub>2</sub> /FTO	0.01–15 $\text{ng mL}^{-1}$	2.8 $\text{pg mL}^{-1}$	Peanut/90–104% corn/95–109%	129
31	PEC	AFB <sub>1</sub>	CdS/CoOOH/FTO	0.01–10 $\text{ng mL}^{-1}$	2.6 $\text{pg mL}^{-1}$	Peanut/unspiked	130
32	DPV	AFB <sub>1</sub>	Ab-AFB <sub>1</sub> /Fc/MWCNTs/Chi/SPCE	0.001–20000 $\text{ng mL}^{-1}$	0.159 $\text{pg mL}^{-1}$	Rice/94% Peanut/102% Corn/96%	131
33	EIS	AFM <sub>1</sub>	Apt/Fc/SINPs/PpPD/SPCE	3.3–165 $\text{fg mL}^{-1}$	1.48 $\text{fg mL}^{-1}$	Milk/unspiked	110
34	EIS	AFM <sub>1</sub>	BSA/Apt/PNPs/MIL-101(Fe)GCE	0.01–80.0 $\text{ng mL}^{-1}$	0.002 $\text{ng mL}^{-1}$	Milk/93–108%	132
35	EIS	AFB <sub>1</sub>	MCH/MCH-Apt/AuNPs/BDD	0.03–3122.8 $\text{pg mL}^{-1}$	0.017 $\text{pg mL}^{-1}$	Peanut/96–109%	99
36	EIS	AFB <sub>1</sub>	Apt/BSA/PS-COOH/PDDA-GN/GCE	0.001–0.1 $\text{ng mL}^{-1}$	0.002 $\text{ng mL}^{-1}$	Oil/98–103% Soy sauce/95–102%	98

Table 1 (Contd.)

S. No.	Method	Analyte	Electrode modifier	Linear range	LOD	Sample	Ref.
37	DPV (HRP)	AFB <sub>1</sub>	DNA-AuNPs-HRP/Apt/cDNA/AuNPs/GCE	0.001–200 ng mL <sup>-1</sup>	0.33 pg mL <sup>-1</sup>	Peanut & corn	133
38	LSV (Au@Ag)	AFB <sub>1</sub>	SPCE-CS-ccdDNA/cDNA-AuNPs	0.05–100 ng mL <sup>-1</sup>	0.43 pg mL <sup>-1</sup>	Corn/93–98%	88
39	ACV	AFB <sub>1</sub>	Fc-Apt/cDNA/AuNPs/THI-rGO/GCE	0.05–20 ng mL <sup>-1</sup>	0.016 ng mL <sup>-1</sup>	Peanut/87–112%	94
40	DPV (ALP)	AFB <sub>1</sub>	SA-ALP/Biotin-Apt/AFB <sub>1</sub> -BSA/AuNPs-PANI/GSPE	0.1–10 ng mL <sup>-1</sup>	0.086 ng mL <sup>-1</sup>	Corn & maize flour	97
41	EIS or DPV	AFB <sub>1</sub>	Apt/Cu <sub>2</sub> O-CQDs/GCE	3 ag mL <sup>-1</sup> –1.9 µg mL <sup>-1</sup>	0.9 ag mL <sup>-1</sup>	Wheat flour/97–104%	134
42	EIS	AFB <sub>1</sub>	Fc-apt/THI-rGO/GCE	0.01–100 ng mL <sup>-1</sup>	0.01 ng mL <sup>-1</sup>	Peanut/94–116%	135
43	LSV	AFB <sub>1</sub>	AuNPs-GQDs/SPE	0.03–15.6 ng mL <sup>-1</sup>	0.15 ng mL <sup>-1</sup>	Malted barley/76–190	102
44	EIS	AFB <sub>2</sub>	ZnO-NPs/CS/PPy/AFB <sub>2</sub>	0.1–1000 fg mL <sup>-1</sup>	0.2 Fg mL <sup>-1</sup>	Milk	136
45	DPV	AFB <sub>1</sub>	ZnO-NPs/CS/AFB <sub>2</sub>	0.01 ng mL <sup>-1</sup> –1 µg mL <sup>-1</sup>	0.6 fg mL <sup>-1</sup>	Maize/99–106%	93
46	PEC CV and EIS	AFB <sub>1</sub>	CuO-g-C <sub>3</sub> N <sub>4</sub> /MIP AP/Ti-MOFs-Pt/GCE	0.1–75 µg mL <sup>-1</sup>	6.8 pg mL <sup>-1</sup> 31 ng mL <sup>-1</sup>	Corn flour/96.05%	100
47	DPV	AFB <sub>1</sub>	BSA/Anti-AFB <sub>1</sub> /Mn <sub>2</sub> O <sub>3</sub> /ITO	1 pg mL <sup>-1</sup> –10 µg mL <sup>-1</sup>	0.54 pg mL <sup>-1</sup>	Rice/104.45%	126
48	DPV	AFB <sub>1</sub>	CCM@ZIF-8/PDA/IgG	0.5 pg mL <sup>-1</sup> –10 ng mL <sup>-1</sup>	0.11 pg mL <sup>-1</sup>	Sweet corn/98.6%	137
49	CV and EIS	AFM <sub>1</sub>	AuNPs/rGO/PGE/aptamer	0.5–800 ng mL <sup>-1</sup>	0.3 ng mL <sup>-1</sup>	Wheat/105.20%	84
50	DPV	AFB <sub>1</sub>	Aptamer/MCH/cDNA/PDA/MXene/ MWCNTs/NiCo <sub>2</sub> O <sub>4</sub> /SGPGE	2.5–200 ng mL <sup>-1</sup>	1.89 ng mL <sup>-1</sup>	Milk Maize flour/92.2%	138
51	EIS	AFB <sub>1</sub>	Anti-AFB <sub>1</sub> /NH <sub>2</sub> -Mo-MOF/Ti <sub>3</sub> C <sub>2</sub> modified SPE	0.06–50 ng mL <sup>-1</sup>	8 pg mL <sup>-1</sup>	Maize residue/109.8%	82
52	DPV	AFB <sub>1</sub>	PS-BSA-Apt-Au/SSE	0.1–10 pg mL <sup>-1</sup>	0.016 pg mL <sup>-1</sup>	Pistachio Wine/87.5%	89
53	EC	AFB <sub>1</sub>	Fc-aDNA/Fc-Apt/MCH/sDNA/AuNPs/GCE	0.1–10000 pg mL <sup>-1</sup>	0.012 pg mL <sup>-1</sup>	Soy sauce/106.7%	81
54	PEC	AFB <sub>1</sub>	PDA@f-MWCNTs/TiO <sub>2</sub> -NTs	0.005–50 ng mL <sup>-1</sup>	1 pg mL <sup>-1</sup>	Corn/96.7–102.9%	85
55	EC	AFB <sub>1</sub>	Apts/AuNPs-CNDs/GCE	0.01–100 ng mL <sup>-1</sup>	0.0052 ng mL <sup>-1</sup>	Groundnut and milk	96
56	CV	AFB <sub>1</sub>	AuNPs/Zn/Ni-ZIF-8-800@graphene	0.18–100 ng mL <sup>-1</sup>	0.18 ng mL <sup>-1</sup>	Corn flour/98.4–101.3%	139
57	LSPR	AFB <sub>1</sub>	AuNPs/Nb <sub>2</sub> CT <sub>x</sub> MXene	0–1000 nM	26.41 nM	Peanut oil	140
58	ELISA	AFB <sub>1</sub>	CdTe/ZnS-Apt/MIP/PC	0.01–20 ng mL <sup>-1</sup>	4.0 pg mL <sup>-1</sup>	—	92
59	FRET	AFM <sub>1</sub>	AFM <sub>1</sub> APT/AFB <sub>1</sub> APT/C1/C2/C3	0.01–200 ng mL <sup>-1</sup>	6.24 pg mL <sup>-1</sup>	(Peanut/98–102.3%) pure milk/98.4–105%) (peanut/99.4–103%) pure milk/98.9–102.5%)	141
		AFB <sub>1</sub>		0.01–150 ng mL <sup>-1</sup>	9.0 pg mL <sup>-1</sup>		



alkaloid, with two samples each having 12. Notably, ergometrine was the most frequently detected alkaloid, appearing in 16 of the 49 samples.<sup>154</sup> Another study utilizing MIP technology focused on the electro-polymerization of dopamine monomers on a GCE, guided by a methylergonovine maleate (MM) template. The improved responsiveness in this electrochemical sensor is attributed to the electrocatalytic activity of the poly-dopamine (PDA)-based MIP film, which enhances electron transfer between the GCE and MM by creating selective recognition cavities. These cavities facilitate specific rebinding through hydrogen bonding and electrostatic interactions between the functional groups of dopamine and MM, accelerating charge transfer and amplifying the electrochemical response. This sensor achieved a LOD of 0.016 nM and exhibited a linear detection range from 0.05 to 300 nM. It was successfully employed to detect MM in Methergin tablets and blood serum samples, demonstrating effective performance in practical applications with recovery rates ranging from 98.8% to 102.3%.<sup>155</sup>

Tajik *et al.* employed SPE in conjunction with a Fe<sub>2</sub>MoO<sub>6</sub> magnetic nanocomposite to create a sensing platform for the detection of cabergoline. The Fe<sub>2</sub>MoO<sub>6</sub> magnetic nanocomposite enhanced the efficiency of the recognition process. The modified electrode demonstrated significantly higher oxidation peak currents for cabergoline compared to traditional screen-printed electrodes. The improved performance of the Fe<sub>2</sub>MoO<sub>6</sub>-modified screen-printed electrode arise from the nanocomposite's high surface area and superior electrical conductivity, which facilitate rapid electron transfer and efficient electrocatalytic oxidation of cabergoline. The sensing mechanism is primarily diffusion-controlled, and the interaction between cabergoline and the modifier likely involves hydrogen bonding and electrostatic interactions between the analyte's amide and amine groups and the oxide surface, enhancing selectivity and signal amplification. A linear analytical response was established for cabergoline concentrations ranging from 0.08 to 300.0 μM, with a detection limit of 0.02 μM.<sup>152</sup> Additionally, another study highlighted the preliminary detection of cabergoline in aqueous solutions using a nanostructure-modified carbon paste electrode integrated with an ionic liquid. This approach employed a SiO<sub>2</sub>@Fe<sub>3</sub>O<sub>4</sub>/GO nanocomposite, designed explicitly as a bromide binder for 1-methyl-3-butylimidazolium. The signal intensification of this sensor is attributed to the synergistic conductivity of the SiO<sub>2</sub>@Fe<sub>3</sub>O<sub>4</sub>/GO nanocomposite and the ionic liquid binder, which enhances electron transfer and expands the electroactive surface area. Meanwhile, cabergoline undergoes electrocatalytic oxidation *via* diffusion-controlled mechanisms. The interaction between cabergoline and the modifier likely involves hydrogen bonding and electrostatic interactions between its amide and amine groups and the carboxyl-functionalized GO surface, facilitating selective recognition and amplified electrochemical response. The SiO<sub>2</sub>@Fe<sub>3</sub>O<sub>4</sub>/GO/CPILE exhibited a cabergoline oxidation peak at 500 mV, which is 200 mV lower than that observed on the conventional carbon paste electrode under similar conditions. Furthermore, the peak current at the SiO<sub>2</sub>@Fe<sub>3</sub>O<sub>4</sub>/GO/CPILE surface was found to be three times

greater than that of the CPE. The detection limit was determined to be 0.01 μM, with a linear response range established between 0.07 and 500.0 μM.<sup>156</sup>

A unique UHPLC-FLD method was used to quantify the six main EAs and their associated epimers in another investigation. The sample preparation involved solid-liquid extraction using acetonitrile and freeze-out cleanup. The high sensitivity of this UHPLC-FLD-based analytical method for ergot alkaloids is attributed to the efficient separation and detection capabilities of the ultra-high-performance liquid chromatography system, coupled with fluorescence detection, which enhances signal intensity through the selective excitation and emission of alkaloid molecules. While no direct electrochemical sensing is involved, the analyte-modifier interaction during sample preparation may include hydrogen bonding and π-π stacking between ergot alkaloid functional groups and matrix components, facilitating selective extraction and quantification. Before analysis, materials were sieved (1.9 × 20 mm) to remove alkaloid-containing sclerotia. However, 23 samples had ergot alkaloid concentrations over the detection limit; the range for the six alkaloids was 0.3 to 2530.1 μg kg<sup>-1</sup>.<sup>157</sup> Twelve EAs were carefully measured in 228 swine feed samples. Analytes were extracted using QuEChERS and Z-Sep + for cleanup. This method reduced the matrix impact, resulting in quantification limits of 2.1 to 21.7 μg kg<sup>-1</sup>. After quantification using UHPLC-MS/MS, 29 samples (12.7%) were found to be contaminated with EA. Interestingly, 65% of infected samples had several alkaloids. Only 6 of the 12 targeted EAs exceeded quantitative limits. The most prevalent alkaloid, ergometrine, had an EA value of 145.3 μg kg<sup>-1</sup>, whereas ergosinine had an EA level of 5.9 μg kg<sup>-1</sup>. The range of the total EA concentration was 5.9 to 158.7 μg kg<sup>-1</sup>.<sup>158</sup> Table 2 depicts the detection of various EAs.

**3.1.3 Fumonisin.** Many fungal species, particularly cereal pathogenic fungi such as *F. verticillioides* and *F. proliferatum*, produce secondary metabolites known as fumonisins. *Aspergillus niger* generates fumonisins in peanuts, maize, and grapes. Most cereals and grain products contain fumonisins, with maize being the most common.<sup>180,181</sup> Over 15 homologs of fumonisins have been identified, including types A, B, C, and P. Among these, fumonisin B<sub>1</sub> (FB<sub>1</sub>), along with its harmful counterparts FB<sub>2</sub> and FB<sub>3</sub>, is particularly concerning, as FB<sub>1</sub> often coexists with the other two forms.<sup>182</sup> FB<sub>1</sub>, FB<sub>2</sub>, and FB<sub>3</sub> are the most common food contaminants. Propane-1,2,3-tricarboxylic acid (TCA) and 2-amino-12,16-dimethyl-3,5,10,14,15-pentahydroxyleicosane combine to form FB<sub>1</sub>, a diester with C-14 and C-15 hydroxyl groups and TCA carboxyl groups. FB<sub>2</sub> and FB<sub>3</sub> are C-5 and C-10 dehydroxy FB<sub>1</sub>. *F. verticillioides*, *F. proliferatum*, and a few other species are primarily responsible for the majority of fumonisin production. Globally, Fusarium saprophytes are present in soil and plants. Fusarium infection is present in the rhizosphere and surrounding systems.<sup>79</sup> Infections in Zea mays are primarily caused by *Fusarium oxysporum*, *F. verticillioides* and *F. proliferatum*, which inflict damage on crops such as corn, carnation, chrysanthemum, and gladiolus throughout their production phase.<sup>183</sup> Fusarium is responsible for infections in orchids, affecting both pathogenic and non-pathogenic varieties.<sup>184</sup> Mutualists and





Table 2 Detection of EAs using different methods

Sr No.	Method	Analyte	Electrode modifier	Linear range	LOD	Sample	Ref.
1	Spectrofluorimetry	Bromocriptine mesylate	—	50–600 ng mL <sup>-1</sup>	14.57 ng mL <sup>-1</sup>	—	159
2	Spectrofluorimetry TLC	Cabergoline	—	50–450 ng mL <sup>-1</sup> 100–1500 ng band <sup>-1</sup>	14.44 ng mL <sup>-1</sup> 25.4 ng band <sup>-1</sup>	—	160
3	HPTLC	Cabergoline and its degradation products	—	0.05–2.0 ng band <sup>-1</sup>	—	Methacarbamol/99.8% Fluphenazine/99.7% Methergine tablet and blood serum	161
4	CV DPV EIS	Methylergonovine maleate	—	1–40 µg mL <sup>-1</sup> 0.05–300 nM	0.016 nM	—	155
5	DPV	Levodopa	2D Ni-MOF NSs/ILCPE	0.09–365.0 µM	0.03 µM	Cabergoline tablet Urine	162
6	CV DPV	Cabergoline and levodopa	GQDs/ZCBF/IL/CPE	0.07–500 µM	0.02 µM	Urine Serum	163
7	SWV	Lysergic acid diethylamide (LSD)	—	5.0–100 µmol L <sup>-1</sup>	0.5 µmol L <sup>-1</sup>	Cabergoline tablets Seized blotter paper samples	164
8	Amperometry	Ergometrine	—	6 nM–1.2 µM	3 nM	Rye flour	165
9	ELISA	Ergometrine	—	—	29.4 µg mL <sup>-1</sup>	Flour and milk	166
10	HPLC-FLD	Ergotamine	—	—	0.05 µg kg <sup>-1</sup> 0.15 µg kg <sup>-1</sup>	Rye-wheat bread and rye-wheat flour	167
11	DPV	Ergocristine	La <sub>2</sub> O <sub>3</sub> /Co <sub>3</sub> O <sub>4</sub> /SPE	0.1–100 µM	0.04 µM	Cabergoline tablets and urine	168
12	LC-FLD	Cabergoline	—	5–100 ng mL <sup>-1</sup>	14.9 µg kg <sup>-1</sup> 12.8 µg kg <sup>-1</sup>	Rye flour and bakery products	169
13	LC-ESI-MS/MS	Ergometrinine Ergosine	—	0.40–4.99 ng g <sup>-1</sup> and 0.45–12.17 ng g <sup>-1</sup> 0.53–9.72 ng g <sup>-1</sup> and 0.52–16.61 ng g <sup>-1</sup>	0.25 ng g <sup>-1</sup> 0.25 ng g <sup>-1</sup>	Swine and dairy feeds	170
14	UHPLC-MS/MS	Ergosinine	—	—	0.10 ng g <sup>-1</sup> 0.07 ng g <sup>-1</sup>	Cereal-based baby food	154
15	UHPLC-MS/MS	Ergocristine Ergocristinine Ergocornine	—	0.25–250 µg kg <sup>-1</sup>	0.0354 µg kg <sup>-1</sup> 0.225 µg kg <sup>-1</sup>	Hard red spring wheat	171
16	UHPLC-MS/MS	Ergocornine	—	1.5–100 µg kg <sup>-1</sup> 1.9–100 µg kg <sup>-1</sup> 0.5–100 µg kg <sup>-1</sup>	0.5 µg kg <sup>-1</sup> 0.6 µg kg <sup>-1</sup> 0.11 µg kg <sup>-1</sup> 0.12 µg kg <sup>-1</sup>	Oat-based products	172
17	LC-MS/MS	Ergokryptine	—	—	2.2 µg kg <sup>-1</sup>	Rye flour and wheat breadcrumbs	173
18	HPLC-FLD	Ergocristine Ergocristinine	—	—	2.6 µg kg <sup>-1</sup> 0.2 µg kg <sup>-1</sup> 0.3 µg kg <sup>-1</sup>	Compound feeds	174
19	LC-MS/MS	Ergotamine Ergotaminine Ergine	—	—	2.6 µg kg <sup>-1</sup> 0.2 µg kg <sup>-1</sup> 0.3 µg kg <sup>-1</sup>	Wheat-rye bread	175
20	UPLC-MS/MS	Ergometrine	—	8.39–200 µg kg <sup>-1</sup> and 9.12–200 µg kg <sup>-1</sup> 9.79–200 µg kg <sup>-1</sup> and 7.64–200 µg kg <sup>-1</sup>	2.54 µg kg <sup>-1</sup> and 2.77 µg kg <sup>-1</sup> 2.97 µg kg <sup>-1</sup> and 2.32 µg kg <sup>-1</sup>	Wheat and maize	176
21	TWIM-MS	Ergometrinine Ergometrine Ergometrinine	—	—	0.6 µg kg <sup>-1</sup> and 0.5 µg kg <sup>-1</sup> 0.3 µg kg <sup>-1</sup> and 0.2 µg kg <sup>-1</sup>	Barley and wheat	177



Table 2 (Contd.)

Sr No.	Method	Analyte	Electrode modifier	Linear range	LOD	Sample	Ref.
22	LC-MS/MS	Ergocornine	—	2.5–13.9 $\mu\text{g kg}^{-1}$	0.4 $\mu\text{g kg}^{-1}$	Cereal grains and its derivatives, wheat flour	178
23	UPLC-MS/MS	Ergocornine Ergosine	—	2.5–12.4 $\mu\text{g kg}^{-1}$	0.2 $\mu\text{g kg}^{-1}$ 0.04 $\mu\text{g kg}^{-1}$	Wheat, oat, rye, wheat gluten and baby food	179
24	LC-FLD	Ergocornine Ergocristine Ergocristinine Ergocryptine	—	5–100 $\text{ng mL}^{-1}$	4.7 $\mu\text{g kg}^{-1}$ 1.5 $\mu\text{g kg}^{-1}$ 0.25 $\text{ng g}^{-1}$	Rye flour and bakery products	169
25	LC-ESI-MS/MS	Ergocryptinine	—	0.63–17.22 $\text{ng g}^{-1}$ and 0.58–13.19 $\text{ng g}^{-1}$ 0.25–100.55 $\text{ng g}^{-1}$ and 0.44–31.57 $\text{ng g}^{-1}$	0.25 $\text{ng g}^{-1}$	Swine feed and dairy feed	170
26	UHPLC-MS/MS	Ergotamine Ergotaminine	—	0.25–250 $\mu\text{g kg}^{-1}$	0.0839 $\mu\text{g kg}^{-1}$ 0.0645 $\mu\text{g kg}^{-1}$	Hard red spring wheat	171
27	LC-MS/MS	Ergosine Ergosimine Ergometrine Ergometrinine	—	0.5–100 $\mu\text{g kg}^{-1}$	0.14 $\mu\text{g kg}^{-1}$	Rye flour and wheat breadcrumbe Barley and wheat	173
28	TWIM-MS	Ergosimine Ergometrine Ergometrinine	—	3.2–100 $\mu\text{g kg}^{-1}$ 0.2–100 $\mu\text{g kg}^{-1}$	1.0 $\mu\text{g kg}^{-1}$ 0.1 $\mu\text{g kg}^{-1}$	Barley and wheat	172

nonpathogenic decomposers enhance seed germination and pigmentation. In certain crops, there is a reduction in non-pathogenic *Fusarium* wilt. *Fusarium* species important to agriculture, such as *F. oxysporum* and *F. solani*, are commonly found in soils that inhibit wilting.<sup>185</sup> Before harvest, maize is susceptible to infection by *Fusarium* species, resulting in the production of fumonisins.<sup>186</sup> Inadequate storage conditions lead to the production of fumonisin after harvest. Fumonisin has detrimental effects on both agricultural and laboratory animals. Horse leukoencephalomalacia, pig pulmonary oedema, rat hepatotoxicity, and nephrotoxicity are consequences of exposure to these toxins.<sup>63</sup>

Climate influences the contamination of food with fumonisins, particularly affecting crops such as oats, millet, rye, barley, maize, rice, and wheat, which are among the most contaminated. Foods that include FB<sub>1</sub> include asparagus, garlic, barley, beers, dried figs, and milk. Most often, FB<sub>1</sub> is found in maize and maize derivatives. Maize is a versatile ingredient used in numerous products, such as tortillas, cornflakes, popcorn, grits, flour, and oils. Research indicates that the levels of fumonisins FB<sub>1</sub> and FB<sub>2</sub> significantly decreased by 59% in tortilla chips made from maize flour, 60% in flour, and 50% in grits and snacks when subjected to extrusion heating. However, contamination with fumonisins persists in other products such as cornflakes, black and herbal teas, corn, and Portuguese maize bread.<sup>187</sup> Endocrine disruptors harm young Nile tilapia. Fumonisin may have an impact on other aquatic creatures and plants, endangering food safety and security. They were found to alter the hepatic expression of the growth hormone receptor (GHR) and insulin-like growth factor 1 (IGF-1) in these species.<sup>188</sup> In humans and animals, mycotoxins can cause poisoning produced by the fungi *Fusarium anthophilum*, *Fusarium proliferatum*, *Fusarium verticillioides*, *Fusarium napiform*, *Fusarium oxysporum*, *Fusarium dlamini*, and *Fusarium nygamai*.<sup>63</sup> These toxins can be found in coffee, barley, sorghum, rice, and maize. Changes in the climate, such as dry periods followed by warm, rainy periods during flowering, can result in ear and kernel rot. Natural strains can reach the ear and kernels due to the insect's maturity damage. Rainfall before harvest could aggravate fumonisin infection in maize. Non-symptomatic maize kernels contain several fumonisins.<sup>189</sup> In US studies, 34% of maize samples and 53% of diets based on corn contained FB<sub>1</sub> and moniliformin.<sup>190</sup> A 2007–2010 Brazilian study revealed the presence of FB<sub>1</sub> and FB<sub>2</sub> in 82% and 51% of corn-based foods, respectively. South Korean chicken broilers and feed-fattening calves had FB<sub>1</sub> and FB<sub>2</sub> contamination.<sup>79</sup> This pollutant is found in roasted coffee beans, green coffee beans, buckwheat flour, rye, oats, and wine. A variety of methods are used for the detection of fumonisins in various analytes as discussed in the subsequent section.

**3.1.3.1 Detection of fumonisins.** Dhiman *et al.* developed an electrochemical microfluidic biosensing technology for the detection of FU-B1, utilizing a maskless lithography approach with a silver-ceria nanocomposite. Structural characterization confirmed the successful creation of impurity-free ceria (CeO<sub>2</sub>) nano-cubes and spherical silver structures. The sensing figures of merit of Ag–CeO<sub>2</sub> nanocomposite-based microfluidic

biosensor stem from rapid electron transfer facilitated by the synergistic conductivity of Ag nanoparticles and the redox-active surface of CeO<sub>2</sub> nanocubes, which enhances charge mobility at the transducer–analyte interface. Specific binding occurs *via* hydrogen bonding and electrostatic interactions between the functional groups of fumonisin-B1 and the nanocomposite surface, promoting selective and efficient electron exchange. The nano-biochip exhibited a linear response to the antigen FU-B<sub>1</sub>, with a detection range spanning from 10 pg mL<sup>-1</sup> to 100 ng mL<sup>-1</sup> and a sensitivity of 7.33 μA log(ng mL<sup>-1</sup>)<sup>-1</sup>cm<sup>-2</sup>. The limits for quantification and detection were determined to be 3.9 and 1.5 pg mL<sup>-1</sup>, respectively.<sup>191</sup> Munawar *et al.* introduced an electrochemical sensor for measuring FB<sub>1</sub> in maize samples, employing molecularly imprinted nanoparticles (nanoMIPs) as the recognition unit. The enhanced current arises from efficient electron transfer of the redox couple through the highly conductive PPy/ZnP underlayer and the analyte-modulated nanoMIP film *via* a gate-effect mechanism, where FB<sub>1</sub> binding triggers local polymer swelling and increased porosity at the Pt interface; FB<sub>1</sub> is selectively captured by hydrogen bonding and electrostatic interactions between its carboxylate/hydroxyl groups and the phosphate/amide functionalities of the EGMP and NAPMA monomers in the imprinted cavities. This nanoMIPs-based chemosensor demonstrated superior performance in terms of sensitivity, low detection limits, reproducibility, repeatability, and shelf life compared to previous research.<sup>192</sup> Another study used a single pot to synthesize AuNPs-doped 2D titanium carbide MXene nanoflakes (Ti<sub>3</sub>C<sub>2</sub>T<sub>x</sub>/Au). The synergistic signal amplification and superior electrical conductivity of Ti<sub>3</sub>C<sub>2</sub>T<sub>x</sub> MXene and AuNPs led to enhanced electrochemical performance. The Ti<sub>3</sub>C<sub>2</sub>T<sub>x</sub>/Au hybrid nanostructure is therefore an effective electrode platform for the electrochemical analysis of various targets. To identify and measure ampicillin (AMP) and FB<sub>1</sub>, SPE with the Ti<sub>3</sub>C<sub>2</sub>T<sub>x</sub>/Au configuration and biorecognition components was employed. The detection limits of 2.284 pM and 1.617 pg mL<sup>-1</sup> for AMP and FB<sub>1</sub>, respectively, are significantly lower than the US FDA's maximum residual limits of 2.8 nM in milk and 2 to 4 mg kg<sup>-1</sup> in maize products for human consumption. Furthermore, 10 pM to 500 nM and 10 pg mL<sup>-1</sup> to 1 μg mL<sup>-1</sup> were chosen as the linear ranges for AMP and FB<sub>1</sub> detection and quantification, respectively.<sup>193</sup>

Dong *et al.* developed a tetrahedral DNA nanostructure (TDN) electrochemical aptasensor that demonstrated a remarkable sevenfold dynamic range, enabling the detection of FB<sub>1</sub> at sub-femtogram per milliliter (fg mL<sup>-1</sup>) concentrations. The 5.67 nm TDN was specifically engineered to immobilize FB<sub>1</sub> aptamers effectively. This approach adjusted TDN assembly density to make the sensing interface assembly controllable and reliable. TDN anchored the aptamer at the electrode, whereas MB absorption generated the signal. To reduce free FB<sub>1</sub> and increase the sensing system's dynamic range, a helper aptamer was added to the sample solution, which negatively charged the TDN blocks and inhibited the absorption of the aptamer. The sensing performance can be related to the tetrahedral DNA scaffold precisely positioning methylene blue labels near the gold electrode to create a low-impedance, high-density redox

interface. At the same time, fumonisin B<sub>1</sub> binding to its aptamer *via* hydrogen bonds and π–π stacking triggers aptamer stripping (reducing steric and electrostatic blocking) and thus enables rapid electron transfer and amplified current. The linear dynamic range of the sensor was 0.500 to 1.00 ng mL<sup>-1</sup>, which was the lowest detection limit of any existing method.<sup>194</sup> Jin *et al.* used bipolar electrodes (BPEs) to analyze FB<sub>1</sub> on an array-based ECL platform visually. The sensor consists of a PDMS cover and a glass substrate with 10 ITO electrodes. A unique sensing interface on the BPE cathode modulates ECL reactions at the anode. The current intensification can be linked to the dense loading of reversible methylene-blue redox centers within porous Zr-MOFs grafted onto highly conductive Au-NP/ITO transducers, which drastically lowers interfacial impedance and boosts electron flux. At the same time, fumonisin B<sub>1</sub> binds its aptamer *via* hydrogen bonds and π–π stacking to trigger DNA-walker/nicking enzyme cycling that modulates MB@Zr-MOF release and amplifies the faradaic signal. The biosensor visibly quantifies FB<sub>1</sub> from 5 × 10<sup>-5</sup> to 0.5 ng mL<sup>-1</sup> utilizing the cyclic amplification activity of the DNA walker and nicking endonuclease. The biosensor detected FB<sub>1</sub> in samples of peanuts and corn. The BPE-ECL biosensor exhibits a recovery rate of 99.2% to 110.6%, indicating its high accuracy for FB<sub>1</sub> detection in foodstuffs.<sup>195</sup>

Zheng and coworkers developed a label-free DNA electrochemical aptasensor to detect FB<sub>1</sub> in maize. The electrochemical signal was enhanced, and the FB<sub>1</sub> identification probe was anchored using chemically modified AuNPs and GO. Using the π–π interaction between thionine and GO, thionine—a potent electrochemical indicator—was conjugated onto the surface of the GO–Au complex. The aptamer was functionalized onto gold particles *via* an Au–S link to improve FB<sub>1</sub> measurement specificity and reduce interference during real sample analysis. The proposed biosensor has a low detection limit of 10 pg mL<sup>-1</sup> and a linear range of 1 × 10<sup>-11</sup> to 1 × 10<sup>-4</sup> g mL<sup>-1</sup>. In real sample detection, it demonstrated commendable practicality and durability.<sup>196</sup> Yu *et al.* developed a disposable bipolar electrode (BPE)-electrochemiluminescence (ECL) device to detect FB<sub>1</sub>. MWCNTs and PDMS were used to produce BPE due to their higher electrical conductivity and mechanical rigidity. The synergistic conductivity of MWCNTs and AuNPs leads to enhanced electron transfer and a larger surface area at the cathode. Meanwhile, the specific binding of FB<sub>1</sub> to the thiolated aptamer involves hydrogen bonding and Ag–S covalent bonding, modulating oxygen reduction and amplifying the ECL signal at the anode through a dual-signal amplification mechanism. Au NPs on the BPE cathode increased the ECL signal by an 89-fold factor. An aptamer-based sensing technique was developed by grafting capture DNA onto the Au surface and hybridizing it with the aptamer. When tagged on an aptamer, Ag NPs catalyzed the oxygen reduction reaction, increasing the ECL signal at the BPE anode by 13.8-fold. Under ideal conditions, the biosensor detected FB<sub>1</sub> concentrations ranging from 0.10 pg mL<sup>-1</sup> to 10 ng mL<sup>-1</sup> linearly.<sup>197</sup> TDNs were employed to precisely bind an Apt in a paper-based electrochemical aptasensor, enhancing its target recognition capabilities. To immobilize complementary DNA–TDNs, AuNPs@MXenes,



a sensing substrate with excellent conductivity, were modified on the electrode. With the help of many Apt–Au@Pt nanocrystals built on the sensing interface and hybridized with cDNA, TMB was able to oxidize with H<sub>2</sub>O<sub>2</sub> and generate a significantly higher DPV signal in the absence of FB<sub>1</sub>. When the target FB<sub>1</sub> linked to its Apt, the electrochemical signal was reduced due to the release of Apt–Au@Pt NCs from double-stranded DNA (dsDNA). Under ideal circumstances, FB<sub>1</sub> triggered the strand displacement response, resulting in a lower detection limit (21 fg mL<sup>-1</sup>) and a more extensive dynamic linear range (50 fg mL<sup>-1</sup> to 100 ng mL<sup>-1</sup>) for the aptasensor.<sup>198</sup>

The detection of FB<sub>1</sub>, a hazardous mycotoxin prevalent in food commodities, has been significantly advanced through innovative biosensing technologies, as illustrated in Fig. 7. Electrochemiluminescence (ECL) biosensors (Fig. 7a) integrate Zr-based metal–organic frameworks and visual bipolar electrode arrays to achieve highly sensitive and spatially resolved FB<sub>1</sub> detection, combining the advantages of MOF-enhanced signal loading with ECL's low background noise. Enzyme-linked oligonucleotide assays (ELONA) (Fig. 7b) utilize aptamer complementary chains and carbon dot conjugates, offering a robust and improved method for FB<sub>1</sub> quantification by combining nucleic acid hybridization with enzymatic signal amplification. Förster resonance energy transfer (FRET)-based methods (Fig. 7c) employ aptamer-mediated fluorescence quenching, allowing precise FB<sub>1</sub> detection through distance-dependent energy transfer between fluorophores. Lastly, surface-enhanced Raman spectroscopy (SERS) platforms (Fig. 7d) utilize aptamer-modified silver-coated porous silicon (Ag-pSi) substrates to achieve ratiometric and reusable FB<sub>1</sub> detection, leveraging the plasmonic enhancement of Raman signals for ultrasensitive and multiplexed analysis. Together, these biosensing approaches highlight the integration of nanomaterials, biorecognition elements (such as antibodies and aptamers), and advanced transduction mechanisms (including electrochemical, optical, and spectrometric) to address the challenges of FB<sub>1</sub> detection in food safety, paving the way for portable, multiplexed, and real-time monitoring systems.

A light-driven biosensor designed for the detection of FB<sub>1</sub> features a hybrid nanoantenna sensing interface. This interface is formed by integrating graphdiyne oxide composites infused with methylene blue and gold nanorods (GDYO-MB-Au NRS) with cadmium selenide quantum dots and DNA nanowires. A TDN, which was both light-driven and amplified, enabled this incorporation. At the sensor interface, MB's chemical characteristics were changed and degraded by light-driven hybrid nanoantennas. Contact with FB<sub>1</sub> may remove the CdSe QDs-DNA nanowire, compromising light-driven activity and enhancing the electrochemical signal by blocking MB degradation. The hybrid nanoantenna was incorporated into the biosensor's design to photodegrade MB, thereby reducing the background signal and improving detection sensitivity. The increase in peak current in this light-driven electrochemical biosensor is attributed to the enhanced electron transfer facilitated by the hybrid nanoantenna, where GDYO-MB-Au NRS amplify conductivity and surface reactivity. At the same time,

CdSe quantum dots–DNA nanowires modulate the photo-degradation of MB. Specific binding of FB<sub>1</sub> to the DNA tetrahedral structure involves hydrogen bonding and  $\pi$ – $\pi$  stacking, which disrupts MB degradation and boosts the electrochemical signal. The produced biosensor attained a linear detection range of 0.5 to 10 pg mL<sup>-1</sup> and a detection limit of 0.45 fg.<sup>202</sup> By electrodepositing AuNPs on chitosan-functionalized nitrogen-doped graphene and polyaniline (N-G@PANI@CS) electrodes, Yang *et al.* developed an electrochemical immunosensor for detecting mycotoxin FB<sub>1</sub> in food. The conductivity and high electroactive surface area of the AuNPs/N-G@PANI@CS composite significantly lower charge-transfer resistance and accelerate electron flow; antibodies are covalently tethered to AuNPs *via* Au–S bonds, and FB<sub>1</sub> binds its antibody through non-covalent hydrogen bonding and electrostatic/hydrophobic interactions, forming immunocomplexes that modulate the redox probe signal. Under ideal conditions, the immunosensor exhibits a linear response from 0.50 to 800.00 ng mL<sup>-1</sup>, with a limit of detection (LOD) of 0.07 ng mL<sup>-1</sup> and a limit of quantification (LOQ) of 0.22 ng mL<sup>-1</sup>. The designed electrochemical immunosensor had 3.26% to 4.73% RSD in real corn samples. The recovery rate ranged from 93.97% to 98.62%, indicating its suitability for FB<sub>1</sub> detection in corn samples. Sensor stability and specificity were also impressive.<sup>203</sup> Table 3 enlists a variety of detection methods and electrode modifiers for Fumonisin, along with their detection limits.

**3.1.4 Trichothecenes.** Fusarium fungi produce sesquiterpenoid mycotoxins known as trichothecenes (T-2 toxin and HT-2 toxin).<sup>221</sup> These toxins can contaminate agricultural products, threatening food safety and public health. Toxicogenic organisms produce TCT because of genetic and environmental factors. In developing countries, fungal proliferation and mycotoxin production are significantly influenced by monsoons, unseasonal rainfall during harvest, flash floods, and temperature as well as moisture level.<sup>222</sup> According to research, crops grown in tropical and subtropical regions are more susceptible to mycotoxin contamination, including TCT, than those grown in temperate areas because these regions provide optimal conditions for toxin production.<sup>223</sup> Due to weather and environmental factors, TCT contamination of feeds and food varies geographically and temporally across continents, regions, and climatic zones. Various crop varieties, agricultural practices, post-harvest storage methods, processing techniques, soil types, and management practices contribute to local variations. Evaluation of co-exposure to diverse TCTs is crucial for risk characterization, as animals and people consume varied diets.<sup>224</sup> Mycotoxin exposure is a severe health concern and productivity constraint for animals, especially monogastric species. Subclinical consequences, including degradation of intestinal integrity and changes in gut flora, are concerning due to their low prevalence. The assessment and management of fungal metabolite hazards to human and animal health have improved as a result of European monitoring procedures for major mycotoxins in food and feed, including TCT.<sup>225</sup> Trichothecenes are a large family of toxic sesquiterpenoids. Trichothecenes of types A and B are widespread and harmful.<sup>226</sup>



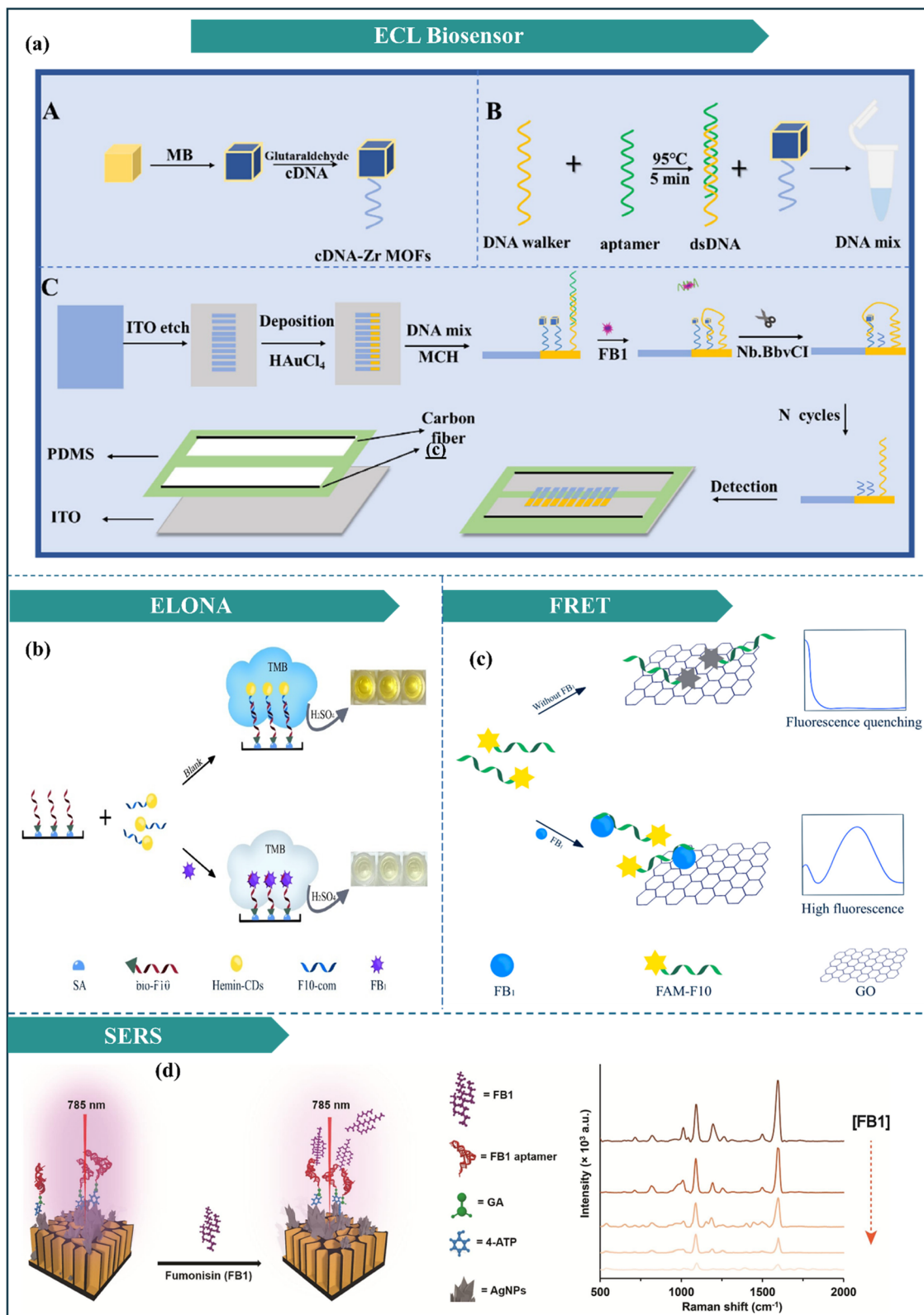


**Fig. 7** ECL Biosensor: (a) Schematic diagram of (A) the preparation process of cDNA-Zr MOFs, (B) synthesis process of DNA mix, and (C) visual bipolar electrode-ECL array electrode for FB<sub>1</sub> detection, reproduced from ref. 195 with permission from MDPI, copyright 2023. Enzyme-linked oligonucleotide assay (ELONA): (b) schematic diagram of the ELONA method based on aptamer complementary chains and CDs conjugates, reproduced from ref. 199 with permission from MDPI, copyright 2022. FRET: (c) schematic diagram of the FRET method for detecting FB<sub>1</sub> based on the aptamer, reproduced from ref. 200 with permission from MDPI, copyright 2022. SERS: (d) schematic representations of FB<sub>1</sub> (target analyte) capturing and detection using aptamer modified Ag-pSi SERS scaffold, reproduced from ref. 201 with permission from Elsevier, copyright 2025.





Table 3 Methods of fumonisins detection and their analytical parameters

S. No.	Method	Analyte	Electrode modifier	Linear range	LOD	Samples/recovery	Ref.
1	DPV EIS	FB <sub>1</sub>	Pt/(PPy/ZnP)/nanoMIPs	1 fM–10 pM	0.03 fM & 0.7 fM	Maize/96–102%	192
2	DPV EIS	FB <sub>1</sub>	Exo-I/Apt/cDNA/AuE	0.001–1000 ng mL <sup>-1</sup>	0.15 pg mL <sup>-1</sup>	Beer/upto 98.6% Corn/upto 106.8%	204
3	EIS	FB <sub>1</sub>	FB <sub>1</sub> /DNA/PGE	2.5–10 µg mL <sup>-1</sup>	3.69 ng mL <sup>-1</sup>	—	205
4	EC	FB <sub>1</sub>	—	10 pg mL <sup>-1</sup> –100 ng mL <sup>-1</sup>	1.5 pg mL <sup>-1</sup>	Corn/85%	191
5	DPV	FB <sub>1</sub>	AuNPs-SE	1 ng L <sup>-1</sup> –1 mg L <sup>-1</sup>	0.08 ng L <sup>-1</sup>	Pork and beef/89.7–113.3%	206
6	DPV	FB <sub>1</sub>	Apt <sub>2</sub> -AuNRs-Fc/ Apt <sub>1</sub> -AuNRs-Th/cDNA/AuE	1 pg mL <sup>-1</sup> –100 ng mL <sup>-1</sup>	0.26 pg mL <sup>-1</sup>	Beer/89–102%	207
7	CV	FB <sub>1</sub>	—	50–400 µg L <sup>-1</sup>	84.17 µg L <sup>-1</sup>	Maize-based and baby foods	208
8	CV	FB <sub>1</sub>	ss-HSDNA/AuNPs/SPCE	0.5–500 ng mL <sup>-1</sup>	0.14 ng mL <sup>-1</sup>	Maize	209
9	ECL	FB <sub>1</sub>	FB <sub>1</sub> /DNA mix/Au NPs/ITO BPE	5 × 10 <sup>-5</sup> –0.5 ng mL <sup>-1</sup>	0.67 pM	Maize/99.6–104.1% Peanut/99.2–110.6%	195
10	CV	FB <sub>1</sub>	GCE/Au-GO-Th/DNAA/FB <sub>1</sub>	1 × 10 <sup>-11</sup> –1 × 10 <sup>-4</sup> g mL <sup>-1</sup>	10 pg mL <sup>-1</sup>	Corn	210
11	EC	FB <sub>1</sub>	Apt/MB/MCH/TDN/Au	0.500 fg mL <sup>-1</sup> –1.00 ng mL <sup>-1</sup>	0.306 fg mL <sup>-1</sup>	Rice/97.9–108%	192
12	EC	FB <sub>1</sub>	Ti <sub>3</sub> C <sub>2</sub> T <sub>x</sub> /Au/l-Cys/anti-FB <sub>1</sub>	10 pg mL <sup>-1</sup> –1 µg mL <sup>-1</sup>	1.617 pg mL <sup>-1</sup>	Corn/102.9–103.8% Wheat/100.3–107.2%	193
13	EC	FB <sub>1</sub>	Silver/FB <sub>1</sub> /Au-aptamer/ Fe <sub>3</sub> O <sub>4</sub> -capture DNA/GCE	10 <sup>-3</sup> –10 ng mL <sup>-1</sup>	—	Corn/109–103.8%	211
14	EC	FB <sub>1</sub>	BSA/ab-FB <sub>1</sub> /GOMn <sub>3</sub> O <sub>4</sub> /ITO	1 pg mL <sup>-1</sup> –800 ng mL <sup>-1</sup>	0.195 pg mL <sup>-1</sup>	Sweet corn/98.91%	212
15	PEC	FB <sub>1</sub>	MIP/GO/Cds/CS/ITO	0.01–1000 ng mL <sup>-1</sup>	4.7 pg mL <sup>-1</sup>	Maize/94.03–102.97% Milk/94.61–105.81%	213
16	EC	FB <sub>1</sub>	—	10 pg mL <sup>-1</sup> –100 ng mL <sup>-1</sup>	—	Corn/85%	214
17	CV EIS	FB <sub>1</sub>	Anti-FB <sub>1</sub> /AuNPs/ N-G@PANI@CS/GCE	0.50 ng mL <sup>-1</sup> –800 ng mL <sup>-1</sup>	0.07 ng mL <sup>-1</sup>	Corn/93.97–98.62%	203
18	DPV	FB <sub>1</sub>	—	50 fg mL <sup>-1</sup> –100 ng mL <sup>-1</sup>	21 fg mL <sup>-1</sup>	Corn and wheat	198
19	CV	FB <sub>1</sub>	—	0.3–140 ppb	97 pg mL <sup>-1</sup>	Ground corn/88.6–95.8%	215
20	LC-MS/MS	FB <sub>1</sub>	cDNA-AuNR/ptamer-Cy5.5	10–250/500 pg mL <sup>-1</sup>	3/5 pg mL <sup>-1</sup>	Corn/92–107%	216
21	Ratiometric EC	FB <sub>1</sub>	FB <sub>1</sub> /TDN/MCH/cDNA/AuE	0.1–100 pg mL <sup>-1</sup>	0.087 pg mL <sup>-1</sup>	Rice powder/97.8–102%	217
22	DPV	FB <sub>1</sub>	MIP-F/ITO/PANI	1 pg mL <sup>-1</sup> –500 ng mL <sup>-1</sup>	0.322 pg mL <sup>-1</sup>	Corn/86.16–102.41%	218
23	EC	FB <sub>1</sub>	GCE/GDYO-MB-Au NRs/CdSe QDs	0.5 fg mL <sup>-1</sup> –10 pg mL <sup>-1</sup>	0.45 fg mL <sup>-1</sup>	Rice/95.4–97.6% Glutinous rice/96–100%	202
24	SERS	FB <sub>1</sub>	α-FB <sub>1</sub> /4-ATP/Ag-psi surface	0.1–1000 ppb	0.05 ppb	Maize/97.6–106.4% Onton/93.4–109.8% Wheat/93.3–107.4%	201
25	FRET	FB <sub>1</sub>	FAM-F10/GO/FB <sub>1</sub>	0–3000 ng mL <sup>-1</sup>	14.42 ng mL <sup>-1</sup>	Defatted milk/98.1–113.6%	200
26	ELONA	FB <sub>1</sub>	F10-com-hemin-CDS	0–100 ng mL <sup>-1</sup>	4.30 ng mL <sup>-1</sup>	Corn/89.13–102.08%	199
27	Fluorometry	FB <sub>1</sub>	—	0.01–100 ng L <sup>-1</sup>	0.003 ng L <sup>-1</sup>	Corn/97.5–99.23%	219
28	PEC	FB <sub>1</sub>	Apt/MnFe <sub>2</sub> O <sub>4</sub> /MCH/sDNA/ Cu <sub>2</sub> Co <sub>0.54</sub> (HITP) <sub>2</sub> /GCE	0.1 pg mL <sup>-1</sup> –10 ng mL <sup>-1</sup>	65 fg mL <sup>-1</sup>	Corn/106.6% Corn/96.4–103% Flour/98.7–108% Corn/104.8–112.8%	220
29	ECL	FB <sub>1</sub>	FB <sub>1</sub> /Ag NPs/ptamer/ MCH/capture DNA/Au	0.10 pg mL <sup>-1</sup> –10 ng mL <sup>-1</sup>	—	Peanut/90.9–112.1%	197

**3.1.4.1 Detection of TCT.** Solis *et al.* developed a competitive immunoassay for detecting T-2 toxin by utilizing monoclonal *anti*-T-2 antibodies within a PMMA microfluidic central channel.<sup>224</sup> At the end of the channel, a platinum wire working electrode was enhanced through a one-step electrodeposition technique that incorporated rGO-nanoporous gold. In this setup, the T-2 toxin present in the sample competed with a T-2-horseradish peroxidase conjugate for binding sites on the immobilized *anti*-T-2 monoclonal antibodies. When exposed to H<sub>2</sub>O<sub>2</sub>, HRP oxidizes 4-*tert*-butylcatechol (4-TBC) and reduces it electrochemically at  $-0.15$  V on the nanostructured electrode. Thus, with lower T-2 concentrations, more enzymatically conjugated T-2 should adhere to the capture antibodies, thereby increasing the current. Electron transfer is accelerated by the 3D graphene-decorated nanoporous gold film, whose enormous electroactive surface area and superior conductivity dramatically lower the charge-transfer resistance and amplify the HRP-H<sub>2</sub>O<sub>2</sub>-4-*tert*-butylcatechol quinone redox current in the competitive immunoassay. Antibodies are covalently tethered *via* PEI/glutaraldehyde and Au-S anchoring, while T-2 toxin binds its specific antibody through noncovalent hydrogen bonds, electrostatic, and hydrophobic interactions. The commercial ELISA method and the electrochemical immunosensor have detection limits of  $10 \mu\text{g kg}^{-1}$  and  $0.10 \mu\text{g kg}^{-1}$ , respectively. Furthermore, the coefficients of variation within and between assays were less than 5.35% and 6.87%, respectively.<sup>227</sup> An inkjet-printed electrochemically reduced graphene oxide (rGO) microelectrode for HT-2 mycotoxin immunoenzymatic biosensing was constructed and utilized, as reported in another study. Following solvent evaporation, single-drop line working microelectrodes with dimensions of  $78 \mu\text{m}$  in width and  $30 \text{ nm}$  in height were inkjet-printed onto poly(ethylene 2,6-naphthalate) substrates using a water-based GO ink. DPV was used to detect 1-naphthol (1-N) by modifying the electrochemical reduction parameters. Reduction timings greatly affected electrode performance. The biosensor exhibited a linear dynamic range of  $6.3$  to  $100.0 \text{ ng mL}^{-1}$  and a detection limit of  $1.6 \text{ ng mL}^{-1}$  during a 5-minute incubation period using the 1-naphthyl phosphate (1-NP) substrate.<sup>228</sup>

Another study utilized AgMOFs and N-CDs to develop a sensitive trilobatin electrochemiluminescence (ECL) sensor. The sensor used AgMOF@N-CD composite as the luminophore, as the integration of both components enhances the stability and intensity of N-CD ECL. AgMOFs exhibited high specific surface area, porosity, and adsorption capabilities, whereas N-CDs displayed high ECL intensity but low stability. The high conductivity of AgMOF@N-CD composite, large porosity, and abundant N-doped sp<sup>2</sup> sites minimize charge-transfer resistance and accelerate electron injection into trilobatin, whose multiple phenolic -OH groups coordinate to Ag<sup>+</sup> centers and form hydrogen bonds and  $\pi$ - $\pi$  stacking with the N-CD matrix to lock the analyte in place and facilitate interfacial electron transfer. Under ideal conditions, the ECL sensor detected trilobatin with a low detection limit of  $5.99 \times 10^{-8} \text{ M}$  (S/N = 3), and a linear range of  $1.0 \times 10^{-7} \text{ M}$  to  $1.0 \times 10^{-3} \text{ M}$ . Additionally, the sensor exhibits excellent stability, interference

resistance, and reproducibility.<sup>229</sup> A label-free aptasensor detects vomitoxin in grains. Cerium-based MOF composite AuNPs (CeMOF@Au) supplied electron transport substrates and DNA binding sites. The CeMOF@Au composite, with dense AuNPs grown on a porous Ce-MOF scaffold, greatly increases electroactive surface area and conductivity lowering charge-transfer resistance and accelerating [Fe(CN)<sub>6</sub>]<sup>3-/4-</sup> shuttling, while Exo III-mediated cDNA recycling further amplifies the electron flux. Thiolated DNA is covalently anchored to AuNPs *via* Au-S bonds, and DON-aptamer recognition is driven by hydrogen bonding and van der Waals (electrostatic) interactions between the toxin's hydroxyl/epoxide groups and the oligonucleotide bases, ensuring specific target capture and signal modulation. With a detection limit of  $1.79 \times 10^{-9} \text{ mg mL}^{-1}$  and an excellent recovery rate in maize, samples spiked with vomitoxin, the aptasensor can detect vomitoxin in the range of  $1 \times 10^{-8}$  to  $5 \times 10^{-4} \text{ mg mL}^{-1}$  under optimal conditions.<sup>230</sup>

The analytical approaches for detecting T-2 toxin, a highly toxic type A trichothecene mycotoxin, are illustrated in Fig. 8, which showcases three distinct yet complementary detection strategies. Electrochemical immunosensors (Fig. 8a) employ a sophisticated nanocomposite platform comprising single-walled carbon nanotubes (SWNTs), chitosan (CS), and gold nanoparticles on a glassy carbon electrode, which enhances both the surface area for antibody immobilization and electron transfer efficiency, enabling sensitive T-2 toxin detection in complex matrices like feed and swine meat. Electrochemical aptasensors (Fig. 8b) employ a dual-signal amplification strategy that involves bimetallic oxide (Ce-In)<sub>x</sub> and covalent organic frameworks, significantly enhancing detection sensitivity through synergistic effects that improve both catalytic activity and aptamer loading capacity. For confirmatory analysis and multi-mycotoxin detection, liquid chromatography-tandem mass spectrometry (LC-MS/MS) (Fig. 8c) provides a gold-standard approach, offering high specificity and accuracy for the simultaneous quantification of T-2 toxin and deoxynivalenol in cereals like maize and oats. Together, these methods illustrate the evolution from conventional antibody-based assays to advanced nanomaterial-enhanced biosensors and exact chromatographic techniques, addressing the critical need for reliable T-2 toxin monitoring across different food and feed commodities. The integration of nanomaterials in electrochemical platforms and the robustness of mass spectrometry highlight the complementary roles of screening and confirmatory methods in comprehensive mycotoxin analysis.

Since T-2 toxin is a significant pollutant of crops, stored grains, and food products, its identification is essential for both human and environmental health. Nanoelectrode arrays are used as gate photoactive materials in the zero-gate-bias organic photoelectrochemical transistor (OPECT) sensor. Due to its extraordinary signal amplification, OPECT's channel current was an order of magnitude higher than that of a typical photoelectrochemical system's photocurrent. Ordered ZnO nanorod arrays act as densely packed nanoelectrodes that, under illumination, generate a large photovoltage and facilitate rapid, low-resistance electron transfer to the FTO gate thanks to



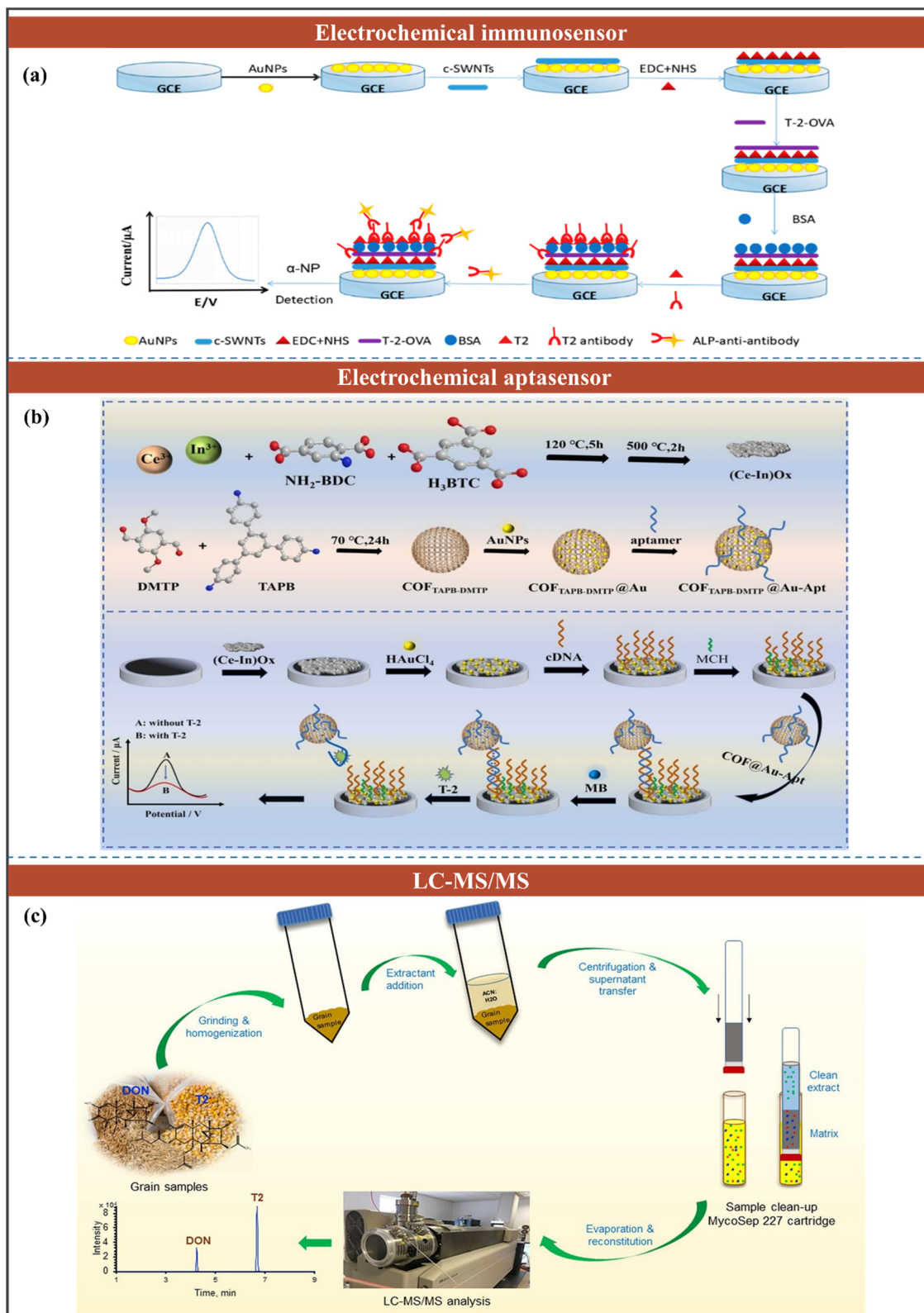


**Fig. 8** Electrochemical immunosensor: (a) the fabrication process of electrochemical biosensor SWNTs/CS/AuNPs/GCE for the detection of T-2 toxin, reproduced from ref. 231 with permission from MDPI, copyright 2018. Electrochemical aptasensor: (b) schematic diagram for the determination of T-2 toxin using a dual-signal amplification, reproduced from ref. 232 with permission from Elsevier, copyright 2023. LC-MS/MS: (c) schematic representation for the simultaneous determination of deoxynivalenol and T-2 toxin in maize and oats, reproduced from ref. 233 with permission from Elsevier, copyright 2021.

their high electroactive surface area and double-layer capacitance. The OPECT channel then amplifies these slight gate-potential shifts into large drain-current outputs. Aptamer probes are covalently anchored *via* Schiff-base ( $-\text{NH}_2/-\text{CHO}$ ) linkages, and T-2 toxin is captured through hydrogen bonding and van der Waals interactions between its hydroxyl/epoxide groups and the oligonucleotide bases. The OPECT aptasensor's detection limit is  $28.8 \text{ pg L}^{-1}$ , which is significantly lower than the standard PEC method's limit of  $0.34 \text{ ng L}^{-1}$ . This indicates that OPECT devices are more effective at measuring T-2 toxins.<sup>234</sup> The *Fusarium* genus produces T-2 toxin, a type A TCT mycotoxin that is genotoxic, cytotoxic, and immunotoxic to animals and humans. As a result, a quick testing process with high reliability, sensitivity, and selectivity is required. By carefully modifying the synthesis parameters, Zhao *et al.* discovered a form of  $\text{NH}_2\text{-UiO-66}$  with a high quenching efficiency. They used a Cy3-labeled aptamer to develop a new fluorescence sensor.  $\text{NH}_2\text{-UiO-66}$  may adsorb and quench Cy3-aptamer fluorescence using FRET and PET principles through coordination, hydrogen bonding, and  $\pi\text{-}\pi$  interactions. The  $\text{NH}_2\text{-UiO-66/Cy3-aptamer}$  complex was disrupted by the T-2 toxin, which was covalently linked to the Cy3-aptamer.

Zhao *et al.* demonstrated that inhibiting energy transfer restored fluorescence intensity, facilitating a sensitive response to T-2 toxin. Their study revealed a strong linear correlation between T-2 toxin concentrations (ranging from 0.5 to  $100 \text{ ng mL}^{-1}$ ) and fluorescence intensity. The developed fluorescent aptasensor exhibited a signal-to-noise ratio of three and achieved a detection limit of  $0.239 \text{ ng mL}^{-1}$ . Additionally, the recovery rates for beer and milk samples were found to be 92.31–111.51% (RSD = 2.3–2.9%) and 89.86–108.99% (RSD = 2.0–2.6%), respectively.<sup>235</sup> Zhang *et al.* developed a colorimetric aptasensor for T-2 toxin detection utilizing pristine Au NPs and an ssDNA aptamer. The solution remained red because the aptamer-wrapped AuNPs inhibited salt-induced aggregation when T-2 was not present. T-2 was added, and the aptamer was complexed with it before being separated from the AuNPs. In a saline environment, this interaction caused the AuNPs to aggregate and change from red to a purple-blue color. The dense AuNPs film on the electrode-aptamer interface, which multiplies electroactive surface area slash charge-transfer resistance and speeds faradaic electron flow, while T-2 binding induces an aptamer fold that further gates tunneling currents; the toxin's hydroxyl and epoxide moieties engage complementary bases *via* multiple hydrogen bonds and van der Waals contacts to secure specific recognition and signal modulation. T-2 was detected by the aptasensor with excellent selectivity and sensitivity. The detection limit and linearity range were  $57.8 \text{ pg mL}^{-1}$  ( $0.124 \text{ nM}$ ) and 0.1 to  $5000 \text{ ng mL}^{-1}$ , respectively.<sup>236</sup> The detection of TCT by different biosensing technologies can be seen in Table 4.

**3.1.5 Zearalenone.** Zearalenone (ZEA) is a resorcylic acid lactone mycotoxin produced by *Fusarium graminearum*, *culmorum* and *cerealis*. Due to its estrogenic properties, this mycotoxin commonly contaminates cereal crops such as maize, wheat, barley, and oats, posing a risk to both animal and human health.<sup>258</sup> Corn, sorghum, wheat, rice, barley, oats, pecans,

soybeans and sesame are among the cereals contaminated with ZEA. Due to its structural resemblance to estrogens, ZEA has been demonstrated in numerous *in vivo* studies to disrupt hormonal homeostasis.<sup>259</sup> Mammals experience problems with reproduction and fertility as a result of mycotoxins' strong binding to estrogen receptors.<sup>260</sup> Cancer is linked to progressive exposure to endocrine-modulatory chemicals. Toxin bioavailability in humans, rats, rabbits, and pigs can exceed 80%, according to a 2014 EFSA assessment.<sup>79</sup> According to recent studies, ZEA is processed in the liver and causes nephrotoxicity, immunotoxicity, cancer, and hepatotoxicity in animals.

**3.1.5.1 Detection of ZEA.** For maize ZEA detection, a dual-signal immunoassay activated by ALP has been reported.<sup>258</sup> The sensitivity may arise from alkaline phosphatase-generated L-ascorbic acid, reducing the  $\text{K}_3[\text{Fe}(\text{CN})_6]$  mediator to  $\text{K}_4[\text{Fe}(\text{CN})_6]$ , whose rapid electron shuttling at the AuNP-modified electrode slashes charge-transfer resistance and produces a large faradaic current. ZEA is captured by its monoclonal antibody *via* multiple non-covalent hydrogen bonds and hydrophobic contacts, localizing ALP-IgG at the interface to ensure specific mediator consumption and signal amplification. The role of  $\text{K}_3[\text{Fe}(\text{CN})_6]$  in multicolor creation and electron transfer allowed colorimetric and electrochemical assays to quantify ZEA. The detection limits for colorimetric and electrochemical techniques were 0.04 and  $0.08 \text{ ng mL}^{-1}$ . ZEA recovery from cornmeal samples was 80–120%, with relative standard deviations below 10%. The dual-signal immunoassay demonstrated high sensitivity in detecting ZEA in corn samples. Another work combined NiO with carboxylated multi-walled carbon nanotubes (MWCNT-COOH) to create an electrochemical sensor that does not require biomolecules and can detect ZEA and OTA. For the first time, ZEA and OTA have been simultaneously detected by a NiO-MWCNT ( $-\text{COOH}$ ) electrochemical sensor. Under optimal conditions, ZEA ( $0.01\text{--}10.24 \text{ }\mu\text{g mL}^{-1}$ ) and OTA ( $0.04\text{--}10.24 \text{ }\mu\text{g mL}^{-1}$ ) showed linear responses, with detection limits of 6 and  $15 \text{ ng mL}^{-1}$ , respectively.<sup>261</sup> For ZEA, Azri *et al.* created an electrochemical aptasensor. A 1,4-phenylene diisocyanate linker and cysteamine hydrochloride were used to bind ZEA to the gold electrode covalently. A shortened ZEA aptamer with a dissociation constant of  $13.4 \pm 2.1 \text{ nM}$  was utilized to develop an aptasensor. Using ferro/ferricyanide as a redox probe, SWV was utilized to examine changes in electron transport. The best measurement of the reaction under suitable experimental conditions was at  $0.20 \text{ V}$  (*vs.*  $\text{Ag}/\text{AgCl}$ ). The competition for the aptamer binding site between the free and immobilized ZEAs was necessary for the signals to occur. Amine-terminated cysteamine/PDIC layers on the Au electrode create a positively charged interface that strongly attracts the  $[\text{Fe}(\text{CN})_6]^{3-/4-}$  redox probe. In the competitive assay, the displacement of the negatively charged aptamer-ZEA complex reduces surface blocking, accelerating electron transfer and amplifying the faradaic current. ZEA is covalently tethered *via* urethane bonds (isocyanate-phenol coupling) and its aptamer recognizes it through hydrogen bonding,  $\pi\text{-}\pi$  stacking, and van der Waals interactions between the phenolic/lactone groups and nucleobases. Aptasensor has a detection limit of  $0.017 \text{ ng mL}^{-1}$  and can detect ZEA in the





Table 4 Detection of TCT using their LODs as determined by various analytical methods

Sr No.	Method	Analyte	Electrode modifier	Linear range	LOD	Samples/recovery	Ref.
1	ECL	Deoxynivalenol (DON)	Ab-biconjugates/BSA/Ag/APTES-PTCA@CNHs/GCE	0.1 ng mL <sup>-1</sup> -20 ng mL <sup>-1</sup>	0.03 pg mL <sup>-1</sup>	Milk/89.3-102.4%	237
2	CV	DON	MIP-SPGE	5-500 ng mL <sup>-1</sup>	0.3 ng mL <sup>-1</sup>	Cornflakes/90.8-98.5%	238
3	EIS	DON	—	610-6210 µg kg <sup>-1</sup>	342.4 µg kg <sup>-1</sup>	Wheat/78-79%	239
4	EC	DON	DON/Anti <sub>DON</sub> /Gel/AE	0.001-0.5 ng mL <sup>-1</sup>	0.43 pg mL <sup>-1</sup>	Apple juice/95-109%	240
5	EC	HT-2	Anti-HT-2 Fab/ERGO	6.3-100.0 ng mL <sup>-1</sup>	1.6 ng mL <sup>-1</sup>	Bovine serum/87.8-108.5%	227
6	EC	T-2	rGO-NPG/Pt	0-1000 µg kg <sup>-1</sup>	0.10 µg kg <sup>-1</sup>	Wheat germ	228
7	Aptasensor	DON	—	1 fg mL <sup>-1</sup> -1 ng mL <sup>-1</sup>	2.11 pg mL <sup>-1</sup>	Plant extract	241
8	Electrochemical DNA sensor	T-2	Aptamer/MCH/CP/MoS <sub>2</sub> -PANI-Chi-Au/GCE	10 fg mL <sup>-1</sup> -100 ng mL <sup>-1</sup>	1.79 fg mL <sup>-1</sup>	Canned beer/94.62-103.52%	242
9	Fluorescence NPs based aptasensor	T-2	T-2/apptamer/KYF <sub>4</sub> Tb <sup>3+</sup>	0.001-100 ng mL <sup>-1</sup>	0.33 pg mL <sup>-1</sup>	Maize/90.0-92.0%	243
10	Silver nanoclusters-based FRET aptasensor	T-2	NC-T5-apt-AgNCs/MoS <sub>2</sub> /T-2	0.005-500 ng mL <sup>-1</sup>	0.93 pg mL <sup>-1</sup>	Maize/89.46-102.08%	244
11	GC-QqQ-MS/MS	DON 3-ADON 15-ADON	—	1.3-1.6 µg kg <sup>-1</sup>	0.1 µg kg <sup>-1</sup>	Wheat/90.41-107.75% Chicken liver/87.9-105.7% —/92.4-108.4% —/89.2-96.7%	245
12	ID-LC/MS/MS	DON DEG	—	0.01-10 µg kg <sup>-1</sup>	0.11 µg kg <sup>-1</sup> 0.02 µg kg <sup>-1</sup>	Grain	246
13	GC-QqQ-MS/MS	NIV(Nivalenol) NIV NEO	—	2.6-7.9 µg kg <sup>-1</sup> 2.7-25 µg kg <sup>-1</sup> 3.7-13.3 µg kg <sup>-1</sup>	0.14 µg kg <sup>-1</sup> 0.05 µg kg <sup>-1</sup> 0.15 µg kg <sup>-1</sup> 0.15 µg kg <sup>-1</sup>	Chicken liver/97.4-103.7% —/88.6-95.4% Chicken liver/96.5-112.3% —/98.1-101.5%	245
15	EC immunosensor	T-2	ALP-anti-antibody/anti-T-2/T-2-SWNTs/GS/AuNPs/GCE	0.01-100 ng mL <sup>-1</sup>	0.14 µg L <sup>-1</sup>	Maize/91.59-102.49% Swine meat/91.42-100.80%	231
16	FRET	T-2	—	0.001-100 ng mL <sup>-1</sup>	0.57 pg mL <sup>-1</sup>	Maize/90-107.77%	247
17	UCNP/MOF fluorescence aptasensor	T-2	—	0.1-100 ng mL <sup>-1</sup>	0.087 ng mL <sup>-1</sup>	Corn meal/97.52-109.53% Beer/90.81-100.02%	248
18	Single cell EC	T-2	GeIMA/AuNP/GCE	0-1000 ng mL <sup>-1</sup> 10-800 µg kg <sup>-1</sup>	0.13807 ng mL <sup>-1</sup> 0.10 µg kg <sup>-1</sup> and 0.12 µg kg <sup>-1</sup>	Flour/81.19-130.17% Maize/89.6-93.3% and Oat/86.3-87.7%	249
19	UPLC-MS/MS	DON T-2	—	5-200 µg kg <sup>-1</sup>	0.04 µg kg <sup>-1</sup>	Maize/86.1-95.3% and oat/85-92.4%	233
20	Photo induced OECT	T-2	T-2/Apt/ZnO NEAs	100 pg L <sup>-1</sup> -1 mg L <sup>-1</sup>	28.8 pg L <sup>-1</sup>	Milk/97.8-102.4%	250
21	Cy3-aptamer/MOFs fluorescence aptasensor	T-2	—	0.5-100 ng mL <sup>-1</sup>	0.239 ng mL <sup>-1</sup>	Milk/89.86-108.99% Beer/92.31-111.51%	235
22	TRFIA	T-2	—	0.0625-50 ng mL <sup>-1</sup>	0.052 ng mL <sup>-1</sup> 0.071 ng mL <sup>-1</sup>	Corn and feed substrate/ 95.31-119.03%	251
23	EIS	DON	Au/Cys/PAMAM/Mab	50-2500 ppb 1-5000 ppb	50 ppb 1 ppb	Dry pasta/98.75-102.60%	252
24	DPV EC	T-2	MCH/S-DNA/AuNPs/ MnO <sub>2</sub> @GO/AuE	2 fg mL <sup>-1</sup> -20 ng mL <sup>-1</sup>	0.107 fg mL <sup>-1</sup>	Milk/96.5-103.4%	232

Table 4 (Contd.)

Str No.	Method	Analyte	Electrode modifier	Linear range	LOD	Samples/recovery	Ref.
25	DPV	T-2	T-2/MB/COF <sub>TAPB-DMTF</sub> @Au-apt/ MCH/cDNA/AuNPs/(Ce-In)Ox/ GCE	$5.0 \times 10^{-7}$ – $5.0 \text{ ng mL}^{-1}$	$7.6 \times 10^{-8} \text{ ng mL}^{-1}$	Crop/94.6–102%	253
26	EC	DON	MB@ZIF-8/SA/sDNA/ DON( $2 \text{ ng mL}^{-1}$ )/Apt/MCH/ cDNA/PEI-rGO/AuNWs/AuE	0.01–100 $\text{ng mL}^{-1}$	0.002 $\text{ng mL}^{-1}$	Maize flour/ 81.85–109.4%	253
27	EC	DON	Label DNA @AgPdNPs/help	$1 \times 10^{-8}$ – $1 \times 10^{-4} \text{ mg mL}^{-1}$	$6.9 \times 10^{-9} \text{ mg mL}^{-1}$		254
28	EIS DPV	T-2	DNA/substrate DNA/ AuONs@GO/AuE	$1 \times 10^{-2}$ – $1 \times 10^4 \text{ pg mL}^{-1}$	6.71 $\text{fg mL}^{-1}$	Beer/86.2–96.1%	255
29	EC	DON	T-2/RecfApt-sDNA/AuNPs/ FeMOF@GO/AuE	0.1–5000 $\text{pg mL}^{-1}$	0.0186 $\text{pg mL}^{-1}$	Grain/85.67–118.0%	256
30	EIS DPV	T-2		$5.0 \times 10^{-1}$ – $5.0 \times 10^6 \text{ pg mL}^{-1}$	0.19 $\text{pg mL}^{-1}$	Beer/92.5–97.8%	257

concentration range of 0.01 to 1000  $\text{ng mL}^{-1}$ . Cross-reactivity with other ZEA analogs was high, but not with other mycotoxins. After quantifying ZEA in maize grain extract, the aptasensor showed 87–110% recovery.<sup>262</sup>

Zaman *et al.* employed a SPE using a 3D carnation flower-like  $\text{Tb}^{3+}/\text{Co}_3\text{O}_4$  nanocomposite to detect ZEA in authentic dairy products, juices, and other liquid foods.<sup>261</sup> The modified electrode was analyzed electrochemically using DPV, EIS, CV, and chronoamperometry. ZEA's proton receptor groups caused its peak current to vary with pH. The maximum signal of the received stream indicated the optimal ZEA signal in PBS at pH 7.0. The improved sensing may derive from the flower-like  $\text{Tb}^{3+}/\text{Co}_3\text{O}_4$  nanocomposite's exceptional conductivity and enlarged electroactive surface area.  $\text{Tb}^{3+}$  induced oxygen vacancies slash charge-transfer resistance and catalyze the diffusion-controlled electrocatalytic oxidation of zearalenone. Zearalenone's phenolic –OH and lactone C=O moieties form hydrogen bonds with surface oxide sites and coordinate to  $\text{Tb}^{3+}$  centers, securing selective adsorption and efficient electron exchange. For ZEA concentration, the sensor exhibited a broad linear range (0.001–500.0  $\mu\text{M}$ ) and an accurate detection limit of 0.34 nM. Zhou *et al.* employed a highly sensitive and selective molecularly imprinted electrochemical sensor to detect ZEA using reduced graphene nanoribbons (GNRs) and AuNPs. To synergistically increase the electrochemical signal, oxidized GNRs are created *via* enhanced Hummers' oxidation, then reduced and modified with AuNPs on a GCE using electrodeposition. With a detection limit of 0.34  $\text{ng mL}^{-1}$ , the sensor's linear detection range for ZEA is 1–500  $\text{ng mL}^{-1}$ .<sup>263</sup> A high-sensitivity signal-off electrochemical aptasensor for detecting ZEA traces was developed in another study. The Ce-based MOF and MWCNTs nanocomposite, functionalized with polyethyleneimine (P-Ce-MOF@MWCNTs), served as a sensing platform due to its wide surface area and high electrochemical activity. The aptamer was then attached using Pt@Au NPs, and the signal probe, toluidine blue, was electrodeposited. The enhanced current arises from the synergy of Ce-MOF's large, catalytically active Ce–O porous network and MWCNT's exceptional conductivity, which together slash charge-transfer resistance and accelerate electron hopping of the toluidine blue tag to the GCE. Zearalenone's phenolic –OH and lactone C=O functionalities form hydrogen bonds with PEI amines and coordinate to  $\text{Ce}^{3+}$  centers, while its aromatic core  $\pi$ – $\pi$  stacks with CNT walls, immobilizing the analyte close to the transducer for efficient sensing. Under optimal conditions, the aptasensor displayed a linear relationship for ZEA in the concentration range of  $5.0 \times 10^{-5}$  to 50.0  $\text{ng mL}^{-1}$ .  $1.0 \times 10^{-5} \text{ ng mL}^{-1}$  was the detection limit (LOD, S/N = 3), and  $2.9 \times 10^{-5} \text{ ng mL}^{-1}$  was the quantitation limit (LOQ, S/N = 10).<sup>264</sup>

Recent advances in electrochemical biosensing for zearalenone detection are comprehensively illustrated in Fig. 9, highlighting three innovative sensor designs that employ distinct signal amplification and recognition strategies. The first approach (Fig. 9a) demonstrates an aptasensor utilizing a phosphorus-doped cerium metal–organic framework (P-Ce-MOF) decorated with multi-walled carbon nanotubes (MWCNTs), which synergistically enhances electrical



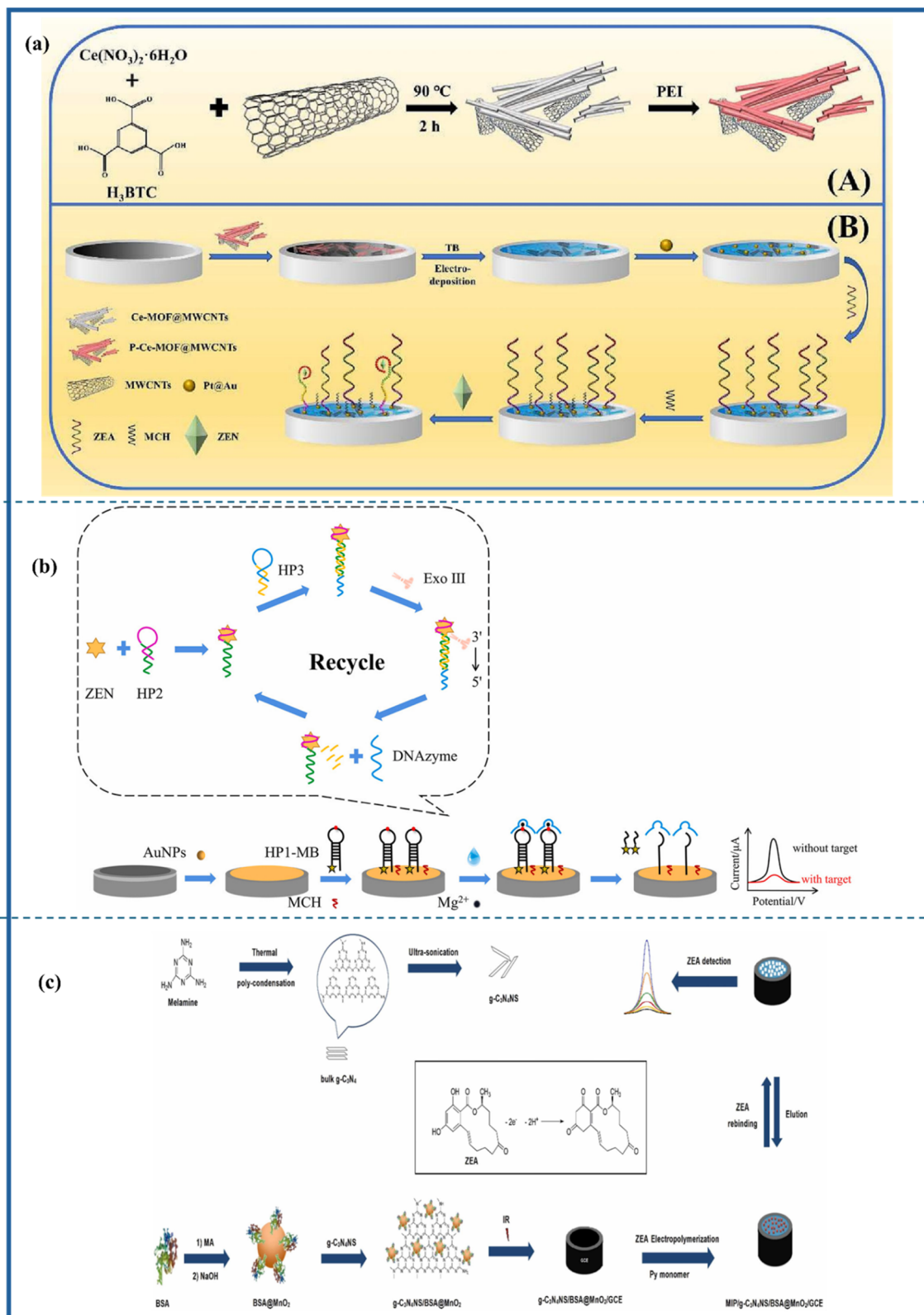


Fig. 9 (a) Schematic diagrams of the synthesis of P-Ce-MOF@MWCNTs and the stepwise construction of the electrochemical aptasensor for the detection of ZEA, reproduced from ref. 264 with permission from Elsevier, copyright 2023. (b) Schematics for the Detection of zearalenone by electrochemical aptasensor based on enzyme-assisted target recycling and DNAzyme release strategy, reproduced from ref. 265 with permission from Elsevier, copyright 2025. (c) Schematic preparation of g-C<sub>3</sub>N<sub>4</sub>NS/BSA@MnO<sub>2</sub> nanocomposite and imprinted electrode for ZEA detection, reproduced from ref. 266 with permission from Elsevier, 2024.



conductivity and provides abundant binding sites for aptamer immobilization, enabling highly sensitive quantification of ZEA. A more sophisticated enzyme-assisted mechanism is shown in Fig. 9b, where target recycling and DNAzyme release strategies are combined to achieve exponential signal amplification, significantly lowering the detection limit through catalytic hairpin assembly and enzymatic signal enhancement. The most autonomous design is presented in Fig. 9c, featuring a self-reporting molecularly imprinted sensor based on copper hexacyanoferrate (CuHCF) modified with reduced graphene nanoribbons-reduced graphene oxide. Here, the redox-active CuHCF serves as both a recognition element and an intrinsic signal reporter, eliminating the need for external probes. These four approaches collectively demonstrate the field's progression from conventional receptor-based detection to intelligent systems that integrate nanozymes, molecular imprinting, and self-signaling materials, all while addressing the critical need for rapid, sensitive, and specific ZEA monitoring in food safety applications. The strategic combination of advanced nanomaterials with clever molecular recognition principles in these designs provides a blueprint for next-generation mycotoxin sensors that strike a balance between sensitivity, selectivity, and practical applicability.

Liu *et al.* developed an electrochemical sensor for ZEA by utilizing a carefully selected mimic peptide from a screened library, validated through molecular modeling and electrochemical methods. The construction of the mimic peptide library involved amino acid mutations, dynamic simulations, molecular docking, and structural analyses. The incorporation of gold nanoparticles (AuNPs) and reduced carboxylated graphene oxide significantly enhanced the electrical signal. The sensor demonstrated a linear detection range from 0.01 to 10 ng mL<sup>-1</sup>, achieving an impressive limit of detection of 0.91 pg mL<sup>-1</sup> under optimal conditions. The commercial ELISA kits varied from 82% to 108.8%, while the grain sample recovery rate ranged from 84% to 105.3%.<sup>267</sup> ZEA in rice flour, maize powder, and morning cereal can be measured using a simple electrochemical nanohybrid sensor. A magnetic Fe<sub>3</sub>O<sub>4</sub>-GO-modified electrode and a Cu-based MOF are key features of this layer-by-layer-built sensor. The synergistic coupling of highly porous, electrocatalytic Cu-MOF with conductive Fe<sub>3</sub>O<sub>4</sub>-GO maximizes the electroactive surface area and minimizes charge-transfer resistance, thereby accelerating electron transfer. ZEA is preconcentrated and recognized through hydrogen bonding between its phenolic -OH and lactone C=O groups and the carboxylates of MOF/GO,  $\pi$ - $\pi$  stacking of its aromatic ring on graphene oxide, and coordination of its carbonyl oxygens to Cu centers. The well-designed sensor is efficient, has a wide surface area, and has exceptional electron transport. Under ideal conditions, the limit of detection for ZEA electrochemical detection was 23.14 ng mL<sup>-1</sup>, with a range of 159.2 to 2865.2 ng mL<sup>-1</sup>.<sup>268</sup>

Wang *et al.* developed CuO@GO nanocomposites as an electrochemical sensor for detecting ZEA mycotoxins in food samples. The toxin's aromatic core  $\pi$ - $\pi$  stacks with graphene, its phenolic -OH hydrogen bonds to GO oxygen functionalities, and its carbonyl oxygen coordinates to Cu<sup>2+</sup> sites, leading to

selective adsorption and rapid electron exchange. The electrochemical characterization of ZEA on CuO@GO/GCE, using CV and DPV techniques, demonstrated a linear detection range of 10 to 150 ng mL<sup>-1</sup>, a sensitivity of 0.4895  $\mu$ A ng<sup>-1</sup> mL<sup>-1</sup>, and a detection limit of 0.012 ng mL<sup>-1</sup>.<sup>269</sup> Additionally, an electrochemical aptamer sensing method utilizing PEI@Ti-MOF@Ti<sub>3</sub>C<sub>2</sub>T<sub>x</sub>-MXene was developed for the identification of ZEA in food products. The synthesis of NH<sub>2</sub>-MIL-125 involved the use of tetra-butyl titanate as the metal center and 2-amino terephthalic acid as the organic ligand. Simultaneous hybridization of Ti<sub>3</sub>C<sub>2</sub>T<sub>x</sub>-MXene resulted in the formation of the Ti-MOF@Ti<sub>3</sub>C<sub>2</sub>T<sub>x</sub>-MXene composite material. The composites were utilized to develop a sensing platform on gold electrodes, following their functionalization with PEI and subsequent covalent bonding. The sensor achieved a LOD of 1.64 fg mL<sup>-1</sup>. Furthermore, it demonstrated remarkable stability, reproducibility, and selectivity in identifying ZEA in beer and cornmeal samples.<sup>270</sup> Table 5 presents the detection of ZEA using different methods along with their LODs.

**3.1.6 Patulin (PAT).** PAT is an electrophilic  $\alpha$ ,  $\beta$ -unsaturated  $\gamma$ -lactone, which interacts with ascorbic acid, free amino groups, sulfur dioxide, and sulfhydryl groups. PAT has been reported to have gastrointestinal, immunotoxic, genotoxic, and mutagenic effects, which can damage vital organs and systems.<sup>311</sup> Therefore, a maximum acceptable concentration of 50  $\mu$ g L<sup>-1</sup> PAT in apple juice and cider has been set by China, the US, the EU, and other countries.<sup>312</sup> Patulin (4-hydroxy-4*H*-furo [3,2-*c*]pyran-2(6*H*)-one, PAT), a mycotoxin found in various foods, is produced by a wide range of fungi.<sup>313</sup> Under optimal temperature and humidity conditions, *Aspergillus* and *Penicillium* species synthesize this secondary metabolite. In 1941, Glister identified, isolated, and designated PAT. Because PAT inhibits both Gram-positive and Gram-negative bacteria (*e.g.*, *Shigella* spp., *Salmonella typhi*, and *E. coli*), it was the focus of earlier clinical trials.<sup>314</sup> Research in the 1960s demonstrated that PAT was detrimental to bacterial cells and animal models. Consequently, PAT is infrequently utilized as a therapeutic agent in clinical environments, with investigations concentrating on its toxicity and contamination of food and feed.<sup>315</sup>

Pears, blueberries, cherries, peaches, plums, mulberries, rotten apples, and pears all contain polyphenolic acids or polyphenols. Due to the higher concentration of PAT in apples, the majority of individuals obtain their PAT from apples and apple-derived products. Recent assessments of PAT by other researchers have been exceptional. These evaluations focus on PAT domains, including synthesis, distribution, and others. An updated evaluation is necessary to incorporate the latest insights from significant studies on the toxicity and detoxification of PAT. This study emphasizes the benefits and potential of the biological approach, highlights the lack of interaction between intestinal microbiota and PAT, and enhances the detoxification model through a thorough analysis of PAT. Regarding PAT toxicity, our findings also included vitamin, trace metal, and probiotic ingestion. We anticipate that compiling perspectives may help mitigate PAT contamination in food and stimulate future studies. Despite clear correlations between PAT contamination numbers and food,





Table 5 Detection of ZEA on various sensing platforms along with their analytical parameters

S. No.	Method	Analyte	Electrode modifier	Linear range	LOD	Sample/recovery	Ref.
1	EC	ZEA	MNPs-aptamer/TRFLNPs-cDNA	0.001–10 ng mL <sup>-1</sup>	0.21 pg mL <sup>-1</sup>	Maize/80.76–119.66% Wheat/90.04–114.75%	271
2	TR-aptasensor	ZEA	—	0.001–100 ng mL <sup>-1</sup>	0.51 pg mL <sup>-1</sup>	Maize/94.4–98.0%	243
3	EC	ZEA	ZEA/CGO-ZBA/BSA/PCS/AuNPs/ CS@AB-MWCNTs/GCE	10 fg mL <sup>-1</sup> –10 ng mL <sup>-1</sup>	3.64 fg mL <sup>-1</sup>	Corn oil/92.81–99.58%	272
4	EC	ZEA	Au/Cys/PPDIC/ZEA/Apt	0.01–1000 ng mL <sup>-1</sup>	0.017 ng mL <sup>-1</sup>	Corn flour/101.12–111.5%	262
5	DPV	ZEA	Thi/GO/MCH/Apt/AuNPs/Nafion/ p-PNTs/AuE	0.5 pg mL <sup>-1</sup> –0.5 µg mL <sup>-1</sup>	0.17 pg mL <sup>-1</sup>	Maize grain/87–110% Maize/97.3–106%	273
6	Colorimetric aptasensor	ZEA	—	10–250 ng mL <sup>-1</sup>	10 ng mL <sup>-1</sup>	Corn oil/101.24–104.92%	274
7	Colorimetric aptasensor	ZEA	—	4–128 ng mL <sup>-1</sup>	4 ng mL <sup>-1</sup>	Corn/92.34–115.59% Maize powder/96.44–99.78%	275
8	Colorimetric aptasensor	ZEA	—	20–8000 ng mL <sup>-1</sup>	10 ng L <sup>-1</sup>	Mouse feed/95.99–103.73%	276
9	Aptamer-based lateral flow test strip	ZEA	—	5–200 ng mL <sup>-1</sup>	20 ng mL <sup>-1</sup>	Human serum/95–103% Corn/93.4–114.2%	277
10	EC	ZEA	GCE/rMoS <sub>2</sub> -Au/Aps/BSA/L-CPs	0.001–10 ng mL <sup>-1</sup>	0.5 pg mL <sup>-1</sup>	Maize/95.9–105.2%	278
11	DPV	ZEA	Anti-ZEA/MCM-41-Fe <sub>3</sub> O <sub>3</sub>	1.88–45 ng mL <sup>-1</sup>	0.57 ng mL <sup>-1</sup>	Amaranthus cruentus seeds	279
12	HPLC	ZEA	—	1.29–16.88 ng mL <sup>-1</sup>	1.29 ng mL <sup>-1</sup>	Field corn	280
13	CV	ZEA	Apt/Pt@AuNPs/TB/ PEI-MoS <sub>2</sub> -MWCNTs/Au	0.5 pg mL <sup>-1</sup> –50 ng mL <sup>-1</sup>	0.17 pg mL <sup>-1</sup>	Beer/85.3–100.2%	281
14	EC	ZEA	Cu@L-GA/NPs/Apt/ PANi-AuNPs/GCE	1 fg mL <sup>-1</sup> –100 ng mL <sup>-1</sup>	0.45 fg mL <sup>-1</sup>	Beer/92–105%	282
15	DPV	ZEN	ZEN-BSA/EDC-NHS/SPCE	8–32 ng mL <sup>-1</sup>	2 ng mL <sup>-1</sup>	Beer/89–97%	283
16	CV	ZEN	CoPC/SPCE	25–400 ng cm <sup>3</sup>	0.15 ng cm <sup>3</sup>	Wine/91.5–96.5% Corn/94.1–103.9%	284
17	DPV	ZEN	—	100–600 ng mL <sup>-1</sup>	29.47 ng mL <sup>-1</sup>	Corn flour, corn starch and Malt	285
18	CV	ZEN	SWCNTs/SPCE	2.5 × 10 <sup>-8</sup> –1 × 10 <sup>-6</sup> M	5 × 10 <sup>-9</sup> M	Cornflakes/98.6–103.3%	286
19	DPV	ZEN	PAN/Glu/PGE	5–30 and 60–100 nM	1.66 nM	Dairy juices	287
20	EC	ZEN	ZEN-xpAb/AuNPs/MWCNTs/ PEI/SPCE	0.1 pg mL <sup>-1</sup> –0.1 ng mL <sup>-1</sup>	0.15 pg mL <sup>-1</sup>	Maize/100.4–104.6%	288
21	CV	ZEN	ZEN/MCH/DNAS2-Apt/AuNPs/ Fe <sub>3</sub> O <sub>4</sub> NRs/rGO/AuE	0.5 pg mL <sup>-1</sup> –0.5 ng mL <sup>-1</sup>	0.105 pg mL <sup>-1</sup>	Maize/91.6–104.4%	289
22	EIS	ZEN	MCH/DNAH1/CoSe <sub>2</sub> /AuNRs/AuE	10 fg mL <sup>-1</sup> –10.0 ng mL <sup>-1</sup>	1.37 fg mL <sup>-1</sup>	Maize/93.6–103.4%	290
23	EC	ZEN	Ab/EDC-NHS/LA/Au	0.010–10 nM	1.9 pg mL <sup>-1</sup>	—	291
24	CV	ZEN	ZEN/BSA/biotin-Ab/ streptavidin/GCE	10 pg mL <sup>-1</sup> –3 ng mL <sup>-1</sup> and 3–12 ng mL <sup>-1</sup>	3.7 pg mL <sup>-1</sup>	Urine/98.5–101%	292
25	EC	ZEN	3D CF-L TB <sup>3+</sup> /Co <sub>3</sub> O <sub>4</sub> NC/SPE	0.001–500.0 µM	0.34 nM	—	293
26	CV	ZEN	MIP/AuNPs/rGNRs/GCE	1–500 ng mL <sup>-1</sup>	0.34 ng mL <sup>-1</sup>	Maize	263



Table 5 (Contd.)

S. No.	Method	Analyte	Electrode modifier	Linear range	LOD	Sample/recovery	Ref.
27	CV EIS DPV	ZEN	ZEN/MCH/L3/AuNPs/ rGO-COOH-apt/GCE	0.01 ng mL <sup>-1</sup> –10 ng mL <sup>-1</sup>	0.91 pg mL <sup>-1</sup>	Corn/98.0–101.3% Wheat/90.0–108.8% Oat/82.0–106.0% Bran/94.0–98.75% <i>Semen coicis</i> /97.06–102.9%	267
28	DPV	ZEN	GCE/P-Ce-MOF@MWCNTs/ TB/Pt@Au/ZEA	50.0 fg mL <sup>-1</sup> –50.0 ng mL <sup>-1</sup>	12.0 fg mL <sup>-1</sup>	Milk/84.4–97.0%	264
29	CV	ZEN	CuO@GO/GCE	10–150 ng mL <sup>-1</sup>	0.012 ng mL <sup>-1</sup>	Maize and oats	269
30	DPV	ZEN	AuNP-SE/ZEN	10 ng kg <sup>-1</sup> –10 mg kg <sup>-1</sup>	1.1 ng kg <sup>-1</sup>	Maize and oats	294
31	SERS	ZEN	Substrate (MSN-Rh6G-AuNPs)	3–200 ng mL <sup>-1</sup>	0.22 µg L <sup>-1</sup>	Corn	295
32	SERS	ZEN	—	10–1000 µg kg <sup>-1</sup>	3.6 µg kg <sup>-1</sup>	Maize/86.06–111.23%	296
33	Fluorescence based aptasensor	ZEN	—	0.01–100 ng mL <sup>-1</sup>	1.2 pg mL <sup>-1</sup>	Corn and oat flour	297
34	EC	ZEN	VMSF/ITO	0.001–1000 ng mL <sup>-1</sup>	1.2 × 10 <sup>-6</sup> ng mL <sup>-1</sup>	Maize/97.1–103%	298
35	ECL	ZEN	ZEN/MB/ZBA/BSA/cDNA/ CS/NGQDs-Ru@SiO <sub>2</sub> /GCE	1.0 × 10 <sup>-15</sup> –5.0 × 10 <sup>-8</sup> g mL <sup>-1</sup>	0.85 fg mL <sup>-1</sup>	Chestnut/96.0–105% Maize flour/93.2–102.8%	299
36	CV	ZEN	MIP/AuSPE	1 × 10 <sup>-4</sup> –1 × 10 <sup>2</sup> ng mL <sup>-1</sup>	3.4 × 10 <sup>-5</sup> ng mL <sup>-1</sup>	Maize/92–108%	300
37	EIS EC	ZEN	B-ZIF@CNP/Ag/Ab/ Anti-IgG-Bio/A-GOX-modified AuE	0.87–1058.5 pg mL <sup>-1</sup>	0.87 pg mL <sup>-1</sup>	Wheat, peanuts and feed/76.4–108.2%	301
38	DPV	ZEN	PEI-rGO/Pt@AuNRs	1–1 × 10 <sup>6</sup> pg mL <sup>-1</sup>	0.02 pg mL <sup>-1</sup>	—	302
39	DPV	ZEN	ZEN/BSA/Apt/PEI@T@M/AuE	1 × 10 <sup>-5</sup> –1 × 10 <sup>-11</sup> mg mL <sup>-1</sup>	1.64 fg mL <sup>-1</sup>	Beer/87.7–105.2% Corn starch/98.2–101.2%	270 and 303
40	EIS EIS CV	ZEN	SPCE/CS-CNT-Pd/EDC-NHS/ ZEN/-MAB/ZEN	0.25–16 ng mL <sup>-1</sup>	0.25 ng mL <sup>-1</sup>	Corn/86.5–98.6%	303
41	OMP	ZEN	GPE/CNH/GNP	10–1000 µg kg <sup>-1</sup>	4.40 µg kg <sup>-1</sup>	Corn/91–105.2%	304
42	CV	ZEN	MIP/g-C <sub>3</sub> N <sub>4</sub> NS/BSA@MnO <sub>2</sub> /GCE	1.0–10.0 ng L <sup>-1</sup>	0.25 ng mL <sup>-1</sup>	Rice	305
43	EIS immunosensor	ZON	APTS/SA/EDC-NHS	0.01–1 pg mL <sup>-1</sup>	0.002 pg mL <sup>-1</sup>	Maize	306
44	FRET	ZEN	(Aptamer-SAF-UNC-P-FO) probe	0.005–100 ng mL <sup>-1</sup>	0.0018 ng mL <sup>-1</sup>	Maize/92.30–110.68%	307
45	EIS	ZEN	ZEN/BSA/Apt/CuBi-BPDC/AE	1 fg mL <sup>-1</sup> –10 ng mL <sup>-1</sup>	0.19 fg mL <sup>-1</sup>	Milk/91.2–109.9%	308
46	DPV	ZEN	0 fg mL <sup>-1</sup> × 10 <sup>9</sup> fg mL <sup>-1</sup>	0 fg mL <sup>-1</sup> × 10 <sup>9</sup> fg mL <sup>-1</sup>	0.73 fg mL <sup>-1</sup>	Rice/92.0–109.9%	268
46	DPASV	ZEA	Cu-MOF/Fe <sub>3</sub> O <sub>4</sub> -GO/GCE	159.2–2865.2 ng mL <sup>-1</sup>	23.14 ng mL <sup>-1</sup>	Maize powder/93.3–97.7% Rice flour/94.9–113.3%	268
47	CV	ZEA	MIP/CuHCF/rGNR-rGO/GCE	0.25–500 ng mL <sup>-1</sup>	0.09 ng mL <sup>-1</sup>	Corn meal/97.30–102.18%	309
48	DPV Amperometry	ZEA	Bi <sub>2</sub> S <sub>3</sub> @CNF/GCE	0.125–375.5 µM	0.61 µM	Wheat and oats/98.9–99.15%	310

epidemiological data about population-level PAT exposure are limited. These investigations did not consider PAT bio-acceptability across various dietary media. Furthermore, fruits and vegetables may exhibit low PAT uptake, thereby reducing mealtime exposure to levels below the provisional maximum allowable daily dose. PAT contamination levels in fruit products exceed permitted limits in several locations, posing a health risk to residents. Future studies should investigate the co-occurrence of PAT with other mycotoxins in food and their combined and synergistic health effects, even if PAT alone poses a negligible risk.

**3.1.6.1 Detection of PAT.** The successful fabrication of a rGO/SnO<sub>2</sub> composite for the electrochemical detection of the fungal contaminant PAT by Shukla *et al.* eliminated the need for specific antibodies or chemical or biological sensors. The resulting rGO/SnO<sub>2</sub> composite demonstrated exceptional performance in the direct assessment of PAT levels in contaminated apple juice samples, exhibiting excellent electrochemical properties. The high DPV current originates from the synergistic coupling of conductive rGO and electrocatalytic SnO<sub>2</sub>, which minimizes charge-transfer resistance and facilitates the rapid two-electron oxidation of patulin. PAT adsorbs onto the composite through  $\pi$ - $\pi$  stacking of its furan-lactone core with the graphene lattice, hydrogen bonding of its hydroxyl and carbonyl groups to GO's oxygen functionalities, and coordination of its carbonyl oxygen to Sn<sup>4+</sup> centers. With a detection limit of 0.6635 nM, the rGO/SnO<sub>2</sub> composite electrode's DPV response showed a linear relationship with PAT concentration over the 50–600 nM range. The sensor electrode showed remarkable selectivity, consistent repeatability, and sensitivity.<sup>316</sup> The harmful properties of increased PAT concentrations underscore the importance of developing new detection methods, which are crucial for advancing research and creating revolutionary control technologies. A new sensor for the SWV method of PAT toxin detection was developed, utilizing a GCE enhanced by an ionic liquid-based MIP and Fe<sub>3</sub>O<sub>4</sub>/GO composite. A linear range of 0.001 nM to 250.0 nM was established under optimized conditions, with a LOQ of 0.001 nM and a LOD of  $3.33 \times 10^{-4}$  nM.<sup>317</sup> To achieve ultra-sensitive and selective PAT detection, a distinct study presented a novel method for creating a molecularly imprinted electrochemical sensor. Initially, N-GQDs were integrated with Au@Cu-MOF to enhance the surface of a GCE. Electro-polymerization was then used to create a layer of MIP on the Au@Cu-MOF/N-GQDs/GCE. The dense AuNPs, conductive N-GQDs, and abundant Cu(II)/Cu(I) redox centers slash charge-transfer resistance and accelerate the  $-0.11$  V Cu-MOF redox signal. Patulin then selectively binds to imprinted cavities and gets locked *via* hydrogen bonds (phenolic -OH to polymer/N-GQD oxides),  $\pi$ - $\pi$  stacking of its furan-lactone ring on graphitic domains, and coordination of its carbonyl oxygens to Cu<sup>2+</sup> nodes, gating electron flow to modulate the current. With an unusually low detection limit of 0.0007 ng mL<sup>-1</sup>, the developed MIP sensor showed a wide linear range from 0.001 to 70.0 ng mL<sup>-1</sup>.<sup>318</sup>

The detection of patulin (PAT), a hazardous mycotoxin commonly found in fruit products, is demonstrated through three advanced sensing platforms in Fig. 10, each employing

distinct detection mechanisms and nanomaterial engineering strategies. Fig. 10a presents an innovative film-like surface-enhanced Raman spectroscopy (SERS) aptasensor utilizing graphene oxide-gold nanosheet composites (GO@Au), where the large surface area and plasmonic properties enable ultra-sensitive PAT detection through aptamer-mediated recognition and significant Raman signal enhancement. Transitioning to electrochemical detection, Fig. 10b illustrates a bioreceptor-free sensor based on a reduced graphene oxide-tin oxide nanocomposite (rGO/SnO<sub>2</sub>), which leverages the synergistic effects of excellent electrical conductivity and metal oxide catalytic activity for rapid PAT quantification without the need for biological recognition elements. The most sophisticated approach is illustrated in Fig. 10c, featuring an *operando* photoelectrochemical-SERS (PEC-SERS) biosensor that combines *in situ* electrochemical characterization with Raman spectroscopy, enabling the simultaneous investigation of interfacial charge transfer mechanisms and highly sensitive PAT detection through dual-mode signal verification. These three platforms collectively demonstrate the evolution from single-mode detection to multifunctional analytical systems, highlighting how strategic nanomaterial design and multimodal sensing can address the challenges of PAT monitoring in complex food matrices. The progression from aptamer-based recognition to bioreceptor-free detection and, ultimately, to *operando* mechanistic analysis reflects the field's shift toward more robust, informative, and practical sensing solutions for food safety applications.

Food PAT poses a significant risk to human health, making the development of a precise and sensitive detection method essential. In this context, Jiang *et al.* developed an electrochemical assay for PAT detection by synthesizing aptamers on a carboxylated hierarchically porous carbon (HPC-COOH)-modified glassy carbon electrode, achieving high sensitivity in their approach. Due to its wide surface area, the HPC-COOH is a unique substrate for immobilizing aptamers, thereby enhancing target PAT capture and identification. The hierarchically porous, carboxylated carbon network of HPC-COOH slashes charge-transfer resistance and boosts Fe(CN)<sub>6</sub><sup>3-/4-</sup> electron shuttling at the GCE. At the same time, amino-terminated aptamers are covalently tethered *via* amide bonds to -COOH sites, and patulin's phenolic -OH and lactone C=O groups engage the aptamer through hydrogen bonding and  $\pi$ - $\pi$  stacking, gating mediator access, and modulating the faradaic current. With a low detection limit of 0.25 ng L<sup>-1</sup>, the modified aptasensor was able to detect PAT at concentrations ranging from 0.5 to  $5.0 \times 10^6$  ng L<sup>-1</sup>.<sup>321</sup> A RuMOF@hydrogel and carbonized polymer dots generated from banana peels were used to create a multimodal PAT aptasensor carefully. The RuMOF@hydrogel-modified magnetic electrode exhibited excellent anodic and cathodic electrochemiluminescence (ECL) emission and stability. The synergistic conductivity and dual-potential electrochemiluminescence of RuMOF@hydrogel and BPPDs@SiO<sub>2</sub> lead to improved electron transport and amplify the anodic ECL response; patulin binds its aptamer *via* hydrogen bonding and  $\pi$ - $\pi$  stacking between its phenolic -OH and lactone C=O groups and the nucleobases, triggering



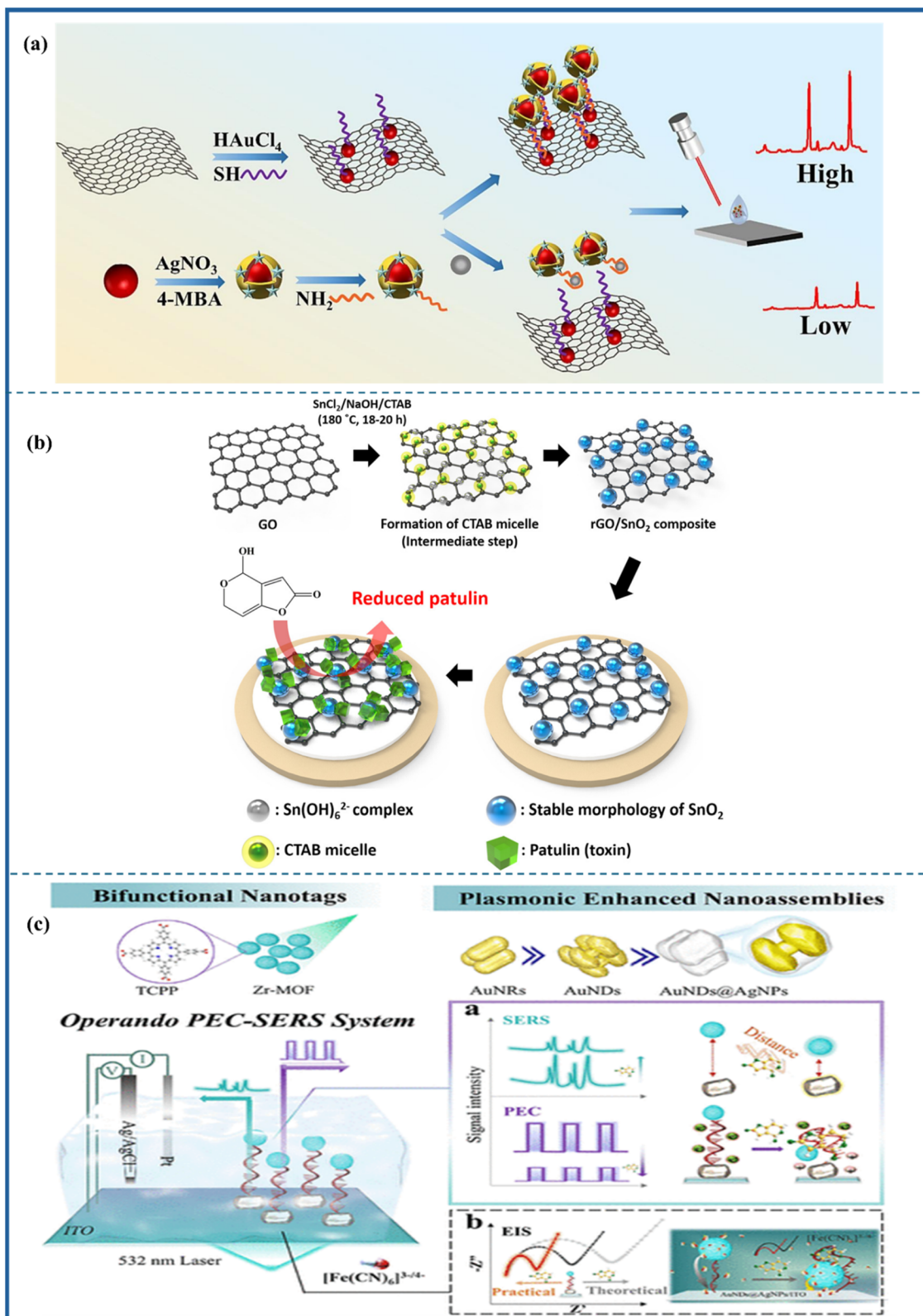


**Fig. 10** (a) Schematic diagram of the film-like SERS aptasensor based on GO@Au nanosheets for the detection of PAT, reproduced from ref. 319 with permission from Elsevier, copyright 2024. (b) Schematic representation of the fabrication of the rGO/SnO<sub>2</sub> nanocomposite and its electrochemical sensing of PAT, reproduced from ref. 316 with permission from Elsevier, copyright 2020. (c) Schematic illustration of the *operando* PEC-SERS biosensor for PAT detection: (a) analysis of biosensing mechanism via the *operando* PEC-SERS method and (b) analysis of biosensing mechanism via the electrochemical characterization method, reprinted from ref. 320 with permission from American Chemical Society, copyright 2025.



a hybridization chain reaction and magnetic enrichment that concentrate signal probes at the electrode interface. The detection limit for ECL was  $2.5 \text{ fg mL}^{-1}$ , resulting in reasonable specificity, stability, and recovery.<sup>322</sup> By modifying electrodes with polyethyleneimine-reduced graphene oxide composites (Pt@AuNRs/Fe-MOFs/PEI-rGO), iron-based MOFs, and gold-platinum core-shell nanorods, a DNA walking machine improves signal quality. For PAT detection, Zr-based MOFs-labeled oligonucleotides loaded with MB (MB@Zr-MOFs-cDNA) serve as signal probes, providing a sensitive electrochemical aptasensor. The Pt@AuNRs/Fe-MOFs/PEI-rGO modified gold electrode shows no change after 60 scans. Its catalytic performance is 250% better than that of a gold electrode. A computed apparent electron transfer rate constant of  $1.64 \text{ s}^{-1}$  confirms high conductivity. With a detection limit of  $4.14 \times 10^{-5} \text{ ng mL}^{-1}$ , the aptasensor with this design has an excellent sensitivity range of  $5.0 \times 10^{-5}$  to  $5.0 \times 10^{-1} \text{ ng mL}^{-1}$ .<sup>323</sup>

Guo *et al.* introduced an innovative assay for detecting PAT contamination in food. Their approach was based on the secondary structure of the aptamer, resulting in a unique truncation strategy. By eliminating the stem-loop structure, they optimized P-30, a truncated version of the PAT aptamer. In this assay, the gold nanocluster-modified aptamer functioned as the fluorescent probe, while BSA-directed  $\text{MnO}_2$  nanoflakes served as the receptor. The intensification of fluorescence signal in this DNase I-assisted aptasensor arises from the efficient Förster resonance energy transfer (FRET) between Au nanocluster-labeled aptamers and  $\text{MnO}_2$  nanoflakes, where patulin binding induces aptamer desorption and fluorescence recovery. Specific recognition is driven by hydrogen bonding (*e.g.*, between PAT's hydroxyl and carbonyl groups and aptamer bases like A3, T5, C4) and  $\pi$ - $\pi$  stacking interactions (*e.g.*, between PAT's furan ring and adenine residues such as A25), ensuring selective target capture and signal amplification. The assay was effective in apple and grape juice samples, with a detection limit of  $8.5 \text{ ng L}^{-1}$ .<sup>324</sup> A GCE sensor was carefully designed for quick and sensitive detection of PAT. Anti-patulin-BSA IgG was produced by rabbits and immobilized on a graphene oxide/gold nanocomposite. Anti-PAT-BSA IgG on the GCE sensor can collect mycotoxin PAT in samples. IgG and PAT interaction reduced electron transfer resistance and IgG's spatial obstruction effect on the GCE sensor. PAT detection was made possible by recent modifications to the immobilized anti-PAT-BSA IgG GCE sensor, which showed a linear relationship with PAT concentration. With a detection limit of  $5 \text{ } \mu\text{g L}^{-1}$ , the immuno-electrochemical GCE sensor can detect PAT in under a minute.<sup>325</sup> In traditional Chinese medicine, PAT produced from *Crataegus pinnatifida* Bge and *Semen Coicis* can be rapidly detected electrochemically using a ratiometric aptasensor that utilizes  $\text{NH}_2\text{-MIL-101@MB}$  and an innovative catalytic  $\text{MnCo@C}$  nanoprobe in conjunction with a straightforward and effective multi-amplification technique.  $\text{NH}_2\text{-MIL-101@MB}$ 's electrode surface modification provided a baseline electrical signal, improving sensor dependability. Redox processes and electron transfer efficiency increased by a new enzyme-mimetic  $\text{MnCo@C}$ . The detection limit of the PAT sensor is  $0.040 \text{ fg mL}^{-1}$  ( $S/N = 3$ ), and its linear range is  $1.00 \times$

$10^{-4}$  to  $1.00 \times 10^1 \text{ pg mL}^{-1}$ . With recovery rates of 90.6–106.3% and 90.2–103.1%, respectively, and RSD values of 1.21–4.70% and 3.18–5.00%, the aptasensor detected PAT in *Crataegus pinnatifida* Bge and *Semen Coicis*.<sup>326</sup> Table 6 enlists the sensing parameters of PAT as determined by various investigators.

**3.1.7 Citrinin.** Before World War II, in 1931, Hetherington and Raistrick isolated citrinin (CIT) from *Penicillium citrinum* Thom. Then, it was discovered in more than a dozen species of *Penicillium*, such as *P. citrinum*, *P. expansum*, *P. radicola*, and *P. verrucosum*, as well as various *Aspergillus* species, including *A. terreus*, *A. oryzae*, and *A. niveus*. Notably, *A. oryzae* is utilized in the production of traditional foods like sake, miso, and soy sauce. Specific strains of *Penicillium camemberti* play a crucial role in cheese-making processes.<sup>360</sup> Industrial strains, such as *Monascus ruber* and *Monascus purpureus*, are used to produce pigments and contribute to the production of CIT.<sup>361</sup> In China, these strains have been harnessed to generate culinary colors, specifically red and yellow hues. Historically, *Monascus* species have been integral to food production and preservation in the Orient, with traditional uses including the fermentation of red wine, the production of red soybean cheese, food coloring, and meat preservation. Additionally, *Monascus* products are recommended for various medical applications.<sup>362</sup>

A study conducted in 1987 revealed that three species of *Penicillium* were capable of producing CIT from around 1400 isolates derived from food and feed cultures. *P. citrinum*, a mesophilic organism, thrives at temperatures between 5 and 40 °C, with an optimal growth range of 26 to 30 °C. It prefers a pH level between 5.0 and 7.0, and as a xerophile, it requires a water activity of 0.8 to 0.84 for development. This fungus typically grows in conditions of 25 to 30 °C and 30 to 35% humidity, making it a significant mycotoxigenic species in rice. While CIT can be produced at temperatures from 15 to 37 °C, with peak production around 30 °C, the influence of water activity on toxin generation remains unclear.<sup>361</sup> Furthermore, recent studies on human toxicokinetics indicate that 40% of CIT is excreted in urine, suggesting effective absorption by the kidneys and liver.<sup>363</sup>

CIT was initially acknowledged for its antibacterial effects against Gram-positive bacteria; however, its therapeutic application has been limited due to the nephrotoxic impacts observed in animals. These adverse effects primarily target the kidneys, while also presenting potential risks to the liver and bone marrow.<sup>364</sup> Notably, Japanese yellow rice sickness is associated with CIT, a significant nephrotoxin in animals, which has been responsible for multiple outbreaks of illness in both animals and humans.<sup>365</sup> The acute toxicity of CIT varies among species, with median lethal doses reported as  $57 \text{ mg kg}^{-1}$  for ducks,  $95 \text{ mg kg}^{-1}$  for chickens, and  $134 \text{ mg kg}^{-1}$  for rabbits. Monogastric animals, such as dogs and pigs, are also susceptible to its toxic effects.<sup>360</sup> CIT induces necrosis in the distal tubule epithelium of the kidneys, disrupts kidney function, and leads to degeneration of renal tubular processes. Additionally, as a hepatonephrotoxin, CIT compromises both kidney structure and function while altering liver metabolism by inhibiting respiratory chain enzymes in the mitochondria of the liver and renal cortex.<sup>366</sup>





Table 6 Sensing parameters of PAT as determined by various analytical techniques

S. No.	Method	Analyte	Electrode modifier	Linear range	LOD	Sample/recovery	Ref.
1	EC impedimetric aptasensor	PAT	—	1–25 ng mL <sup>-1</sup>	1.25 ng mL <sup>-1</sup>	Apple juice/92.5–96%	327
2	DPV	PAT	rGO/SnO <sub>2</sub> /GCE	50–600 nM	0.6635 nM	Apple juice/74.33–99.26%	316
3	EC	PAT	MIP/Au@Cu-MOF/N-GQDs/GCE	0.001–70 ng mL <sup>-1</sup>	0.0007 ng mL <sup>-1</sup>	Apple juice/97.6–99.4%	318
4	EC	PAT	MIP/thionine-PtNP-NGE/GCE	0.002–2 ng mL <sup>-1</sup>	0.001 ng mL <sup>-1</sup>	Apple juice/99.8–113.0%	328
5	EC	PAT	PAT/aptamer-AuNP-BP NSs/GCE	0.1–10 μM	0.03 nM	Grape juice/95.4–104.8%	329
6	DPV	PAT	PAT/MCH/Apt/DpAu/ZnONRs-CS/AuE	50 ng mL <sup>-1</sup> –0.5 pg mL <sup>-1</sup>	0.27 pg mL <sup>-1</sup>	Apple juice/96.2–104%	330
7	CE	PAT	—	1–100 μg kg <sup>-1</sup>	0.3 μg kg <sup>-1</sup>	Apple juice/94–98%	331
8	HPLC-DAD	PAT	—	5 ng mL <sup>-1</sup> –10 μg mL <sup>-1</sup>	1.5 μg kg <sup>-1</sup>	Strawberries/53.1–103.6%	332
9	UPLC-MS/MS	PAT	—	42–757 μg kg <sup>-1</sup>	50 μg L <sup>-1</sup>	Apple/76–84%	333
10	EC	PAT	MIP/Fe <sub>3</sub> O <sub>4</sub> /GO/GCE	42–1298 μg kg <sup>-1</sup>	12.5 μg kg <sup>-1</sup>	Apple juice/102–108%	317
11	SWV	PAT	Anti-patulin-BSA/IgG/GCE	0.001 nM–250.0 nM	3.33 × 10 <sup>-4</sup> nM	Apple juice	317
12	EIS	PAT	Fe <sub>3</sub> O <sub>4</sub> NPs/rGO/PAT/TDNs-Apt/AuE	5–200 μg L <sup>-1</sup>	5 μg L <sup>-1</sup>	—	325
13	DPV	PAT	—	5 × 10 <sup>-8</sup> –5 × 10 <sup>-1</sup> μg L <sup>-1</sup>	30.4 fg mL <sup>-1</sup>	Apple juice/96.9–105%	334
14	CV	PAT	MIP/PPD-NPC/GCE	1–25 μM	3.56 ng mL <sup>-1</sup>	Apple juice/94.4%	335
15	EIS	PAT	—	0.01–10 μg L <sup>-1</sup>	7.5 × 10 <sup>-3</sup> μg L <sup>-1</sup>	Juice (apple & grape)/94–99.8%	336
16	SPES	PAT	Aptamer/G-Bi <sub>2</sub> S <sub>3</sub> /ITO	5.0–500 nM	0.28 nM	Apple juice/97.7–104.8%	337
17	DPV	PAT	BSA/Apt/HPC-COOH/GCE	0.5–5.0 × 10 <sup>6</sup> ng L <sup>-1</sup>	0.25 ng L <sup>-1</sup>	Apple juice and haw juice/86.2–105.4%	321
18	CV	PAT	—	0.0154–15.4 ng mL <sup>-1</sup>	0.043 ng mL <sup>-1</sup>	Apple, pear, and tomato/95.0–106.7%	338
19	SWV	PAT	cDNA/aptamer/AuNPs-BPNS/GCE	0.01–10 ng mL <sup>-1</sup>	9.8 pg mL <sup>-1</sup>	Apple juice/86%	339
20	EIS	PAT	Patulin/pAb-patulin/GO/GCE	50 fg mL <sup>-1</sup> –500 ng mL <sup>-1</sup>	30 fg mL <sup>-1</sup>	Apple	340
21	EC	PAT	CdTe QDs/Au NRS	0.01 × 10 <sup>-7</sup> –0.10 μg mL <sup>-1</sup>	—	Apple juice/98.20–102.70%	341
22	PEC	PAT	MCH/PAT-aptamer & AuNPs-BSA/GCE	In buffer & apple juice medium	In buffer (0.18 pg mL <sup>-1</sup> ) & In apple juice (0.47 pg mL <sup>-1</sup> )	Apple juice/91.24–93.47%	342
23	Amperometry EC (EIS, CV & DPV)	PAT	Ni-NiO-streptavidin-BSA-aptamer-GCE	(1–10 <sup>4</sup> pg mL <sup>-1</sup> )	(0.47 pg mL <sup>-1</sup> )	Apple juice/more than 85%	343
24	Dual-EATR	PAT	AgPdNPs/c-DNA/reaction solution/MCH/DNAMix/AuNFS(Ig-C <sub>3</sub> N <sub>4</sub> /AuE)	10–10 <sup>6</sup> fg mL <sup>-1</sup>	1.65 fg mL <sup>-1</sup>	Apple juice/95.5–110%	344
25	SPR	PAT	AuNPs/FeMOF-PEI-GO/AuE	5 × 10 <sup>-6</sup> –50 μg L <sup>-1</sup>	0.92 fg mL <sup>-1</sup>	Apple juice/91.0–103%	345
26	SERS	PAT	—	5 × 10 <sup>-7</sup> –5 ng mL <sup>-1</sup>	0.217 fg mL <sup>-1</sup>	Apple juice/98.24–98.32%	346
27	EC	PAT	MIP-ir-Au/PDMS/AO NH <sub>2</sub> -MIL-101@MB	5 × 10 <sup>-10</sup> –5 × 10 <sup>-6</sup> M	0.011 nM	Apple juice/96.43–112.83%	347
28	FRET	PAT	—	1.00 × 10 <sup>-4</sup> –1.00 × 10 <sup>1</sup> pg mL <sup>-1</sup>	0.040 fg mL <sup>-1</sup>	Grataegus pinnatifida Bgel/90.6–106.3%	326
29	FRET	PAT	—	0.01–100 ng mL <sup>-1</sup>	0.003 ng mL <sup>-1</sup>	Semen <i>Coicis</i> /90.2–103.1%	348
30	MIP-SERS	PAT	—	15–35 μg L <sup>-1</sup>	6 ng L <sup>-1</sup>	Apple juice/93.33–105.21%	349
31	Fluorescence-apta assay	PAT	—	7.00 × 10 <sup>-12</sup> –5.00 × 10 <sup>-8</sup> M	5.37 × 10 <sup>-12</sup> M	Fruit products/96–108%	350
				5–600 ng mL <sup>-1</sup>	0.13 μg L <sup>-1</sup>	Apple juice/96–98%	351



Table 6 (Contd.)

S. No.	Method	Analyte	Electrode modifier	Linear range	LOD	Sample/recovery	Ref.
32	SWV DPV	PAT	Pep&Apta/AuNPs/SPE	0.1 fM–10 nM	0.03 fM	Apple and orange juices/99.3–101.2%	352
33	ECL	PAT	Apt/PTCA/Tb MOG/GCE	0.1 fg mL <sup>-1</sup> –0.1 µg mL <sup>-1</sup>	0.02 fg mL <sup>-1</sup>	Apple and orange juices/96.28–104.0%	353
34	SERS	PAT	—	1–70 ng mL <sup>-1</sup>	0.46 ng mL <sup>-1</sup>	Apple puree/88.77–102.20% Apple juice/90.50–97.36%	319
35	EC	PAT	SINP-CHIT/SPCE	3.2–20 µg mL <sup>-1</sup>	1.15 µg mL <sup>-1</sup>	—	354
36	Fluorescence	PAT	NCDs-SH	0.1–400 ng mL <sup>-1</sup>	0.053 ng mL <sup>-1</sup>	Apple juice/88.9–99.2% Grape juice/92.5–101.8%	355
37	Fluorescence assay	PAT	CM6Iip-SH/NH <sub>2</sub> -Au@Fe <sub>3</sub> O <sub>4</sub>	0.05–20 ng mL <sup>-1</sup>	0.033 ng mL <sup>-1</sup>	Apple and grape juices/ 96.2–107.6%	356
38	FRET-based ratiometric fluorescence	PAT	—	01–50 ng mL <sup>-1</sup>	0.16 ng mL <sup>-1</sup>	Grapes/95.9–105.4%	357
39	ECL	PAT	Anth-CQDs@SiO <sub>2</sub> /Ru@Tri/GE	0.1 pg mL <sup>-1</sup> –10 ng mL <sup>-1</sup>	0.05 pg mL <sup>-1</sup>	Fruits/96–106%	358
40	ECL	PAT	MIP-IL/CS-UiO66@CN/ITO	0.1–10 <sup>3</sup> pg mL <sup>-1</sup>	50 fg mL <sup>-1</sup>	Apple/95.3–102.7%	359

**3.1.7.1 Detection of CIT.** A europium nanoparticle-based fluorescence immunochromatographic assay has been developed to detect CIT in corn samples, achieving limits of detection and IC<sub>50</sub> values with an average recovery rate ranging from 86.3% to 111.6%. The high conductivity and large-surface-area network of metal–MOF composites accelerates electron tunneling of the redox probe, while specific adsorption of the analyte *via* hydrogen bonds (phenolic –OH, lactone C=O), π–π stacking (aromatic cores), and metal–ligand coordination locks it at the interface to modulate local electron density and amplify the faradaic response.<sup>367</sup> Additionally, a ratiometric electrochemical sensor based on a molecularly imprinted polymer (MIP-RECS) has been created to identify CIT. This sensor was produced through the electro-polymerization of thionine and CIT, leveraging a hierarchical porous carbon structure co-doped with boron and nitrogen, which provides a substantial surface area for the anchoring of thionine and citrinin, further enhanced by the presence of an ionic liquid. In this setup, poly(thionine) serves as both a reference probe and a molecularly imprinted polymer. The sensor achieved a low detection limit (1 × 10<sup>-4</sup> ng mL<sup>-1</sup>) and a broad linear detection range (1 × 10<sup>-3</sup>–10 ng mL<sup>-1</sup>) by using [Fe(CN)<sub>6</sub>]<sup>3-/4-</sup> as an indicator probe. When the sensor recognized spiked CIT in samples, a recovery rate of 97–110% was achieved.<sup>368</sup> TDN nanostructures were utilized to construct a dual-signal mode CIT aptasensor in another study. A Fenton-like reaction generated significant electrochemical signals from mesoporous nanozymes of PtPdCo, which exhibit catalase-like catalytic capabilities. Meanwhile, their MB loading capacity ensured autonomous dual signal outputs. The high current derives from the honeycomb-like, large-surface-area PtPdCo mesoporous nanozymes whose trimetallic synergy and mesoporosity slash charge-transfer resistance and catalyze H<sub>2</sub>O<sub>2</sub> in a Fenton-like process to generate electron-rich redox species that tunnel rapidly to the Au transducer, while tetrahedral DNA scaffolds minimize probe entanglement and RecJf Exo cycling amplifies target binding; citrinin is captured through hydrogen bonds between its phenolic –OH/lactone C=O groups and aptamer nucleobases and π–π stacking with its aromatic backbone. Under optimal conditions, the aptasensor demonstrated exceptional detection capabilities, achieving LODs of 1.57 × 10<sup>-3</sup> in SWV mode and 7.67 × 10<sup>-3</sup> ng mL<sup>-1</sup> in DPV mode. This aptasensor shows promise for *in situ* detection due to its accurate dual-signal mode identification and multiple signal amplification.<sup>369</sup>

Tang *et al.* used TDN and *p*-PtNTs to build an electrochemical aptasensor that is both sensitive and accurate for CIT detection. An electrode-anchored TDN-Apt complex was formed when the probe support material, TDN, hybridized with the aptamer. This effectively controls probe spacing and reduces the tangling of Apt electrodes. *p*-PtNTs' large surface area boosts MB loading and DNA strand binding. To form the CIT-Apt complex and detach from the electrode surface, CIT favored binding to Apt. The greater surface area of the porous Pt nanotubes accommodates a large number of MB/DNA1 probes. Together with the spatially organized tetrahedral DNA scaffold that prevents probe entanglement, this enables rapid redox

cycling and seamless electron transfer to the Au electrode. Citrinin is selectively captured *via* hydrogen bonds between its phenolic –OH/lactone C=O groups, and its aptamer bases, as well as by  $\pi$ – $\pi$  stacking with its aromatic core, locking it at the interface to modulate local electron density and amplify the faradaic signal. With a detection limit of  $1.95 \times 10^{-2}$  ng mL<sup>-1</sup> (S/N = 3), the electrochemical aptasensor efficiently detects CIT between 0.1 and  $1 \times 10^4$  ng mL<sup>-1</sup>.<sup>370</sup> Elfadil and colleagues used graphene nanoflakes (GF) from sodium cholate-facilitated solvent-free water-phase exfoliation of graphite to determine CIT quickly electrochemically. The current enhancement occurs because the 2D graphene nanoflakes form a highly conductive, large-surface-area layer that cuts charge-transfer resistance (from  $\sim 3$  k $\Omega$  to  $\sim 0.5$  k $\Omega$ ) and drives an adsorption-controlled, irreversible oxidation of citrinin's phenolic –OH group, while the toxin is “locked” at the interface by  $\pi$ – $\pi$  stacking of its aromatic rings with the sp<sup>2</sup> graphene domains and by hydrogen bonds between its phenolic –OH/lactone C=O groups and the methacrylamide functional monomer, thereby amplifying the faradaic signal. The GF-SC outperformed conventional carbon materials in CIT sensing, enabling repeatable determination at concentrations below the maximum residual limit (LOD = 5  $\mu$ g L<sup>-1</sup>) in food, with a relative standard deviation of 4.5% ( $n = 8$ ). CIT was extracted and purified from red rice, blueberries, turmeric, corn, wheat germ, and rice starch using MIP. The effectiveness of the suggested technology was demonstrated by the reproducible results (RSD < 5.7%,  $n = 3$ ) and precise recoveries (85.8–111.4%) obtained from all samples, which were significantly correlated with CIT quantification *via* LC-MS/MS (relative errors: 9.9–9.1%).<sup>371</sup>

The detection of citrinin, a nephrotoxic mycotoxin commonly found in food products, is illustrated through three innovative biosensing techniques in Fig. 11, highlighting notable improvements in both sensitivity and specificity. Fig. 11a illustrates a molecularly imprinted electrochemical sensor that generates artificial recognition sites through polymerization, offering exceptional selectivity and stability for citrinin detection while addressing the limitations of traditional biological receptors. In Fig. 11b, a groundbreaking nucleic acid-based method is presented, which merges double isothermal amplification with CRISPR-Cas12a technology, resulting in remarkable sensitivity through dual signal amplification and the precise targeting capabilities of the CRISPR system. Lastly, Fig. 11c showcases a state-of-the-art electrochemical aptasensor that combines porous platinum nanotubes with tetrahedral DNA nanostructures, utilizing the enhanced signal amplification of nanomaterials alongside the structural benefits of DNA nanotechnology for highly sensitive quantification of citrinin. These three platforms collectively demonstrate the field's progression from traditional imprinting techniques to sophisticated biomolecular engineering strategies, highlighting how the integration of nanotechnology, molecular biology, and electrochemistry can address the challenges of mycotoxin monitoring. The evolution from synthetic receptor-based detection to nucleic acid amplification technologies and finally to hybrid nanomaterial-DNA systems reflects the growing

demand for more sensitive, specific, and reliable detection methods in food safety applications.

The NH<sub>2</sub>-Fe-MOF nanomaterial serves as an optimal loading platform for aptamers, enhancing sensor detection due to its high specific surface area, biocompatibility, straightforward production process, and low synthesis costs. In the context of CIT, the aptamer binds with specificity, leading to a conformational change that hinders electron transport to the electrode surface. The quantification of CIT can be achieved by examining the DPV responses associated with the peak current of the [Fe(CN)<sub>6</sub>]<sup>3-/4-</sup> system. After thorough experimental optimization, the aptasensor exhibited an impressive detection limit of  $4.52 \times 10^{-11}$  g mL<sup>-1</sup>. Given its remarkable stability and selectivity, this aptasensor shows significant potential for the ultra-sensitive detection of CIT in practical applications.<sup>374</sup> Additionally, a molecularly imprinted polymer combined with SiO<sub>2</sub> nanoparticles infused with Ru(bpy)<sub>3</sub> and NCQDs was utilized to develop an ECL sensor for CIT detection. High ECL current and sensitivity stem from the dual-coreactant electron transfer between Ru(bpy)<sub>3</sub><sup>3+</sup> and NCQDs on the high-surface-area SiO<sub>2</sub> support, which slashes charge-transfer resistance and accelerates Ru(bpy)<sub>3</sub><sup>\*</sup> formation, while citrinin's phenolic –OH and lactone/carboxyl C=O groups form hydrogen bonds with the poly(*p*-aminothiophenol) MIP's –NH<sub>2</sub> sites and  $\pi$ – $\pi$  stack with its aromatic backbone to secure selective binding and signal gating. This ECL sensor demonstrated sensitivity, stability, and reproducibility, with a detection limit of 5 fg mL<sup>-1</sup>. The ECL intensity showed a strong correlation with the logarithm of CIT concentration, spanning from 1.0 to 100 pg mL<sup>-1</sup>. Furthermore, the relative standard deviation for CIT detection in rice and millet remained below 6.1%, while recovery rates for spiked standards ranged from 95.5% to 102.0%.<sup>375</sup> A comparison of the CIT detection parameters across various sensing platforms is presented in Table 7.

### 3.2 Bacterial toxins

Foodborne pathogens, primarily bacteria, account for approximately 40% of infections, posing significant challenges to public health and the economy.<sup>389,390</sup> The prevalence of foodborne illnesses increasingly burdens healthcare systems worldwide. In the United States alone, around 48 million individuals are affected by these diseases annually, resulting in 128 000 hospitalizations, 3000 fatalities, and an economic impact of \$15.6 billion.<sup>391</sup> These pathogens contaminate food and water supplies, leading to severe health issues. While bacteria, viruses, and parasites are the primary culprits behind most foodborne diseases, fungal infections have also been recognized as a significant contributor. Bacteria are particularly concerning, accounting for the majority of hospitalizations (63.9%) and fatalities (63.7%). Infections caused by these microorganisms can lead to a range of health complications, including gastrointestinal distress, kidney disease, cognitive decline, inflammatory joint disorders, vision impairment, and even death.<sup>392</sup> Foodborne illnesses can arise from toxins produced by bacteria and fungi that may remain even after food has been prepared. These harmful agents can contaminate



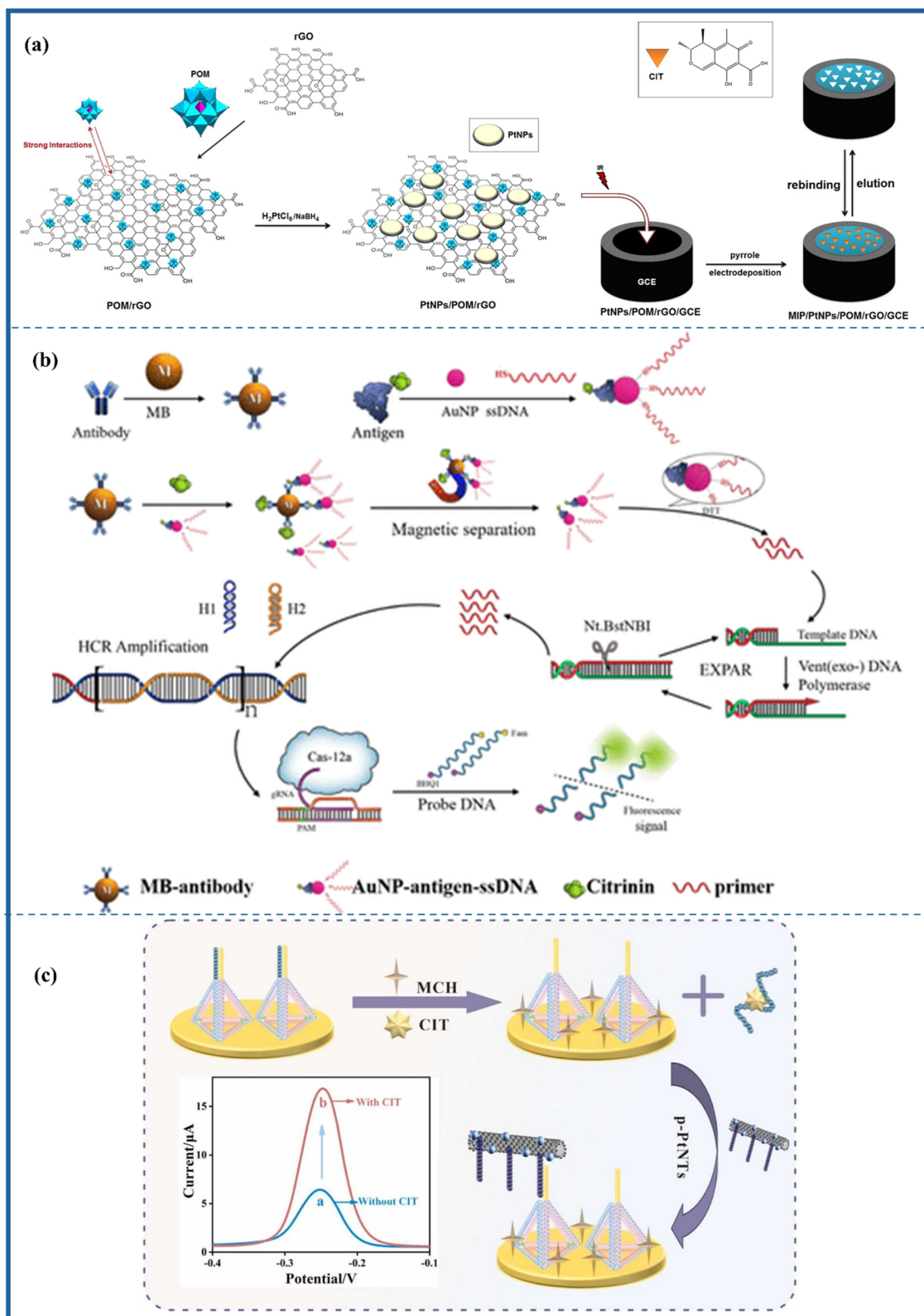


**Fig. 11** (a) Schematic representation for the determination of citrinin based on a molecularly imprinted electrochemical sensor, reproduced from ref. 372 with permission from Elsevier, copyright 2016. (b) Principle of using double isothermal amplification and CRISPR-Cas12a for detection of citrinin, reproduced from ref. 373 with permission from American Chemical Society, copyright 2021. (c) Schematic representation for the ultrasensitive detection of citrinin using an electrochemical aptasensor, reproduced from ref. 370 with permission from Elsevier, copyright 2024.





Table 7 Detection of CIT using a variety of analytical methods along with their LODs

S. No.	Method	Analyte	Electrode modifier	Linear range	LOD	Sample/recovery	Ref.
1	ECL	CIT	MIP/NCQDs/ Ru(bpy) <sub>3</sub> @SiO <sub>2</sub>	$1.0 \times 10^{-3}$ – $1.0 \times 10^{-1}$ ng mL <sup>-1</sup>	$5.0 \times 10^{-6}$ ng mL <sup>-1</sup>	Red rice/95.5–102% Millet/99.2–102%	375
2	SWV	CIT	MIP/[APMim]Br/ BN-HPC/GCE	$1.0 \times 10^{-2}$ – $10$ ng mL <sup>-1</sup>	$1.0 \times 10^{-4}$ ng mL <sup>-1</sup>	Red yeast rice/98.4–102% Rice/97.3–112% Wheat/102–107% Oat/97–104% Flour/105–111% Human serum	368 373 376 and 377
3	Cas12a/EXPAR-HCR	CIT	—	0.005–500 µg mL <sup>-1</sup>	0.127 ng mL <sup>-1</sup>	—	373
4	FRET-based immunosensor	CIT	—	$1 \times 10^{-12}$ – $6 \times 10^{-12}$ M	$1 \times 10^{-13}$ M	—	376 and 377
5	Spectrofluorimetry	CIT	—	0–0.15 µg mL <sup>-1</sup>	1.0 µg kg <sup>-1</sup>	Red fermented rice/91.6–95.0%	377
6	UiO66-MOF	CIT	—	0.08–1.00 µM	0.042 µM	Wheat and feeds	378
7	DF-ICA	CIT	—	—	0.06 ng mL <sup>-1</sup>	Corn/86.3–111.6%	367
8	HPLC-FLD	CIT	DNAI/MB/p-PNTs/ MCH/TDN-Apt/AuE	$0.1$ – $1 \times 10^4$ ng mL <sup>-1</sup>	$1.95 \times 10^{-2}$ ng mL <sup>-1</sup>	Corn/97.02–99.04%	370
9	ic-ELISA	CIT	—	5.9–230 µg mL <sup>-1</sup>	0.6 µg mL <sup>-1</sup>	Wine/intra-assay (84.7–92.0%) and inter-assay (83.6–91.6%)	379
10	HPLC	CIT	—	0.005–50 µg g <sup>-1</sup>	0.001 µg g <sup>-1</sup>	Apple and pear/84–101%	380
11	DPV	CIT	cDNA/MB/PPdCo MNZs/MCH/TDN-Apt/AuE	$0.01$ – $1 \times 10^4$ ng mL <sup>-1</sup>	$7.67 \times 10^{-3}$ ng mL <sup>-1</sup> (DPV)	Cornmeal/96.98–104.15% (DPV) and 101.17–108.01% (SWV)	369
	SWV	—	—	—	$1.57 \times 10^{-3}$ ng mL <sup>-1</sup> (SWV)	Red yeast rice/96.81–103.84% (DPV) and 102.49–107.22% (SWV)	381
12	UHPLC-MS/MS	CIT	—	1–1000 µg kg <sup>-1</sup>	0.07 µg kg <sup>-1</sup>	Red rice/82–92% RYR/90–104%	382
13	X27-based real time immune-PCR (rtIPCR)	CIT	—	0.1–1000 ng mL <sup>-1</sup>	0.08 ng mL <sup>-1</sup> 20 ng mL <sup>-1</sup>	Rice flour/90.0–104.6% Flour/75.8–110.0%	382
14	LC-MS/MS	CIT	—	—	(in <i>Monascus</i> -rice or <i>Monascus</i> products)	Urine/94.8–107%	383
15	CZE	CIT	—	4.5–150.0 µg kg <sup>-1</sup>	0.14 ng mL <sup>-1</sup> (in urine)	Plasma/96.2–109%	384
16	UHPLC-HRMS	CIT	—	>LOD–4.0 ng mg <sup>-1</sup>	1.5 µg kg <sup>-1</sup>	Peper/98%	385
17	ciELISA	CIT	—	—	0.003 ng mL <sup>-1</sup>	Urine/70–86%	386
18	RAFTPP-HPLC	CIT	MIP/NIP	1–100 µg kg <sup>-1</sup>	0.04 ng mL <sup>-1</sup>	Wheat/87.1–115.6%	387
19	DPV	CIT	—	0.1– 0.1–10000 ng mL <sup>-1</sup>	0.35 µg kg <sup>-1</sup>	Corn/86.6–107.9	374
20	HPLC	CIT	—	50–200 µg kg <sup>-1</sup>	$4.52 \times 10^{-11}$ g mL <sup>-1</sup> 3 µg kg <sup>-1</sup>	Rye/98–100.0% Dark tea/89.87–98.92%	388

a variety of foods, including raw meat, poultry, vegetables, fruits, eggs, dairy products, and cooked seafood. The prevalence of foodborne diseases represents a significant public health challenge in both developed and developing nations.<sup>393,394</sup> Certain foods can enhance the interaction between bacterial toxins and host cells, leading to alterations in signaling pathways and changes in cell structure. This interaction may result in symptoms such as nausea, vomiting, and diarrhea. To improve food safety, it is crucial to enhance the identification of harmful bacteria. Traditional methods for biochemical identification and targeted microbiological diagnosis of microbial pathogens are often costly and time-consuming. Consequently, there is a growing trend towards the development of rapid, accurate, and portable detection methods.<sup>394</sup> Fig. 12 illustrates a range of detection techniques, including electrochemical biosensors that translate toxin interactions into quantifiable electrical signals, colorimetric biosensors that facilitate visual detection through observable color changes, immunosensors that leverage antibody–antigen interactions for targeted identification, and fluorescence assays that utilize fluorescent markers for enhanced sensitivity. Collectively, these technologies address the need for rapid, sensitive and field-deployable toxin monitoring in food safety applications.

**3.2.1 Detection of bacterial toxins.** Zhou *et al.* developed a method for detecting bacterial toxins by leveraging the “collateral effect” of RNase activity that occurs after the recognition of target RNA, in conjunction with the programmability

of crRNA. This approach, known as CCB detection (CRISPR-Cas13a-based bacterial detection), utilized *Staphylococcus aureus* (*S. aureus*) as the model organism for testing. The analyte's key functional groups (phenolic –OH, carbonyl C=O and aromatic moieties) engage the modifier *via* hydrogen bonds,  $\pi$ – $\pi$  stacking and metal–ligand coordination, locking the target at the interface and amplifying the faradaic current. The CCB detection method successfully identified target genomic DNA, demonstrating a limit of detection of 1 CFU mL<sup>–1</sup>.<sup>395</sup> In parallel, the need for rapid screening tests for botulinum neurotoxins (BoNTs), which are produced by the soil bacterium *Clostridium botulinum* and can cause botulism, has become increasingly critical. Traditional methods, such as the mouse lethality assay, require 2–5 days for results, hindering timely food safety and medical responses. To address this, Caratelli *et al.* introduced an innovative paper-based sensor that detects BoNT/A and BoNT/C without the use of antibodies. This sensor utilizes a synthetic peptide that mimics SNAP-25, coupled with an electroactive chemical, MB, on an AuNPs-enhanced electrode. The biosensor, designed to work with a smartphone-assisted potentiostat, achieved a detection limit of 10 pM and demonstrated linearity up to 1 nM, marking a significant advancement in rapid toxin detection. Using spiked orange juice samples, this biosensor demonstrated recovery values of 104 ± 6% and 98 ± 9% for BoNT/A concentrations of 1 nM and 0.5 nM.<sup>396</sup> Due to its severe toxicity and potential for use in bioterrorism, BoNT identification is crucial for both national security and public

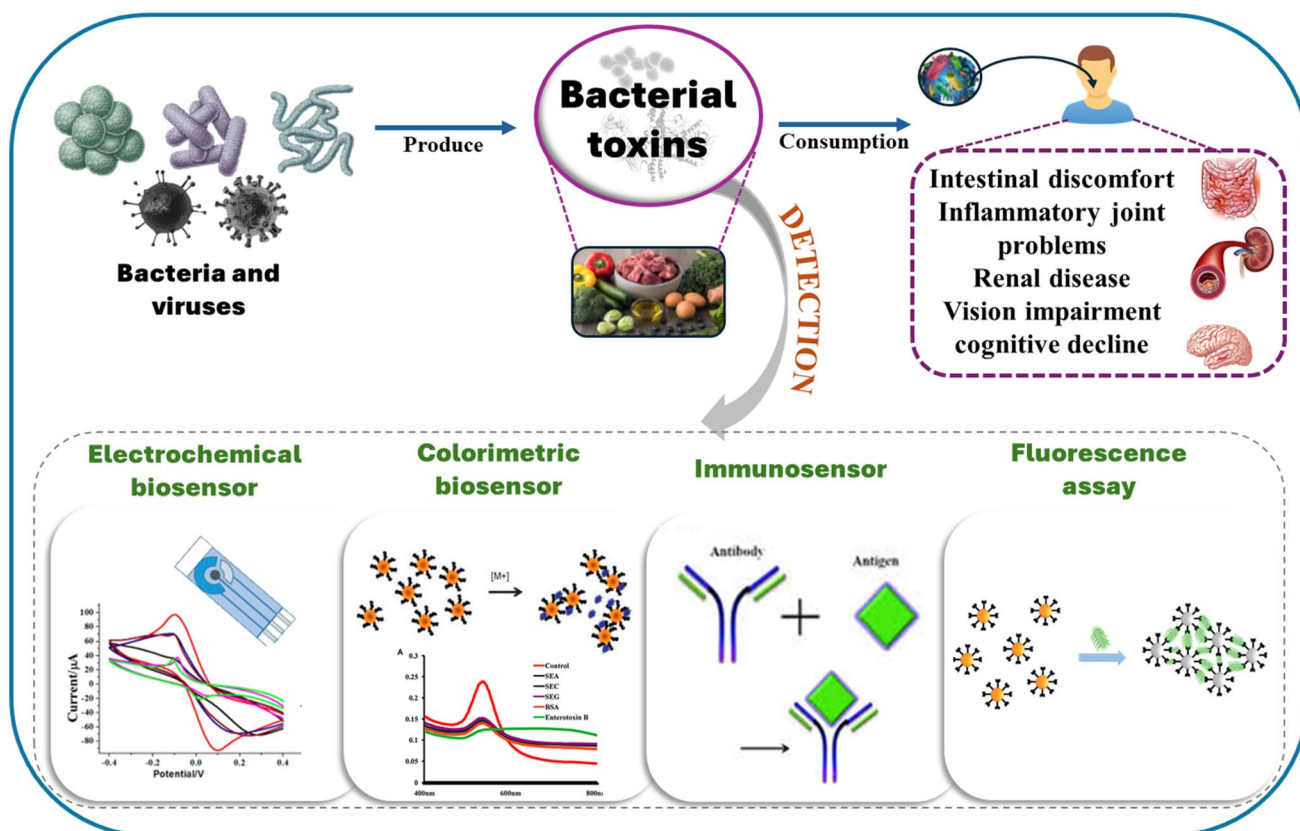


Fig. 12 Schematic representation of major biosensor types employed for detecting biological (bacteria, viruses) and chemical food toxins.



health. Another study used structural switching, systematic evolution of ligands by exponential enrichment, and BOSS-SELEX to find a BoNT-specific aptamer. When attached to BoNT with high affinity, a novel aptamer (BoNT-A4) undergoes structural modification, resulting in a more refined colorimetric detection method that utilizes tyramide signal amplification. The ultrahigh current stems from the modifier's highly conductive, large-surface-area network, which reduces charge-transfer resistance and accelerates faradaic electron flow to the transducer. Meanwhile, target binding drives a structural switch in the aptamer that further gates electron tunneling. BoNT is detected at  $5.72 \text{ ng mL}^{-1}$ . It has no response with other toxins or bovine serum albumin, proving its BoNT specificity.<sup>397</sup>

Pathogenic *Staphylococcus aureus* is identified using an electrochemical detector that incorporates a functional two-dimensional MOF nanozyme. This method enables the precise targeting of *S. aureus* through a dual recognition approach, utilizing vancomycin in conjunction with an *anti-S. aureus* antibody. The two-dimensional MOF serves as an effective electrochemical signal transducer for measuring bacterial concentration, thanks to its peroxidase-like activity, which facilitates the conversion of *o*-phenylenediamine into 2,2-diaminoazobenzene. Under optimal conditions, this bioassay achieves a detection limit of  $6 \text{ CFU mL}^{-1}$ .<sup>398</sup> A conductive poly(3-thiopheneacetic acid) (BICP) film, imprinted with bacteria, served as an impedimetric sensor for the rapid, sensitive, and label-free detection of *S. aureus*. The BICP film was applied directly to a gold electrode, streamlining the process by eliminating the need for harmful organic solvents or cross-linkers, thereby promoting an environmentally friendly approach. Extensive evaluations of the imprinting and recognition components were conducted to enhance sensing performance. Under optimal conditions, the BICP-based impedimetric sensor demonstrated a wide linear detection range of 10 to  $108 \text{ CFU mL}^{-1}$ , a low detection limit of  $2 \text{ CFU mL}^{-1}$ , and a swift recognition time of just 10 minutes, while also exhibiting remarkable selectivity, universality, and repeatability.<sup>399</sup>

Pathogenic microorganisms present significant health hazards, necessitating the rapid identification and eradication of bacteria. Robby *et al.* developed a wireless sensor capable of detecting bacteria through electrochemical and luminescent methods. This sensor employs fluorescent carbon dots (FCDs) derived from electrochemically produced cationic polymers, which are further enhanced by the application of catechol moieties. These modifications improve the photothermal antibacterial properties when combined with near-infrared-responsive cesium tungsten oxide ( $\text{CsWO}_3$ ). While the fluorescence emitted by the  $\text{CsWO}_3$ -FCD nanohybrids is substantial, the cationic nature of the FCD surface diminishes this emission, whereas the anionic bacterial cell wall amplifies it. Electrochemical techniques can evaluate the interaction between the sensor and bacteria by measuring changes in resistance before and after bacterial attachment. This research established a limit of detection for *Staphylococcus aureus* at  $131 \text{ CFU mL}^{-1}$  and for *Escherichia coli* at  $70 \text{ CFU mL}^{-1}$  using the luminescent approach. In contrast, the electrochemical method demonstrated remarkable sensitivity, with detection limits

below  $10 \text{ CFU mL}^{-1}$  for both bacterial strains.<sup>400</sup> Due to the health risks associated with consuming contaminated food, foodborne bacteria must be identified promptly. Using a rGO-CNT nanocomposite, Appaturi *et al.* developed a hydrothermal biosensor for the rapid, accurate, and label-free electrochemical detection of harmful microbes, such as *Salmonella enterica*. An amino-modified DNA aptamer improved the nanocomposite on GCE. To detect DPV bacteria, the ssDNA/rGO-CNT/GCE aptasensor was used. By integrating the improved electrical characteristics and ease of chemical operation of rGO and CNT to create a stable interface, the aptasensor yields synergistic results. Under ideal conditions, *S. Typhimurium* was detected by the aptasensor at concentrations ranging from  $10^1$  to  $10^8 \text{ CFU mL}^{-1}$ , with a detection limit of  $10^1 \text{ CFU mL}^{-1}$ .<sup>401</sup>

### 3.3 Marine biotoxins

Marine biotoxins (MBs) infiltrate the food chain primarily through organisms such as algae-eating fish, prawns, and shellfish. Among the diverse array of marine toxins, those found in shellfish are particularly hazardous.<sup>401</sup> These biotoxins are produced by marine algae, bacteria, and invertebrates, posing significant risks to human health, aquatic species, and overall ecosystems. The classification of biotoxins is determined by their chemical structure, origin, and mechanism of action, with three main categories identified: peptide, polyether, and alkaloid.<sup>402</sup> Chemically classified peptide poisons are small organic entities composed of multiple amino acid molecules. Peptide poison research has focused on conotoxins obtained from sea anemones and sea snakes.<sup>403</sup> The venom of *Conus vulgaris* produces conotoxin, a compact neurotoxin with disulfide bonds. Conotoxins are categorized by neuromuscular targets:  $\alpha$ -,  $\mu$ -,  $\omega$ -,  $\sigma$ -,  $\kappa$ -, and  $\lambda$ -conotoxin. The venom of sea anemone cnidocytes contains anemone polypeptide toxin, a neurotoxin.<sup>404</sup> Voltage-gated  $\text{Na}^+$ ,  $\text{K}^+$ , and other ion channels are the targets of the toxins. Enzymes, polypeptides, and small peptides, including  $\alpha$ -neurotoxins, are released by sea snakes, which operate as postsynaptic neurotoxins.<sup>405</sup>

A significant heteroatom-to-carbon ratio and the presence of multiple oxygenated ether rings are characteristic of organic polyether toxins. These toxins are primarily categorized into trapezoidal, linear, and macrolide structures. Notable examples include ciguatoxin, palytoxin, and brevetoxin. The organism *Gambierdiscus toxicus* is known to produce ciguatoxin (CTX), a particularly potent trapezoidal polyether toxin.<sup>406</sup> Human health is threatened by trophic-level bioaccumulation in aquatic species. Palythoa's linear polyether toxin PTX is one of the most dangerous and complex marine biotoxins.<sup>407</sup> Nudibranch species produce the macrolide polyether toxin BTX, threatening marine fish and humans.<sup>404</sup> Nitrogenous alkaloid poisons with complex carbon frameworks are secondary metabolites in aquatic organisms. Alkaloid poisons include tetrodotoxin, saxitoxin, and gonyautoxin.<sup>60</sup> Pufferfish and other creatures have TTX, an amino pyrroloquinazoline neurotoxin that paralyzes neurons and muscles. Clams and mussels are rich in STX, a potent guanidinoamine neurotoxin.<sup>60</sup>



Marine biotoxins present considerable threats to human health, wildlife, and the economy. When marine biotoxin levels exceed safety thresholds, they can lead to a range of health issues, including acute and chronic conditions, allergic reactions, and even cancer. These potent toxins primarily affect the digestive, neurological, and cardiovascular systems. For instance, adults ingesting over 40.00  $\mu\text{g}$  of okadaic acid (OA) may experience symptoms such as chills, nausea, vomiting, diarrhea, and abdominal pain. While fatalities are rare, OA is closely linked to an increased risk of cancers affecting the liver, pancreas, colon, stomach, and esophagus.<sup>404</sup> Although STX is not harmful to shellfish, at a deadly dose of 300.00  $\mu\text{g}$ , it can cause paralysis, headaches, fever, and respiratory failure in people. Acute, potent, mild, and relatively toxic are the four levels of CTX affecting the neurological, cardiovascular, and digestive systems.<sup>408</sup> Marine biotoxins directly affect poisoning symptoms and can cause irreparable harm or death. Marine biotoxin events are closely monitored because they affect the area's economic and industrial development. The sale of algae, mussels, prawns, and fish with excessive marine biotoxin levels is illegal. The stability of these poisons makes food processing difficult and unprofitable. Thus, exceeding the safe marine biotoxin limit not only costs the aquaculture company money but also harms tourists and the aquatic ecosystem.

**3.3.1 Detection of marine biotoxins.** STX, a potent small-molecule cyanotoxin, is characterized by its high toxicity, water solubility, and resistance to both acids and heat, raising

significant health and environmental concerns in marine ecosystems. Consequently, detecting STX, even at trace levels, is crucial. Raju *et al.* developed an electrochemical peptide-based biosensor that utilizes differential pulse voltammetry signals to accurately identify STX across various sample types. This biosensor incorporates a nanocomposite of Pt-Ru@C/ZIF-67, created by infusing zeolitic imidazolate framework-67 (ZIF-67) with bimetallic Pt-Ru nanoparticles. The STX-binding peptide adsorbs *via* coordination to unsaturated Co sites and  $\pi$ - $\pi$  interactions, and saxitoxin's guanidinium and carbonyl moieties engage the peptide through hydrogen bonds and hydrophobic (aromatic) stacking to gate the faradaic signal. With a detection limit of 26.7  $\text{pg mL}^{-1}$ , the enhanced screen-printed electrode can identify STX concentrations ranging from 1 to 1000  $\text{ng mL}^{-1}$ . The biosensor's exceptional sensitivity and selectivity for STX detection suggest its potential for developing portable bioassays to monitor aquatic food chains for various harmful substances.<sup>409</sup> Additionally, Fig. 13 categorizes three main groups of shellfish toxins, detailing their representative toxins, health effects, and relevant biosensing technologies. This figure highlights the significance of advanced biosensors in detecting these toxins, thereby reducing public health risks.

Najeeb *et al.* used two-dimensional layered  $\text{Ti}_3\text{C}_2\text{T}_x$  nano-sheets modified with aptamers to create an electrolyte-insulator-semiconductor STX sensor. Aptamer modification and STX interactions were made possible by MXene's high surface area and functional groups. Capacitance-voltage and

Toxin family	Toxin	Effects	Detection
Paralytic shellfish toxins	 Saxitoxin (STX)	Paralysis, headaches, fever, and respiratory failure	Electrochemical biosensor  Fluorescence biosensor 
Amnesic shellfish toxins	 Domoic acid (DA)	Neurological and gastrointestinal disorders	Colorimetric biosensor 
Diarrhetic shellfish toxins	 Okadaic acid (OA)	Liver, pancreas, colon, stomach, and esophageal cancers	SERS biosensor  SPR Sensor 

Fig. 13 Classification of three principal shellfish toxin groups, their representative toxins, associated health effects, and corresponding bi-sensing technologies.





Table 8 Analytical parameters of various methods used for the detection of bacterial &amp; marine biotoxins

Sr No.	Method	Analyte	Electrode modifiers	Linear range	LOD	Sample/recovery	Ref.
1	CCB	<i>Staphylococcus aureus</i>		$10^6$ – $10^7$ CFU mL <sup>-1</sup>	1 CFU mL <sup>-1</sup>		395
2	Signal-off	Botulinum neurotoxins (BoNTs)	—	0.01–10 nM	10 pM	Orange juice/98–104%	396
3	SELEX	Botulinum neurotoxins (BoNTs)	—	0–500 ng mL <sup>-1</sup>	5.72 ng mL <sup>-1</sup>	—	397
4	DPV	<i>Staphylococcus aureus</i>	Ab <sub>2</sub> /AuNPs/ MOFs/BSA/GCE	$10$ – $7.5 \times 10^7$ CFU mL <sup>-1</sup>	6 CFU mL <sup>-1</sup>	—	398
5	EIS	<i>Staphylococcus aureus</i>	BICP/PTAA/S. aureus	$10$ – $10^8$ CFU mL <sup>-1</sup>	2 CFU mL <sup>-1</sup>	Milk/103.6–122.5%	399
6	DPV	Saxitoxin (STX)	Pt–Ru@C/ZIF-67/SPE	1–1000 ng mL <sup>-1</sup>	26.7 pg mL <sup>-1</sup>	Fresh water	409
7	EIS	Saxitoxin (STX)	—	1.0–200 nM	0.03 nM	—/103%	410
8	SWV	Saxitoxin (STX)	pPtNPs/STX aptamer	10 pg mL <sup>-1</sup> –1 μg mL <sup>-1</sup>	4.669 pg mL <sup>-1</sup>	Freshwater	411
9	EIS	Ciguatoxins (CTXs)	O + V + CTX1B/MB	0.5–32 pg mL <sup>-1</sup>	—	Fish	412
10	DPV	Saxitoxin (STX)	Au/APT/MCH/STX	0.3–30 μg L <sup>-1</sup>	0.3 μg L <sup>-1</sup>	—	413
11	CV	Tetrodotoxin (TTX)	MIP/SPGE	5.0–25.0 μg mL <sup>-1</sup>	1.14 μg mL <sup>-1</sup>	Muscle/81.0–110.2%	414
12	DPV	Domoic acid (DA)	CB-SPEs	5000–0.016 ng mL <sup>-1</sup>	1.7 ng mL <sup>-1</sup> (in buffer) and 1.9 ng mL <sup>-1</sup> (in mussel extract)	—	415
		Okadaic acid (OA)		100–0.01 ng mL <sup>-1</sup>	0.15 ng mL <sup>-1</sup> (in buffer) and 0.18 ng mL <sup>-1</sup> (in mussel extract)		
13	EC	Domoic acid (DA)	PDA-rGO/PAM/GCE	1–600 nM	0.31 nM	Mussel extract	416

constant-capacitance experiments demonstrated that the apta-sensor could detect STX, exhibiting good sensitivity and specificity. The highly conductive scaffold enables dense aptamer loading and ultralow interfacial impedance, allowing STX-induced aptamer conformational shifts to produce pronounced charge redistribution and capacitance/potential changes. STX binds the aptamer through electrostatic attraction of its guanidinium groups to the phosphate backbone and hydrogen bonds between its hydroxyl/carbonyl moieties and nucleobase functionalities. With a detection limit of 0.03 nM, the range of detection was between 1.0 and 200 nM.<sup>410</sup> To identify STX in natural freshwater samples with high signal fidelity, a round-type micro-gap electrode (RMGE) was developed. With 15 pairs of equal electrode wire lengths between gaps, the RMGE improves signal fidelity. The effectiveness of the biosensor was evaluated using LOD and selectivity studies on natural freshwater samples. With a detection limit of 4.669 pg mL<sup>-1</sup>, the biosensor showed good selectivity in freshwater samples ranging from 10 pg mL<sup>-1</sup> to 1 µg mL<sup>-1</sup>.<sup>411</sup>

Cell-based biosensors (CBBs) designed to detect marine neurotoxins, including CTXs, have gained significant popularity due to their ability to achieve low limits of quantification by leveraging sensitive brain cells that produce a comprehensive toxicological response. The development and validation of these biosensors are intricate processes, primarily because they involve living materials and necessitate effective signal transduction methods. In this study, Neuro-2a cells were integrated onto thin-film gold electrodes. The viability of these cells after exposure to CTX1B was evaluated using methylene blue as a redox indicator, in conjunction with light optical microscopy, cyclic voltammetry, and differential pulse voltammetry. The resulting LOQ was determined to be 0.93 pg CTX1B mL<sup>-1</sup>.<sup>412</sup> Additionally, an electrochemical impedimetric biosensor employing a specific aptamer was utilized to detect saxitoxin, leveraging the exceptional sensing capabilities of aptamers in conjunction with a non-invasive, label-free electrochemical impedance approach. The enhanced sensitivity is driven by electrostatic repulsion and aptamer-analyte complex formation *via* non-covalent interactions such as hydrogen bonding and van der Waals forces, rather than direct covalent bonding between functional groups. The device demonstrated significant selectivity and high sensitivity in negative control tests, successfully identifying saxitoxin concentrations above 0.3 µg L<sup>-1</sup>, suggesting its potential as a viable alternative for monitoring waterborne toxins.<sup>413</sup>

Marine biotoxin tetrodotoxin (TTX) is closely associated with the biosynthesis of pufferfish. The distribution is mainly in Asian and tropical maritime environments. Climate change may be a contributing factor to the spread of this class of toxins across Europe. Following this incident, the European Union and the European Food Safety Authority introduced TTX control and monitoring systems for marine products throughout the European Union. Therefore, it is essential to improve analytical technologies to guarantee food safety, particularly for fish and shellfish. Rocha *et al.* developed an electrochemical sensor that measures TTX using MIP. Using voglibose as a template, *ortho*-phenylenediamine was electro-polymerized to form an MIP. The

screen-printed gold electrode MIP sensor was examined using cyclic voltammetry. DPV and [Fe(CN)<sub>6</sub>]<sup>3-/4-</sup> were used as a redox probe in the study. With a detection limit of 1.14 µg, the designed sensor exhibited a linear response over the range of 5.0 to 25.0 µg mL<sup>-1</sup>. TTX had excellent selectivity due to its high imprinting efficiency. Recoveries of 81.0, 110.2, and 102.5 percent for external standard addition at doses of 30.0, 44.0, and 60.0 µg kg<sup>-1</sup> with relative standard deviations below 15% were obtained from recovery assays on spiked mussel samples, confirming the utility of the sensor.<sup>414</sup>

An electrochemical immunosensor was developed by Nelis *et al.* to detect marine biotoxins, including okadaic acid and domoic acid (DA). The sensors employed high-throughput carbon black-modified screen-printed electrodes (CB-SPE). To assess the electrochemical performance and stability, CV and EIS were conducted on both carbon black-modified and bare carbon solid polymer electrolytes. The results indicated that CB-SPEs demonstrated superior stability and electrocatalytic properties compared to conventional solid polymer electrodes, maintaining these advantages for at least six months. Two indirect competitive immunosensors were developed using DPV after biofunctionalizing the CB-SPEs with DA or okadaic acid protein conjugates. The DPV signals from these immunosensors showed impressive detection limits (LOD = 1.7 ng mL<sup>-1</sup> for DA in buffer; LOD = 1.9 ng mL<sup>-1</sup> for DA in mussel extract; LOD = 0.15 ng mL<sup>-1</sup> for OA in buffer; LOD = 0.18 ng mL<sup>-1</sup> for OA in mussel extract) and aligned well with dose-response curves ( $R^2 > 0.98$ ).<sup>415</sup> Both humans and marine life are neurotoxically affected by amnesic shellfish toxin, also known as DA. The development of precise and rapid DA monitoring systems is necessary to reduce poisoning incidents. An electrochemical MIP sensor using PDA-rGO/PAM was able to detect dopamine (DA). PDA-rGO enhanced the PAM loading capacity and charge transfer rate, thereby improving the MIP sensor's electrical signal responsiveness. The domoic acid is selectively captured in PAM's imprinted cavities *via* hydrogen bonds between its carboxyl/hydroxyl groups and the polymer's amide moieties, gating local electron flow and delivering excellent sensitivity. With a linear range of 1 to 600 nM and the ability to detect as low as 0.31 nM, the SPE modified with PDA-rGO/PAM responded well to toxin-contaminated samples.<sup>416</sup> Table 8 presents the LODs and linearity ranges of various analytical methods for the detection of bacterial & marine biotoxins.

## 4. Chemical toxins

### 4.1 Pesticides

Pesticides play a crucial role in agriculture for controlling pests due to their effective fungicidal and insecticidal properties.<sup>417</sup> They play a vital role in safeguarding food and animal feed throughout various stages, including production, processing, storage, transportation, and marketing. Pesticides can be categorized based on the type of organism they target, such as herbicides, insecticides, fungicides, rodenticides, and pediculicides. Additionally, they can be classified according to their physical characteristics and chemical makeup, which includes synthetic, organic, inorganic, and biological (biopesticide)



varieties.<sup>418</sup> Among the most frequently utilized pesticides are organochlorines, organophosphates, and carbamates. However, it is crucial to implement effective detection and control measures, as pesticides can lead to adverse health effects, including skin and eye irritation, headaches, dizziness, nausea, and more serious conditions like cancer, asthma, and diabetes.

**4.1.1 Detection of pesticides.** Wu *et al.* developed a homogeneous electrochemical sensor for detecting organophosphate pesticides by utilizing nanozymes, specifically 2D MnO<sub>2</sub> sheets, which exhibit both oxidase and peroxidase-like activities. This sensor utilizes dissolved O<sub>2</sub> as a co-reactant, effectively eliminating the interference from H<sub>2</sub>O<sub>2</sub> and color changes. The MnNS facilitates the oxidation of tetramethylbenzidine, resulting in a decrease in the DPV current due to its extensive surface area and distinctive catalytic properties. Additionally, acetylcholinesterase hydrolyzes acetylthiocholine, prompting a strong reaction from MnNS. This innovative approach enables reliable electrochemical detection of organophosphates while inhibiting AChE activity, achieving an LOD of 0.025 ng mL<sup>-1</sup>.<sup>417</sup> MnO<sub>2</sub> nanosheets on paper and a laser-induced graphene electrode on polyimide foil were used to create a novel electrochemical biosensor for the detection of OP residues at the point of care. The ferrocene-tagged hairpin probes are tethered *via* robust Au-S bonds and held in intimate electronic contact, which accelerates redox cycling. At the same time, organophosphorus pesticide inhibition of AChE prevents MnO<sub>2</sub>-triggered probe cleavage, preserving abundant Fc labels at the interface to produce a strong “signal-on” response. No direct covalent or hydrogen bonding occurs between the pesticide and the electrode modifier, since sensing relies on enzyme inhibition rather than analyte-surface interactions. The proposed biosensor exhibited a linear range of 3 to 4000 ng mL<sup>-1</sup> and a detection limit of 1.2 ng mL<sup>-1</sup>, demonstrating exemplary performance in the organophosphate experiment.<sup>418</sup>

Maheshwaran and coauthors hydrothermally synthesized a hybrid AgWO<sub>4</sub>-rGO nanocomposite for the rapid electrochemical detection of Cr(vi). AgWO<sub>4</sub>-rGO nanocomposites are used as electrode enhancers in electrochemical investigations for CQT detection (rGO@AgWO<sub>4</sub>/GCE). With a linear detection range of 1–1108 μM and a sensitive detection limit of 0.0661 μM for electrochemical CQT detection, the rGO@AgWO<sub>4</sub>/GCE showed outstanding catalytic activity. The rGO@AgWO<sub>4</sub>/GCE CQT sensor demonstrated high sensitivity (0.6306 μA μM<sup>-1</sup> cm<sup>-2</sup>), selectivity, and reproducibility.<sup>419</sup> Rashed *et al.* developed a nanocomposite of silver nanoparticles on mesoporous carbon and naturally obtained hematite ore to detect Imidacloprid (IMC) insecticide sensitively and selectively. Electrocatalysis's irreversible, diffusion-governed kinetics involves the exchange of four electrons and four protons during electroreduction. LSV has a linear detection range of 63–870 M, a detection limit of 1.06 μM, and a sensitivity of 0.1955 μA μM<sup>-1</sup> cm<sup>-2</sup> for IMC detection. The amperometric method achieved a detection limit of 0.257 μM and a sensitivity of 0.8113 μA μM<sup>-1</sup> cm<sup>-2</sup> between 10.80 and 195.50 μM.<sup>420</sup> Singh *et al.* created a gold electrode biosensing platform modified with a nanocomposite for the detection of monocrotophos, achieving a low detection limit and high sensitivity. A ZnONFs-rGO nanocomposite was

produced and electrodeposited onto the Au electrode to increase the sensor's catalytic efficiency. The enzymatically generated thiocholine at the electrode; organophosphorus pesticides covalently phosphorylate AChE's active Ser-OH (phosphoester bond), inhibiting ATCl hydrolysis and gating the faradaic response. The linear operating range of the designed biosensor was 0.01–100 nM. The sensor demonstrated good reproducibility, high sensitivity (0.384 μA nM<sup>-1</sup>), and a low detection limit of 0.01 nM.<sup>421</sup> Kumaravel and Muruganathan developed a nanosilver-dodecane electrode for electrochemical fenitrothion detection in potatoes and paddy. In comparison to the electrodes, the LOD was low. The electrode remained stable and sensitive after many analysis cycles.<sup>422</sup>

An electrochemical device utilizing Cu-based MOFs and rGO exhibited enhanced charge transfer, stability, and structural adhesion on electrode surfaces. Paraquat is irreversibly pre-concentrated in the MOF pores *via* the coordination of its bipyridinium nitrogen centers to Cu(II) sites, locking the analyte at the interface and amplifying the faradaic response. Under optimal conditions, DPV (−0.8 to 0.3 V against Ag/AgCl) was used to recognize paraquat in standard solutions. The device exhibited a linear response range from 0.30 to 5.00 μmol L<sup>-1</sup>, achieving detection and quantification limits of 50.0 and 150.0 nmol L<sup>-1</sup>, respectively.<sup>423</sup> In a separate study, Suzan *et al.* developed a CPE augmented with bismuth ferrite microflowers (BiFeO<sub>3</sub>/CPE) for the detection of the neonicotinoid insecticide imidacloprid (IMD) in aqueous samples, alongside fipronil (FIP). The square wave voltammetry technique was employed to evaluate the electrode's performance in spiked water samples, yielding calibration curves for all analytes within the range of 1.0 to 100.0 μM. The LODs for IMD and FIP were determined to be 0.97 and 0.81 μM, respectively, with environmental water samples recovering between 90.0% and 105.0% of both compounds.<sup>424</sup> Additionally, Chen *et al.* addressed the health risks posed by carbendazim (CBZ) residues by developing an electrochemical sensor using polyethyleneimine-carbon nanotubes (PEI-CNTs) and nitrogen-doped carbon nanohorns (N-CNHs) for the detection of CBZ in water. The incorporation of PEI facilitated N-H bonding, resulting in a positively charged surface on the CNT, which enhanced the enrichment of CBZ and allowed for the electrostatic assembly of N-CNHs and PEI-CNTs. This composite exhibited improved electron transfer capacity, electrochemical active surface area, and catalytic activity due to ultrasound-assisted assembly, achieving a remarkable recovery rate of 87.33% to 117.67%, a low detection limit of 4 nmol L<sup>-1</sup>, and a broad linear range from 15 nmol L<sup>-1</sup> to 70 μmol L<sup>-1</sup> under optimal conditions.<sup>425</sup>

## 4.2 Heavy metals

Heavy metals are known to be five times denser than water, and their prevalence in the environment has increased due to urbanization and industrialization. These metals are now found in the air, water, and soil, making their presence a daily concern.<sup>426</sup> The accumulation of heavy metals in mammals can occur through various pathways, including inhalation, ingestion, and skin absorption. Unfortunately, the human body



tends to accumulate these metals at a rate that surpasses its ability to detoxify them, leading to levels that can exceed safe limits.<sup>427</sup> While certain heavy metals serve as essential cofactors and prosthetic groups for various enzymes, the body requires them only in specific amounts.<sup>428</sup> Organic vegetables, leafy greens, fruits, grains, and pulses can provide beneficial heavy metals such as potassium, manganese, molybdenum, and copper. However, exposure to inorganic sources like cadmium, zinc, cobalt, nickel, lead, and iron in their various forms can be toxic, with dietary intake of chromium, cadmium, nickel, and lead posing significant risks to systemic health.

**4.2.1 Detection of heavy metals in food.** Electrochemical detection methods have typically relied on pre-enrichment phases to enhance the detection of heavy metals, a process that can complicate sensing and increase energy consumption. In a novel approach, Gao and colleagues developed a one-step electrodeposition technique to grow Mo-doped WO<sub>3</sub> directly on carbon cloth. This innovative electrode is capable of simultaneously detecting heavy metal ions such as Cd<sup>2+</sup>, Pb<sup>2+</sup>, Cu<sup>2+</sup>, and Hg<sup>2+</sup> across a concentration range of 0.1 to 100.0 μM, with detection limits ranging from 11.2 to 17.1 nM. The effectiveness of this electrode was demonstrated through its application in various food samples.<sup>429</sup> In another study, Bagheri *et al.* explored the use of Cr<sub>2</sub>TiC<sub>2</sub>T<sub>x</sub>, a relatively under-researched MXene, as an adsorbent in ultrasonic-assisted dispersive micro-solid-phase extraction (d-μ-SPE) to identify trace levels of heavy metals in food and soil. This MXene exhibited remarkable performance, achieving detection limits of 0.09 and 1.9 ng mL<sup>-1</sup>, along with dynamic ranges of 0.3–90 μg L<sup>-1</sup> for Cd<sup>2+</sup> and 6–120 μg L<sup>-1</sup> for Pb<sup>2+</sup>.<sup>430</sup>

Huang *et al.* investigated a new boron and nitrogen co-doped carbon (BCN) material derived from metal-organic frameworks (MOFs) for the detection of heavy metal ions. Utilizing square-wave anodic stripping voltammetry, the BCN-modified GCE demonstrated significant electrochemical responses to cadmium (Cd(II)) and lead (Pb(II)), achieving sensitivities of 0.459 and 0.509 μA μM<sup>-1</sup> cm<sup>-2</sup>, respectively, under optimal conditions. Furthermore, the sensor corroborated the results obtained from inductively coupled plasma-mass spectrometry by successfully identifying Cd(II) and Pb(II) in samples of *Beta vulgaris* var. *cicla* L.<sup>431</sup> Cd<sup>2+</sup>, Pb<sup>2+</sup>, Cu<sup>2+</sup>, and Hg<sup>2+</sup> were among the heavy metal ions tested separately and simultaneously using a simple and sensitive Fe<sub>3</sub>O<sub>4</sub>@SiO<sub>2</sub>-based extraction and direct electrochemical detection method. Heavy metal ions were mixed with Fe<sub>3</sub>O<sub>4</sub>@SiO<sub>2</sub> and transferred onto the working electrode to form an electrochemical sensor following alkali treatment. The proposed electrochemical analytical method had a sizeable linear range and a low detection limit for heavy metals. Cd<sup>2+</sup>, Pb<sup>2+</sup>, Cu<sup>2+</sup>, and Hg<sup>2+</sup> had detection limits of 56.1, 16.5, 79.4, and 56.7 nM, respectively. The analytical approach has a 96.0–104.3% recovery rate in real samples and can quantify Cd<sup>2+</sup>, Pb<sup>2+</sup>, Cu<sup>2+</sup>, and Hg<sup>2+</sup>.<sup>432</sup>

Square-wave anodic stripping voltammetry was employed to investigate a fluorinated graphene-gold nanocomposite for the detection of heavy metals. Optimal results were achieved under specific conditions: a buffer pH of 5.0, a deposition potential of –1.25 V, and a deposition time of 140 seconds. The FGP/AuNC

electrode exhibited significant stripping peaks for Zn<sup>2+</sup>, Cd<sup>2+</sup>, and Pb<sup>2+</sup> at voltages of –1.10, –0.77, and –0.50 V, respectively, with large linear ranges of 6–7000, 4–6000, and 6–5000 μg L<sup>-1</sup>, and low detection limits of 0.08, 0.09, and 0.05 μg L<sup>-1</sup>. Furthermore, the electrode was utilized to analyze Zn<sup>2+</sup>, Cd<sup>2+</sup>, Pb<sup>2+</sup>, Cu<sup>2+</sup>, and Hg<sup>2+</sup> in samples of tea, peanuts, and rape bolts.<sup>433</sup> Li *et al.* developed an electrochemical sensing platform that can detect Pb<sup>2+</sup> and Cd<sup>2+</sup> in real food samples without requiring pretreatment. This platform utilizes a combination of silica nanochannels and polydimethylsiloxane, employing differential pulse anodic stripping voltammetry for electrochemical detection. This method involves the electrodeposition of metal species, which are subsequently stripped within the modified silica nanochannels. Under optimized conditions, the linear detection ranges for Pb<sup>2+</sup> and Cd<sup>2+</sup> were determined to be 4 to 1500 μg L<sup>-1</sup> and 30 to 900 μg L<sup>-1</sup>, respectively.<sup>434</sup>

Wang *et al.* developed an electrochemical device for detecting Cd<sup>2+</sup> ions using voltammetry, which utilizes MWCNTs and an amine-functionalized zirconium(IV) metal-organic framework (UiO-66-NH<sub>2</sub>). The UiO-66-NH<sub>2</sub>@MWCNTs composites were synthesized *via* a one-pot hydrothermal method. The combination of MWCNTs, known for their excellent conductivity, and the octahedral structure of UiO-66-NH<sub>2</sub>, which offers a larger surface area, significantly enhances the sensor's efficacy. Under optimal conditions, the sensor demonstrated a linear response range from 0.5 to 170 μg L<sup>-1</sup>, with a detection limit of 0.2 μg L<sup>-1</sup>. It successfully identified Cd<sup>2+</sup> in 21 meat samples, achieving a recovery rate between 95.1% and 107.5% and a relative standard deviation of less than 4.5%.<sup>435</sup> Additionally, a sensitive lead ion sensor for tobacco leaves was developed using a reduced graphene oxide (rGO)/MoS<sub>2</sub>/chitosan (CS) nanocomposite-modified GCE. The incorporation of rGO enhanced the sensor's conductivity, while the nano-flowered MoS<sub>2</sub> provided active sites for heavy metal detection and a significant reaction-specific surface area. Chitosan further enhanced the heavy metal enrichment and electrocatalytic activity of the electrode, resulting in an electrochemical sensor characterized by exceptional stability, repeatability, and resistance to interference. The performance of the Pb<sup>2+</sup> stripping and sensor operation was evaluated using square wave anodic stripping voltammetry, revealing a limit of detection of 0.0016 μM and sensitivity within the range of 0.005 to 2.0 μM.<sup>436</sup>

A cost-effective voltammetric sensor was created for the detection of toxic ions Cd<sup>2+</sup> and Pb<sup>2+</sup> by integrating β-Bi<sub>2</sub>O<sub>3</sub> microspheres with shuttle-like α-Fe<sub>2</sub>O<sub>3</sub> nanoparticles. The synergistic effects of Fe<sub>2</sub>O<sub>3</sub>/Bi<sub>2</sub>O<sub>3</sub> nanocomposites enhanced the deposition-stripping process, resulting in improved electrocatalytic activity compared to other modified electrodes. The Fe<sub>2</sub>O<sub>3</sub>/Bi<sub>2</sub>O<sub>3</sub>/GCE facilitated the simultaneous detection of Cd<sup>2+</sup> and Pb<sup>2+</sup> at nanomolar concentrations, exhibiting a dynamic range of 0.002–4 μM.<sup>437</sup> Additionally, an electrochemical sensor utilizing UiO-66 was developed for the concurrent measurement of these heavy metals, demonstrating a linear detection range of 10–50 μg L<sup>-1</sup> and detection limits of 1.16 μg L<sup>-1</sup> for Cd<sup>2+</sup> and 1.14 μg L<sup>-1</sup> for Pb<sup>2+</sup>. The carbonized UiO-66/Bi/GCE electrode showcased remarkable detection



capabilities, attributed to the increased availability of active sites for Bi and the co-deposition of heavy metal ions, which enhanced electron transport. Furthermore, a decorating method applied to disposable SPCEs yielded detection limits of  $4.67 \mu\text{g L}^{-1}$  for  $\text{Cd}^{2+}$  and  $1.24 \mu\text{g L}^{-1}$  for  $\text{Pb}^{2+}$ , with a linear detection range of 20–120  $\mu\text{g L}^{-1}$ .<sup>438</sup>

### 4.3 Veterinary drug residues

Animal husbandry practices have led to a decrease in disease prevalence and an increase in animal welfare. In this context, the use of antibiotics plays a significant role. However, a lack of awareness regarding proper medical practices and the overuse of these drugs has resulted in antibiotic residues being present in milk, meat, eggs, and honey. These residues pose serious health risks, including mutagenicity, teratogenicity, carcinogenicity, antimicrobial resistance, hypersensitivity reactions, and disruptions to the internal microbiota. While most antibiotics administered to animals are metabolized and excreted, traces that remain in animal tissues can still lead to health issues if ingested.<sup>439</sup> Bacteria gain antibiotic resistance through mutations. After developing antibiotic resistance, bacteria use various self-protection mechanisms, including disrupting the cell wall and nucleic acid synthesis, inhibiting protein synthesis, and changing the outer membrane to alter permeability.<sup>440</sup> Several antibiotics are commonly used, including tetracycline,  $\beta$ -lactamase inhibitors, penicillin, sulfonamides, aminoglycosides such as streptomycin, and macrolides like erythromycin. Oxytetracyclines are frequently used to treat animal infections. Overuse causes accumulation in milk, pork, eggs, and chicken, posing health hazards.<sup>441</sup> While Staphylococcus infections are treated with cloxacillin, a penicillin resistant to  $\beta$ -lactamases, residual microbial diseases in domestic animals may contaminate milk because animal-derived products include varied antibiotic residues that are harmful to humans.<sup>442</sup>

**4.3.1 Detection of veterinary drug residues.** Huang *et al.* developed a flexible electrode device called Co nanoparticle-modified 3D N-doped porous carbon (Co@3D NPC) by integrating a Co-based metal-organic framework (ZIF-67) with polyimide (ZIF-67/PI) using a room-temperature laser ablation technique.<sup>445</sup> This Co@3D NPC electrode exhibited improved electron transport, enhanced physical adsorption, and a larger electrochemically active surface area compared to 3D NPC electrodes made solely from polyimide film. Additionally, the Co@3D NPC electrode technology proved effective in detecting two widely used veterinary drugs and insecticides, clozapine and albendazole, achieving detection limits of 2.8 nM and 2.5 nM, respectively, along with detection sensitivities of  $410.47 \mu\text{A } \mu\text{M}^{-1} \text{cm}^{-2}$  for clozapine and  $580.33 \mu\text{A } \mu\text{M}^{-1} \text{cm}^{-2}$  for albendazole. The Co@3D NPC electrode device exhibited remarkable stability and precision, highlighting its potential for practical applications.<sup>443</sup> Promethazine (PHZ), a sedative used in veterinary medicine, poses potential risks to humans. Detecting PHZ through electrochemical methods presents a practical solution; however, conventional electroanalytical techniques face challenges when applied directly to meat

samples due to matrix interference. In a pioneering study, Yang *et al.* achieved sensitive and selective detection of PHZ in beef and beef liver using differential pulse voltammetry (DPV) combined with magnetic solid-phase extraction. They developed a magnetic adsorbent by coating  $\text{CoFe}_2\text{O}_4$ /graphene with C18-functionalized mesoporous silica (MG@mSiO<sub>2</sub>-C18), which effectively isolates PHZ, minimizing the influence of contaminants and concentrating the analyte on the magnetic electrode. The modified N-doped hollow carbon microspheres (HCM) further enhance the electrochemical signal of PHZ. This integrated detection method demonstrates a low detection limit of  $9.8 \text{ nmol L}^{-1}$  and a wide linear range from  $0.08 \mu\text{mol L}^{-1}$  to  $300 \mu\text{mol L}^{-1}$ , with promising recovery rates in beef samples, indicating its potential for rapid and efficient identification of PHZ in meat products.<sup>444</sup>

Dimetridazole (DMZ), a derivative of nitroimidazole, has been utilized as an antibiotic for treating bacterial and protozoal infections in poultry. However, the presence of DMZ residues poses health risks to humans. To enhance the detection of DMZ, Behera and colleagues developed a novel electrocatalyst. They created a Cu-integrated poly(aniline) (PANI) electrocatalyst, termed PANI-Cu@BSA, through a one-step biomimetic mineralization and polymerization process that employed bovine serum albumin (BSA) as a stabilizing agent. This synthesized PANI-Cu@BSA was further encapsulated with rGO using ultrasonication. The resulting nanocomposite, PANI-Cu@BSA/rGO, exhibited remarkable electrical conductivity, water dispersibility, and effective nanoscale particle performance. A screen-printed carbon electrode modified with the PANI-Cu@BSA/rGO nanocomposite was then utilized for the sensitive electrochemical detection of DMZ. Compared to both the PANI-Cu@BSA/rGO/SPCE and the bare SPCE in phosphate-buffered saline, the modified electrode exhibited a significantly higher current intensity. The combination of PANI-Cu@BSA and rGO facilitated the formation of analyte-electrode junctions characterized by high conductivity and increased active surface areas, thereby enhancing electron transfer between the electrode and the analyte. The PANI-Cu@BSA/rGO/SPCE demonstrated linear detection ranges of 1.78 nM, a sensitivity of  $5.96 \mu\text{A } \mu\text{M}^{-1} \text{cm}^{-2}$ , and a detection limit that underscores its effectiveness for analytical applications.<sup>445</sup> Furaltadone (FTD), a nitrofurantoin derivative used in veterinary medicine, poses environmental and health risks due to the toxic nature of its organic components. To facilitate the electrochemical detection of FTD, an activated SPCE was modified with hydrothermally synthesized  $\text{CuCoO}_2$ , employing CV and DPV. This modified SPCE/ $\text{CuCoO}_2$  electrode demonstrated a broad linear detection range of 0.1–316  $\mu\text{M}$ , significantly improved sensitivity of  $21.03 \mu\text{A } \mu\text{M}^{-1} \text{cm}^{-2}$ , and a detection limit of 1.79 nM.<sup>446</sup>

Veterinary medicine employs the broad-spectrum antibiotic tetracycline (TC) to address various health issues; however, the presence of its residues in food and beverages raises significant concerns. This necessitates the development of an efficient, cost-effective, and straightforward method for detecting TC in aquatic environments. Wang *et al.* introduced a nanocomposite sensor for tetracycline detection, utilizing bismuth carbide (BiC) nanofibers modified with AuNPs and a TC aptamer. The



incorporation of AuNPs enhances electrochemical detection and facilitates the binding of the TC aptamer. The electrochemical performance of the BiC@Au@Apta sensor was assessed using CV and DPV, revealing a detection range of 0.001–100  $\mu\text{M}$  and LOD of 2.92 nM under optimal conditions, along with impressive stability ( $I = 97.30\%$ ), repeatability, and resistance to interference. Additionally, antimicrobial resistance (AMR) poses a significant socioeconomic challenge to public health, with  $\beta$ -lactams being the most frequently prescribed treatments for various bacterial infections. The routine use of antibiotics contributes to the emergence of AMR in both humans and animals. In response, Kolhe *et al.* developed an electro-immunosensor designed to detect and mitigate antibiotic misuse in food products derived from animals. This sensor utilized a recessed nano-disk array electrode (RNE) created from a PEO-*b*-PMMA amphiphilic block copolymer, which was subsequently immobilized with Penicillin and Cefalexin antibodies. The RNE working electrode demonstrated limits of detection of 14.8 and 13.8 pM for penicillin and cefalexin, respectively, showcasing strong selectivity against non-specific antibiotics.<sup>447</sup>

#### 4.4 Food additives

Food additives are deliberately incorporated into food products to fulfill specific technological or sensory roles that improve the quality of these items, as long as they remain within legally established limits. Any substance that is meant to modify the properties of food, whether directly or indirectly, and thus becomes part of the food itself, is categorized as a food additive.<sup>448,449</sup> To be recognized as such, a substance must be deemed safe for its intended use by qualified experts based on scientific evidence. However, many synthetic preservatives, including sulfites, benzoates, sorbates, and nitrates, raise health concerns due to their potential harmful effects.<sup>450</sup> While these artificial preservatives are effective in preventing spoilage and prolonging shelf life, the impact of natural preservatives, such as nisin, on gut microbiota remains under-researched. Research has shown that certain dietary additives can trigger inflammation and worsen metabolic diseases by altering gut microbiota,<sup>449</sup> particularly affecting vulnerable populations such as children, who are more susceptible to the adverse effects of these additives. Therefore, it is essential to investigate further the significant influence of food additives on gut microbiota, potentially utilizing *in vitro* models of the human gastrointestinal system.<sup>451</sup> Some additives, like monosodium glutamate (MSG) and artificial sweeteners, have been associated with addictive properties that may influence eating behaviors, resulting in compulsive consumption and overeating due to their impact on brain function.<sup>452</sup> The ongoing debate regarding the health implications of food additives is fueled by inconsistent research findings on their toxicity and effects. Nonetheless, these additives must be used within legal limits, raising concerns about their proper identification and regulation.

**4.4.1 Detection of food additives.** The excessive reliance on flavor enhancers in food marketing diminishes the nutritional integrity of products. Vanillin (VAN), a widely used flavor

enhancer, necessitates accurate detection methods. This study introduces an electrochemical sensor utilizing a modified electrode made from  $\text{La}_2\text{NiO}_4$ -functionalized carbon nanofibers (f-CNF) to identify VAN in food samples. Through electrochemical analysis employing CV and DPV, the sensor exhibited a sensitivity of  $0.2899 \mu\text{A} \mu\text{M}^{-1} \text{cm}^{-2}$  and LOD of 6 nM. Testing with food samples confirmed the modified electrode's effective electrocatalytic properties for VAN detection, achieving a high recovery rate.<sup>453</sup> Taouri *et al.* conducted measurements of VAN in food samples utilizing an electrochemical sensor.<sup>457</sup> The sensor incorporated a carbon paste electrode featuring a fullerene (FNT) nanostructure along with functionalized multi-walled carbon nanotubes. For the electrochemical analysis, cyclic voltammetry was applied after optimizing parameters such as pH, accumulation time, and supporting electrolytes. Following this optimization, the nanostructured sensor demonstrated a detection limit of  $3.4 \times 10^{-8} \text{ mol L}^{-1}$ , with linear responses observed between  $5 \times 10^{-8}$  and  $9 \times 10^{-6} \text{ mol L}^{-1}$  at trace levels, and from  $10^{-5}$  to  $10^{-4} \text{ mol L}^{-1}$  for higher concentrations. Notably, VAN was removed entirely after 300 seconds of adsorption at concentrations below  $10^{-5} \text{ mol L}^{-1}$ .<sup>454</sup> Nehru *et al.* developed a hydrothermal method to synthesize  $\text{g-C}_3\text{N}_4\text{NTs@MoS}_2$  and evaluated its electrochemical performance for VAN detection. This sensor was engineered to produce a stronger current signal by utilizing various electrolytes and optimizing its settings. Under ideal conditions, the sensor demonstrated sensitivity of  $3.48 \mu\text{A} \mu\text{M}^{-1} \text{cm}^{-2}$ , limit of detection (4 nM), and extensive linear ranges (0.005–458.9  $\mu\text{M}$ ) using DPV.<sup>455</sup>

Sebastian *et al.* investigated the electrochemical detection of tert-butylhydroquinone (TBHQ), a potentially harmful food preservative.<sup>456</sup> They employed sonochemical techniques to develop a nanocomposite by combining  $\beta$ -cyclodextrin ( $\beta$ -CD)-functionalized carbon black with various metal oxides, such as ZnO, CuO, and MgO. The resulting nanocomposite underwent extensive characterization through multiple methods. Notably, the screen-printed carbon electrode-based nanocomposite exhibited remarkable electrocatalytic performance for TBHQ detection, achieving a sensitivity of  $22.67 \mu\text{A} \mu\text{M}^{-1} \text{cm}^{-2}$  and a detection limit of 1 nM. In a related study, Balram *et al.* developed an electrochemical sensor for TBHQ by sonochemically integrating spinel  $\text{Co}_3\text{O}_4$  nanorods with surface-functionalized carbon black (FCB), resulting in a hybrid nanocomposite. The synthesis involved co-precipitation with oxalic acid to create highly porous  $\text{Co}_3\text{O}_4$  nanorods, while acid treatment was employed to oxidize the carbon black. The modified electrode exhibited excellent electrochemical performance, allowing for TBHQ detection with a sensitivity of  $7.94 \mu\text{A} \mu\text{M}^{-1} \text{cm}^{-2}$  and a detection limit of 1 nM.<sup>457</sup>

Rajaji and his team utilized traditional solvothermal and hydrothermal methods to produce binary nanosheets of  $\text{Bi}_2\text{Te}_3$ . To enhance electrocatalytic performance, they synthesized  $\text{Bi}_2\text{Te}_3/\text{g-C}_3\text{N}_4$  binary nanosheets *via* a hydrothermal process. The electrochemical characteristics of the modified GCEs featuring  $\text{Bi}_2\text{Te}_3/\text{g-C}_3\text{N}_4$  BNs were assessed using DPV, EIS, and CV. The  $\text{Bi}_2\text{Te}_3/\text{g-C}_3\text{N}_4$  BNs electrode demonstrated high sensitivity and a low detection limit in identifying ractopamine



in food samples.<sup>458</sup> Nejad *et al.* designed a screen-printed graphite electrode (SPGE) incorporating MnO<sub>2</sub> nanorods within a graphene oxide nanocomposite (MnO<sub>2</sub> NRs/GO) for the detection of sunset yellow. Electrochemical techniques, including chronoamperometry, DPV, CV, and LSV, confirmed the effective oxidation of sunset yellow on the MnO<sub>2</sub> NRs/GO/SPGE. The CV results indicated that the MnO<sub>2</sub> NRs/GO nanocomposite exhibited electrocatalytic activity, with the electrode showing a linear response for sunset yellow concentrations ranging from 0.01 to 115.0 μM under optimal DPV conditions, achieving an LOD of 0.008 μM. Fig. 14 illustrates the identification of chemical toxins through various biosensing technologies, while Table 9 summarizes the detection of pesticides, heavy metals, veterinary drug residues, and food additives using diverse analytical methods.

Reported literatures predominantly focus on sensor performance in controlled environments; however, it is crucial to comprehend the physical and chemical interactions that influence sensor effectiveness within complex food matrices. Each sensor type has specific known interferences from the matrix, such as lipid and protein fouling in electrochemical sensors, and background fluorescence or quenching in optical techniques. The current document discusses typical sample

preparation methods necessary for achieving low detection limits, while also addressing common causes of false positives and negatives. It presents the validation levels as reported by the original authors, which may include buffer-only limits of detection, multi-matrix laboratory validations, inter-laboratory assessments, or field pilot studies. To emphasize the applicability of the data, a specific column for sample recovery has been incorporated into the tables, connecting the reported sensors to practical applications.

## 5. Future prospects and conclusions

The food toxin detection field is advancing thanks to innovations in sensor technology, including biosensors and chromatographic sensors. These improvements in sensitivity, specificity, and response speed, along with portable, user-friendly devices, drive this progress. Biosensors, leveraging biological recognition elements like enzymes, antibodies, and nucleic acids, now incorporate nanomaterials such as graphene and gold nanoparticles to enhance signals and lower detection limits. Flexible and wearable biosensors enable continuous, real-time food monitoring and early contamination alerts. Their

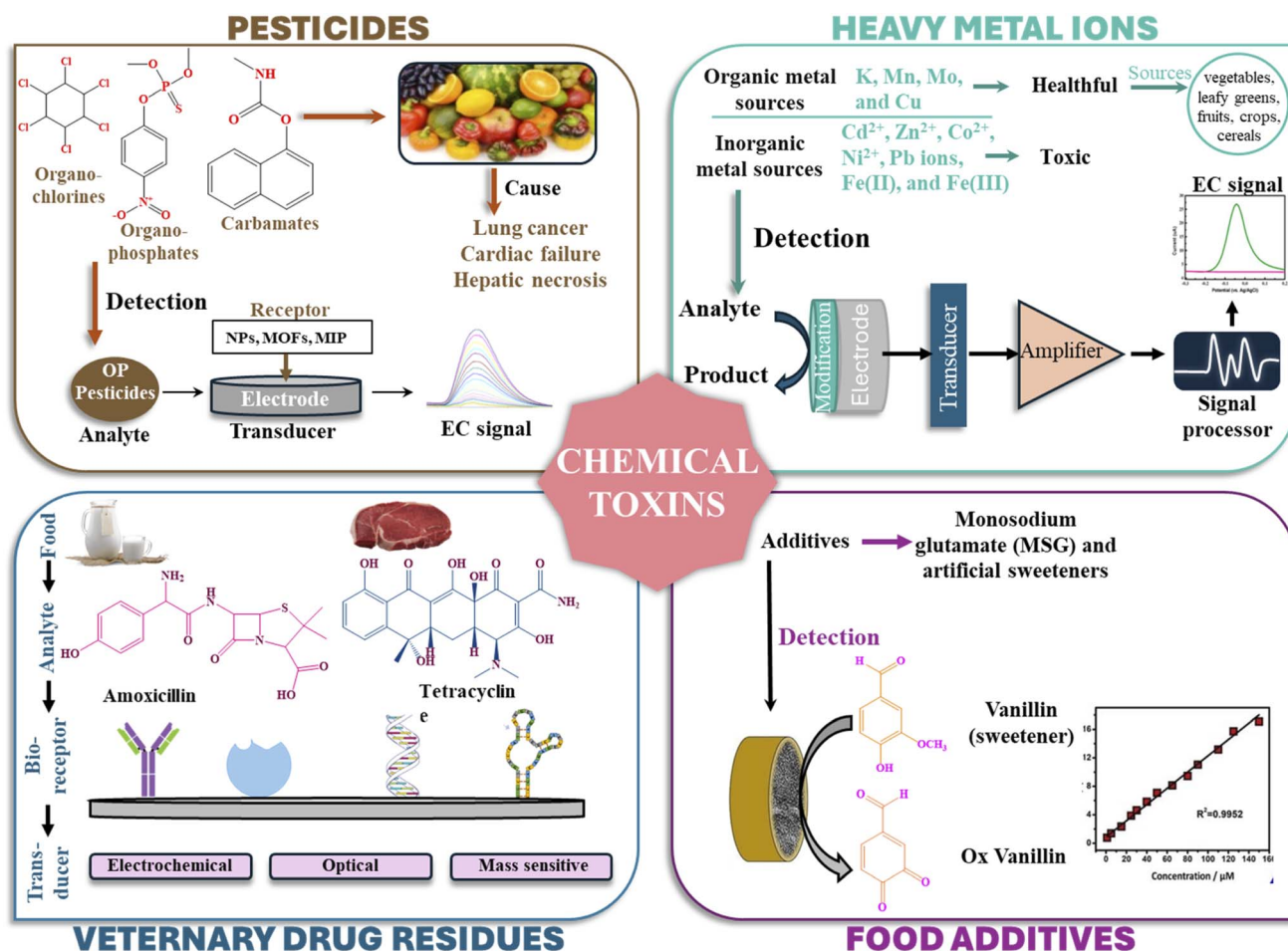


Fig. 14 Chemical toxins and their identification through various biosensing technologies.





Table 9 Detection of pesticides, heavy metals, veterinary drug residues, and food additives by electrochemical methods

Sr No.	Method	Analyte	Electrode modifier	Linear range	LOD	Sample/recovery	Ref.
1	DPV	Organophosphate pesticides (Ops)	TMB-MnNS-ATCh-AChE	0.1–20 ng mL <sup>-1</sup>	0.025 ng mL <sup>-1</sup>	Pakchoi/99.72–102.41%	417
2		Pesticides (Ops)		3–4000 ng mL <sup>-1</sup>	1.2 ng mL <sup>-1</sup>		418
3	EC	Chrisquat	rGO@AgWO <sub>4</sub> /GCE	1–1108 μM	0.0661 μM		419
4		Imidacloprid (IMC) pesticide		10.80–195.50 μM	0.257 μM		420
5	EC	Monocrotophos pesticide	ZnONFs/rGO/Au	0.01–100 nM	0.01 nM		421
6	DPV	Paraquat	CuMOF/rGO/Au	0.30–5.00 μmol L <sup>-1</sup>	50.0 nmol L <sup>-1</sup>	River, tap water and human blood serum/98–104%	423
7	SWV	Imidacloprid (IMD)	N-CNHS/PEI-CNTs/GCE	15 nmol L <sup>-1</sup> –70 μmol L <sup>-1</sup>	0.97 μM	Environmental water/90.0–105.0%	424
8	EC	Carbendazium (CBZ)	ChOx/PBCB <sup>ethalin</sup> e-HNO <sub>3</sub> <sup>rTD</sup> /MWCNT/GCE	0.8–30 μM	4 nmol L <sup>-1</sup>	Water/87.33–117.67%	425
9	EC	Dichlorvos			1.59 nM	Orange juice/99.7–103.2%	459
10	CV	Profenofos Phorate	BSA/Apt/rGO-CuNPs/SPCE	0.01–100 nM	3 pM	River water/80–92%	460
		Isocarphos		1–1000 nM	300 pM		
		Omethoate		0.1–1000 nM	30 pM		
		Diazinon (DZN)		1–500 nM	300 pM		
11	CV		DZN/thiolated aptamer/AuNPs/SPGES	0.0304–304 ng mL <sup>-1</sup>	0.005 ng mL <sup>-1</sup>	Plasma of Male Wistar rat/96.0–99.30%	461
12	SWV	Sulfentrazone (SFZ)	SPE-MWCNT	1.0–25 μmol L <sup>-1</sup>	0.8 μmol L <sup>-1</sup>	Soy milk/98.67%	462
13	Electrodeposition	Heavy metal ions (HMIs)	Mo-WO <sub>3</sub> /CC	0.1–100.0 μM	11.2–17.1 nM	Groundwater/99.00%	429
14	d-μ-SPE	Heavy metal ions (Cd <sup>2+</sup> and Pb <sup>2+</sup> )	—	0.3–90 μg L <sup>-1</sup>	0.09 ng mL <sup>-1</sup>	Food and soil	463
				6–120 μg L <sup>-1</sup>	1.9 ng mL <sup>-1</sup>		
				1–150 μg L <sup>-1</sup>	0.41 μg L <sup>-1</sup>		
15	SWASV	Cd(II) Pb(II) (HMIs)	BCN-Nafion/GCE	2–150 μg L <sup>-1</sup>	0.93 μg L <sup>-1</sup>	<i>Beta vulgaris</i> var. <i>Cicla</i> L/101.56–104.81%	431
16	DPSV	HMIs					432
17	CV	Zn <sup>2+</sup>	FGP/AuNC/GCE	6–7000 μg L <sup>-1</sup>	0.08 μg L <sup>-1</sup>	Milk/96.0–104.3% Peanut/98.5% (Zn <sup>2+</sup> ), 105% (Cd <sup>2+</sup> ), and 104% (Pb <sup>2+</sup> )	433
				4–6000 μg L <sup>-1</sup>	0.09 μg L <sup>-1</sup>	Rape bolt/94.5% (Zn <sup>2+</sup> ), 105% (Cd <sup>2+</sup> ), and 101% (Pb <sup>2+</sup> )	
				6–5000 μg L <sup>-1</sup>	0.05 μg L <sup>-1</sup>	Tea/99.0% (Zn <sup>2+</sup> ), 102% (Cd <sup>2+</sup> ), and 102% (Pb <sup>2+</sup> )	
18	EIS	Cd <sup>2+</sup> Pb <sup>2+</sup> Cu <sup>2+</sup> Hg <sup>2+</sup>	FGP/AuNC/GCE	4–4000 μg L <sup>-1</sup>	0.19 μg L <sup>-1</sup>	Peanut/104% (Cu <sup>2+</sup> ) and 95.5% (Hg <sup>2+</sup> )	433
				6–5000 μg L <sup>-1</sup>	0.01 μg L <sup>-1</sup>	Rape bolt/102% (Cu <sup>2+</sup> ) and 104% (Hg <sup>2+</sup> )	
						Tea/93.5% (Cu <sup>2+</sup> ) and 101% (Hg <sup>2+</sup> )	
19	DPV	Pb <sup>2+</sup> Cd <sup>2+</sup>	<i>p</i> -PDMS@MSF/ITO			Fruit juice/ Beverage/	434
20	EC	Cd <sup>2+</sup>	UiO-66-NH <sub>2</sub> @MWCNTs/GCE	0.5–170 μg L <sup>-1</sup>	0.2 μg L <sup>-1</sup>	Meat/95.1–107.5%	435
21	SWASV	Pb(II)	rGO/MoS <sub>2</sub> /CS/GCE	0.005–0.05 μM	0.0016 μM	Tobacco leaves	436
22	SWASV	Pb(II) Cd(II)	Fe <sub>2</sub> O <sub>3</sub> /Bi <sub>2</sub> O <sub>3</sub> /GCE	0.002–4 μM		Water and milk	437

Table 9 (Contd.)

Sr No.	Method	Analyte	Electrode modifier	Linear range	LOD	Sample/recovery	Ref.
23	CV EIS	Cd(II) Pb(II)	UiO-66/Bi/GCE	10–50 $\mu\text{g L}^{-1}$	1.16 $\mu\text{g L}^{-1}$ 1.14 $\mu\text{g L}^{-1}$	Tap water/97% (Cd <sup>2+</sup> ) and 105% (Pb <sup>2+</sup> ) The Songhua river/93% (Cd <sup>2+</sup> ) and 91% (Pb <sup>2+</sup> )	438
24	CV EIS	Cd(II) Pb(II)	UiO-66/Bi/GCE	20–60 $\mu\text{g L}^{-1}$	1.73 $\mu\text{g L}^{-1}$ 1.00 $\mu\text{g L}^{-1}$	Tap water/96% (Cd <sup>2+</sup> ) and 93% (Pb <sup>2+</sup> ) The Songhua river/94% (Cd <sup>2+</sup> ) and 95% (Pb <sup>2+</sup> )	438
25		Clozapine Albendazole			2.8 nM 2.5 nM		443
26	CV	Promethazine (PHZ)	MG@mSiO <sub>2</sub> -C <sub>18</sub> -HCM/MGCE	0.08–300 $\mu\text{mol L}^{-1}$	9.8 nmol L <sup>-1</sup>	Beef/82.5–97.2%	444
27	DPV LSV	Dimetridazole (DMZ)	PANI-Cu@BSA/rGO/SPCE	0.79–2057 $\mu\text{M}$	1.78 nM	Beef liver/81.5–96.1% Human blood serum/90.0–100.0% Rat blood serum/98.0–101.0%	445
28	CV DPV	Furaltadone (FTD)	ASPCe/CuCoO <sub>2</sub>	0.1–316 $\mu\text{M}$	1.79 nM	Egg/97.0–100% Antibiotic 1/90–93%	446
29	CV EIS DPV	Tetracycline (TC)	BiC@Au@Apta/AuE	0.001–100 $\mu\text{M}$	2.92 nM	Tap water/97.52–125.18 Milk/78.73–103.80	464
30	Fluorescent	Tetracycline (TC)	—	0.1–100 $\mu\text{M}$	0.23 $\mu\text{M}$	Antibiotics	465
31	SERS	Tetracycline (TC)	CoNi-ZIFs@Ag@NF	10 <sup>-10</sup> –10 <sup>-5</sup> M	1.0 × 10 <sup>-11</sup> M	—/94.45–114.25%	466
32	DPV	Dimetridazole (DMZ)	Mn-SnO@rGO/GCE	0.009–1291 $\mu\text{M}$	2.0 $\mu\text{M}$	Milk and egg	467
33	DPV	Dimetridazole (DMZ)	Se-Co <sub>3</sub> O <sub>4</sub> @GO-NC/GCE	0.02–83.72 $\mu\text{M}$	3.4 nM	Milk/98.5% Pigeon egg/99.6%	468
34	DPV	Dimetridazole (DMZ)	DM/Nd <sub>2</sub> Sn <sub>2</sub> O <sub>7</sub> /GCE	0.01–1453 $\mu\text{M}$	6.0 nM	Pigeon meat/100.4% Human blood serum and human urine	469
35	CV DPV	Vanillin	La <sub>2</sub> NiO <sub>4</sub> /f-CNF/GCE		6 nM	Chocolat/	453
36	CV	Vanillin	f-MWCNTs-FNTs/CPE	5 × 10 <sup>-8</sup> –9 × 10 <sup>-6</sup> mol L <sup>-1</sup>	3.4 × 10 <sup>-8</sup> mol L <sup>-1</sup>	Ice cream/ Sugar/100–107%	454
37	DPV	Vanillin	g-C <sub>3</sub> N <sub>4</sub> NTs@MoS <sub>2</sub> /GCE	0.005–458.9 $\mu\text{M}$	4 nM	—	455
38	CV	<i>Ter</i> -butyl hydroquinone (TBHQ)	Co <sub>3</sub> O <sub>4</sub> NRs/FCB/SPCE		1 nM	Beef tallow/ Peanut oil/ Lake water/ Pork, beef, and chicken	457
39	DPV EIS CV	Ractopamine (RAC)	Bi <sub>2</sub> Te <sub>3</sub> /g-C <sub>3</sub> N <sub>4</sub> BNs/GCEs	0.015–456.4 $\mu\text{M}$	1.07 nM		458
40	DPV CV LSV	Sunset yellow	MnO <sub>2</sub> NRs/GO/SPGE	0.01–115.0 $\mu\text{M}$	0.008 $\mu\text{M}$	Apple juice and orange juice/97.3–104.6%	470



integration with smartphones further makes detection and data analysis accessible to non-experts, boosting practical use.

Recent years have seen significant progress in chemical sensors, driven by innovative materials like metal–organic frameworks and covalent organic frameworks that improve sensitivity and selectivity through high surface area and tunable porosity. Molecularly imprinted polymers offer cost-effective, precise toxin detection *via* tailored binding sites. The move toward miniaturized sensors expands their use in food safety, enabling quick on-site testing. Advances in electrochemical sensors, improved electrode materials, and the addition of nanomaterials like carbon nanotubes boost sensitivity and response times. Combining electrochemical sensors with microfluidics allows for simultaneous multi-toxin detection, simplifying analysis and reducing reagent use. Self-powered sensors, powered by environmental energy or the sample itself, promise sustainable, maintenance-free operation, thereby boosting reliability and versatility in food toxin detection.

Fluorescent sensors are increasingly recognized for their sensitivity and quick response times. Fluorescent nanomaterials like quantum dots and carbon dots have enhanced these sensors with bright, stable signals. Recent advancements include ratiometric sensors using dual-emission probes to improve accuracy and reduce environmental interference. Integrating fluorescent sensors with microfluidic chips allows high-throughput food sample screening, streamlining detection. Optical sensors utilize techniques like surface plasmon resonance (SPR), surface-enhanced Raman scattering (SERS), and interferometry, with recent focus on boosting sensitivity and lowering detection limits. SPR utilizes nanostructured materials to amplify signals for the detection of low-level toxins, whereas SERS relies on molecular spectral fingerprints for the precise identification of contaminants. Coupling these sensors with portable devices like smartphones enables on-site, real-time food testing. Spectroscopic sensors have evolved with advanced materials and signal enhancement, using mid-IR quantum cascade lasers for increased sensitivity, facilitating quick, non-destructive toxin detection based on spectral characteristics. Combining spectroscopic sensors with chemometrics improves data analysis, allowing detection of multiple toxins simultaneously. Chromatographic sensors remain vital for their separation efficiency and accuracy, with recent miniaturization of systems like microchip chromatography reducing analysis time and sample volume. Coupling chromatographic sensors with mass spectrometry offers sensitive, specific toxin identification. Automated, high-throughput systems further improve toxin screening efficiency.

Recent advancements in the integration of machine learning with nanosensing technologies have revealed significant advantages alongside distinct challenges. Supervised learning algorithms, such as support vector machines, random forests, and gradient-boosted trees, have proven effective in classifying intricate signal patterns from multi-channel sensors, enhancing selectivity by distinguishing target toxins from potential interferents. Meanwhile, unsupervised techniques like principal component analysis and *t*-SNE aid in reducing

dimensionality and exploring clustering within spectral or multi-electrode datasets, thereby revealing concealed interference patterns. Additionally, deep learning approaches, including convolutional and recurrent neural networks, have been utilized on raw spectral or time-series data to identify features that traditional methods might miss, thus broadening detection capabilities in noisy environments.

Practical challenges in sensor studies remain significant. Data scarcity and class imbalance often result in biased models due to the limited number of positive samples, necessitating strategies such as targeted data augmentation, synthetic data generation through physics-based simulations, and transfer learning from similar analytes. Additionally, label noise and inconsistent protocols, stemming from variations in sample preparation and inter-laboratory discrepancies, compromise model generalizability; addressing this requires standardized protocols, matrix-matched training sets, and robust algorithms that can tolerate label noise. Furthermore, sensor drift and batch variability can diminish model performance over time, which can be mitigated through online calibration, domain adaptation techniques, and periodic retraining with calibration standards. Lastly, deployment constraints due to limited computing power on portable devices necessitate the use of lightweight models, model compression, and edge-optimized inference frameworks. Systematic efforts to address these issues are essential for advancing machine learning from theoretical concepts to practical, field-ready enhancements in nanosensor technology.

When interpreting reported LODs, it is crucial to take into account the complexity of the matrix, the difficulties associated with sample preparation, and the validation phase. Sensors that present LODs solely under buffer conditions require further laboratory validation and field testing to be considered appropriate for regulatory use. The current document connects theoretical performance with these practical aspects, providing essential context for assessing translational readiness without necessitating the replication of experimental data.

In conclusion, the future of food toxin detection is poised for remarkable advancements driven by innovations in sensor technology. The ongoing enhancement of various sensor types, including biosensors, chemical, electrochemical, fluorescent, colorimetric, optical, spectroscopic, and chromatographic sensors, holds significant potential to improve food safety and public health. These technological improvements enable the more sensitive, specific, and rapid identification of toxins, allowing for proactive strategies to mitigate foodborne illnesses and safeguard consumers. As the field evolves, the integration of these sophisticated sensors into portable, user-friendly devices, along with the utilization of artificial intelligence for data analysis, will further increase their practicality and accessibility. This review highlights the vital role of advanced sensor technologies in protecting public health. It underscores the need for ongoing research and development to address the evolving challenges in food safety. By adopting these innovations, researchers, industry stakeholders, and regulatory agencies can work together to strive for a safer and more secure global food supply chain.



## Conflicts of interest

Authors declare no conflict of interest.

## Data availability

No primary research results, software or code have been included and no new data were generated or analysed as part of this review.

## References

- P. K. Gupta and P. K. Gupta, Poisonous and Venomous Organisms, *Concepts and Applications in Veterinary Toxicology: an Interactive Guide*, 2019, pp.165–185.
- M. A. Kabir, I. Lee, C. B. Singh, G. Mishra, B. K. Panda and S.-H. Lee, Detection of Mycotoxins in Cereal Grains and Nuts Using Machine Learning Integrated Hyperspectral Imaging: A Review, *Toxics*, 2025, **17**, 219.
- A. Alengebawy, S. T. Abdelkhalek, S. R. Qureshi and M.-Q. Wang, Heavy Metals and Pesticides Toxicity in Agricultural Soil and Plants: Ecological Risks and Human Health Implications, *Toxics*, 2021, **9**, 42.
- M. M. Uddin, M. C. M. Zakeel, J. S. Zavahir, F. M. M. T. Marikar and I. Jahan, Heavy Metal Accumulation in Rice and Aquatic Plants Used as Human Food: A General Review, *Toxics*, 2021, **9**, 360.
- N. M. Aljamali, F. W. El-Taei and D. Alasady, Review on Types of Toxins (Pharmaceutical, Biological, Chemical), *Glob. Acad. J. Pharm. Drug. Res.*, 2021, **3**, 44–53.
- V. R. Askari, Z. Najafi, V. Baradaran Rahimi and M. H. Boskabady, Comparative Study on the Impacts of Visnagin and Its Methoxy Derivative Khellin on Human Lymphocyte Proliferation and Th1/Th2 Balance, *Pharmacol. Rep.*, 2023, **75**, 411–422.
- P. N. Chávez-Dulanto, A. A. A. Thiry, P. Glorio-Paulet, O. Vögler and F. P. Carvalho, Increasing the Impact of Science and Technology to Provide More People with Healthier and Safer Food, *Food Energy Secur.*, 2021, **10**, e259.
- M. Gallo, L. Ferrara, A. Calogero, D. Montesano and D. Naviglio, Relationships between Food and Diseases: What to Know to Ensure Food Safety, *Food Res. Int.*, 2020, **137**, 109414.
- M. M. Aung and Y. S. Chang, Traceability in a Food Supply Chain: Safety and Quality Perspectives, *Food Control*, 2014, **39**, 172–184.
- N. Pasdar, P. Mostashari, R. Greiner, A. Khelfa, A. Rashidinejad, H. Eshpari, J. M. Vale, S. M. T. Gharibzahedi and S. Roohinejad, Advancements in Non-Thermal Processing Technologies for Enhancing Safety and Quality of Infant and Baby Food Products: A Review, *Foods*, 2024, **13**, 2659.
- L. Sheng and L. Wang, The Microbial Safety of Fish and Fish Products: Recent Advances in Understanding Its Significance, Contamination Sources, and Control Strategies, *Compr. Rev. Food Sci. Food Saf.*, 2021, **20**, 738–786.
- M. Hashemi, M. Salayani, A. Afshari, H. S. Kafil and S. M. A. Noori, The Global Burden of Viral Food-Borne Diseases: A Systematic Review, *Current Pharm. Biotechnol.*, 2023, **24**, 1657–1672.
- M. Shirani, *Assessing Food Safety Risk in Global Supply Chain*, 2016.
- H. A. D. Ruwandeepika, D. N. Madushanka and T. S. P. Jayaweera, Foodborne Organisms: General Characteristics, Virulence Factors, and Clinical Manifestations, in *Food Microbial and Molecular Biology*, Apple Academic Press, 2023, pp 213–285.
- Z. Wu, X. Gu, L. Zha, Q. Yang, Y. Zhou and Z. Zeng, Structural and Functional Insights into Yeast Tbf1 as an Atypical Telomeric Repeat-Binding Factor, *Structure*, 2024, **32**(7), 889–898, DOI: [10.1016/j.str.2024.04.002](https://doi.org/10.1016/j.str.2024.04.002).
- H. Liu, P. Bing, M. Zhang, G. Tian, J. Ma, H. Li, M. Bao, K. He, J. He, B. He and J. Yang, MNNMDA: Predicting Human Microbe-Disease Association via a Method to Minimize Matrix Nuclear Norm, *Comput. Struct. Biotechnol. J.*, 2023, **21**, 1414–1423, DOI: [10.1016/J.CSBJ.2022.12.053](https://doi.org/10.1016/J.CSBJ.2022.12.053).
- J. Yi, W. Xiao, G. Li, P. Wu, Y. He, C. Chen, Y. He, P. Ding and T. Kai, *The Research of Aptamer Biosensor Technologies for Detection of Microorganism*, DOI: [10.1007/s00253-020-10940-1](https://doi.org/10.1007/s00253-020-10940-1)/Published.
- L. A. Dave, S. M. Hodgkinson, N. C. Roy, N. W. Smith and W. C. McNabb, The Role of Holistic Nutritional Properties of Diets in the Assessment of Food System and Dietary Sustainability, *Crit. Rev. Food Sci. Nutr.*, 2023, **63**, 5117–5137.
- B. Fang, S. Xu, Y. Huang, F. Su, Z. Huang, H. Fang, J. Peng, Y. Xiong and W. Lai, Gold Nanorods Etching-Based Plasmonic Immunoassay for Qualitative and Quantitative Detection of Aflatoxin M1 in Milk, *Food Chem.*, 2020, **329**, 127160.
- Y. Zhao, L. Li, R. Ma, L. Wang, X. Yan, X. Qi, S. Wang and X. Mao, A Competitive Colorimetric Aptasensor Transduced by Hybridization Chain Reaction-Facilitated Catalysis of AuNPs Nanozyme for Highly Sensitive Detection of Saxitoxin, *Anal. Chim. Acta*, 2021, **1173**, 338710.
- X. Tang, J. Zuo, C. Yang, J. Jiang, Q. Zhang, J. Ping and P. Li, Current Trends in Biosensors for Biotoxins (Mycotoxins, Marine Toxins, and Bacterial Food Toxins): Principles, Application, and Perspective, *TrAC, Trends Anal. Chem.*, 2023, **165**, 117144.
- A. De Girolamo, V. Lippolis and M. Pascale, Overview of Recent Liquid Chromatography Mass Spectrometry-Based Methods for Natural Toxins Detection in Food Products, *Toxics*, 2022, **14**, 328.
- A. T. Rosário and J. C. Dias, How Industry 4.0 and Sensors Can Leverage Product Design: Opportunities and Challenges, *Sensors*, 2023, **23**, 1165.
- S. Abdulmalek, A. Nasir, W. A. Jabbar, M. A. M. Almuahaya, A. K. Bairagi, M. A.-M. Khan and S.-H. Kee, IoT-Based Healthcare-Monitoring System towards Improving Quality of Life: A Review, in *Healthcare*, MDPI, 2022, vol. 10, p. 1993.



- 25 T. Miller, I. Durlík, E. Kostecka, P. Kozłowska, A. Łobodzińska, S. Sokołowska and A. Nowy, Integrating Artificial Intelligence Agents with the Internet of Things for Enhanced Environmental Monitoring: Applications in Water Quality and Climate Data, *Electronics*, 2025, **14**, 696.
- 26 R. Feng and Y. Yu, ZHANG Heng's Seismometer and Longxi Earthquake in AD 134, *Acta Seismol. Sin.*, 2006, **19**, 704–719.
- 27 S. Kapse, S. Kausley and B. Rai, Portable Food Diagnostic Devices and Methods: A Review, *J. Food Process Eng.*, 2022, **45**, e14159.
- 28 Z. Deng, J. Ding, J. Bu, J. Li, H. Liu, P. Gao, Z. Gong, X. Qin, Y. Yang and S. Zhong, Fluorophore Label-Free Light-up Near Infrared Deoxyribonucleic Acid Nanosensor for Monitoring Extracellular Potassium Levels, *Anal. Chem.*, 2024, **96**(10), 4023–4030, DOI: [10.1021/acs.analchem.3c03881](https://doi.org/10.1021/acs.analchem.3c03881).
- 29 P. Arora, A. Sindhu, N. Dilbaghi and A. Chaudhury, Biosensors as Innovative Tools for the Detection of Food Borne Pathogens, *Biosens. Bioelectron.*, 2011, **28**, 1–12.
- 30 M. S. Thakur and K. V. Ragavan, Biosensors in Food Processing, *J. Food Sci. Technol.*, 2013, **50**, 625–641.
- 31 J. Kirsch, C. Siltanen, Q. Zhou, A. Revzin and A. Simonian, Biosensor Technology: Recent Advances in Threat Agent Detection and Medicine, *Chem. Soc. Rev.*, 2013, **42**, 8733–8768.
- 32 R. Gupta, N. Raza, S. K. Bhardwaj, K. Vikrant, K.-H. Kim and N. Bhardwaj, Advances in Nanomaterial-Based Electrochemical Biosensors for the Detection of Microbial Toxins, Pathogenic Bacteria in Food Matrices, *J. Hazard. Mater.*, 2021, **401**, 123379.
- 33 S. Kogularasu, Y.-Y. Lee, G.-P. Chang-Chien, M. Govindasamy and J.-K. Sheu, Nanofibers: Empowering Electrochemical Sensors for Reliable Detection of Food and Environmental Toxins, *J. Electrochem. Soc.*, 2023, **170**, 77514.
- 34 M. Javed, A. Shah and I. Shah, Electrochemical Sensor for Levosulpiride Detection and Its Adsorptive Removal from Wastewater, *ACS Omega*, 2025, **10**(17), 17529–17542, DOI: [10.1021/acsomega.4c11218](https://doi.org/10.1021/acsomega.4c11218).
- 35 V. S. Manikandan, B. Adhikari and A. Chen, Nanomaterial Based Electrochemical Sensors for the Safety and Quality Control of Food and Beverages, *Analyst*, 2018, **143**, 4537–4554.
- 36 K. Sakthivel, S. Balasubramanian, G.-P. Chang-Chien, S.-F. Wang, W. Billey, J. Platero, T. Soundappan and P. Sekhar, Editors' Choice—Review—Advances in Electrochemical Sensors: Improving Food Safety, Quality, and Traceability, *ECS Sens. Plus*, 2024, **3**, 20605.
- 37 J. Li, L. Li, Junjie Fei, P. Zhao, J. Zhao and Y. Xie, Ultrasensitive Electrochemical Sensor for Fenitrothion Based on MIL-125 Derived Iron/Titanium Bimetallic Oxides Doped Porous Carbon Composite, *Microchem. J.*, 2024, **200**, 110426, DOI: [10.1016/j.microm.2024.110426](https://doi.org/10.1016/j.microm.2024.110426).
- 38 H. Singh, D. Kumar, A. Deep, S. Puri, M. Khatri and N. Bhardwaj, Fluorescent Nanosensors for Detection of Microbial Toxins in Food Matrices: A Review, *J. Food Meas. Charact.*, 2024, **18**, 7669–7699.
- 39 M. K. Goshisht and N. Tripathi, Fluorescence-Based Sensors as an Emerging Tool for Anion Detection: Mechanism, Sensory Materials and Applications, *J. Mater. Chem. C*, 2021, **9**, 9820–9850.
- 40 X. Huang, Q. Guo, R. Zhang, Z. Zhao, Y. Leng, J. W. Y. Lam, Y. Xiong and B. Z. Tang, AIEgens: An Emerging Fluorescent Sensing Tool to Aid Food Safety and Quality Control, *Compr. Rev. Food Sci. Food Saf.*, 2020, **19**, 2297–2329.
- 41 H. Chen, S. Yan, L. Zhang, B. Zhao, C. Zhu, G. Deng and J. Liu, A Self-Degrading and NIR-II Emissive Type I/II Photosensitizer with Synergistic Photodynamic and Photothermal Properties for Antibacterial and Anticancer, *Sens. Actuators, B*, 2024, **405**, 135346, DOI: [10.1016/J.SNB.2024.135346](https://doi.org/10.1016/j.snb.2024.135346).
- 42 H. Ling, L. Xiao, T. Li, Y. Yang and S. Zhong, Construction of Fluorescence-Sensing Molecularly Imprinted Membranes Based on Hydrophilic-Hydrophobic Multifunctional Monomers for the Detection of LPS Molecules, *Sens. Actuators, B*, 2024, **419**, 136451, DOI: [10.1016/J.SNB.2024.136451](https://doi.org/10.1016/J.SNB.2024.136451).
- 43 G. S. Geleta, A Colorimetric Aptasensor Based on Gold Nanoparticles for Detection of Microbial Toxins: An Alternative Approach to Conventional Methods, *Anal. Bioanal. Chem.*, 2022, **414**, 7103–7122.
- 44 Z. Jia, C. Shi, X. Yang, J. Zhang, X. Sun, Y. Guo and X. Ying, QD-based Fluorescent Nanosensors: Production Methods, Optoelectronic Properties, and Recent Food Applications, *Compr. Rev. Food Sci. Food Saf.*, 2023, **22**, 4644–4669.
- 45 W. Yachuan, L. Zhang, A. Halimov, M. Fu, J. Tu, H. Liu, S. Zhang, X. Nie and J. Liu, A Triarylboron-Based Fluorescent Probe with Activatable Photosensitivity for Imaging MitoDNA, *Talanta*, 2025, **294**, 128196, DOI: [10.1016/J.TALANTA.2025.128196](https://doi.org/10.1016/J.TALANTA.2025.128196).
- 46 Y. Ding, C. Deng, Y. Yang, J. Zhang, W. Liu, O. Aras, F. An, J. Liu and Y. Chai, Carrier-Free Nanoparticles for Cancer Theranostics with Dual-Mode Magnetic Resonance Imaging/Fluorescence Imaging and Combination Photothermal and Chemodynamic Therapy, *Int. J. Pharm.*, 2025, **671**, 125285, DOI: [10.1016/J.IJPHARM.2025.125285](https://doi.org/10.1016/J.IJPHARM.2025.125285).
- 47 K. Narsaiah, S. N. Jha, R. Bhardwaj, R. Sharma and R. Kumar, Optical Biosensors for Food Quality and Safety Assurance—a Review, *J. Food Sci. Technol.*, 2012, **49**, 383–406.
- 48 K. L. Diehl and E. V. Anslyn, Array Sensing Using Optical Methods for Detection of Chemical and Biological Hazards, *Chem. Soc. Rev.*, 2013, **42**, 8596–8611.
- 49 P. Yeh, N. Yeh, C.-H. Lee and T.-J. Ding, Applications of LEDs in Optical Sensors and Chemical Sensing Device for Detection of Biochemicals, Heavy Metals, and Environmental Nutrients, *Renewable Sustainable Energy Rev.*, 2017, **75**, 461–468.
- 50 B. A. Prabowo, A. Purwidyantri and K.-C. Liu, Surface Plasmon Resonance Optical Sensor: A Review on Light Source Technology, *Biosensors*, 2018, **8**, 80.
- 51 R. S. Rodriguez, T. L. O'Keefe, C. Froehlich, R. E. Lewis, T. R. Sheldon and C. L. Haynes, Sensing Food



- Contaminants: Advances in Analytical Methods and Techniques, *Anal. Chem.*, 2020, **93**, 23–40.
- 52 S. Sforza, C. Dall'Asta and R. Marchelli, Recent Advances in Mycotoxin Determination in Food and Feed by Hyphenated Chromatographic Techniques/Mass Spectrometry, *Mass Spectrom. Rev.*, 2006, **25**, 54–76.
- 53 E. Ibañez and A. Cifuentes, New Analytical Techniques in Food Science, *Crit. Rev. Food Sci. Nutr.*, 2001, **41**, 413–450.
- 54 Z. Li, J. R. Askim and K. S. Suslick, The Optoelectronic Nose: Colorimetric and Fluorometric Sensor Arrays, *Chem. Rev.*, 2018, **119**, 231–292.
- 55 R. Apak, S. D. Çekiç, A. Üzer, E. Çapanoğlu, S. E. Çelik, M. Bener, Z. Can and S. Durmazel, Colorimetric Sensors and Nanoprobes for Characterizing Antioxidant and Energetic Substances, *Anal. Methods*, 2020, **12**, 5266–5321.
- 56 M. J. Kangas, R. M. Burks, J. Atwater, R. M. Lukowicz, P. Williams and A. E. Holmes, Colorimetric Sensor Arrays for the Detection and Identification of Chemical Weapons and Explosives, *Crit. Rev. Anal. Chem.*, 2017, **47**, 138–153.
- 57 Y. Gao, S. Zhang, T. Aili, J. Yang, Z. Jia, J. Wang, H. Li, L. Bai, X. Lv and X. Huang, Dual Signal Light Detection of Beta-Lactoglobulin Based on a Porous Silicon Bragg Mirror, *Biosens. Bioelectron.*, 2022, **204**, 114035, DOI: [10.1016/J.BIOS.2022.114035](https://doi.org/10.1016/j.bios.2022.114035).
- 58 A. R. Nwaji, O. Arieri, A. S. Anyang, K. Nguedia, E. B. Abiade, G. E. Forcados, O. O. Oladipo, S. Makama, I. L. Elisha and N. Ozele, Natural Toxins and One Health: A Review, *Sci. One Health*, 2022, **1**, 100013.
- 59 M. Pohanka, Immunosensors for Assay of Toxic Biological Warfare Agents, *Biosensors*, 2023, **13**, 402.
- 60 P. Katikou, C. Gokbulut, A. R. Kosker, M. Campàs and F. Ozogul, An Updated Review of Tetrodotoxin and Its Peculiarities, *Mar. Drugs*, 2022, **20**, 47.
- 61 J. I. Pitt and J. D. A. Miller, Concise History of Mycotoxin Research, *J. Agric. Food Chem.*, 2017, **65**, 7021–7033.
- 62 T. Ahmed and M. Z. Hashmi, Hazardous Environmental Micro-Pollutants, *Health Impacts and Allied Treatment Technologies*, Springer Nature, 2022.
- 63 C. G. Awuchi, E. N. Ondari, C. U. Ogbonna, A. K. Upadhyay, K. Baran, C. O. R. Okpala, M. Korzeniowska and R. P. F. Guiné, Mycotoxins Affecting Animals, Foods, Humans, and Plants: Types, Occurrence, Toxicities, Action Mechanisms, Prevention, and Detoxification Strategies—A Revisit, *Foods*, 2021, **10**, 1279.
- 64 S. Shahba, J. Mehrzad and A. M. Malvandi, Neuroimmune Disruptions from Naturally Occurring Levels of Mycotoxins, *Environ. Sci. Pollut. Res.*, 2021, **28**, 32156–32176.
- 65 A. Barac, Mycotoxins and Human Disease, in *Clinically relevant mycoses: a practical approach*, Springer, 2018, pp. 213–225.
- 66 C. Gurikar, D. P. Shivaprasad, L. Sabillón, N. A. N. Gowda and K. Siliveru, Impact of Mycotoxins and Their Metabolites Associated with Food Grains, *Grain Oil Sci. Technol.*, 2023, **6**, 1–9.
- 67 N. K. Kortei, T. Annan, P. T. Akonor, S. A. Richard, H. A. Annan, V. Kyei-Baffour, F. Akuamo, P. G. Akpaloo and P. Esua-Amofo, The Occurrence of Aflatoxins and Human Health Risk Estimations in Randomly Obtained Maize from Some Markets in Ghana, *Sci. Rep.*, 2021, **11**, 4295.
- 68 D. Pickova, V. Ostry and F. Malir, A Recent Overview of Producers and Important Dietary Sources of Aflatoxins, *Toxins*, 2021, **13**, 186.
- 69 D. Pickova, V. Ostry, J. Toman and F. A. Malir, History, Significant Milestones, Recent Data on Their Toxicity and Ways to Mitigation, *Toxins*, 2021, **13**, 399.
- 70 D. K. Mahato, K. E. Lee, M. Kamle, S. Devi, K. N. Dewangan, P. Kumar and S. G. Kang, Aflatoxins in Food and Feed: An Overview on Prevalence, Detection and Control Strategies, *Front. Microbiol.*, 2019, **10**, 2266.
- 71 W. Cao, P. Yu, K. Yang and D. Cao, Aflatoxin B1: Metabolism, Toxicology, and Its Involvement in Oxidative Stress and Cancer Development, *Toxicol. Mech. Methods*, 2022, **32**, 395–419.
- 72 T. Omara, A. K. Kiprof, P. Wangila, A. P. Wacoo, S. Kagoya, P. Nteziyaremye, M. Peter Odero, C. Kiwanuka Nakiguli and S. Baker Obakiro, The Scourge of Aflatoxins in Kenya: A 60-Year Review (1960 to 2020), *J. Food Qual.*, 2021, 8899839.
- 73 A. A. Mohamed, M. Armanious, R. W. Bedair, N. S. Amin and H. M. El Tayebi, When Less Is More: The Association between the Expression of Polymorphic CYPs and AFB1-induced HCC, *Eur. J. Clin. Invest.*, 2024, **54**, e14297.
- 74 S. Abrehame, V. R. Manoj, M. Hailu, Y.-Y. Chen, Y.-C. Lin and Y.-P. A. Chen, Source, Detection, Clinical Features and Prevention, *Processes*, 2023, **11**, 204.
- 75 N. Benkerroum, Chronic and Acute Toxicities of Aflatoxins: Mechanisms of Action, *Int. J. Environ. Res. Public Health*, 2020, **17**, 423.
- 76 M. Carvajal-Moreno, Metabolic Changes of Aflatoxin B1 to Become an Active Carcinogen and the Control of This Toxin, *Immunome Res.*, 2015, **11**, 1.
- 77 V. Dohnal, Q. Wu and K. Kuča, Metabolism of Aflatoxins: Key Enzymes and Interindividual as Well as Interspecies Differences, *Arch. Toxicol.*, 2014, **88**, 1635–1644.
- 78 R. R. M. Paterson and N. Lima, Toxicology of Mycotoxins. Molecular, Clinical and Environmental Toxicology, *Clin. Toxicol.*, 2010, **2**, 31–63.
- 79 R. A. El-Sayed, A. B. Jebur, W. Kang and F. M. El-Demerdash, An Overview on the Major Mycotoxins in Food Products: Characteristics, Toxicity, and Analysis, *J. Future Foods*, 2022, **2**, 91–102.
- 80 C. Wang, Y. Li and Q. A. Zhao, Signal-on Electrochemical Aptasensor for Rapid Detection of Aflatoxin B1 Based on Competition with Complementary DNA, *Biosens. Bioelectron.*, 2019, **144**, 111641.
- 81 T. Chen, Y. Li, S. Meng, C. Liu, D. Liu, D. Dong and T. You, Temperature and PH Tolerance Ratiometric Aptasensor: Efficiently Self-Calibrating Electrochemical Detection of Aflatoxin B1, *Talanta*, 2022, **242**, 123280.
- 82 G. Kaur, S. Sharma, N. Bhardwaj, M. K. Nayak and A. Deep, Highly Sensitive and Selective Electrochemical Detection of Aflatoxin B1 in Water and Pistachio Samples with MOF/



- MXene Composite Based Sensor, *Food Control*, 2024, **165**, 110694.
- 83 M. Wood and S. M. Mugo, A MIP-Enabled Stainless-Steel Hypodermic Needle Sensor for Electrochemical Detection of Aflatoxin B1, *Anal. Methods*, 2022, **14**, 2063–2071.
- 84 S. F. Ahmadi, M. Hojjatoleslami, H. Kiani and H. Molavi, Monitoring of Aflatoxin M1 in Milk Using a Novel Electrochemical Aptasensor Based on Reduced Graphene Oxide and Gold Nanoparticles, *Food Chem.*, 2022, **373**, 131321.
- 85 G. B. Asl, M. Arvand and M. F. Habibi, High Affinity Aptamers for Ultra-Sensitive Detection of Aflatoxin B1 in Milk and Groundnut Samples with Label-Free Photo-Electrochemical Aptasensor, *Food Chem.*, 2022, **397**, 133829.
- 86 T. N. Kulikova, A. V. Porfireva, G. A. Evtugyn and T. Hianik, Electrochemical Aptasensor with Layer-by-layer Deposited Polyaniline for Aflatoxin M1 Voltammetric Determination, *Electroanalysis*, 2019, **31**, 1913–1924.
- 87 H. Bhardwaj, M. K. Pandey, Rajesh and G. Sumana, Electrochemical Aflatoxin B1 Immunosensor Based on the Use of Graphene Quantum Dots and Gold Nanoparticles, *Microchim. Acta*, 2019, **186**, 1–12.
- 88 J. Qian, C. Ren, C. Wang, K. An, H. Cui, N. Hao and K. Wang, Gold Nanoparticles Mediated Designing of Versatile Aptasensor for Colorimetric/Electrochemical Dual-Channel Detection of Aflatoxin B1, *Biosens. Bioelectron.*, 2020, **166**, 112443.
- 89 Y. Zhang, T. Lin, Y. Shen and H. Li, A High-Performance Self-Supporting Electrochemical Biosensor to Detect Aflatoxin B1, *Biosensors*, 2022, **12**, 897.
- 90 C. Wang, Y. Li and Q. Zhao, A Competitive Electrochemical Aptamer-Based Method for Aflatoxin B1 Detection with Signal-off Response, *Anal. Methods*, 2020, **12**, 646–650.
- 91 X. Hu, K. Wang, Y. Yang, B. Ding and C. Yu, Fluorescence/Colorimetric Sensor Based on Aptamers-Molecular Imprinted Polymers Synergistic Recognition for Ultrasensitive and Interference-Free Detection of Aflatoxin B1, *Food Chem.*, 2025, **467**, 142387.
- 92 H. Chi and G. Liu, A Fluorometric Sandwich Biosensor Based on Molecular Imprinted Polymer and Aptamer Modified CdTe/ZnS for Detection of Aflatoxin B1 in Edible Oil, *Lwt*, 2023, **180**, 114726.
- 93 L. Mao, X. Xue, X. Xu, W. Wen, M.-M. Chen, X. Zhang and S. Wang, Heterostructured CuO-g-C3N4 Nanocomposites as a Highly Efficient Photocathode for Photoelectrochemical Aflatoxin B1 Sensing, *Sens. Actuators, B*, 2021, **329**, 129146.
- 94 Y. Li, D. Liu, C. Zhu, X. Shen, Y. Liu and T. You, Sensitivity Programmable Ratiometric Electrochemical Aptasensor Based on Signal Engineering for the Detection of Aflatoxin B1 in Peanut, *J. Hazard. Mater.*, 2020, **387**, 122001.
- 95 Y. Chen, W. Cheng, Y. Yang, D. Wu, Y. Zhang and X. Tang, Development of an Ultrasensitive SERS Aptasensor for Determination of Aflatoxin B1 by Modifying Magnetic Beads with UiO-66-NH2 for Enhanced Signal Probe Capturing, *Sens. Actuators, B*, 2023, **393**, 134329.
- 96 F. Jahangiri-Dehaghani, H. R. Zare and Z. Shekari, Simultaneous Measurement of Ochratoxin A and Aflatoxin B1 Using a Duplexed-Electrochemical Aptasensor Based on Carbon Nanodots Decorated with Gold Nanoparticles and Two Redox Probes Hemin@ HKUST-1 and Ferrocene@ HKUST-1, *Talanta*, 2024, **266**, 124947.
- 97 G. Selvolini, M. Lettieri, L. Tassoni, S. Gastaldello, M. Grillo, C. Maran and G. Marrazza, Electrochemical Enzyme-Linked Oligonucleotide Array for Aflatoxin B1 Detection, *Talanta*, 2019, **203**, 49–57.
- 98 T. Lin and Y. Shen, Fabricating Electrochemical Aptasensors for Detecting Aflatoxin B1 via Layer-by-Layer Self-Assembly, *J. Electroanal. Chem.*, 2020, **870**, 114247.
- 99 Z. Feng, N. Gao, J. Liu and H. Li, Boron-Doped Diamond Electrochemical Aptasensors for Trace Aflatoxin B1 Detection, *Anal. Chim. Acta*, 2020, **1122**, 70–75.
- 100 D. Meng, X. Gan and T. Tian, An Electrochemical Sensing Method for Aflatoxin B1 Detection Based on Pt-Coordinated Titanium-Based Porphyrin MOF, *Int. J. Electrochem. Sci.*, 2022, **17**, 220247.
- 101 B. Pérez-Fernández, B. M. Maestroni, S. Nakaya, S. Bussalino, C. Vlachou and A. D. de la Escosura-Muñiz, Optimization and Validation of an Electrochemical Immunosensor for Determination of Total Aflatoxins in Pistachio, *Food Control*, 2023, **152**, 109859.
- 102 A. Gevaerd, C. E. Banks, M. F. Bergamini and L. H. Marcolino-Junior, Nanomodified Screen-Printed Electrode for Direct Determination of Aflatoxin B1 in Malted Barley Samples, *Sens. Actuators, B*, 2020, **307**, 127547.
- 103 A. Beheshti-Marnani, A. Hatefi-Mehrjardi and Z. Es' hagh, A Sensitive Biosensing Method for Detecting of Ultra-Trace Amounts of AFB1 Based on “Aptamer/Reduced Graphene Oxide” Nano-Bio Interaction, *Colloids Surf., B*, 2019, **175**, 98–105.
- 104 G. S. Geleta, Z. Zhao and Z. Wang, A Novel Reduced Graphene Oxide/Molybdenum Disulfide/Polyaniline Nanocomposite-Based Electrochemical Aptasensor for Detection of Aflatoxin B1, *Analyst*, 2018, **143**, 1644–1649.
- 105 G. Peng, X. Li, F. Cui, Q. Qiu, X. Chen and H. Huang, Aflatoxin B1 Electrochemical Aptasensor Based on Tetrahedral DNA Nanostructures Functionalized Three Dimensionally Ordered Macroporous MoS2–AuNPs Film, *ACS Appl. Mater. Interfaces*, 2018, **10**, 17551–17559.
- 106 G. S. Geleta, Z. Zhao and Z. Wang, A Sensitive Electrochemical Aptasensor for Detection of Aflatoxin B2 Based on a Polyacrylamide/Phytic Acid/Polydopamine Hydrogel Modified Screen Printed Carbon Electrode, *Anal. Methods*, 2018, **10**, 4689–4694.
- 107 S. H. Jalalian, M. Ramezani, N. M. Danesh, M. Alibolandi, K. Abnous and S. M. Taghdisi, A Novel Electrochemical Aptasensor for Detection of Aflatoxin M1 Based on Target-Induced Immobilization of Gold Nanoparticles on the Surface of Electrode, *Biosens. Bioelectron.*, 2018, **117**, 487–492.
- 108 C. Wang, J. Qian, K. An, C. Ren, X. Lu, N. Hao, Q. Liu, H. Li, X. Huang and K. Wang, Fabrication of Magnetically



- Assembled Aptasensing Device for Label-Free Determination of Aflatoxin B1 Based on EIS, *Biosens. Bioelectron.*, 2018, **108**, 69–75.
- 109 V. Smolko, D. Shurpik, A. Porfireva, G. Evtugyn, I. Stoikova and T. Hianik, Electrochemical Aptasensor Based on Poly (Neutral Red) and Carboxylated Pillar [5] Arene for Sensitive Determination of Aflatoxin M1, *Electroanalysis*, 2018, **30**, 486–496.
- 110 S. B. Aissa, A. Mars, G. Catanante, J.-L. Marty and N. Raouafi, Design of a Redox-Active Surface for Ultrasensitive Redox Capacitive Aptasensing of Aflatoxin M1 in Milk, *Talanta*, 2019, **195**, 525–532.
- 111 S. S. Wu, M. Wei, W. Wei, Y. Liu and S. Liu, Electrochemical Aptasensor for Aflatoxin B1 Based on Smart Host-Guest Recognition of  $\beta$ -Cyclodextrin Polymer, *Biosens. Bioelectron.*, 2019, **129**, 58–63.
- 112 C. Wang, J. Qian, K. An, X. Lu and X. Huang, A Semiconductor Quantum Dot-Based Ratiometric Electrochemical Aptasensor for the Selective and Reliable Determination of Aflatoxin B1, *Analyst*, 2019, **144**, 4772–4780.
- 113 D. Pan, G. Li, H. Hu, H. Xue, M. Zhang, M. Zhu, X. Gong, Y. Zhang, Y. Wan and Y. Shen, Direct Immunoassay for Facile and Sensitive Detection of Small Molecule Aflatoxin B1 Based on Nanobody, *Chem.–Eur. J.*, 2018, **24**, 9869–9876.
- 114 R. Mo, L. He, X. Yan, T. Su, C. Zhou, Z. Wang, P. Hong, S. Sun and C. Li, A Novel Aflatoxin B1 Biosensor Based on a Porous Anodized Alumina Membrane Modified with Graphene Oxide and an Aflatoxin B1 Aptamer, *Electrochem. Commun.*, 2018, **95**, 9–13.
- 115 S. M. Khoshfetrat, H. Bagheri and M. A. Mehrgardi, Visual Electrochemiluminescence Biosensing of Aflatoxin M1 Based on Luminol-Functionalized, Silver Nanoparticle-Decorated Graphene Oxide, *Biosens. Bioelectron.*, 2018, **100**, 382–388.
- 116 W.-J. Zeng, N. Liao, Y.-M. Lei, J. Zhao, Y.-Q. Chai, R. Yuan and Y. Zhuo, Hemin as Electrochemically Regenerable Co-Reaction Accelerator for Construction of an Ultrasensitive PTCA-Based Electrochemiluminescent Aptasensor, *Biosens. Bioelectron.*, 2018, **100**, 490–496.
- 117 Y. Wang, G. Zhao, X. Li, L. Liu, W. Cao and Q. Wei, Electrochemiluminescent Competitive Immunosensor Based on Polyethyleneimine Capped SiO<sub>2</sub> Nanomaterials as Labels to Release Ru (Bpy)<sub>3</sub><sup>2+</sup> Fixed in 3D Cu/Ni Oxalate for the Detection of Aflatoxin B1, *Biosens. Bioelectron.*, 2018, **101**, 290–296.
- 118 J. Ge, Y. Zhao, C. Li and G. Jie, Versatile Electrochemiluminescence and Electrochemical “on-off” Assays of Methyltransferases and Aflatoxin B1 Based on a Novel Multifunctional DNA Nanotube, *Anal. Chem.*, 2019, **91**, 3546–3554.
- 119 L. Kong, J. Chen, Z. Chen, J. Feng, D. Fan and Q. Wei, A Label-Free Photoelectrochemical Aptasensor Based on N-GQDs Sensitized Zn-SnS<sub>2</sub> for Aflatoxin B1 Detection, *IEEE Sens. J.*, 2018, **19**, 1633–1639.
- 120 Y. Tang, X. Liu, H. Zheng, L. Yang, L. Li, S. Zhang, Y. Zhou and S. Alwarappan, A Photoelectrochemical Aptasensor for Aflatoxin B1 Detection Based on an Energy Transfer Strategy between Ce-TiO<sub>2</sub>@MoSe<sub>2</sub> and Au Nanoparticles, *Nanoscale*, 2019, **11**, 9115–9124.
- 121 Q. Yuan, C. He, R. Mo, L. He, C. Zhou, P. Hong, S. Sun and C. Li, Detection of AFB1 via TiO<sub>2</sub> Nanotubes/Au Nanoparticles/Enzyme Photoelectrochemical Biosensor, *Coatings*, 2018, **8**, 90.
- 122 B. Zhang, Y. Lu, C. Yang, Q. Guo and G. Nie, Simple “Signal-on” Photoelectrochemical Aptasensor for Ultrasensitive Detecting AFB1 Based on Electrochemically Reduced Graphene Oxide/Poly (5-Formylindole)/Au Nanocomposites, *Biosens. Bioelectron.*, 2019, **134**, 42–48.
- 123 L. Shi, Z. Wang, G. Yang, H. Yang and F. Zhao, A Novel Electrochemical Immunosensor for Aflatoxin B1 Based on Au Nanoparticles-Poly 4-Aminobenzoic Acid Supported Graphene, *Appl. Surf. Sci.*, 2020, **527**, 146934.
- 124 L. Shi, Z. Wang, N. Wu, X. Chen, G. Yang and W. A. Liu, Simple Electrochemical Immunosensor for Highly Sensitive Detection of Aflatoxin B1 Based on Gold Nanoparticle Decorated Carboxylated Graphene Oxide, *Int. J. Electrochem. Sci.*, 2020, **15**, 1655–1668.
- 125 Z. B. Abdallah, C. Grauby-Heywang, L. Beven, S. Cassagnere, F. Moroté, E. Maillard, H. Sghaier and T. C. Bouhacina, Development of an Ultrasensitive Label-Free Immunosensor for Fungal Aflatoxin B1 Detection, *Biochem. Eng. J.*, 2019, **150**, 107262.
- 126 A. K. Singh, T. K. Dhiman and P. R. Solanki, Dimanganese Trioxide (Mn<sub>2</sub>O<sub>3</sub>) Based Label-Free Electrochemical Biosensor for Detection of Aflatoxin-B1, *Bioelectrochemistry*, 2021, **137**, 107684.
- 127 F. A. Azri, R. Sukor, J. Selamat, F. Abu Bakar, N. A. Yusof and R. Hajian, Electrochemical Immunosensor for Detection of Aflatoxin B1 Based on Indirect Competitive ELISA, *Toxins*, 2018, **10**, 196.
- 128 B. D. Abera, A. Falco, P. Ibba, G. Cantarella, L. Petti and P. Lugli, Development of Flexible Dispense-Printed Electrochemical Immunosensor for Aflatoxin M1 Detection in Milk, *Sensors*, 2019, **19**, 3912.
- 129 L. Su, P. Tong, L. Zhang, Z. Luo, C. Fu, D. Tang and Y. Zhang, Photoelectrochemical Immunoassay of Aflatoxin B1 in Foodstuff Based on Amorphous TiO<sub>2</sub> and CsPbBr<sub>3</sub> Perovskite Nanocrystals, *Analyst*, 2019, **144**, 4880–4886.
- 130 L. Su, Y. Song, C. Fu and D. Tang, Etching Reaction-Based Photoelectrochemical Immunoassay of Aflatoxin B1 in Foodstuff Using Cobalt Oxyhydroxide Nanosheets-Coating Cadmium Sulfide Nanoparticles as the Signal Tags, *Anal. Chim. Acta*, 2019, **1052**, 49–56.
- 131 H. Zhang, Z. Shi, S. Cheng, Q. Yang, X. Sun and Y. Guo, Ultrasensitive Immunosensor for Aflatoxin B1 Detection Based on Screen-Printed Carbon Electrode Modified by Ferrocene@ Multi-Walled Carbon Nanotubes, *Int. J. Electrochem. Sci.*, 2019, **14**, 9170–9180.
- 132 F. Jahangiri-Dehaghani, H. R. Zare and Z. Shekari, Measurement of Aflatoxin M1 in Powder and Pasteurized Milk Samples by Using a Label-Free Electrochemical Aptasensor Based on Platinum Nanoparticles Loaded on



- Fe-Based Metal–Organic Frameworks, *Food Chem.*, 2020, **310**, 125820.
- 133 Y. Hui, B. Wang, R. Ren, A. Zhao, F. Zhang, S. Song and Y. He, An Electrochemical Aptasensor Based on DNA-AuNPs-HRP Nanoprobes and Exonuclease-Assisted Signal Amplification for Detection of Aflatoxin B1, *Food Control*, 2020, **109**, 106902.
- 134 F. Rahimi, H. Roshanfekar and H. Peyman, Ultra-Sensitive Electrochemical Aptasensor for Label-Free Detection of Aflatoxin B1 in Wheat Flour Sample Using Factorial Design Experiments, *Food Chem.*, 2021, **343**, 128436.
- 135 Y. Li, D. Liu, C. Zhu, M. Wang, Y. Liu and T. You, A Ratiometry-Induced Successive Reusable Electrochemical Aptasensing Platform: Efficient Monitoring of Aflatoxin B1 in Peanut, *Sens. Actuators, B*, 2021, **336**, 129021.
- 136 N. E. A. El Hassani, B. Bouchikhi and N. El Bari, Recent Development of an Electrochemical Imprinted Sensor for the Detection of Trace-Level of Unmetabolized Aflatoxin B2 in Dairy Milk, *J. Electroanal. Chem.*, 2020, **865**, 114123.
- 137 H. Dai, X. Wu, S. Duan, Z. Li, Q. Zhang, Y. Shen, J. Bi, Z. Shu, A. Xiao and F. Pi, An Electrochemical Sensor Based on Curcumin-Encapsulated Zeolitic Imidazolate Framework-8 for the Sensitive Determination of Aflatoxin B1 in Grain Products, *Microchem. J.*, 2023, **191**, 108852.
- 138 J. Shen, J. Liu, S. Yang, X. Yao, H. Fa, C. Hou and M. Yang, Novel Electrochemical Sensor Based on PDA/MXene/MWCNTs/NiCo<sub>2</sub>O<sub>4</sub> Nanocomposites for Rapid, Sensitive, and Selective Detection of Aflatoxin B1, *Food Anal. Methods*, 2023, **16**, 1055–1068.
- 139 N. Wang, Q. Liu, X. Hu, F. Wang, M. Hu, Q. Yu and G. Zhang, Electrochemical Immunosensor Based on AuNPs/Zn/Ni-ZIF-8-800@ Graphene for Rapid Detection of Aflatoxin B1 in Peanut Oil, *Anal. Biochem.*, 2022, **650**, 114710.
- 140 X. Liu, R. Singh, M. Li, G. Li, R. Min, C. Marques, B. Zhang and S. Kumar, Plasmonic Sensor Based on Offset-Splicing and Waist-Expanded Taper Using Multicore Fiber for Detection of Aflatoxins B1 in Critical Sectors, *Opt. Express*, 2023, **31**, 4783–4802.
- 141 G. Ge, T. Wang, Z. Liu, X. Liu, T. Li, Y. Chen, J. Fan, E. Bukye, X. Huang and L. Song, A Self-Assembled DNA Double-Crossover-Based Fluorescent Aptasensor for Highly Sensitivity and Selectivity in the Simultaneous Detection of Aflatoxin M1 and Aflatoxin B1, *Talanta*, 2023, **265**, 124908.
- 142 R. Krska and C. S. Crews, Chemistry and Determination of Ergot Alkaloids: A Review, *Food Addit. Contam.*, 2008, **25**, 722–731.
- 143 A. Sofia, Ergot Alkaloids and Anti-Mycotoxin Strategies in Food and Feed. *Anti-Mycotoxin Strategies for Food and Feed*, 2024, pp. 237–254.
- 144 A. Grzybowski, K. Pawlikowska-Łagód and A. Polak, Ergotism and Saint Anthony's Fire, *Clin. Dermatol.*, 2021, **39**, 1088–1094.
- 145 C. De Costa, St Anthony's Fire and Living Ligatures: A Short History of Ergometrine, *Lancet*, 2002, **359**, 1768–1770.
- 146 C. S. Jamieson, J. Misa, Y. Tang and J. M. Billingsley, Biosynthesis and Synthetic Biology of Psychoactive Natural Products, *Chem. Soc. Rev.*, 2021, **50**, 6950–7008.
- 147 R. A. El-Sayed, A. B. Jeburb, W. Kange and F. M. El-Demerdash, Journal of Future Foods. J, *Future Foods*, 2022, **2**, 91–102.
- 148 M. Kuner, S. Kühn, H. Haase, K. Meyer and M. Koch, Cleaving Ergot Alkaloids by Hydrazinolysis—a Promising Approach for a Sum Parameter Screening Method, *Toxins*, 2021, **13**, 342.
- 149 F. K. Kazungu, E. M. Muindi and J. M. Mulinge, Overview of Sorghum (*Sorghum Bicolor*. L), Its Economic Importance, Ecological Requirements and Production Constraints in Kenya, *Int. J. Plant Soil Sci.*, 2023, **35**, 62–71.
- 150 K. Singh and A. Kumari, *Mycotoxins and Mycotoxicoses*, Springer, 2022.
- 151 A. L. Frederick and G. D. Stanwood, Drugs, Biogenic Amine Targets and the Developing Brain, *Dev. Neurosci.*, 2009, **31**, 7–22.
- 152 S. Berraies, M. Liu, J. G. Menzies, S. A. Tittlemier, D. P. Overy and S. Walkowiak, Ergot of Cereals: Toxins, Pathogens and Management, *Plant Pathol.*, 2024, **73**, 1301–1316.
- 153 S. Belser-Ehrlich, A. Harper, J. Hussey and R. Hallock, Human and Cattle Ergotism since 1900: Symptoms, Outbreaks, and Regulations, *Toxicol. Ind. Health*, 2013, **29**, 307–316.
- 154 B. Huybrechts, S. V. Malysheva and J. Masquelier, A Targeted UHPLC-MS/MS Method Validated for the Quantification of Ergot Alkaloids in Cereal-Based Baby Food from the Belgian Market, *Toxins*, 2021, **13**, 531.
- 155 N. M. Ali, M. Roushani and Z. M. Karazan, Novel Electrochemical Sensor Based on Polydopamine Molecularly Imprinted Polymer for Selective Determination of Methylergonovine Maleate, *IEEE Sens. J.*, 2023, **24**, 1140–1146.
- 156 M. Baniyadi, H. Maaref, A. Dorzadeh and P. Mohammad Alizadeh, A Sensitive SiO<sub>2</sub>@Fe<sub>3</sub>O<sub>4</sub>/GO Nanocomposite Modified Ionic Liquid Carbon Paste Electrode for the Determination of Cabergoline, *Iran. J. Chem. Chem. Eng.*, 2020, **39**, 11–22.
- 157 C. Schummer, L. Brune and G. Moris, Development of a UHPLC-FLD Method for the Analysis of Ergot Alkaloids and Application to Different Types of Cereals from Luxembourg, *Mycotoxin Res.*, 2018, **34**, 279–287.
- 158 N. Arroyo-Manzanares, V. Rodríguez-Estévez, A. M. García-Campaña, E. Castellón-Rendón and L. Gámiz-Gracia, Determination of Principal Ergot Alkaloids in Swine Feeding, *J. Sci. Food Agric.*, 2021, **101**, 5214–5224.
- 159 S. G. Abdulrazik, T. Z. Attia and S. M. Derayea, The First Spectrofluorimetric Protocol for Sensitive Quantitative Analysis of Bromocriptine in Its Pure and Pharmaceutical Forms: Evaluation of the Greenness of the Method, *RSC Adv.*, 2023, **13**, 35733–35740.
- 160 M. Rizk, Z. M. Mahmoud and M. M. Azab, Spectrofluorimetric and Stability-Indicating Thin Layer Chromatographic Methods for Determination of



- Cabergoline, a Prolactin Inhibitor in Pharmaceuticals, *Spectrochim. Acta, Part A*, 2022, **281**, 121639.
- 161 N. F. Farid and N. S. Abdelwahab, Development and Validation of Different Chromatographic Methods for Analysis of Cabergoline in the Presence of Its Degradation Products: Studying Degradation Profile, *Chromatographia*, 2019, **82**, 1555–1569.
- 162 L. Mohammadipoor-Ghasemabad, H. Oloumi, S. Tajik and F. Garkani Nejad, Electrochemical Sensing Platform Based on Two-Dimensional Ni-MOF and Ionic Liquid Modified Carbon Paste Electrode for Simultaneous Determination of Levodopa and Cabergoline, *J. Mater. Sci.: Mater. Electron.*, 2024, **35**, 1287.
- 163 P. M. Jahani, Electrocatalytic Determination of Levodopa in Presence of Cabergoline Using Carbon Paste Electrode Modified with Graphene Quantum Dots/2-Chlorobenzoyl Ferrocene/Ionic Liquid, *J. Electrochem. Sci. Eng.*, 2022, **12**, 81–90.
- 164 D. M. Pimentel, L. C. Arantes, L. M. Santos, K. A. O. Souza, R. M. Verly, S. L. Barbosa and W. T. P. dos Santos, Rapid and Simple Voltammetric Screening Method for Lysergic Acid Diethylamide (LSD) Detection in Seized Samples Using a Boron-Doped Diamond Electrode, *Sens. Actuators, B*, 2021, **344**, 130229.
- 165 S. Höfs, V. Jaut and R. J. Schneider, Ergometrine Sensing in Rye Flour by a Magnetic Bead-Based Immunoassay Followed by Flow Injection Analysis with Amperometric Detection, *Talanta*, 2023, **254**, 124172.
- 166 M. Pohanka, Quartz Crystal Microbalance Biosensor for Ergotamine Detection, *Int. J. Electrochem. Sci.*, 2020, **15**, 4179–4187.
- 167 M. Gross, V. Curtui and E. Usleber, Detection of Total Ergot Alkaloids in Cereal Flour and in Bread by a Generic Enzyme Immunoassay Method, *J. AOAC Int.*, 2018, **101**, 618–626.
- 168 S. Z. Mohammadi, H. Beitollahi, H. Allahabadi and T. Rohani, Disposable Electrochemical Sensor Based on Modified Screen Printed Electrode for Sensitive Cabergoline Quantification, *J. Electroanal. Chem.*, 2019, **847**, 113223.
- 169 I. Holderied, M. Rychlik and P. W. Elsingerhorst, Optimized Analysis of Ergot Alkaloids in Rye Products by Liquid Chromatography-Fluorescence Detection Applying Lysergic Acid Diethylamide as an Internal Standard, *Toxins*, 2019, **11**, 184.
- 170 S. Poapolathep, N. Klangkaew, Z. Zhang, M. Giorgi, A. F. Logrieco and A. Poapolathep, Simultaneous Determination of Ergot Alkaloids in Swine and Dairy Feeds Using Ultra High-Performance Liquid Chromatography-Tandem Mass Spectrometry, *Toxins*, 2021, **13**, 724.
- 171 J. Cherewyk, T. Grusie-Ogilvie, B. Blakley and A. Al-Dissi, Validation of a New Sensitive Method for the Detection and Quantification of R and S-Epipimers of Ergot Alkaloids in Canadian Spring Wheat Utilizing Deuterated Lysergic Acid Diethylamide as an Internal Standard, *Toxins*, 2021, **14**, 22.
- 172 L. Carbonell-Rozas, L. Gámiz-Gracia, F. J. Lara and A. M. García-Campaña, Determination of the Main Ergot Alkaloids and Their Epimers in Oat-Based Functional Foods by Ultra-High Performance Liquid Chromatography Tandem Mass Spectrometry, *Molecules*, 2021, **26**, 3717.
- 173 A. García-Juan, N. León, S. Armenta and O. Pardo, Development and Validation of an Analytical Method for the Simultaneous Determination of 12 Ergot, 2 Tropane, and 28 Pyrrolizidine Alkaloids in Cereal-Based Food by LC-MS/MS, *Food Res. Int.*, 2023, **174**, 113614.
- 174 E. Kowalczyk and K. Kwiatek, Development, in-House Validation and Application of a Method Using High-Performance Liquid Chromatography with Fluorescence Detection (HPLC-FLD) for the Quantification of 12 Ergot Alkaloids in Compound Feeds, *J. Vet. Res.*, 2023, **67**, 603.
- 175 A. Veršilovskis, P. P. J. Mulder, D. P. K. H. Pereboom-de Fauw, J. de Stoppelaar and M. de Nijs, Simultaneous Quantification of Ergot and Tropane Alkaloids in Bread in the Netherlands by LC-MS/MS, *Food Addit. Contam.:Part B*, 2020, **13**, 215–223.
- 176 N. Arroyo-Manzanares, K. De Ruyck, V. Uka, L. Gámiz-Gracia, A. M. García-Campaña, S. De Saeger and J. Diana Di Mavungu, In-House Validation of a Rapid and Efficient Procedure for Simultaneous Determination of Ergot Alkaloids and Other Mycotoxins in Wheat and Maize, *Anal. Bioanal. Chem.*, 2018, **410**, 5567–5581.
- 177 L. Carbonell-Rozas, M. Hernández-Mesa, L. Righetti, F. Monteau, F. J. Lara, L. Gámiz-Gracia, B. Le Bizec, C. Dall'Asta, A. M. García-Campaña and G. Dervilly, Ion Mobility-Mass Spectrometry to Extend Analytical Performance in the Determination of Ergot Alkaloids in Cereal Samples, *J. Chromatogr. A*, 2022, **1682**, 463502.
- 178 V. M. T. Lattanzio, E. Verdini, S. Sdogati, A. Caporali, B. Ciasca and I. Pecorelli, Undertaking a New Regulatory Challenge: Monitoring of Ergot Alkaloids in Italian Food Commodities, *Toxins*, 2021, **13**, 871.
- 179 E. Rollo, D. Catellani, C. Dall'Asta, N. Dreolin and M. Suman, Determination of Ergot Alkaloids: Comparison of Extraction Efficiencies in Several Cereal Production Chains by UPLC-MS/MS, 2024.
- 180 A. Perochon and F. M. Doohan, Trichothecenes and Fumonisin: Key Players in Fusarium–Cereal Ecosystem Interactions, *Toxins*, 2024, **16**, 90.
- 181 K. Gasser, M. Sulyok, B. Spangl, R. Krska, S. Steinkellner and K. Hage-Ahmed, Fusarium Proliferatum Secondary Metabolite Profile *in Vitro* Depends on the Origin of the Isolates and Is Clearly Reduced in Stored Garlic, *Postharvest Biol. Technol.*, 2023, **200**, 112312.
- 182 T. Li, X. Su, H. Qu, X. Duan and Y. Jiang, Biosynthesis, Regulation, and Biological Significance of Fumonisin in Fungi: Current Status and Prospects, *Crit. Rev. Microbiol.*, 2022, **48**, 450–462.
- 183 A. K. Singh, V. B. Singh, J. N. Srivastava, S. K. Singh and A. Gupta, Diseases of Maize Crops and Their Integrated Management, in *Diseases of Field Crops Diagnosis and Management*, Apple Academic Press, 2020, pp. 105–140.



- 184 E. A. Tsavkelova and G. L. Kolomeitseva, Fusarium–Orchid Interactions under Greenhouse Conditions, *S. Afr. J. Bot.*, 2022, **146**, 889–896.
- 185 I. Todorović, Y. Moënné-Loccoz, V. Raičević, J. Jovičić-Petrović and D. Muller, Microbial Diversity in Soils Suppressive to Fusarium Diseases, *Front. Plant Sci.*, 2023, **14**, 1228749.
- 186 M. I. Dinolfo, M. Martínez, E. Castañares and A. F. Arata, Fusarium in Maize during Harvest and Storage: A Review of Species Involved, Mycotoxins, and Management Strategies to Reduce Contamination, *Eur. J. Plant Pathol.*, 2022, **164**, 151–166.
- 187 S. Schaarschmidt and C. Fahl-Hassek, Mycotoxins during the Processes of Nixtamalization and Tortilla Production, *Toxins*, 2019, **11**, 227.
- 188 S. C. C. da Silva, B. Lala, C. H. de Oliveira Carniatto, C. R. Schamber, C. S. Nascimento, G. L. Braccini, C. Porto, G. Roldi, F. Tanamati and E. Gasparino, Fumonisin Affects Performance and Modulates the Gene Expression of IGF-1 and GHR in Nile Tilapia Fingerlings and Juveniles, *Aquaculture*, 2019, **507**, 233–237.
- 189 M. Kamle, D. K. Mahato, S. Devi, K. E. Lee, S. G. Kang and P. Kumar, Fumonisin: Impact on Agriculture, Food, and Human Health and Their Management Strategies, *Toxins*, 2019, **11**, 328.
- 190 T. Gutema, C. Munimbazi and L. B. Bullerman, Occurrence of Fumonisin and Moniliformin in Corn and Corn-Based Food Products of US Origin, *J. Food Prot.*, 2000, **63**, 1732–1737.
- 191 T. K. Dhiman, G. Lakshmi, K. Dave, A. Roychoudhury, N. Dalal, S. K. Jha, A. Kumar, K.-H. Han and P. R. Solanki, Rapid and Label-Free Electrochemical Detection of Fumonisin-B1 Using Microfluidic Biosensing Platform Based on Ag-CeO<sub>2</sub> Nanocomposite, *J. Electrochem. Soc.*, 2021, **168**, 77510.
- 192 H. Munawar, A. Garcia-Cruz, M. Majewska, K. Karim, W. Kutner and S. A. Piletsky, Electrochemical Determination of Fumonisin B1 Using a Chemosensor with a Recognition Unit Comprising Molecularly Imprinted Polymer Nanoparticles, *Sens. Actuators, B*, 2020, **321**, 128552.
- 193 W. Wang, Y. Yin and S. Gunasekaran, Gold Nanoparticles-Doped MXene Heterostructure for Ultrasensitive Electrochemical Detection of Fumonisin B1 and Ampicillin, *Microchim. Acta*, 2024, **191**, 294.
- 194 N. Dong, D. Liu, S. Meng, S. Liu and T. You, Tetrahedral DNA Nanostructure-Enabled Electrochemical Aptasensor for Ultrasensitive Detection of Fumonisin B1 with Extended Dynamic Range, *Sens. Actuators, B*, 2022, **354**, 130984.
- 195 L. Jin, H. Yu, W. Liu, Z. Xiao, H. Yang, B. Jin and M. Wu, Visual Measurement of Fumonisin B1 with Bipolar Electrodes Array-Based Electrochemiluminescence Biosensor, *Chemosensors*, 2023, **11**, 451.
- 196 Y. Zheng, Z. Shi, W. Wu, C. He and H. Zhang, Label-Free DNA Electrochemical Aptasensor for Fumonisin B 1 Detection in Maize Based on Graphene and Gold Nanocomposite, *J. Anal. Chem.*, 2021, **76**, 252–257.
- 197 H. Yu, H. Yang, W. Liu, L. Jin, B. Jin and M. Wu, Novel Electrochemiluminescence Biosensor of Fumonisin B1 Detection Using MWCNTs-PDMS Flexible Bipolar Electrode, *Talanta*, 2023, **257**, 124379.
- 198 X. Zhang, Z. Li, L. Hong, X. Wang and J. Cao, Tetrahedral DNA Nanostructure-Engineered Paper-Based Electrochemical Aptasensor for Fumonisin B1 Detection Coupled with Au@ Pt Nanocrystals as an Amplification Label, *J. Agric. Food Chem.*, 2023, **71**, 19121–19128.
- 199 X. Zhao, J. Gao, Y. Song, J. Zhang and Q. Han, Establishment of an Improved ELONA Method for Detecting Fumonisin B1 Based on Aptamers and Hemin-CDs Conjugates, *Sensors*, 2022, **22**, 6714.
- 200 X. Zhao, J. Gao, Y. Song, J. Zhang and Q. Han, Determination of Fumonisin B1 by Aptamer-Based Fluorescence Resonance Energy Transfer, *Sensors*, 2022, **22**, 8598.
- 201 N. R. Nirala, S. Sadhasivam, R. K. Singh, E. Sionov and G. Shtenberg, Sensitive Ratiometric Detection of Fumonisin B1 Using a Reusable Ag-PSi SERS Platform, *Food Chem.: X*, 2025, **25**, 102151.
- 202 N. Dong, S. Liu, S. Meng, Z. Chen, Y. Li, D. Liu and T. You, Light-Driven Electrochemical Biosensing with DNA Origami-Assisted Hybrid Nanoantenna for Fumonisin B1 Monitoring, *Anal. Chem.*, 2024, **96**, 12809–12816.
- 203 Y. Yang, B. Sun, Q. Ma, H. Shi, Q. Dang, Y. Liu, S. Yu, L. Bao, L. Yang and X. Shi, A Novel Electrochemical Immunosensor Based on AuNPs/NG@ PANI@ CS Was Constructed for the Highly Sensitive and Selective Detection of Mycotoxin FB1 in Food, *J. Food Compos. Anal.*, 2025, **139**, 107083.
- 204 M. Wei, F. Zhao, S. Feng and H. Jin, A Novel Electrochemical Aptasensor for Fumonisin B 1 Determination Using DNA and Exonuclease-I as Signal Amplification Strategy, *BMC Chem.*, 2019, **13**, 1–6.
- 205 E. Kesici and A. Erdem, Impedimetric Detection of Fumonisin B1 and Its Biointeraction with FsDNA, *Int. J. Biol. Macromol.*, 2019, **139**, 1117–1122.
- 206 L. Zhao, L. Zhou, D. M. Dansou, C. Tang, J. Zhang, Y. Qin and Y. Yu, Development of an Electrochemical Sensor Modified with Gold Nanoparticles for Detecting Fumonisin B1 in Packaged Foods, *RSC Adv.*, 2024, **14**, 29254–29259.
- 207 M. Wei, L. Xin, S. Feng and Y. Liu, Simultaneous Electrochemical Determination of Ochratoxin A and Fumonisin B1 with an Aptasensor Based on the Use of a Y-Shaped DNA Structure on Gold Nanorods, *Microchim. Acta*, 2020, **187**, 1–7.
- 208 E. M. Abu El Azm and T. Razek, Cyclic voltammetric study of fumonisin b1 on screen printed electrode sensor, *J. Environ. Sci.*, 2022, **51**, 1–22.
- 209 B. Naghshbandi, M. Adabi, K. Pooshang Bagheri and H. Tavakolipour, Design of a New Electrochemical Aptasensor Based on Screen Printed Carbon Electrode Modified with Gold Nanoparticles for the Detection of



- Fumonisin B1 in Maize Flour, *J. Nanobiotechnol.*, 2022, **20**, 534.
- 210 Y. Zheng, Z. Shi, W. Wu, C. He and H. Zhang, Label-Free DNA Electrochemical Aptasensor for Fumonisin B1 Detection in Maize Based on Graphene and Gold Nanocomposite, *J. Anal. Chem.*, 2021, **76**, 252–257.
- 211 Y.-T. Zheng, B.-S. Zhao, H.-B. Zhang, H. Jia and M. Wu, Colorimetric Aptasensor for Fumonisin B1 Detection by Regulating the Amount of Bubbles in Closed Bipolar Platform, *J. Electroanal. Chem.*, 2020, **877**, 114584.
- 212 S. Sarpal, A. K. Singh, H. Bhardwaj, N. K. Puri and P. R. Solanki, Graphene Oxide-Mn<sub>3</sub>O<sub>4</sub> Nanocomposites for Advanced Electrochemical Biosensor for Fumonisin B1 Detection, *Nanotechnology*, 2023, **34**, 465708.
- 213 L. Mao, K. Ji, L. Yao, X. Xue, W. Wen, X. Zhang and S. Wang, Molecularly Imprinted Photoelectrochemical Sensor for Fumonisin B1 Based on GO-CdS Heterojunction, *Biosens. Bioelectron.*, 2019, **127**, 57–63.
- 214 N. Dalal, Microfluidic Based Electrochemical Detection of Fumonisin-B1 Using Silver-Ceria Nanocomposite, *SGS-Eng. Sci.*, 2021, **1**, <https://spast.org/techrep/article/view/1387>.
- 215 L. Lu and S. Gunasekaran, Dual-Channel ITO-Microfluidic Electrochemical Immunosensor for Simultaneous Detection of Two Mycotoxins, *Talanta*, 2019, **194**, 709–716.
- 216 D. He, Z. Wu, B. Cui and E. Xu, Aptamer and Gold Nanorod-Based Fumonisin B1 Assay Using Both Fluorometry and SERS, *Microchim. Acta*, 2020, **187**, 215.
- 217 N. Dong, Y. Li, S. Meng, S. Liu, Y. Liu, D. Liu and T. You, Tetrahedral DNA Nanostructure-Based Ratiometric Electrochemical Aptasensor for Fumonisin B1: A Unity of Opposites in Binding Site and Steric Hindrance of Large-Sized DNA for Signal Amplification, *Sens. Actuators, B*, 2023, **394**, 134341.
- 218 A. K. Singh, G. Lakshmi, M. Fernandes, T. Sarkar, P. Gulati, R. P. Singh and P. R. Solanki, A Simple Detection Platform Based on Molecularly Imprinted Polymer for AFB1 and FuB1 Mycotoxins, *Microchem. J.*, 2021, **171**, 106730.
- 219 D. He, Z. Wu, B. Cui, Z. Jin and E. Xu, A Fluorometric Method for Aptamer-Based Simultaneous Determination of Two Kinds of the Fusarium Mycotoxins Zearalenone and Fumonisin B1 Making Use of Gold Nanorods and Upconversion Nanoparticles, *Microchim. Acta*, 2020, **187**, 254.
- 220 Z. Li, Y. Wang, X. Ji, C. Guo, S. Zhang, Q. Jia, M. Wang, L. He, M. Du and Z. Zhang, Ultrasensitive “Signal-Inversion” Photoelectrochemical Aptasensor Based on Semiconductive MOF Integrated with the Manganese Ferrite Nanozyme-Regulation for the Selective Detection of Fumonisin B1, *Sens. Actuators, B*, 2024, **420**, 136473.
- 221 M. Torp and W. Langseth, Production of T-2 Toxin by a Fusarium Resembling Fusarium Poae, *Mycopathologia*, 1999, **147**, 89–96.
- 222 G. Perrone, M. Ferrara, A. Medina, M. Pascale and N. Magan, Toxicogenic Fungi and Mycotoxins in a Climate Change Scenario: Ecology, Genomics, Distribution, Prediction and Prevention of the Risk, *Microorganisms*, 2020, **8**, 1496.
- 223 Q. N. Nji, O. O. Babalola, T. I. Ekwomadu, N. Nleya and M. Mwanza, Six Main Contributing Factors to High Levels of Mycotoxin Contamination in African Foods, *Toxins*, 2022, **14**, 318.
- 224 W.-H. Chang, P.-H. Chen, S. Herianto, H.-L. Chen and C.-C. Lee, Aggregating Exposures and Toxicity Equivalence Approach into an Integrated Probabilistic Dietary Risk Assessment for Perchlorate, Nitrate, and Thiocyanate: Results from the National Food Monitoring Study and National Food Consumption Database, *Environ. Res.*, 2022, **211**, 112989.
- 225 M. Polak-Śliwińska and B. Paszczyk, Trichothecenes in Food and Feed, Relevance to Human and Animal Health and Methods of Detection: A Systematic Review, *Molecules*, 2021, **26**, 454.
- 226 M. C. Paul and R. S. Dass, Trichothecenes: Toxicogenic Effects and Detoxification Strategies, *Anti-Mycotoxin Strategies for Food and Feed*, 2024, pp. 109–131.
- 227 L. N. F. Solis, G. J. S. Junior, M. Bertotti, L. Angnes, S. V. Pereira, M. A. Fernández-Baldo and M. Regiart, Electrochemical Microfluidic Immunosensor with Graphene-Decorated Gold Nanoporous for T-2 Mycotoxin Detection, *Talanta*, 2024, **273**, 125971.
- 228 J. Kudr, L. Zhao, E. P. Nguyen, H. Arola, T. K. Nevanen, V. Adam, O. Zitka and A. Merkoçi, Inkjet-Printed Electrochemically Reduced Graphene Oxide Microelectrode as a Platform for HT-2 Mycotoxin Immunoenzymatic Biosensing, *Biosens. Bioelectron.*, 2020, **156**, 112109.
- 229 L. Yao, X. Mei, J. Zhi, W. Wang, Q. Li, D. Jiang, X. Chen and Z. Chen, A Novel Electrochemiluminescent Sensor Based on AgMOF@ N-CD Composites for Sensitive Detection of Trilobatin, *Analyst*, 2024, **149**, 5265–5276.
- 230 K. Wang, H. Yan, B. He, L. Xie, R. Liu, M. Wei, H. Jin, W. Ren, Z. Suo and Y. Xu, Electrochemical Aptasensor Based on Exonuclease III-Mediated Signal Amplification for Sensitive Detection of Vomitoxin in Cornmeal, *Sci. Total Environ.*, 2023, **875**, 162561.
- 231 Y. Wang, L. Zhang, D. Peng, S. Xie, D. Chen, Y. Pan, Y. Tao and Z. Yuan, Construction of Electrochemical Immunosensor Based on Gold-Nanoparticles/Carbon Nanotubes/Chitosan for Sensitive Determination of T-2 Toxin in Feed and Swine Meat, *Int. J. Mol. Sci.*, 2018, **19**, 3895.
- 232 P. Ming, H. Lai, Y. Liu, J. Wang, F. You, D. Sun and H. Zhai, Aptasensor Development for T-2 Toxin Detection Utilizing a Dual Signal Amplification Strategy: Synergistic Effects of Bimetallic Oxide (Ce-In) Ox and COFTAPB-DMTP, *Sens. Actuators, B*, 2023, **396**, 134602.
- 233 I. F. Tahoun, M. A. Gab-Allah, R. N. Yamani and A. B. Shehata, Development and Validation of a Reliable LC-MS/MS Method for Simultaneous Determination of Deoxynivalenol and T-2 Toxin in Maize and Oats, *Microchem. J.*, 2021, **169**, 106599.



- 234 J. Lai, L. Ding, Y. Liu, C. Fan, F. You, J. Wei, J. Qian and K. Wang, A Miniaturized Organic Photoelectrochemical Transistor Aptasensor Based on Nanorod Arrays toward High-Sensitive T-2 Toxin Detection in Milk Samples, *Food Chem.*, 2023, **423**, 136285.
- 235 X. Zhao, Y. Wang, J. Li, B. Huo, Y. Qin, J. Zhang, M. Chen, Y. Peng, J. Bai and S. Li, A Fluorescence Aptasensor Based on Controlled Zirconium-Based MOFs for the Highly Sensitive Detection of T-2 Toxin, *Spectrochim. Acta, Part A*, 2021, **259**, 119893.
- 236 W. Zhang, Y. Wang, M. Nan, Y. Li, J. Yun, Y. Wang and Y. Bi, Novel Colorimetric Aptasensor Based on Unmodified Gold Nanoparticle and SsDNA for Rapid and Sensitive Detection of T-2 Toxin, *Food Chem.*, 2021, **348**, 129128.
- 237 H. Zheng, H. Yi, H. Dai, D. Fang, Z. Hong, D. Lin, X. Zheng and Y. Lin, Fluoro-Coumarin Silicon Phthalocyanine Sensitized Integrated Electrochemiluminescence Bioprobe Constructed on TiO<sub>2</sub> MOFs for the Sensing of Deoxynivalenol, *Sens. Actuators, B*, 2018, **269**, 27–35.
- 238 A.-E. Radi, A. Eissa and T. Wahdan, Impedimetric Sensor for Deoxynivalenol Based on Electropolymerised Molecularly Imprinted Polymer on the Surface of Screen-Printed Gold Electrode, *Int. J. Environ. Anal. Chem.*, 2021, **101**, 2586–2597.
- 239 E. Valera, R. García-Febrero, C. T. Elliott, F. Sánchez-Baeza and M.-P. Marco, Electrochemical Nanoprobe-Based Immunosensor for Deoxynivalenol Mycotoxin Residues Analysis in Wheat Samples, *Anal. Bioanal. Chem.*, 2019, **411**, 1915–1926.
- 240 Y. Peng, L. Geng, X. Liu, M. Liu, H. Wu and J. Li, A Label-Free Small Molecular Hydrogel-Based Electrochemical Immunosensor for Ultrasensitive Detection of Deoxynivalenol, *Anal. Methods*, 2019, **11**, 5948–5952.
- 241 C. C. Ong, S. S. Sangu, N. M. Illias, S. C. B. Gopinath and M. S. M. Saheed, Iron Nanoflorets on 3D-Graphene-Nickel: A 'Dandelion' Nanostructure for Selective Deoxynivalenol Detection, *Biosens. Bioelectron.*, 2020, **154**, 112088.
- 242 H. Zhong, C. Yu, R. Gao, J. Chen, Y. Yu, Y. Geng, Y. Wen and J. He, A Novel Sandwich Aptasensor for Detecting T-2 Toxin Based on RGO-TEPA-Au@ Pt Nanorods with a Dual Signal Amplification Strategy, *Biosens. Bioelectron.*, 2019, **144**, 111635.
- 243 S. Niazi, I. M. Khan, Y. Yu, I. Pasha, M. Shoaib, A. Mohsin, B. S. Mushtaq, W. Akhtar and Z. A. Wang, "Turnon" Aptasensor for Simultaneous and Time-Resolved Fluorometric Determination of Zearalenone, Trichothecenes A and Aflatoxin B1 Using WS2 as a Quencher, *Microchim. Acta*, 2019, **186**, 575.
- 244 I. M. Khan, S. Zhao, S. Niazi, A. Mohsin, M. Shoaib, N. Duan, S. Wu and Z. Wang, Silver Nanoclusters Based FRET Aptasensor for Sensitive and Selective Fluorescent Detection of T-2 Toxin, *Sens. Actuators, B*, 2018, **277**, 328–335.
- 245 A. F. Mahmoud, L. Escrivá, Y. Rodríguez-Carrasco, J. C. Moltó and H. Berrada, Determination of Trichothecenes in Chicken Liver Using Gas Chromatography Coupled with Triple-Quadrupole Mass Spectrometry, *LWT*, 2018, **93**, 237–242.
- 246 M. A. Gab-Allah, K. Choi and B. Kim, Accurate Determination of Type B Trichothecenes and Conjugated Deoxynivalenol in Grains by Isotope Dilution-Liquid Chromatography Tandem Mass Spectrometry, *Food Control*, 2021, **121**, 107557.
- 247 I. M. Khan, S. Niazi, Y. Yu, I. Pasha, L. Yue, A. Mohsin, M. Shoaib, M. W. Iqbal, A. Khaliq and Z. Wang, Fabrication of PAA Coated Green-Emitting AuNCs for Construction of Label-Free FRET Assembly for Specific Recognition of T-2 Toxin, *Sens. Actuators, B*, 2020, **321**, 128470.
- 248 X. Zhao, Y. Wang, J. Li, B. Huo, H. Huang, J. Bai, Y. Peng, S. Li, D. Han and S. Ren, A Fluorescence Aptasensor for the Sensitive Detection of T-2 Toxin Based on FRET by Adjusting the Surface Electric Potentials of UCNPs and MIL-101, *Anal. Chim. Acta*, 2021, **1160**, 338450.
- 249 L. Gao, J. Sun, L. Wang, Q. Fan, G. Zhu, H. Guo and X. Sun, Highly Sensitive Real-Time Detection of Intracellular Oxidative Stress and Application in Mycotoxin Toxicity Evaluation Based on Living Single-Cell Electrochemical Sensors, *Analyst*, 2021, **146**, 1444–1454.
- 250 J. Lai, L. Ding, Y. Liu, C. Fan, J. Wei, N. Hao, J. Qian and K. Wang, Highly Sensitive Detection of T-2 Toxin Using Photo Induced Zero-Gating Voltage Organic Electrochemical Transistor Aptasensor Based on Zn Nanorod Arrays, Available at SSRN 4049612.
- 251 F. Malvano, R. Pilloton, A. Rubino and D. Albanese, Rapid Detection of Deoxynivalenol in Dry Pasta Using a Label-Free Immunosensor, *Biosensors*, 2022, **12**, 240.
- 252 L. Wang, H. Jin, M. Wei, W. Ren, Y. Zhang, L. Jiang, T. Wei and B. He, A DNzyme-Assisted Triple-Amplified Electrochemical Aptasensor for Ultra-Sensitive Detection of T-2 Toxin, *Sens. Actuators, B*, 2021, **328**, 129063.
- 253 J. Wu, B. He, Y. Wang, R. Zhao, Y. Zhang, C. Bai, M. Wei, H. Jin, W. Ren and Z. Suo, ZIF-8 Labelled a New Electrochemical Aptasensor Based on PEI-PrGO/AuNWs for DON Detection, *Talanta*, 2024, **267**, 125257.
- 254 K. Wang, B. He, L. Xie, L. Li, J. Yang, R. Liu, M. Wei, H. Jin and W. Ren, Exonuclease III-Assisted Triple-Amplified Electrochemical Aptasensor Based on PtPd NPs/PEI-RGO for Deoxynivalenol Detection, *Sens. Actuators, B*, 2021, **349**, 130767.
- 255 X. Lu, L. Wang, B. He, R. Zhao, C. Bai, Y. Zhang, W. Ren, L. Jiang, Z. Suo and Y. Xu, AgPdNFs and AuNOs@GO Nanocomposites for T-2 Toxin Detection by Catalytic Hairpin Assembly, *Microchim. Acta*, 2023, **190**, 120.
- 256 Z. Yuan, H. Dai, X. Liu, S. Duan, Y. Shen, Q. Zhang, Z. Shu, A. Xiao and J. Wang, An Electrochemical Immunosensor Based on Prussian Blue@ Zeolitic Imidazolate Framework-8 Nanocomposites Probe for the Detection of Deoxynivalenol in Grain Products, *Food Chem.*, 2023, **405**, 134842.
- 257 L. Wang, X. Lu, R. Zhao, Z. Qu and B. He, FeMOF-Based Nanostructured Platforms for T-2 Toxin Detection in Beer



- by a “Fence-Type” Aptasensing Principle, *Anal. Bioanal. Chem.*, 2022, **414**, 7999–8008.
- 258 M. Mostrom, Trichothecenes and Zearalenone, in *Reproductive and Developmental Toxicology*, Elsevier, 2011, pp. 739–751.
- 259 A. Balló, K. Busznyákné Székvári, P. Czétány, L. Márk, A. Török, Á. Szántó and G. Máté, Estrogenic and Non-Estrogenic Disruptor Effect of Zearalenone on Male Reproduction: A Review, *Int. J. Mol. Sci.*, 2023, **24**, 1578.
- 260 K. Kościelecka, A. Kuć, D. Kubik-Machura, T. Męcik-Kronenberg, J. Włodarek and L. Radko, Endocrine Effect of Some Mycotoxins on Humans: A Clinical Review of the Ways to Mitigate the Action of Mycotoxins, *Toxins*, 2023, **15**, 515.
- 261 K. Veenuttranon, X. Lu and J. Chen, Ultrasensitive Electrochemical Sensing for Simultaneous Rapid Detection of Zearalenone and Ochratoxin A in Feedstuffs and Foodstuffs, *Chem. Eng. J.*, 2024, **497**, 154807.
- 262 F. A. Azri, S. Eissa, M. Zourob, R. Chinnappan, R. Sukor, N. A. Yusof, N. H. A. Raston, A. Alhoshani and S. Jinap, Electrochemical Determination of Zearalenone Using a Label-Free Competitive Aptasensor, *Microchim. Acta*, 2020, **187**, 266.
- 263 B. Zhou, H. Xie, S. Zhou, X. Sheng, L. Chen and M. Zhong, Construction of AuNPs/Reduced Graphene Nanoribbons Co-Modified Molecularly Imprinted Electrochemical Sensor for the Detection of Zearalenone, *Food Chem.*, 2023, **423**, 136294.
- 264 H. Lai, P. Ming, M. Wu, S. Wang, D. Sun and H. Zhai, An Electrochemical Aptasensor Based on P-Ce-MOF@MWCNTs as Signal Amplification Strategy for Highly Sensitive Detection of Zearalenone, *Food Chem.*, 2023, **423**, 136331.
- 265 J. Wang, Y. Zhang, C. Qi, H. Xu, X. Lu, X. Ma and W. Zhang, Detection of Zearalenone by Electrochemical Aptasensor Based on Enzyme-Assisted Target Recycling and DNAzyme Release Strategy, *Talanta*, 2025, **286**, 127533, DOI: [10.1016/j.talanta.2025.127533](https://doi.org/10.1016/j.talanta.2025.127533).
- 266 N. Ç. Rehman, N. Özdemir, H. Boyacıoğlu and M. L. Yola, A Novel Molecularly Imprinted Electrochemical Sensor Based on Graphitic Carbon Nitride Nanosheets Decorated Bovine Serum Albumin@ MnO<sub>2</sub> Nanocomposite for Zearalenone Detection, *J. Food Compos. Anal.*, 2024, **125**, 105857.
- 267 B. Liu, X. Zhao, J. Peng, L. Chen, H. Wang and S. Wang, An Electrochemical Sensor for the Rapid Detection of Zearalenone Based on the Mimic Peptide Screened by Molecular Simulation, *Food Chem.*, 2024, **460**, 140364, DOI: [10.1016/j.foodchem.2024.140364](https://doi.org/10.1016/j.foodchem.2024.140364).
- 268 Y. Zeng, M. B. Camarada, X. Lu, K. Tang, W. Li, D. Qiu, Y. Wen, G. Wu, Q. Luo and L. Bai, Detection and Electrocatalytic Mechanism of Zearalenone Using Nanohybrid Sensor Based on Copper-Based Metal-Organic Framework/Magnetic Fe<sub>3</sub>O<sub>4</sub>-Graphene Oxide Modified Electrode, *Food Chem.*, 2022, **370**, 131024, DOI: [10.1016/j.foodchem.2021.131024](https://doi.org/10.1016/j.foodchem.2021.131024).
- 269 C. Wang, X. Zhu, L. Zhang, Q. Song, H. Xu and X. Liu, Electrochemical Sensor Based on CuO Nanoparticles-Modified Graphene Oxide (CuO@GO) Nanocomposites for Determination of Zearalenone Mycotoxins in Food Samples, *Int. J. Electrochem. Sci.*, 2021, **16**(4), 210435, DOI: [10.20964/2021.04.59](https://doi.org/10.20964/2021.04.59).
- 270 K. Zhao, B. Zhang, X. Cui, X. Chao, F. Song, H. Chen and B. He, An Electrochemical Aptamer-Sensing Strategy Based on a Ti<sub>3</sub>C<sub>2</sub>T<sub>x</sub> MXene Synergistic Ti-MOF Amplification Signal for Highly Sensitive Detection of Zearalenone, *Food Chem.*, 2024, **461**, 140828, DOI: [10.1016/j.foodchem.2024.140828](https://doi.org/10.1016/j.foodchem.2024.140828).
- 271 S. Niazi, X. Wang, I. Pasha, I. M. Khan, S. Zhao, M. Shoaib, S. Wu and Z. Wang, A Novel Bioassay Based on Aptamer-Functionalized Magnetic Nanoparticle for the Detection of Zearalenone Using Time Resolved-Fluorescence NaYF<sub>4</sub>: Ce/Tb Nanoparticles as Signal Probe, *Talanta*, 2018, **186**, 97–103, DOI: [10.1016/j.talanta.2018.04.013](https://doi.org/10.1016/j.talanta.2018.04.013).
- 272 Z. Mu, L. Ma, J. Wang, J. Zhou, Y. Yuan and L. Bai, A Target-Induced Amperometric Aptasensor for Sensitive Zearalenone Detection by CS@AB-MWCNTs Nanocomposite as Enhancers, *Food Chem.*, 2021, **340**, 128128, DOI: [10.1016/j.foodchem.2020.128128](https://doi.org/10.1016/j.foodchem.2020.128128).
- 273 B. He and X. Yan, An Amperometric Zearalenone Aptasensor Based on Signal Amplification by Using a Composite Prepared from Porous Platinum Nanotubes, Gold Nanoparticles and Thionine-Labelled Graphene Oxide, *Microchim. Acta*, 2019, **186**, 383, DOI: [10.1007/s00604-019-3500-z](https://doi.org/10.1007/s00604-019-3500-z).
- 274 S. Sun, R. Zhao, S. Feng and Y. Xie, Colorimetric Zearalenone Assay Based on the Use of an Aptamer and of Gold Nanoparticles with Peroxidase-like Activity, *Microchim. Acta*, 2018, **185**(12), 535, DOI: [10.1007/s00604-018-3078-x](https://doi.org/10.1007/s00604-018-3078-x).
- 275 S. Sun, R. Zhao, S. Feng and Y. Xie, Colorimetric Zearalenone Assay Based on the Use of an Aptamer and of Gold Nanoparticles with Peroxidase-like Activity, *Microchim. Acta*, 2018, **185**(12), 535, DOI: [10.1007/s00604-018-3078-x](https://doi.org/10.1007/s00604-018-3078-x).
- 276 S. M. Taghdisi, N. M. Danesh, M. Ramezani, A. S. Emrani and K. Abnous, Novel Colorimetric Aptasensor for Zearalenone Detection Based on Nontarget-Induced Aptamer Walker, Gold Nanoparticles, and Exonuclease-Assisted Recycling Amplification, *ACS Appl. Mater. Interfaces*, 2018, **10**(15), 12504–12509, DOI: [10.1021/acsami.8b02349](https://doi.org/10.1021/acsami.8b02349).
- 277 S. Wu, L. Liu, N. Duan, Q. Li, Y. Zhou and Z. Wang, Aptamer-Based Lateral Flow Test Strip for Rapid Detection of Zearalenone in Corn Samples, *J. Agric. Food Chem.*, 2018, **66**(8), 1949–1954, DOI: [10.1021/acs.jafc.7b05326](https://doi.org/10.1021/acs.jafc.7b05326).
- 278 Z. Han, Z. Tang, K. Jiang, Q. Huang, J. Meng, D. Nie and Z. Zhao, Dual-Target Electrochemical Aptasensor Based on Co-Reduced Molybdenum Disulfide and Au NPs (RMOs2-Au) for Multiplex Detection of Mycotoxins, *Biosens. Bioelectron.*, 2020, **150**, 111894, DOI: [10.1016/j.bios.2019.111894](https://doi.org/10.1016/j.bios.2019.111894).
- 279 M. Regiart, O. Fernández, A. Vicario, J. Villarroel-Rocha, K. Sapag, G. A. Messina, J. Raba and F. A. Bertolino,



- Mesoporous Immunosensor Applied to Zearalenone Determination in *Amaranthus Cruentus* Seeds, *Microchem. J.*, 2018, **141**, 388–394, DOI: [10.1016/j.microc.2018.05.051](https://doi.org/10.1016/j.microc.2018.05.051).
- 280 Y. Chen, X. Meng, Y. Zhu, M. Shen, Y. Lu, J. Cheng and Y. Xu, Rapid Detection of Four Mycotoxins in Corn Using a Microfluidics and Microarray-Based Immunoassay System, *Talanta*, 2018, **186**, 299–305, DOI: [10.1016/j.talanta.2018.04.064](https://doi.org/10.1016/j.talanta.2018.04.064).
- 281 L. Ma, L. Bai, M. Zhao, J. Zhou, Y. Chen and Z. Mu, An Electrochemical Aptasensor for Highly Sensitive Detection of Zearalenone Based on PEI-MoS<sub>2</sub>-MWCNTs Nanocomposite for Signal Enhancement, *Anal. Chim. Acta*, 2019, **1060**, 71–78, DOI: [10.1016/j.aca.2019.02.012](https://doi.org/10.1016/j.aca.2019.02.012).
- 282 X. Ji, C. Yu, Y. Wen, J. Chen, Y. Yu, C. Zhang, R. Gao, X. Mu and J. He, Fabrication of Pioneering 3D Sakura-Shaped Metal-Organic Coordination Polymers Cu@L-Glu Phenomenal for Signal Amplification in Highly Sensitive Detection of Zearalenone, *Biosens. Bioelectron.*, 2019, **129**, 139–146, DOI: [10.1016/j.bios.2019.01.012](https://doi.org/10.1016/j.bios.2019.01.012).
- 283 K. Yugender Goud, V. Sunil Kumar, A. Hayat, K. Vengatajalabathy Gobi, H. Song, K. H. Kim and J. L. Marty, A Highly Sensitive Electrochemical Immunosensor for Zearalenone Using Screen-Printed Disposable Electrodes, *J. Electroanal. Chem.*, 2019, **832**, 336–342, DOI: [10.1016/j.jelechem.2018.10.058](https://doi.org/10.1016/j.jelechem.2018.10.058).
- 284 A. E. Radi, A. Eissa and T. Wahdan, Electrocatalytic Oxidation of Zearalenone on Cobalt Phthalocyanine-Modified Screen-Printed Carbon Electrode, *Monatsh. Chem.*, 2020, **151**(1), 45–50, DOI: [10.1007/s00706-019-02532-1](https://doi.org/10.1007/s00706-019-02532-1).
- 285 A. Erdem, E. Eksin, E. Kesici, E. Yaralı and E. Kanat, Single-Use Sensor Technology for Monitoring of Zearalenone in Foods: ZentoSens, *Microchem. J.*, 2019, **147**, 37–42, DOI: [10.1016/j.microc.2019.03.001](https://doi.org/10.1016/j.microc.2019.03.001).
- 286 A. E. Radi, A. Eissa and T. Wahdan, Voltammetric Behavior of Mycotoxin Zearalenone at a Single Walled Carbon Nanotube Screen-Printed Electrode, *Anal. Methods*, 2019, **11**(35), 4494–4500, DOI: [10.1039/c9ay01400d](https://doi.org/10.1039/c9ay01400d).
- 287 S. Moradi, M. Azizi-Lalabadi, V. Bagheri and E. Sadeghi, Fabrication of Electrospun Sensor Based on a Synthesized Component Doped into PAN (Polyacrylonitrile) Nanofibers for Electrochemical Detection of Zearalenone Mycotoxin in Foods Simulant, *Sens. Biosensing. Res.*, 2020, **28**, 100321, DOI: [10.1016/j.sbsr.2020.100321](https://doi.org/10.1016/j.sbsr.2020.100321).
- 288 W. I. Riberi, L. V. Tarditto, M. A. Zon, F. J. Arévalo and H. Fernández, Development of an Electrochemical Immunosensor to Determine Zearalenone in Maize Using Carbon Screen Printed Electrodes Modified with Multi-Walled Carbon Nanotubes/Polyethyleneimine Dispersions, *Sens. Actuators, B*, 2018, **254**, 1271–1277, DOI: [10.1016/j.snb.2017.07.113](https://doi.org/10.1016/j.snb.2017.07.113).
- 289 B. He and X. A. Yan, “Signal-on” Voltammetric Aptasensor Fabricated by HcPt@AuNFs/PEI-RGO and Fe<sub>3</sub>O<sub>4</sub>NRs/RGO for the Detection of Zearalenone, *Sens. Actuators, B*, 2019, **290**, 477–483, DOI: [10.1016/j.snb.2019.04.005](https://doi.org/10.1016/j.snb.2019.04.005).
- 290 B. He and X. Yan, Ultrasensitive Electrochemical Aptasensor Based on CoSe<sub>2</sub>/AuNRs and 3D Structured DNA-PtNi@Co-MOF Networks for the Detection of Zearalenone, *Sens. Actuators, B*, 2020, **306**, 127558, DOI: [10.1016/j.snb.2019.127558](https://doi.org/10.1016/j.snb.2019.127558).
- 291 A. Foubert, N. V. Beloglazova, M. Hedström and S. De Saeger, Antibody Immobilization Strategy for the Development of a Capacitive Immunosensor Detecting Zearalenone, *Talanta*, 2019, **191**, 202–208, DOI: [10.1016/j.talanta.2018.08.062](https://doi.org/10.1016/j.talanta.2018.08.062).
- 292 Y. Wang, G. Zhao, H. Wang, Y. Zhang, N. Zhang, D. Wei, R. Feng and Q. Wei, Label-Free Electrochemical Immunosensor Based on Biocompatible Nanoporous Fe<sub>3</sub>O<sub>4</sub> and Biotin-Streptavidin System for Sensitive Detection of Zearalenone, *Analyst*, 2020, **145**(4), 1368–1375, DOI: [10.1039/c9an02543j](https://doi.org/10.1039/c9an02543j).
- 293 G. S. Zaman, I. Waleed, R. A. Obeid, S. A. Khudair, S. A. Abd Al-Kahdum, K. Al-Majdi, A. S. Abed, A. Alsalamy, M. T. Qasim and A. H. R. Alawadi, Electrochemical Determination of Zearalenone in Agricultural Food Samples Using a Flower like Nanocomposite-Modified Electrode, *Mater. Chem. Phys.*, 2023, **305**, 127986.
- 294 L. Zhao, L. Zhou, D. M. Dansou, C. Tang, J. Zhang, Y. Qin and Y. Yu, Ultrasensitive Analyses of Zearalenone in Grain Samples with a Catalytic Oxidation Platform Involving Gold Nanomaterials, *Food Chem.: X*, 2024, **23**, 101666, DOI: [10.1016/j.FOCHX.2024.101666](https://doi.org/10.1016/j.FOCHX.2024.101666).
- 295 Z. Guo, L. Gao, L. Yin, M. Arslan, H. R. El-Seedi and X. Zou, Novel Mesoporous Silica Surface Loaded Gold Nanocomposites SERS Aptasensor for Sensitive Detection of Zearalenone, *Food Chem.*, 2023, **403**, 134384, DOI: [10.1016/j.foodchem.2022.134384](https://doi.org/10.1016/j.foodchem.2022.134384).
- 296 L. Yin, T. You, H. R. El-Seedi, I. M. El-Garawani, Z. Guo, X. Zou and J. Cai, Rapid and Sensitive Detection of Zearalenone in Corn Using SERS-Based Lateral Flow Immunosensor, *Food Chem.*, 2022, **396**, 133707, DOI: [10.1016/j.foodchem.2022.133707](https://doi.org/10.1016/j.foodchem.2022.133707).
- 297 W. Zhu, G. Ji, R. Chen, Y. Xiang, S. Ji, S. Zhang, Z. Gao, H. Liu, Y. Wang and T. A. Han, Fluorescence Aptasensor Based on Hybridization Chain Reaction for Simultaneous Detection of T-2 Toxins and Zearalenone, *Talanta*, 2023, **255**, 124249, DOI: [10.1016/j.talanta.2022.124249](https://doi.org/10.1016/j.talanta.2022.124249).
- 298 Z. Huang, X. Luo, F. Yan and B. Zhou, Homogeneous Electrochemical Aptasensor for Sensitive Detection of Zearalenone Using Nanocomposite Probe and Silica Nanochannel Film, *Molecules*, 2023, **28**(21), 7241, DOI: [10.3390/molecules28217241](https://doi.org/10.3390/molecules28217241).
- 299 L. Luo, X. Liu, X. Bi, L. Li and T. You, Dual-Quenching Effects of Methylene Blue on the Luminophore and Co-Reactant: Application for Electrochemiluminescent-Electrochemical Ratiometric Zearalenone Detection, *Biosens. Bioelectron.*, 2023, **222**, 114991, DOI: [10.1016/j.bios.2022.114991](https://doi.org/10.1016/j.bios.2022.114991).
- 300 K. Guo, Design and Fabrication of a Molecularly Imprinted Electrochemical Sensor with High Sensitivity for Zearalenone Assessment in Maize, *Int. J. Electrochem. Sci.*, 2024, **19**(6), 100612, DOI: [10.1016/j.IJOES.2024.100612](https://doi.org/10.1016/j.IJOES.2024.100612).



- 301 G. Liu, Z. Liu, Y. Sun, M. Sun, J. Duan, Y. Tian, D. Du and M. Li, Cascade Amplifying Electrochemical Bioanalysis for Zearalenone Detection in Agricultural Products: Utilizing a Glucose–Fenton–HQ System on Bimetallic–ZIF@CNP Nanocomposites, *Foods*, 2024, **13**(19), 3192, DOI: [10.3390/foods13193192](https://doi.org/10.3390/foods13193192).
- 302 H. Yan, B. He, W. Ren, Z. Suo, Y. Xu, L. Xie, L. Li, J. Yang and R. Liu, A Label-Free Electrochemical Immunosensing Platform Based on PEI-RGO/Pt@Au NRs for Rapid and Sensitive Detection of Zearalenone, *Bioelectrochemistry*, 2022, **143**, 107955, DOI: [10.1016/j.bioelechem.2021.107955](https://doi.org/10.1016/j.bioelechem.2021.107955).
- 303 V. S. Kumar, S. Kummari, G. Catanante, K. V. Gobi, J. L. Marty and K. Y. Goud, A Label-Free Impedimetric Immunosensor for Zearalenone Based on CS-CNT-Pd Nanocomposite Modified Screen-Printed Disposable Electrodes, *Sens. Actuators, B*, 2023, **377**, 133077, DOI: [10.1016/j.snb.2022.133077](https://doi.org/10.1016/j.snb.2022.133077).
- 304 A. Laza, S. V. Pereira, G. A. Messina, M. A. Fernández-Baldo, J. Raba, M. D. Regiart and F. A. Bertolino, Origami Paper-Based Electrochemical Immunosensor with Carbon Nanohorns-Decorated Nanoporous Gold for Zearalenone Detection, *Chemosensors*, 2024, **12**(1), 10, DOI: [10.3390/chemosensors12010010](https://doi.org/10.3390/chemosensors12010010).
- 305 N. Ç. Rehman, N. Özdemir, H. Boyacıoğlu and M. L. Yola, A Novel Molecularly Imprinted Electrochemical Sensor Based on Graphitic Carbon Nitride Nanosheets Decorated Bovine Serum Albumin@MnO<sub>2</sub> Nanocomposite for Zearalenone Detection, *J. Food Compos. Anal.*, 2024, **125**, 105857, DOI: [10.1016/j.jfca.2023.105857](https://doi.org/10.1016/j.jfca.2023.105857).
- 306 I. Székács, N. Adányi, I. Szendrő and A. Székács, Direct and Competitive Optical Grating Immunosensors for Determination of Fusarium Mycotoxin Zearalenone, *Toxins*, 2021, **13**(1), 43, DOI: [10.3390/TOXINS13010043](https://doi.org/10.3390/TOXINS13010043).
- 307 Y. Li, Y. Li, D. Zhang, W. Tan, J. Shi, Z. Li, H. Liu, Y. Yu, L. Yang, X. Wang, Y. Gong and X. Zou, A Fluorescence Resonance Energy Transfer Probe Based on Functionalized Graphene Oxide and Upconversion Nanoparticles for Sensitive and Rapid Detection of Zearalenone, *LWT*, 2021, **147**, 111541, DOI: [10.1016/j.lwt.2021.111541](https://doi.org/10.1016/j.lwt.2021.111541).
- 308 M. Kang, Y. Yao, B. Yuan, S. Zhang, O. Oderinde and Z. Zhang, A Sensitive Bimetallic Copper/Bismuth Metal-Organic Frameworks-Based Aptasensors for Zearalenone Detection in Foodstuffs, *Food Chem.*, 2024, **437**, 137827, DOI: [10.1016/j.foodchem.2023.137827](https://doi.org/10.1016/j.foodchem.2023.137827).
- 309 B. Zhou, H. Xie, X. Li, Y. Zhu, L. Huang, M. Zhong and L. Chen, Construction of a Self-Reporting Molecularly-Imprinted Electrochemical Sensor Based on CuHCF Modified by RGNR–RGO for the Detection of Zearalenone, *Food Chem.*, 2024, **448**, 139154.
- 310 S. J. Huang, K. Gokulkumar, G. Mani, Y. Y. Lee, S. Kogularasu and G. P. Chang-Chien, Synthesis and Characterization of Bi<sub>2</sub>S<sub>3</sub>-Embedded Carbon Nanofibers as a Novel Electrochemical Biosensor for the Detection of Mycotoxin Zearalenone in Food Crops, *FlatChem*, 2024, **45**, 100652, DOI: [10.1016/j.flatc.2024.100652](https://doi.org/10.1016/j.flatc.2024.100652).
- 311 S. Pal, N. Singh and K. M. Ansari, Toxicological Effects of Patulin Mycotoxin on the Mammalian System: An Overview, *Toxicol. Res.*, 2017, 764–771, DOI: [10.1039/c7tx00138j](https://doi.org/10.1039/c7tx00138j).
- 312 S. Duan, F. Liu, Q. Qin, Q. Jia, X. Cao, Z. Hua, Y. Fan and C. Wang, Implementation of the HACCP System for Apple Juice Concentrate Based on Patulin Prevention and Control, *Foods*, 2023, **12**(4), 786, DOI: [10.3390/foods12040786](https://doi.org/10.3390/foods12040786).
- 313 M. Sajid, S. Mehmood, Y. Yuan and T. Yue, Mycotoxin Patulin in Food Matrices: Occurrence and Its Biological Degradation Strategies, *Drug Metab. Rev.*, 2019, 105–120, DOI: [10.1080/03602532.2019.1589493](https://doi.org/10.1080/03602532.2019.1589493).
- 314 W. Chen and A. Narbad, *Lactic Acid Bacteria in Foodborne Hazards Reduction*, 2018, DOI: [10.1007/978-981-13-1559-6](https://doi.org/10.1007/978-981-13-1559-6).
- 315 S. A. S. Bacha, Y. Li, J. Nie, G. Xu, L. Han and S. Farooq, Comprehensive Review on Patulin and Alternaria Toxins in Fruit and Derived Products, *Front. Plant Sci.*, 2023, **14**, 1139757, DOI: [10.3389/fpls.2023.1139757](https://doi.org/10.3389/fpls.2023.1139757).
- 316 S. Shukla, Y. Haldorai, I. Khan, S. M. Kang, C. H. Kwak, S. Gandhi, V. K. Bajpai, Y. S. Huh and Y. K. Han, Bioreceptor-Free, Sensitive and Rapid Electrochemical Detection of Patulin Fungal Toxin, Using a Reduced Graphene Oxide@SnO<sub>2</sub> Nanocomposite, *Mater. Sci. Eng., C*, 2020, **113**, 110916, DOI: [10.1016/j.msec.2020.110916](https://doi.org/10.1016/j.msec.2020.110916).
- 317 Z. Afzali, A. Mohadesi, M. Ali Karimi and F. Fathirad, A Highly Selective and Sensitive Electrochemical Sensor Based on Graphene Oxide and Molecularly Imprinted Polymer Magnetic Nanocomposite for Patulin Determination, *Microchem. J.*, 2022, **177**, 107215, DOI: [10.1016/j.microc.2022.107215](https://doi.org/10.1016/j.microc.2022.107215).
- 318 B. Hatamluyi, M. Rezayi, H. R. Beheshti and M. T. Boroushaki, Ultra-Sensitive Molecularly Imprinted Electrochemical Sensor for Patulin Detection Based on a Novel Assembling Strategy Using Au@Cu-MOF/N-GQDs, *Sens. Actuators, B*, 2020, **318**, 128219, DOI: [10.1016/j.snb.2020.128219](https://doi.org/10.1016/j.snb.2020.128219).
- 319 S. Xue, L. Yin, S. Gao, R. Zhou, Y. Zhang, H. Jayan, H. R. El-Seedi, X. Zou and Z. Guo, A Film-like SERS Aptasensor for Sensitive Detection of Patulin Based on GO@Au Nanosheets, *Food Chem.*, 2024, **441**, 138364, DOI: [10.1016/j.foodchem.2024.138364](https://doi.org/10.1016/j.foodchem.2024.138364).
- 320 S. Liu, N. Dong, S. Meng, Y. Li, Y. Li, S. Wang, D. Liu and T. You, Operando Photoelectrochemical Surface-Enhanced Raman Spectroscopy: Interfacial Mechanistic Insights and Simultaneous Detection of Patulin, *Anal. Chem.*, 2025, **97**(2), 1329–1337, DOI: [10.1021/acs.analchem.4c05669](https://doi.org/10.1021/acs.analchem.4c05669).
- 321 C. Jiang, Y. Wang, J. Liang, L. Xie, Z. Liang, K. Huang, H. Li, T. Li, D. Ning, L. Tang, X. Huang, L. Luo, Y. Ya and F. Yan, High Sensitive and Selective Electrochemical Aptasensor for Patulin Detection Based on a Novel Assembling Strategy Using Hierarchically Porous Carbon, *J. Food Compos. Anal.*, 2024, **131**, 106217, DOI: [10.1016/j.jfca.2024.106217](https://doi.org/10.1016/j.jfca.2024.106217).
- 322 L. Lv, Q. Tao, Y. Kuang, T. Zhang and X. Wang, A Novel Multimodal Aptasensor for Patulin Detection in Fruit



- Products Based on High-Performance RuMOF@hydrogel and Versatile Pericarp-Derived Carbonized Polymer Dots, *Food Chem.*, 2024, **461**, 140930, DOI: [10.1016/J.FOODCHEM.2024.140930](https://doi.org/10.1016/J.FOODCHEM.2024.140930).
- 323 B. He and X. Nb. Dong, BbvCI Powered DNA Walking Machine-Based Zr-MOFs-Labeled Electrochemical Aptasensor Using Pt@AuNRs/Fe-MOFs/PEI-RGO as Electrode Modification Material for Patulin Detection, *Chem. Eng. J.*, 2021, **405**, 126642, DOI: [10.1016/J.CEJ.2020.126642](https://doi.org/10.1016/J.CEJ.2020.126642).
- 324 H. Guo, Y. Sun, P. Ma, I. M. Khan, N. Duan and Z. Wang, Sensitive Detection of Patulin Based on DNase I-Assisted Fluorescent Aptasensor by Using AuNCs-Modified Truncated Aptamer, *Food Control*, 2022, **131**, 108430, DOI: [10.1016/j.foodcont.2021.108430](https://doi.org/10.1016/j.foodcont.2021.108430).
- 325 X. Song, D. Wang and M. Kim, Development of an Immuno-Electrochemical Glass Carbon Electrode Sensor Based on Graphene Oxide/Gold Nanocomposite and Antibody for the Detection of Patulin, *Food Chem.*, 2021, **342**, 128257, DOI: [10.1016/j.foodchem.2020.128257](https://doi.org/10.1016/j.foodchem.2020.128257).
- 326 Y. Liu, H. Lai, P. Ming, P. Chen, Q. Zhou, D. Sun and H. Zhai, Ultrasensitive Ratiometric Electrochemical Aptasensor Based on Novel MnCo@C as Nonenzyme Catalysis for the Detection of Patulin, *Sens. Actuators, B*, 2024, **401**, 135077, DOI: [10.1016/j.snb.2023.135077](https://doi.org/10.1016/j.snb.2023.135077).
- 327 R. Khan, S. B. Aissa, T. A. Sherazi, G. Catanante, A. Hayat and J. L. Marty, Development of an Impedimetric Aptasensor for Label Free Detection of Patulin in Apple Juice, *Molecules*, 2019, **24**(6), 1017, DOI: [10.3390/molecules24061017](https://doi.org/10.3390/molecules24061017).
- 328 S. Xue, L. Yin, S. Gao, R. Zhou, Y. Zhang, H. Jayan, H. R. El-Seedi, X. Zou and Z. Guo, A Film-like SERS Aptasensor for Sensitive Detection of Patulin Based on GO@Au Nanosheets, *Food Chem.*, 2024, **441**, 138364, DOI: [10.1016/j.foodchem.2024.138364](https://doi.org/10.1016/j.foodchem.2024.138364).
- 329 J. Xu, X. Qiao, Y. Wang, Q. Sheng, T. Yue, J. Zheng and M. Zhou, Electrostatic Assembly of Gold Nanoparticles on Black Phosphorus Nanosheets for Electrochemical Aptasensing of Patulin, *Microchim. Acta*, 2019, **186**(4), 238, DOI: [10.1007/s00604-019-3339-3](https://doi.org/10.1007/s00604-019-3339-3).
- 330 B. He and X. Dong, Aptamer Based Voltammetric Patulin Assay Based on the Use of ZnO Nanorods, *Microchim. Acta*, 2018, **185**(10), 462, DOI: [10.1007/s00604-018-3006-0](https://doi.org/10.1007/s00604-018-3006-0).
- 331 D. Moreno-González, P. Jáč, P. Riasová and L. Nováková, In-Line Molecularly Imprinted Polymer Solid Phase Extraction-Capillary Electrophoresis Coupled with Tandem Mass Spectrometry for the Determination of Patulin in Apple-Based Food, *Food Chem.*, 2021, **334**, 127607, DOI: [10.1016/j.foodchem.2020.127607](https://doi.org/10.1016/j.foodchem.2020.127607).
- 332 I. Sadok, A. Szmagara and M. M. Staniszewska, The Validated and Sensitive HPLC-DAD Method for Determination of Patulin in Strawberries, *Food Chem.*, 2018, **245**, 364–370, DOI: [10.1016/j.foodchem.2017.10.093](https://doi.org/10.1016/j.foodchem.2017.10.093).
- 333 J. V. Dias, R. C. da Silva, I. R. Pizzutti, I. D. dos Santos, M. Dassi and C. D. Cardoso, Patulin in Apple and Apple Juice: Method Development, Validation by Liquid Chromatography-Tandem Mass Spectrometry and Survey in Brazilian South Supermarkets, *J. Food Compos. Anal.*, 2019, **82**, 103242, DOI: [10.1016/j.jfca.2019.103242](https://doi.org/10.1016/j.jfca.2019.103242).
- 334 B. He and X. Lu, An Electrochemical Aptasensor Based on Tetrahedral DNA Nanostructures as a Signal Probe Carrier Platform for Sensitive Detection of Patulin, *Anal. Chim. Acta*, 2020, **1138**, 123–131, DOI: [10.1016/j.aca.2020.09.025](https://doi.org/10.1016/j.aca.2020.09.025).
- 335 N. Küçük, Ş. Kaya, S. Şahin and M. O. Çağlayan, Structural Switching Aptamer-Based Electrochemical Sensor for Mycotoxin Patulin Detection, *Toxicon*, 2024, **239**, 107583, DOI: [10.1016/j.toxicon.2023.107583](https://doi.org/10.1016/j.toxicon.2023.107583).
- 336 X. Hu, Y. Xia, Y. Liu, F. Zhao and B. Zeng, Determination of Patulin Using Dual-Dummy Templates Imprinted Electrochemical Sensor with PtPd Decorated N-Doped Porous Carbon for Amplification, *Microchim. Acta*, 2021, **188**(5), 148, DOI: [10.1007/s00604-021-04812-2](https://doi.org/10.1007/s00604-021-04812-2).
- 337 Y. Ding, J. Li, K. Yan and J. Zhang, A Miniature Self-Powered Electrochemical Sensor for the Determination of Patulin Based on an Integrated Photocatalytic Fuel Cell, *Sens. Actuators, B*, 2022, **369**, 132259, DOI: [10.1016/j.snb.2022.132259](https://doi.org/10.1016/j.snb.2022.132259).
- 338 J. Xu, J. Liu, W. Li, Y. Wei, Q. Sheng and Y. Shang, A Dual-Signaling Electrochemical Aptasensor Based on an In-Plane Gold Nanoparticles-Black Phosphorus Heterostructure for the Sensitive Detection of Patulin, *Foods*, 2023, **12**(4), 846, DOI: [10.3390/foods12040846](https://doi.org/10.3390/foods12040846).
- 339 W. I. Riberi, M. A. Zon, H. Fernández and F. J. Arévalo, Impedimetric Immunosensor to Determine Patulin in Apple Juices Using a Glassy Carbon Electrode Modified with Graphene Oxide, *Microchem. J.*, 2020, **158**, 105192, DOI: [10.1016/j.microc.2020.105192](https://doi.org/10.1016/j.microc.2020.105192).
- 340 S. Liu, S. Meng, M. Wang, W. Li, N. Dong, D. Liu, Y. Li and T. You, In-Depth Interpretation of Aptamer-Based Sensing on Electrode: Dual-Mode Electrochemical-Photoelectrochemical Sensor for the Ratiometric Detection of Patulin, *Food Chem.*, 2023, **410**, 135450, DOI: [10.1016/j.foodchem.2023.135450](https://doi.org/10.1016/j.foodchem.2023.135450).
- 341 H. Zhao, X. Qiao, X. Zhang, C. Niu, T. Yue and Q. Sheng, Simultaneous Electrochemical Aptasensing of Patulin and Ochratoxin A in Apple Juice Based on Gold Nanoparticles Decorated Black Phosphorus Nanomaterial, *Anal. Bioanal. Chem.*, 2021, **413**(11), 3131–3140, DOI: [10.1007/s00216-021-03253-3](https://doi.org/10.1007/s00216-021-03253-3).
- 342 A. Erdem and H. Senturk, Smartphone-Controlled Aptasensor for Voltammetric Detection of Patulin in Apple Juice, *Sensors*, 2024, **24**(3), 754, DOI: [10.3390/s24030754](https://doi.org/10.3390/s24030754).
- 343 B. Datta, P. Bhatt and G. Dutta, A Redox Mediator-Free Highly Selective and Sensitive Electrochemical Aptasensor for Patulin Mycotoxin Detection in Apple Juice Using Ni-NiO Pseudocapacitive Nanomaterials, *J. Agric. Food Chem.*, 2024, **72**(11), 5993–6005, DOI: [10.1021/acs.jafc.3c07886](https://doi.org/10.1021/acs.jafc.3c07886).
- 344 X. Lu, B. He, Y. Liang, J. Wang, M. Wei, H. Jin, W. Ren, Z. Suo and Y. Xu, Ultrasensitive Detection of Patulin Based on a Ag<sup>+</sup>-Driven One-Step Dual Signal Amplification, *J. Hazard. Mater.*, 2022, **438**, 129530, DOI: [10.1016/j.jhazmat.2022.129530](https://doi.org/10.1016/j.jhazmat.2022.129530).



- 345 X. Lu, B. He, Y. Liang, J. Wang, Q. Jiao, Y. Liu, R. Guo, M. Wei, H. Jin, W. Ren and Z. Suo, An Electrochemical Aptasensor Based on Dual-Enzymes-Driven Target Recycling Strategy for Patulin Detection in Apple Juice, *Food Control*, 2022, **137**, 108907, DOI: [10.1016/j.foodcont.2022.108907](https://doi.org/10.1016/j.foodcont.2022.108907).
- 346 D. Çimen, N. Bereli and A. Denizli, Patulin Imprinted Nanoparticles Decorated Surface Plasmon Resonance Chips for Patulin Detection, *Photonic Sens.*, 2022, **12**(2), 117–129, DOI: [10.1007/s13320-021-0638-1](https://doi.org/10.1007/s13320-021-0638-1).
- 347 Y. Zhu, L. Wu, H. Yan, Z. Lu, W. Yin and H. Han, Enzyme Induced Molecularly Imprinted Polymer on SERS Substrate for Ultrasensitive Detection of Patulin, *Anal. Chim. Acta*, 2020, **1101**, 111–119, DOI: [10.1016/j.aca.2019.12.030](https://doi.org/10.1016/j.aca.2019.12.030).
- 348 Z. Wu, E. Xu, Z. Jin and J. Irudayaraj, An Ultrasensitive Aptasensor Based on Fluorescent Resonant Energy Transfer and Exonuclease-Assisted Target Recycling for Patulin Detection, *Food Chem.*, 2018, **249**, 136–142, DOI: [10.1016/j.foodchem.2018.01.025](https://doi.org/10.1016/j.foodchem.2018.01.025).
- 349 A. Ahmadi, N. M. Danesh, M. Ramezani, M. Aliboland, P. Lavaee, A. S. Emrani, K. Abnous and S. M. Taghdisi, A Rapid and Simple Ratiometric Fluorescent Sensor for Patulin Detection Based on a Stabilized DNA Duplex Probe Containing Less Amount of Aptamer-Involved Base Pairs, *Talanta*, 2019, **204**, 641–646, DOI: [10.1016/j.talanta.2019.06.057](https://doi.org/10.1016/j.talanta.2019.06.057).
- 350 L. Wu, H. Yan, G. Li, X. Xu, L. Zhu, X. Chen and J. Wang, Surface-Imprinted Gold Nanoparticle-Based Surface-Enhanced Raman Scattering for Sensitive and Specific Detection of Patulin in Food Samples, *Food Anal. Methods*, 2019, **12**(7), 1648–1657, DOI: [10.1007/s12161-019-01498-4](https://doi.org/10.1007/s12161-019-01498-4).
- 351 R. Khan, T. A. Sherazi, G. Catanante, S. Rasheed, J. L. Marty and A. Hayat, Switchable Fluorescence Sensor toward PAT via CA-MWCNTs Quenched Aptamer-Tagged Carboxyfluorescein, *Food Chem.*, 2020, **312**, 126048, DOI: [10.1016/j.foodchem.2019.126048](https://doi.org/10.1016/j.foodchem.2019.126048).
- 352 X. Qiao, W. Sun, Z. Kong, T. Yue, P. Wang, S. Lv and Q. Sheng, An Antifouling Biosensor with Dual Modality Readouts for Detection of Patulin in Complex Fruit Juice, *Microchem. J.*, 2023, **194**, 109229, DOI: [10.1016/j.microc.2023.109229](https://doi.org/10.1016/j.microc.2023.109229).
- 353 S. Xiang, J. Li, M. Shi, H. Yang, R. Cai and W. Tan, A Novel ECL Aptasensor for Ultra-Highly Sensitive Detection of Patulin Based on Terbium Organic Gels as Co-Reaction Accelerator in a 3, 4, 9, 10-Perylenetetracarboxylic Acid/K<sub>2</sub>S<sub>2</sub>O<sub>8</sub> System, *Sens. Actuators, B*, 2023, **394**, 134365, DOI: [10.1016/j.snb.2023.134365](https://doi.org/10.1016/j.snb.2023.134365).
- 354 F. Akpınar, Ş. G. Çalışkan and M. Muti, Disposable Nanosensor for the Electrochemical Determination of the Interaction between DNA, and a Mycotoxin, Patulin, *J. Pharm. Biomed. Anal.*, 2023, **236**, 115713, DOI: [10.1016/j.jpba.2023.115713](https://doi.org/10.1016/j.jpba.2023.115713).
- 355 K. Liu, Y. Guo, H. Yu, Y. Cheng, Y. Xie and W. Yao, Sulfhydryl-Functionalized Carbon Dots as Effective Probes for Fluorescence Enhancement Detection of Patulin, *Food Chem.*, 2023, **420**, 136037, DOI: [10.1016/j.foodchem.2023.136037](https://doi.org/10.1016/j.foodchem.2023.136037).
- 356 D. Nie, D. Guo, Q. Huang, W. Guo, J. Wang, Z. Zhao and Z. Han, A Novel Insight into Fluorescent Sensor for Patulin Detection Using Thiol-Terminated Liposomes with Encapsulated Coumarin-6 as Signal Probe, *Sens. Actuators, B*, 2021, **345**, 130366, DOI: [10.1016/j.snb.2021.130366](https://doi.org/10.1016/j.snb.2021.130366).
- 357 M. Yao, H. Zhan, L. Liu, T. Gai, D. Zhao and W. Wei, A Ratiometric Fluorescent Biosensing Platform Based on CDs and AuNCs@CGO for Patulin Detection, *Anal. Chim. Acta*, 2024, **1330**, 343279, DOI: [10.1016/J.ACA.2024.343279](https://doi.org/10.1016/J.ACA.2024.343279).
- 358 L. Lv, Q. Q. Chen, C. Jing and X. Wang, An Ultrasensitive Ratiometric Aptasensor Based on the Dual-Potential Electrochemiluminescence of Ru(Bpy)<sub>3</sub><sup>2+</sup> in a Novel Ternary System for Detection of Patulin in Fruit Products, *Food Chem.*, 2023, **415**, 135780, DOI: [10.1016/j.foodchem.2023.135780](https://doi.org/10.1016/j.foodchem.2023.135780).
- 359 Q. Tao, L. Lv, T. Liu and X. Wang, A Fluorescence-Validated MIP-ECL Sensor Based on UiO66 Loaded Carbon Nitride for Detection of Trace Patulin in Series Fruit Products, *Microchem. J.*, 2024, **207**, 111627, DOI: [10.1016/J.MICROC.2024.111627](https://doi.org/10.1016/J.MICROC.2024.111627).
- 360 L. J. G. Silva, A. M. P. T. Pereira, A. Pena and C. M. Lino, Citrinin in Foods and Supplements: A Review of Occurrence and Analytical Methodologies, *Foods*, 2021, **10**(1), 14, DOI: [10.3390/foods10010014](https://doi.org/10.3390/foods10010014).
- 361 S. Moradi and S. A. Mortazavi, Evaluation of *Monascus Purpureus* Fermentation in Dairy Sludge-Based Medium for Enhanced Production of Vibrant Red Pigment with Minimal Citrinin Content, *PLoS One*, 2024, **19**(12), e0315006, DOI: [10.1371/journal.pone.0315006](https://doi.org/10.1371/journal.pone.0315006).
- 362 F. Vendruscolo, R. M. M. Bühler, J. C. de Carvalho, D. de Oliveira, D. E. Moritz, W. Schmidell and J. L. Ninow, *Monascus*: A Reality on the Production and Application of Microbial Pigments, *Appl. Biochem. Biotechnol.*, 2016, **178**(2), 211–223, DOI: [10.1007/s12010-015-1880-z](https://doi.org/10.1007/s12010-015-1880-z).
- 363 N. Ali and G. H. Degen, Citrinin Biomarkers: A Review of Recent Data and Application to Human Exposure Assessment, *Arch. Toxicol.*, 2019, **93**(11), 3057–3066, DOI: [10.1007/s00204-019-02570-y](https://doi.org/10.1007/s00204-019-02570-y).
- 364 A. A. P. M. de Menezes, R. P. S. Aguiar, J. V. O. Santos, C. Sarkar, M. T. Islam, A. L. Braga, M. M. Hasan, F. C. C. da Silva, J. Sharif-Rad, A. Dey, D. Calina, A. A. C. Melo-Cavalcante and J. M. C. Sousa, Citrinin as a Potential Anti-Cancer Therapy: A Comprehensive Review, *Chem.-Biol. Interact.*, 2023, **381**, 110561, DOI: [10.1016/j.cbi.2023.110561](https://doi.org/10.1016/j.cbi.2023.110561).
- 365 J. H. Doughari, The Occurrence, Properties and Significance of Citrinin Mycotoxin, *J. Plant Pathol. Microbiol.*, 2015, **6**(11), 2, DOI: [10.4172/2157-7471.1000321](https://doi.org/10.4172/2157-7471.1000321).
- 366 S. Samyal and A. Sharma, Mycotoxins: Structure, Biosynthesis, Health Effects, and Their Biological Detoxification, in *Fungal Resources for Sustainable Economy: Current Status and Future Perspectives*, 2023, DOI: [10.1007/978-981-19-9103-5\\_18](https://doi.org/10.1007/978-981-19-9103-5_18).



- 367 S. Samyál and A. Sharma, Mycotoxins: Structure, Biosynthesis, Health Effects, and Their Biological Detoxification, in *Fungal Resources for Sustainable Economy: Current Status and Future Perspectives*, 2023, DOI: [10.1007/978-981-19-9103-5\\_18](https://doi.org/10.1007/978-981-19-9103-5_18).
- 368 X. Hu, Y. Liu, Y. Xia, F. Zhao and B. Zeng, A Novel Ratiometric Electrochemical Sensor for the Selective Detection of Citrinin Based on Molecularly Imprinted Poly(Thionine) on Ionic Liquid Decorated Boron and Nitrogen Co-Doped Hierarchical Porous Carbon, *Food Chem.*, 2021, **363**, 130385, DOI: [10.1016/j.foodchem.2021.130385](https://doi.org/10.1016/j.foodchem.2021.130385).
- 369 S. Tang, B. He, Y. Liu, L. Wang, Y. Liang, J. Wang, H. Jin, M. Wei, W. Ren, Z. Suo and Y. Xu, A Dual-Signal Mode Electrochemical Aptasensor Based on Tetrahedral DNA Nanostructures for Sensitive Detection of Citrinin in Food Using PtPdCo Mesoporous Nanozymes, *Food Chem.*, 2024, **460**, 140739, DOI: [10.1016/J.FOODCHEM.2024.140739](https://doi.org/10.1016/J.FOODCHEM.2024.140739).
- 370 S. Tang, B. He, J. Yang, Y. Liu, Y. Liang, J. Wang, H. Jin, M. Wei, W. Ren, Z. Suo and Y. Xu, A Signal-Amplification Electrochemical Aptasensor Based on Porous Pt Nanotubes and Tetrahedral DNA Nanostructures for Ultrasensitive Detection of Citrinin, *Sens. Actuators, B*, 2024, **408**, 135519, DOI: [10.1016/j.snb.2024.135519](https://doi.org/10.1016/j.snb.2024.135519).
- 371 D. Elfadil, F. Silveri, S. Palmieri, F. Della Pelle, M. Sergi, M. Del Carlo, A. Amine and D. Compagnone, Liquid-Phase Exfoliated 2D Graphene Nanoflakes Electrochemical Sensor Coupled to Molecularly Imprinted Polymers for the Determination of Citrinin in Food, *Talanta*, 2023, **253**, 124010, DOI: [10.1016/j.talanta.2022.124010](https://doi.org/10.1016/j.talanta.2022.124010).
- 372 N. Atar, M. L. Yola and T. Eren, Sensitive Determination of Citrinin Based on Molecular Imprinted Electrochemical Sensor, *Appl. Surf. Sci.*, 2016, **362**, 315–322, DOI: [10.1016/j.apsusc.2015.11.222](https://doi.org/10.1016/j.apsusc.2015.11.222).
- 373 M. Zhang, X. Xue, H. Gong, B. Liu and L. Ye, Double Isothermal Amplification and CRISPR-Cas12a for Sensitive Detection of Citrinin, *ACS Food Sci. Technol.*, 2021, **1**(10), 1997–2005, DOI: [10.1021/acsfoodscitech.1c00321](https://doi.org/10.1021/acsfoodscitech.1c00321).
- 374 H. Yan, B. He, L. Xie and X. Cao, A Label-Free Electrochemical Aptasensor Based on NH<sub>2</sub>-MIL-235(Fe) for the Sensitive Detection of Citrinin, *Anal. Methods*, 2022, **14**(37), 3702–3708, DOI: [10.1039/d2ay01243j](https://doi.org/10.1039/d2ay01243j).
- 375 Y. He, T. Wang, J. Cao, F. Zhao and B. Zeng, Molecular Imprinting Electrochemiluminescence Sensor Based on Nitrogen-Doped Carbon Quantum Dots/Ru(Bpy)<sub>3</sub>@SiO<sub>2</sub> for the Determination of Citrinin, *Microchim. Acta*, 2023, **190**(4), 155, DOI: [10.1007/s00604-023-05735-w](https://doi.org/10.1007/s00604-023-05735-w).
- 376 B. Shojaee Sadi, M. Bayat, P. Tajik and S. J. Hashemi, Citrinin Detection by Intensified Fluorescence Signal of a FRET-Based Immunosensor Using Magnetic/Silica Core-Shell, *Saudi J. Biol. Sci.*, 2018, **25**(1), 171–177, DOI: [10.1016/j.sjbs.2016.08.006](https://doi.org/10.1016/j.sjbs.2016.08.006).
- 377 M. Sun, S. Li, J. Xu, Y. Zhou and R. Fu, Simple and Accurate Spectrofluorimetric Method for Detecting Citrinin in Red Fermented Rice, *Anal. Lett.*, 2020, **53**(9), 1446–1454, DOI: [10.1080/00032719.2019.1709076](https://doi.org/10.1080/00032719.2019.1709076).
- 378 A. Hitabatuma, P. Wang, M. Ma, R. Wang and X. Su, Determination of Citrinin with a Stable Fluorescent Zirconium(IV)-Based Metal–Organic Framework, *Chem. Pap.*, 2023, **77**(6), 2957–2966, DOI: [10.1007/s11696-023-02679-6](https://doi.org/10.1007/s11696-023-02679-6).
- 379 X. Yang, Y. Qu, C. Wang, L. Wu and X. Hu, Development of an Enzyme-Linked Immunosorbent Assay Based on a Monoclonal Antibody for the Rapid Detection of Citrinin in Wine, *Foods*, 2024, **14**(1), 27, DOI: [10.3390/foods14010027](https://doi.org/10.3390/foods14010027).
- 380 S. Sadhasivam, O. Barda, V. Zakin, R. Reifen and E. Sionov, Rapid Detection and Quantification of Patulin and Citrinin Contamination in Fruits, *Molecules*, 2021, **26**(15), 4545, DOI: [10.3390/molecules26154545](https://doi.org/10.3390/molecules26154545).
- 381 P. Ponz-Perelló, F. A. Esteve-Turrillas, M. Á. Cortés, J. Herranz and O. Pardo, Development and Validation of an Analytical Method for Determination of Citrinin in Red Rice and Red Yeast Rice-Based Food Supplements by Ultra-High Performance Liquid Chromatography Tandem Mass Spectrometry, *Food Chem.*, 2024, **455**, 139941, DOI: [10.1016/J.FOODCHEM.2024.139941](https://doi.org/10.1016/J.FOODCHEM.2024.139941).
- 382 W. Huang, Z. Tu, Z. Ning, Q. He and Y. Li, Development of Real-Time Immuno-PCR Based on Phage Displayed an Anti-Idiotypic Nanobody for Quantitative Determination of Citrinin in *Monascus*, *Toxins*, 2019, **11**(10), 572, DOI: [10.3390/toxins11100572](https://doi.org/10.3390/toxins11100572).
- 383 S. Ouhibi, A. Vidal, C. Martins, R. Gali, A. Hedhili, S. De Saeger and M. De Boevre, LC-MS/MS Methodology for Simultaneous Determination of Patulin and Citrinin in Urine and Plasma Applied to a Pilot Study in Colorectal Cancer Patients, *Food Chem. Toxicol.*, 2020, **136**, 110994, DOI: [10.1016/j.fct.2019.110994](https://doi.org/10.1016/j.fct.2019.110994).
- 384 M. Li, Z. Tong, X. Gao, L. Zhang and S. Li, Simultaneous Detection of Zearalenone, Citrinin, and Ochratoxin A in Pepper by Capillary Zone Electrophoresis, *Food Addit. Contam. Part A. Chem. Anal. Control Expo. Risk Assess.*, 2020, **37**(8), 1388–1398, DOI: [10.1080/19440049.2020.1769197](https://doi.org/10.1080/19440049.2020.1769197).
- 385 A. Narváez, L. Izzo, Y. Rodríguez-Carrasco and A. Ritieni, Citrinin Dietary Exposure Assessment Approach through Human Biomonitoring High-Resolution Mass Spectrometry-Based Data, *J. Agric. Food Chem.*, 2021, **69**(22), 6330–6338, DOI: [10.1021/acs.jafc.1c01776](https://doi.org/10.1021/acs.jafc.1c01776).
- 386 A. R. Jalalvand, M. Farshadnia, F. Jalili and C. Jalili, A Novel, Intelligent and Computer-Assisted Electrochemical Sensor for Extraction and Simultaneous Determination of Patulin and Citrinin in Apple and Pear Fruit Samples, *Chemom. Intell. Lab. Syst.*, 2024, **252**, 105188, DOI: [10.1016/J.CHEMOLAB.2024.105188](https://doi.org/10.1016/J.CHEMOLAB.2024.105188).
- 387 İ. Meydan, M. Bilici, E. Turan and A. Zengin, Selective Extraction and Determination of Citrinin in Rye Samples by a Molecularly Imprinted Polymer (MIP) Using Reversible Addition Fragmentation Chain Transfer Precipitation Polymerization (RAFTPP) with High-Performance Liquid Chromatography (HPLC) Detection,



- Anal. Lett.*, 2021, **54**(10), 1697–1708, DOI: [10.1080/00032719.2021.1892125](https://doi.org/10.1080/00032719.2021.1892125).
- 388 W. Xu, L. Xiang, Y. Chen, Y. Zhao, S. Liao, Y. Li, Y. Li, B. Tunyaluk and L. Lin, Risk Assessment of Citrinin in Chinese Dark Tea and Inhibitory Effects of Tea Polyphenols on Citrinin Production, *LWT*, 2024, **205**, 116527, DOI: [10.1016/J.LWT.2024.116527](https://doi.org/10.1016/J.LWT.2024.116527).
- 389 E. Todd, Food-Borne Disease Prevention and Risk Assessment, *Int. J. Environ. Health Res.*, 2020, **17**(14), 5129, DOI: [10.3390/ijerph17145129](https://doi.org/10.3390/ijerph17145129).
- 390 Y. Tang, Y. Li, P. Chen, S. Zhong and Y. Yang, *Nucleic Acid Aptamer-Based Sensors for Bacteria Detection: A Review*, BioEssays. John Wiley and Sons Inc March 1, 2025, DOI: [10.1002/bies.202400111](https://doi.org/10.1002/bies.202400111).
- 391 F. Ali, K. J. Harris and K. Ryu, Consumers' Return Intentions towards a Restaurant with Foodborne Illness Outbreaks: Differences across Restaurant Type and Consumers' Dining Frequency, *Food Control*, 2019, **98**, 424–430, DOI: [10.1016/j.foodcont.2018.12.001](https://doi.org/10.1016/j.foodcont.2018.12.001).
- 392 A. A. Ali, A. B. Altemimi, N. Alhelfi and S. A. Ibrahim, Application of Biosensors for Detection of Pathogenic Food Bacteria: A Review, *Biosensors*, 2020, DOI: [10.3390/BIOS10060058](https://doi.org/10.3390/BIOS10060058).
- 393 T. Bintsis, Foodborne Pathogens, *AIMS Microbiol.*, 2017, **3**(3), 529, DOI: [10.3934/microbiol.2017.3.529](https://doi.org/10.3934/microbiol.2017.3.529).
- 394 S. Panwar, K. S. Duggirala, P. Yadav, N. Debnath, A. K. Yadav and A. Kumar, Advanced Diagnostic Methods for Identification of Bacterial Foodborne Pathogens: Contemporary and Upcoming Challenges, *Crit. Rev. Biotechnol.*, 2023, **43**(7), 982–1000, DOI: [10.1080/07388551.2022.2095253](https://doi.org/10.1080/07388551.2022.2095253).
- 395 J. Zhou, L. Yin, Y. Dong, L. Peng, G. Liu, S. Man and L. Ma, CRISPR-Cas13a Based Bacterial Detection Platform: Sensing Pathogen *Staphylococcus Aureus* in Food Samples, *Anal. Chim. Acta*, 2020, **1127**, 225–233, DOI: [10.1016/j.aca.2020.06.041](https://doi.org/10.1016/j.aca.2020.06.041).
- 396 V. Caratelli, S. Fillo, N. D'Amore, O. Rossetto, M. Pirazzini, M. Moccia, C. Avitabile, D. Moscone, F. Lista and F. Arduini, Paper-Based Electrochemical Peptide Sensor for on-Site Detection of Botulinum Neurotoxin Serotype A and C, *Biosens. Bioelectron.*, 2021, **183**, 113210, DOI: [10.1016/j.bios.2021.113210](https://doi.org/10.1016/j.bios.2021.113210).
- 397 G. H. Lee, Y. Kim, E. S. Lee, D. Nam, B. S. Cha, S. Kim, S. Kim and K. S. Park, Development of a Structure-Switching Aptamer for Sensitive Colorimetric Detection of Botulinum Neurotoxin, *Biochip J.*, 2024, **18**(4), 601–610, DOI: [10.1007/s13206-024-00170-2](https://doi.org/10.1007/s13206-024-00170-2).
- 398 W. C. Hu, J. Pang, S. Biswas, K. Wang, C. Wang and X. H. Xia, Ultrasensitive Detection of Bacteria Using a 2D MOF Nanozyme-Amplified Electrochemical Detector, *Anal. Chem.*, 2021, **93**(24), 8544–8552, DOI: [10.1021/acs.analchem.1c01261](https://doi.org/10.1021/acs.analchem.1c01261).
- 399 R. Wang, L. Wang, J. Yan, D. Luan, sun Tao, J. Wu and X. R. Bian, Sensitive and Label-Free Detection of Pathogenic Bacteria Using a Bacteria-Imprinted Conducting Polymer Film-Based Electrochemical Sensor, *Talanta*, 2021, **226**, 122135, DOI: [10.1016/j.talanta.2021.122135](https://doi.org/10.1016/j.talanta.2021.122135).
- 400 A. I. Robby, S. G. Kim, U. H. Lee, I. In, G. Lee and S. Y. Park, Wireless Electrochemical and Luminescent Detection of Bacteria Based on Surface-Coated CsWO<sub>3</sub>-Immobilized Fluorescent Carbon Dots with Photothermal Ablation of Bacteria, *Chem. Eng. J.*, 2021, **403**, 126351, DOI: [10.1016/j.cej.2020.126351](https://doi.org/10.1016/j.cej.2020.126351).
- 401 J. N. Appaturi, T. Pulingam, K. L. Thong, S. Muniandy, N. Ahmad and B. F. Leo, Rapid and Sensitive Detection of Salmonella with Reduced Graphene Oxide-Carbon Nanotube Based Electrochemical Aptasensor, *Anal. Biochem.*, 2020, **589**, 113489, DOI: [10.1016/j.ab.2019.113489](https://doi.org/10.1016/j.ab.2019.113489).
- 402 E. Ettoubi, F. Akif, F. Genten and M. Blaghen, Marine Biotoxins: Origins, Effects, Distribution, Prevention and Treatment, *Int. J. Innov. Sci. Res. Technol.*, 2020, **5**(11), 928–941.
- 403 H. Maru, V. Bagga, A. Dhrangadhriya and J. J. Georrgie, A review on marine fish toxins and venoms, DOI: [10.5281/zenodo.7951206](https://doi.org/10.5281/zenodo.7951206).
- 404 X. Zhu, Y. Zhao, L. Wu, X. Gao, H. Huang, Y. Han and T. Zhu, *Advances in Biosensors for the Rapid Detection of Marine Biotoxins: Current Status and Future Perspectives*. Biosensors, Multidisciplinary Digital Publishing Institute MDPI, 2024, DOI: [10.3390/bios14040203](https://doi.org/10.3390/bios14040203).
- 405 A. K. AlShammari, T. M. Abd El-Aziz and A. Al-Sabi, Snake Venom: A Promising Source of Neurotoxins Targeting Voltage-Gated Potassium Channels, *Toxins*, 2023, **16**(1), 12, DOI: [10.3390/toxins16010012](https://doi.org/10.3390/toxins16010012).
- 406 A. Anadon, I. Ares, M. Martinez, M. R. Martinez-Larranaga and M. A. Martinez, Ciguatera Toxins: Toxicity and Food Safety, *Toxicological Risk Assessment and Multi-System Health Impacts from Exposure*, 2021, pp. 579–599, DOI: [10.1016/B978-0-323-85215-9.00019-2](https://doi.org/10.1016/B978-0-323-85215-9.00019-2).
- 407 V. Ramos and V. Vasconcelos, Palytoxin and Analogs: Biological and Ecological Effects, *Mar. Drugs*, 2010, **8**(7), 2021–2037, DOI: [10.3390/md8072021](https://doi.org/10.3390/md8072021).
- 408 K. L'Herondelle, M. Talagas, O. Mignen, L. Misery and R. Le Garrec, Neurological Disturbances of Ciguatera Poisoning: Clinical Features and Pathophysiological Basis, *Cells*, 2020, **9**(10), 2291, DOI: [10.3390/cells9102291](https://doi.org/10.3390/cells9102291).
- 409 C. V. Raju, Y. V. Manohara Reddy, C. H. Cho, H. H. Shin, T. J. Park and J. P. Park, Highly Sensitive Electrochemical Peptide-Based Biosensor for Marine Biotxin Detection Using a Bimetallic Platinum and Ruthenium Nanoparticle-Tethered Metal–Organic Framework Modified Electrode, *Food Chem.*, 2023, **428**, 136811, DOI: [10.1016/j.foodchem.2023.136811](https://doi.org/10.1016/j.foodchem.2023.136811).
- 410 N. Ullah, W. Chen, B. Noureen, Y. Tian, L. Du, C. Wu and J. Ma, An Electrochemical Ti<sub>3</sub>c<sub>2</sub>t<sub>x</sub> Aptasensor for Sensitive and Label-Free Detection of Marine Biological Toxins, *Sensors*, 2021, **21**(14), 4938, DOI: [10.3390/s21144938](https://doi.org/10.3390/s21144938).
- 411 J. A. Park, N. Kwon, E. Park, Y. Kim, H. Jang, J. Min and T. Lee, Electrochemical Biosensor with Aptamer/Porous Platinum Nanoparticle on Round-Type Micro-Gap Electrode for Saxitoxin Detection in Fresh Water, *Biosens.*



- Bioelectron.*, 2022, **210**, 114300, DOI: [10.1016/j.bios.2022.114300](https://doi.org/10.1016/j.bios.2022.114300).
- 412 M. Campàs, S. Leonardo, A. Sanchez-Henao, F. Real and J. Diogène, Electrochemical Biosensor for the Assessment of Cell Viability Using Methylene Blue. Application to the Detection of Ciguatoxins in Fish from the Canary Islands, *Anal. Chem.*, 2024, **96**(49), 19207–19212, DOI: [10.1021/acs.analchem.4c05174](https://doi.org/10.1021/acs.analchem.4c05174).
- 413 P. C. Serrano, G. E. Nunes, L. B. Avila, C. P. S. Reis, A. M. C. Gomes, F. T. Reis, M. L. Sartorelli, S. P. Melegari, W. G. Matias and I. H. Bechtold, Electrochemical Impedance Biosensor for Detection of Saxitoxin in Aqueous Solution, *Anal. Bioanal. Chem.*, 2021, **413**(25), 6393–6399, DOI: [10.1007/s00216-021-03603-1](https://doi.org/10.1007/s00216-021-03603-1).
- 414 P. Rocha, P. Rebelo, J. G. Pacheco, D. Geraldo, F. Bento, J. M. Leão-Martins, C. Delerue-Matos and H. P. A. Nouws, Electrochemical Molecularly Imprinted Polymer Sensor for Simple and Fast Analysis of Tetrodotoxin in Seafood, *Talanta*, 2025, **282**, 127002, DOI: [10.1016/J.TALANTA.2024.127002](https://doi.org/10.1016/J.TALANTA.2024.127002).
- 415 J. L. D. Nelis, D. Migliorelli, L. Mühlebach, S. Generelli, L. Stewart, C. T. Elliott and K. Campbell, Highly Sensitive Electrochemical Detection of the Marine Toxins Okadaic Acid and Domoic Acid with Carbon Black Modified Screen Printed Electrodes, *Talanta*, 2021, **228**, 122215, DOI: [10.1016/j.talanta.2021.122215](https://doi.org/10.1016/j.talanta.2021.122215).
- 416 M. Jiang, J. Tang, N. Zhou, J. Liu, F. Tao, F. Wang and C. Li, Rapid Electrochemical Detection of Domoic Acid Based on Polydopamine/Reduced Graphene Oxide Coupled with in-Situ Imprinted Polyacrylamide, *Talanta*, 2022, **236**, 122885, DOI: [10.1016/j.talanta.2021.122885](https://doi.org/10.1016/j.talanta.2021.122885).
- 417 J. Wu, Q. Yang, Q. Li, H. Li and F. Li, Two-Dimensional MnO<sub>2</sub> Nanozyme-Mediated Homogeneous Electrochemical Detection of Organophosphate Pesticides without the Interference of H<sub>2</sub>O<sub>2</sub> and Color, *Anal. Chem.*, 2021, **93**(8), 4084–4091, DOI: [10.1021/acs.analchem.0c05257](https://doi.org/10.1021/acs.analchem.0c05257).
- 418 X. Liu, H. Cheng, Y. Zhao, Y. Wang and F. Li, Portable Electrochemical Biosensor Based on Laser-Induced Graphene and MnO<sub>2</sub> Switch-Bridged DNA Signal Amplification for Sensitive Detection of Pesticide, *Biosens. Bioelectron.*, 2022, **199**, 113906, DOI: [10.1016/j.bios.2021.113906](https://doi.org/10.1016/j.bios.2021.113906).
- 419 S. Maheshwaran, V. Renganathan, S. M. Chen, R. Balaji, C. R. Kao, N. Chandrasekar, S. Ethiraj, M. S. Samuel and M. Govarthanan, Hydrothermally Constructed AgWO<sub>4</sub>-RGO Nanocomposites as an Electrode Enhancer for Ultrasensitive Electrochemical Detection of Hazardous Herbicide Crisquat, *Chemosphere*, 2022, **299**, 134434, DOI: [10.1016/j.chemosphere.2022.134434](https://doi.org/10.1016/j.chemosphere.2022.134434).
- 420 M. A. Rashed, M. Faisal, S. A. Alsareii, M. Alsaieri, M. Jalalah and F. A. Harraz, Highly Sensitive and Selective Electrochemical Sensor for Detecting Imidacloprid Pesticide Using Novel Silver Nanoparticles/Mesoporous Carbon/Hematite Ore Ternary Nanocomposite, *J. Environ. Chem. Eng.*, 2022, **10**(5), 108364, DOI: [10.1016/j.jece.2022.108364](https://doi.org/10.1016/j.jece.2022.108364).
- 421 A. P. Singh, S. Balayan, V. Hooda, R. K. Sarin and N. Chauhan, Nano-Interface Driven Electrochemical Sensor for Pesticides Detection Based on the Acetylcholinesterase Enzyme Inhibition, *Int. J. Biol. Macromol.*, 2020, **164**, 3943–3952, DOI: [10.1016/j.ijbiomac.2020.08.215](https://doi.org/10.1016/j.ijbiomac.2020.08.215).
- 422 A. Kumaravel and M. Muruganathan, Electrochemical Detection of Fenitrothion Usingnanosilver/Dodecane Modified Glassy Carbon Electrode, *Sens. Actuators, B*, 2021, **331**, 129467, DOI: [10.1016/j.snb.2021.129467](https://doi.org/10.1016/j.snb.2021.129467).
- 423 D. Wachholz Junior, P. B. Deroco and L. T. Kubota, A Copper-Based Metal-Organic Framework/Reduced Graphene Oxide-Modified Electrode for Electrochemical Detection of Paraquat, *Microchim. Acta*, 2022, **189**(8), 278, DOI: [10.1007/s00604-022-05358-7](https://doi.org/10.1007/s00604-022-05358-7).
- 424 S. El-Akaad, M. A. Mohamed, M. M. Elmasri, N. S. Abdelwahab, E. A. Abdelaleem, S. De Saeger and N. Beloglazova, 3D Bismuth Ferrite Microflowers Electrochemical Sensor for the Multiple Detection of Pesticides, *J. Electrochem. Soc.*, 2020, **167**(2), 027543, DOI: [10.1149/1945-7111/ab6cf0](https://doi.org/10.1149/1945-7111/ab6cf0).
- 425 X. Chen, W. Li, C. Lu, J. Chu, R. Lin, P. Wang, G. Xie, Q. Gu, D. Wu and B. Chu, Highly Sensitive Electrochemical Detection of Carbendazim Residues in Water by Synergistic Enhancement of Nitrogen-Doped Carbon Nanohorns and Polyethyleneimine Modified Carbon Nanotubes, *Sci. Total Environ.*, 2022, **851**, 158324, DOI: [10.1016/j.scitotenv.2022.158324](https://doi.org/10.1016/j.scitotenv.2022.158324).
- 426 S. J. Hawkes, *Information Textbooks Media Resources What Is a "Heavy Metal"?*; UTC, 1997, vol. 74, <https://pubs.acs.org/sharingguidelines>.
- 427 D. Witkowska, J. Słowik and K. Chilicka, Review Heavy Metals and Human Health: Possible Exposure Pathways and the Competition for Protein Binding Sites, *Molecules*, 2021, **26**(19), 6060, DOI: [10.3390/molecules26196060](https://doi.org/10.3390/molecules26196060).
- 428 A. Singh and I. Kostova, Health Effects of Heavy Metal Contaminants Vis-à-Vis Microbial Response in Their Bioremediation, *Inorg. Chim. Acta*, 2024, **568**, 122068, DOI: [10.1016/J.ICA.2024.122068](https://doi.org/10.1016/J.ICA.2024.122068).
- 429 J. Gao, J. Yin, G. Wang, X. Wang, J. Zhang, B. Sun, D. He, H. Suo and C. Zhao, A Novel Electrode for Simultaneous Detection of Multiple Heavy Metal Ions without Pre-Enrichment in Food Samples, *Food Chem.*, 2024, **448**, 138994, DOI: [10.1016/j.foodchem.2024.138994](https://doi.org/10.1016/j.foodchem.2024.138994).
- 430 S. Bagheri, R. K. Khurana, M. I. Kholil, M. J. Loes, S. Luo and A. Sinitskii, Cr<sub>2</sub>TiC<sub>2</sub>Tx MXene as an Adsorbent Material in Ultrasonic-Assisted d-μ-Solid Phase Extraction for Trace Detection of Heavy Metals, *Nanoscale*, 2024, **17**(5), 2545–2553, DOI: [10.1039/d4nr02556c](https://doi.org/10.1039/d4nr02556c).
- 431 R. Huang, J. Lv, J. Chen, Y. Zhu, J. Zhu, T. Wågberg and G. Hu, Three-Dimensional Porous High Boron-Nitrogen-Doped Carbon for the Ultrasensitive Electrochemical Detection of Trace Heavy Metals in Food Samples, *J. Hazard. Mater.*, 2023, **442**, 130020, DOI: [10.1016/j.jhazmat.2022.130020](https://doi.org/10.1016/j.jhazmat.2022.130020).
- 432 M. Zhang and W. Guo, Simultaneous Electrochemical Detection of Multiple Heavy Metal Ions in Milk Based on



- Silica-Modified Magnetic Nanoparticles, *Food Chem.*, 2023, **406**, 135034, DOI: [10.1016/j.foodchem.2022.135034](https://doi.org/10.1016/j.foodchem.2022.135034).
- 433 Z. Tan, W. Wu, C. Feng, H. Wu and Z. Zhang, Simultaneous Determination of Heavy Metals by an Electrochemical Method Based on a Nanocomposite Consisting of Fluorinated Graphene and Gold Nanocage, *Microchim. Acta*, 2020, **187**(7), 414, DOI: [10.1007/s00604-020-04393-6](https://doi.org/10.1007/s00604-020-04393-6).
- 434 G. Li, T. Belwal, Z. Luo, Y. Li, L. Li, Y. Xu and X. Lin, Direct Detection of Pb<sup>2+</sup> and Cd<sup>2+</sup> in Juice and Beverage Samples Using PDMS Modified Nanochannels Electrochemical Sensors, *Food Chem.*, 2021, **356**, 129632, DOI: [10.1016/j.foodchem.2021.129632](https://doi.org/10.1016/j.foodchem.2021.129632).
- 435 X. Wang, Y. Xu, Y. Li, Y. Li, Z. Li, W. Zhang, X. Zou, J. Shi, X. Huang, C. Liu and W. Li, Rapid Detection of Cadmium Ions in Meat by a Multi-Walled Carbon Nanotubes Enhanced Metal-Organic Framework Modified Electrochemical Sensor, *Food Chem.*, 2021, **357**, 129762, DOI: [10.1016/j.foodchem.2021.129762](https://doi.org/10.1016/j.foodchem.2021.129762).
- 436 C. Guo, C. Wang, H. Sun, D. Dai and H. Gao, A Simple Electrochemical Sensor Based on RGO/MoS<sub>2</sub>/CS Modified GCE for Highly Sensitive Detection of Pb(II) in Tobacco Leaves, *RSC Adv.*, 2021, **11**(47), 29590–29597, DOI: [10.1039/d1ra05350g](https://doi.org/10.1039/d1ra05350g).
- 437 G. Li, X. Qi, G. Zhang, S. Wang, K. Li, J. Wu, X. Wan, Y. Liu and Q. Li, Low-Cost Voltammetric Sensors for Robust Determination of Toxic Cd(II) and Pb(II) in Environment and Food Based on Shuttle-like  $\alpha$ -Fe<sub>2</sub>O<sub>3</sub> Nanoparticles Decorated  $\beta$ -Bi<sub>2</sub>O<sub>3</sub> Microspheres, *Microchem. J.*, 2022, **179**, 107515, DOI: [10.1016/J.MICROC.2022.107515](https://doi.org/10.1016/J.MICROC.2022.107515).
- 438 Y. Ding, F. Wei, C. Dong, J. Li, C. Zhang and X. Han, UiO-66 Based Electrochemical Sensor for Simultaneous Detection of Cd(II) and Pb(II), *Inorg. Chem. Commun.*, 2021, **131**, 108785, DOI: [10.1016/J.INOCHE.2021.108785](https://doi.org/10.1016/J.INOCHE.2021.108785).
- 439 Y. M. Mesfin, B. A. Mitiku and H. Tamrat Admasu, *Veterinary Drug Residues in Food Products of Animal Origin and Their Public Health Consequences: A Review. Veterinary Medicine and Science*, John Wiley and Sons Inc November, vol. 1, 2024, DOI: [10.1002/vms3.70049](https://doi.org/10.1002/vms3.70049).
- 440 F. Zhang and W. Cheng, The Mechanism of Bacterial Resistance and Potential Bacteriostatic Strategies, *Antibiotics*, 2022, **11**(9), 1215, DOI: [10.3390/antibiotics11091215](https://doi.org/10.3390/antibiotics11091215).
- 441 N. De Briyne, J. Atkinson, S. P. Borriello and L. Pokludová, Antibiotics Used Most Commonly to Treat Animals in Europe, *Vet. Rec.*, 2014, **175**(13), 325, DOI: [10.1136/vr.102462](https://doi.org/10.1136/vr.102462).
- 442 R. F. Rabello, R. R. Bonelli, B. A. Penna, J. P. Albuquerque, R. M. Souza and A. M. F. Cerqueira, Antimicrobial Resistance in Farm Animals in Brazil: An Update Overview, *Animals*, 2020, **10**(4), 552, DOI: [10.3390/ani10040552](https://doi.org/10.3390/ani10040552).
- 443 J. Huang, Y. Xu, M. Liu, P. Jiang, X. Guo, T. Gan, C. Wu and K. Wu, Rapid Room-Temperature Synthesis of Disposable Co Nanoparticles Modified 3D N-Doped Porous Carbon Electrode Device for Efficient Electrochemical Detection of Veterinary Drug and Pesticide Residue, *Carbon N Y*, 2024, **219**, 118806, DOI: [10.1016/j.carbon.2024.118806](https://doi.org/10.1016/j.carbon.2024.118806).
- 444 X. Yang, S. M. Ying, S. Zhang, J. Dai, W. Gao, T. Q. Wang, J. Q. Qiao, H. Z. Lian and L. Mao, CoFe<sub>2</sub>O<sub>4</sub> Decorated Graphene/C18-Functionalized Mesoporous Silica Nanocomposites Prepared for Magnetic Enrichment and Electrochemical Detection of Promethazine in Beef, *Chin. Chem. Lett.*, 2024, **35**(3), 108674, DOI: [10.1016/j.cclet.2023.108674](https://doi.org/10.1016/j.cclet.2023.108674).
- 445 K. Behera, B. Mutharani, Y. H. Chang, M. Kumari and F. C. Chiu, Protein-Aided Synthesis of Copper-Integrated Polyaniline Nanocomposite Encapsulated with Reduced Graphene Oxide for Highly Sensitive Electrochemical Detection of Dimetridazole in Real Samples, *Polymers*, 2024, **16**(1), 162, DOI: [10.3390/polym16010162](https://doi.org/10.3390/polym16010162).
- 446 K. Mariappan, T. W. Chen, S. M. Chen, T. W. Tseng, Y. Bian, T. T. Sun, J. Jiang and J. Yu, Fabrication of Hexagonal CuCoO<sub>2</sub> Modified Screen-Printed Carbon Electrode for the Selective Electrochemical Detection of Furaltadone, *Int. J. Electrochem. Sci.*, 2022, **17**, 220644, DOI: [10.20964/2022.06.21](https://doi.org/10.20964/2022.06.21).
- 447 P. Kolhe, M. Shah, A. Nathani, C. Shekhar Sharma and S. Gandhi, Block Copolymer-Derived Recessed Nanodisk-Array Electrodes for Electrochemical Detection of  $\beta$ -Lactam Antibiotics, *Food Chem.*, 2024, **435**, 137557, DOI: [10.1016/j.foodchem.2023.137557](https://doi.org/10.1016/j.foodchem.2023.137557).
- 448 M. Medhi, A. K. Gupta, S. Dhua and P. Mishra, Food Additives, in *Advances in Food Chemistry: Food Components, Processing and Preservation*, 2022, DOI: [10.1007/978-981-19-4796-4\\_7](https://doi.org/10.1007/978-981-19-4796-4_7).
- 449 P. Raoul, M. Cintoni, M. Palombaro, L. Basso, E. Rinninella, A. Gasbarrini and M. C. Mele, Food Additives, a Key Environmental Factor in the Development of IBD through Gut Dysbiosis, *Microorganisms*, 2022, **10**(1), 167, DOI: [10.3390/microorganisms10010167](https://doi.org/10.3390/microorganisms10010167).
- 450 P. Rathee, R. Sehrawat, P. Rathee, A. Khatkar, E. K. Akkol, S. Khatkar, N. Redhu, G. Türkcanoğlu and E. Sobarzo-Sánchez, Polyphenols: Natural Preservatives with Promising Applications in Food, Cosmetics and Pharma Industries; Problems and Toxicity Associated with Synthetic Preservatives; Impact of Misleading Advertisements; Recent Trends in Preservation and Legislation, *Materials*, 2023, **16**(3), 4793, DOI: [10.3390/ma16134793](https://doi.org/10.3390/ma16134793).
- 451 Z. Knezovic, B. Jurcevic Zidar, A. Pribisalic, S. Luetic, K. Jurcic, N. Knezovic and D. Sutlovic, Artificial Sweeteners in Food Products: Concentration Analysis, Label Practices, and Cumulative Intake Assessment in Croatia, *Nutrients*, 2025, **17**(7), 1110, DOI: [10.3390/nu17071110](https://doi.org/10.3390/nu17071110).
- 452 M. V. Martinez-Vega, S. Galván-Menéndez-Conde and V. Freyre-Fonseca, Possible Signaling Pathways in the Gut Microbiota-Brain Axis for the Development of Parkinson's Disease Caused by Chronic Consumption of Food Additives, *ACS Chem. Neurosci.*, 2023, **14**(11), 1950–1962, DOI: [10.1021/acchemneuro.3c00170](https://doi.org/10.1021/acchemneuro.3c00170).
- 453 E. J. Nixon, R. Sakthivel, Z. A. ALOthman, P. S. Ganesh and R. J. Chung, Lanthanum Nickelate Spheres Embedded Acid



- Functionalized Carbon Nanofiber Composite: An Efficient Electrocatalyst for Electrochemical Detection of Food Additive Vanillin, *Food Chem.*, 2023, **409**, 135324, DOI: [10.1016/j.foodchem.2022.135324](https://doi.org/10.1016/j.foodchem.2022.135324).
- 454 L. Taouri, M. Bourouina, S. Bourouina-Bacha and D. Hauchard, Fullerene-MWCNT Nanostructured-Based Electrochemical Sensor for the Detection of Vanillin as Food Additive, *J. Food Compos. Anal.*, 2021, **100**, 103811, DOI: [10.1016/j.jfca.2021.103811](https://doi.org/10.1016/j.jfca.2021.103811).
- 455 R. Nehru, C. W. Chen and C. Di. Dong, In-Situ Growth of MoS<sub>2</sub> Nanosheets on g-C<sub>3</sub>N<sub>4</sub> Nanotube: A Novel Electrochemical Sensing Platform for Vanillin Determination in Food Samples, *Carbon N Y*, 2023, **208**, 410–420, DOI: [10.1016/j.carbon.2023.03.053](https://doi.org/10.1016/j.carbon.2023.03.053).
- 456 N. Sebastian, W. C. Yu, D. Balram, F. S. Al-Mubaddel and M. Tayyab Noman, Nanomolar Detection of Food Additive Tert-Butylhydroquinone in Edible Oils Based on Novel Ternary Metal Oxide Embedded  $\beta$ -Cyclodextrin Functionalized Carbon Black, *Food Chem.*, 2022, **377**, 131867, DOI: [10.1016/j.foodchem.2021.131867](https://doi.org/10.1016/j.foodchem.2021.131867).
- 457 D. Balram, K. Y. Lian, N. Sebastian, F. S. Al-Mubaddel and M. T. Noman, A Sensitive and Economical Electrochemical Platform for Detection of Food Additive Tert-Butylhydroquinone Based on Porous Co<sub>3</sub>O<sub>4</sub> Nanorods Embellished Chemically Oxidized Carbon Black, *Food Control*, 2022, **136**, 108844, DOI: [10.1016/j.foodcont.2022.108844](https://doi.org/10.1016/j.foodcont.2022.108844).
- 458 U. Rajaji, T. W. Chen, S. Chinnapaiyan, S. M. Chen and M. Govindasamy, Two-Dimensional Binary Nanosheets (Bi<sub>2</sub>Te<sub>3</sub>@g-C<sub>3</sub>N<sub>4</sub>): application toward the Electrochemical Detection of Food Toxic Chemical, *Anal. Chim. Acta*, 2020, **1125**, 220–230, DOI: [10.1016/j.aca.2020.05.033](https://doi.org/10.1016/j.aca.2020.05.033).
- 459 W. da Silva, M. E. Ghica and C. M. A. Brett, Choline Oxidase Inhibition Biosensor Based on Poly(Brilliant Cresyl Blue) – Deep Eutectic Solvent/Carbon Nanotube Modified Electrode for Dichlorvos Organophosphorus Pesticide, *Sens. Actuators, B*, 2019, **298**, 126862, DOI: [10.1016/j.snb.2019.126862](https://doi.org/10.1016/j.snb.2019.126862).
- 460 J. Fu, X. An, Y. Yao, Y. Guo and X. Sun, Electrochemical Aptasensor Based on One Step Co-Electrodeposition of Aptamer and GO-CuNPs Nanocomposite for Organophosphorus Pesticide Detection, *Sens. Actuators, B*, 2019, **287**, 503–509, DOI: [10.1016/j.snb.2019.02.057](https://doi.org/10.1016/j.snb.2019.02.057).
- 461 S. Hassani, M. R. Akmal, A. Salek-Maghsoudi, S. Rahmani, M. R. Ganjali, P. Norouzi and M. Abdollahi, Novel Label-Free Electrochemical Aptasensor for Determination of Diazinon Using Gold Nanoparticles-Modified Screen-Printed Gold Electrode, *Biosens. Bioelectron.*, 2018, **120**, 122–128, DOI: [10.1016/j.bios.2018.08.041](https://doi.org/10.1016/j.bios.2018.08.041).
- 462 R. de O. Silva, É. A. da Silva, A. R. Fiorucci and V. S. Ferreira, Electrochemically Activated Multi-Walled Carbon Nanotubes Modified Screen-Printed Electrode for Voltammetric Determination of Sulfentrazone, *J. Electroanal. Chem.*, 2019, **835**, 220–226, DOI: [10.1016/j.jelechem.2019.01.018](https://doi.org/10.1016/j.jelechem.2019.01.018).
- 463 S. Bagheri, R. K. Khurana, M. I. Kholil, M. J. Loes, S. Luo and A. Sinitskii, Cr<sub>2</sub>TiC<sub>2</sub>T<sub>x</sub> MXene as an Adsorbent Material in Ultrasonic-Assisted d- $\mu$ -Solid Phase Extraction for Trace Detection of Heavy Metals, *Nanoscale*, 2024, **17**(5), 2545–2553, DOI: [10.1039/d4nr02556c](https://doi.org/10.1039/d4nr02556c).
- 464 H. Wang, X. Wei, F. Shao, Y. He, Y. Luo, Y. Sun and D. Xu, Synthesis of BiC@Au@Apta by Electrospinning as an Electrochemical Sensor for Detection of Tetracycline, *Ionics*, 2025, **31**(1), 981–991, DOI: [10.1007/s11581-024-05943-1](https://doi.org/10.1007/s11581-024-05943-1).
- 465 M. Nehra, R. Kumar, N. Dilbaghi and S. Kumar, Controlled Synthesis of Cu-MOF Possessing Peroxidase-Mimetic Activity for the Colorimetric Detection of Tetracycline in Aqueous Solution, *New J. Chem.*, 2023, **47**(16), 7595–7603, DOI: [10.1039/d3nj00218g](https://doi.org/10.1039/d3nj00218g).
- 466 Y. Zhao, X. Wang, Y. Chen, Q. Wang, Z. Yao and L. Wang, Electrochemical Synthesis of Co/Ni Bimetal-Organic Frameworks: A High-Performance SERS Platform for Detection of Tetracycline, *Spectrochim. Acta A Mol. Biomol. Spectrosc.*, 2023, **285**, 121843, DOI: [10.1016/j.saa.2022.121843](https://doi.org/10.1016/j.saa.2022.121843).
- 467 S. V. Selvi, U. Rajaji, S. M. Chen and J. N. Jebaranjitham, Floret-like Manganese Doped Tin Oxide Anchored Reduced Graphene Oxide for Electrochemical Detection of Dimetridazole in Milk and Egg Samples, *Colloids Surf., A*, 2021, **631**, 127733, DOI: [10.1016/j.colsurfa.2021.127733](https://doi.org/10.1016/j.colsurfa.2021.127733).
- 468 N. M. Umesh, J. A. Jesila, S. F. Wang, K. S. S. Devi, M. Govindasamy, A. A. Alothman and R. A. Alshgari, An Enhanced Electrochemical Performance of in Milk, Pigeon Meat and Eggs Samples Using Se Nanorods Capped with Co<sub>3</sub>O<sub>4</sub> Nanoflowers Decorated on Graphene Oxide, *Colloids Surf., B*, 2021, **200**, 111577, DOI: [10.1016/j.colsurfb.2021.111577](https://doi.org/10.1016/j.colsurfb.2021.111577).
- 469 R. Rajakumaran, K. Balamurugan, S. M. Chen and R. Sukanya, Facile Synthesis of Neodymium Stannate Nanoparticles an Effective Electrocatalyst for the Selective Detection of Dimetridazole in Biological Samples, *Anal. Chim. Acta*, 2022, **1190**, 339234, DOI: [10.1016/j.aca.2021.339234](https://doi.org/10.1016/j.aca.2021.339234).
- 470 F. Garkani Nejad, M. H. Asadi, I. Sheikhshoaie, Z. Dourandish, R. Zaimbashi and H. Beitollahi, Construction of Modified Screen-Printed Graphite Electrode for the Application in Electrochemical Detection of Sunset Yellow in Food Samples, *Food Chem. Toxicol.*, 2022, **166**, DOI: [10.1016/j.fct.2022.113243](https://doi.org/10.1016/j.fct.2022.113243).

